IRE Transactions

n Microwave Theory and Techniques

Volume MTT-9 **JULY, 1961** Number 4

Published Bimonthly

In This Issue

PUBLISHED BY THE

fessional Group on Microwave Theory and Techniques

IRE PROFESSIONAL GROUP ON MICROWAVE THEORY AND TECHNIQUES

The Professional Group on Microwave Theory and Techniques is an association of IRE members with professional interest in the field of Microwave Theory and Techniques. All IRE members are eligible for membership and will receive all Group publications upon payment of the prescribed annual fee of $3.00. Members of the American Physical Society and the Institution of Electrical Engineers of Great Britain may become affiliated with PGMTT and receive all Group publications upon payment of the Affiliate fee of $7.50 per year.

IRE TRANSACTIONS®
on Microwave Theory and Techniques

Published by The Institute of Radio Engineers, Inc., for the Professional Group on Microwave Theory and Techniques, at 1 East 79 Street, New York 21, N.Y. Responsibility for the contents rests upon the authors, and not upon the IRE, the Group, or its members. Individual copies of this issue and all available back issues may be purchased at the following prices: IRE members (one copy) $2.25, libraries and colleges $3.25, all others $4.50. Annual subscription price: non-members, $17.00; colleges and public libraries, $12.75.

Address all manuscripts to Donald D. King, PGMTT Editor, Electronic Communications, Inc., 1830 York Road, Timonium, Md. Submission of three copies of manuscripts, including figures, will expedite the review.

IRE Transactions on Microwave Theory and Techniques

Volume MTT-9 JULY, 1961 Number 4
Published Bimonthly

TABLE OF CONTENTS

CORRESPONDENCE

Report on Advances in Microwave Theory and Techniques—1960*

R. C. HANSEN†, SENIOR MEMBER, IRE, AND M. T. WEISS†, SENIOR MEMBER, IRE

THIS is a compendium of the principal advances in the microwave area for the calendar year 1960; only United States journals are included in this report which is not a catalog of all published papers, but rather, is intended to be a semicritical review of the major accomplishments in the field. The report is divided into four major sections which cover, respectively, tube sources, electromagnetic devices, solid-state devices, and measurements.

The year has seen outstanding accomplishments in the realization of new types of solid-state devices such as low-noise amplifiers, tunnel-diode oscillators and amplifiers, and quantum devices. Other highlights include new structures for traveling-wave interaction, resolution of the single-mode ferrite-slab-in-guide paradox, advances in high-power component testing, and in plasma analysis/diagnostics. A major advance has occurred in the testing and operation of various low-noise systems.

This report continues a series which started with the report for 1954; 1958 was the last year covered by the series. Survey reports covering the interim that might be useful include three papers on MTT progress outside of the United States [1]–[3], and the URSI USA National Commission report to the 13th General Assembly of URSI. This last report [4], [5] covers USA progress during the triennium 1957–1959 on a variety of topics including radio measurements and standards, parametric amplifiers, masers, ferrites, microwave tubes, and plasmas.

[1] J. Brown, "Report of advances in microwave theory and techniques in Great Britain—1959," IRE TRANS. ON MICROWAVE THEORY AND TECHNIQUES, vol. MTT-8, pp. 382–386; July, 1960.
[2] G. Goudet, "Report of advances in microwave theory and techniques in Western Europe—1959," IRE TRANS. ON MICROWAVE THEORY AND TECHNIQUES, vol. MTT-8, pp. 387–394; July, 1960.
[3] K. Morita, "Report of advances in microwave theory and techniques in Japan—1959," IRE TRANS. ON MICROWAVE THEORY AND TECHNIQUES, vol. MTT-8, pp. 395–397; July, 1960.
[4] E. A. Gerber, *et al.*, "USA National Committee URSI Report: radio measurement methods and standards," *J. Res. NBS*, vol. 64D, pp. 592–605; November–December, 1960.
[5] P. K. Tien, *et al.*, "USA National Committee URSI Report: radio electronics," *J. Res. NBS*, vol. 64D, pp. 751–767; November–December, 1960.

I. SOURCES

A. Klystrons

Large signal studies [6], [7], noise studies [8], [9], and the cascading of reflex tubes as regenerative amplifiers [10], [11] are the major areas of work. A hybrid tube has been developed [12] which is a combination of klystron and TWT. Cavities are used for bunching of the beam, and a traveling-wave section is the output coupler. Development of a Ku band electrostatically-focused tube [13] and a novel scheme for wide-band tuning using ferrite material have been reported [14].

[6] S. E. Webber, "Some calculations on the large signal energy exchange mechanisms in linear beam tubes," IRE TRANS. ON ELECTRON DEVICES, vol. ED-7, pp. 154–162; July, 1960.
[7] S. V. Yadavalli, "On the large-signal aspect of the broadband multicavity klystron problem—theory and experiment," PROC. IRE (Correspondence), vol. 48, pp. 953–954; May, 1960.
[8] G. A. Espersen, "Noise studies on two-cavity CW klystrons," IRE TRANS. ON MICROWAVE THEORY AND TECHNIQUES, vol. MTT-8, pp. 474–477; September, 1960.
[9] K. Ishii, "Noise figures of reflex klystron amplifiers," IRE TRANS. ON MICROWAVE THEORY AND TECHNIQUES, vol. MTT-8, pp. 291–294; May, 1960.
[10] ——, "Phase adjustment effects on cascaded reflex klystron amplifiers," IRE TRANS. ON MICROWAVE THEORY AND TECHNIQUES, vol. MTT-8, pp. 445–449; July, 1960.
[11] ——, "Isolator effect on cascaded reflex klystron amplifiers," PROC. IRE (Correspondence), vol. 48, pp. 1503–1504; August, 1960.
[12] S. V. Yadavalli, "On the performance of a class of hybrid tubes," PROC. IRE (Correspondence), vol 48, p. 263; February, 1960.
[13] R. G. Rockwell, "A four-cavity, electrostatically focused, Ku-band klystron amplifier," 1960 IRE WESCON CONVENTION RECORD, pt. 3, pp. 109–113.
[14] G. R. Jones and J. C. Cacheris, "Magnetically tuned klystrons for wide-band frequency modulation applications," IRE TRANS. ON ELECTRON DEVICES, vol. ED-7, pp. 206–214; October, 1960.

B. Magnetron and Crossed-Field Tubes

Relatively little effort is being expended in this area; a new use (as a detector) of the original-type smooth-anode magnetron has appeared [15]. An analysis of the crossed-field amplifier which uses a boundary-value approach to include the effects of evanescent modes at the input boundary has been made by Hershenov [16]. Velocity sorting for secondary emission reduction is used in a crossed-field collector applicable to both TW and klystron tubes [17]. Noise measurements have been reported on "M"-type tubes [18].

[15] R. M. Hill and F. A. Olson, "Microwave oscillation and detection by a smooth anode coaxial magnetron," PROC. IRE (Correspondence), vol. 48, pp. 1906–1907; November, 1960.
[16] B. Hershenov, "A small-signal field theory analysis of crossed-field amplifiers applicable to thick beams," IRE TRANS. ON ELECTRON DEVICES, vol. ED-7, pp. 163–171; July, 1960.
[17] D. A. Dunn, *et al.*, "A crossed-field multisegment depressed collector for beam-type tubes," IRE TRANS. ON ELECTRON DEVICES, vol. ED-7, pp. 262–267; October, 1960.
[18] J. R. Anderson, "Noise measurements on an M-type backward-wave amplifier," PROC. IRE (Correspondence), vol. 48, pp. 946–947; May, 1960.

C. Traveling-Wave Tubes

Theoretical work probably represents most of the advancement in this area. A general analysis of the

* Received by the PGMTT, May 11, 1960.
† Electronics Lab., Aerospace Corp., Los Angeles, Calif.

dependence of output power on various factors for dispersive structures is given by Sobol and Rowe [19]. Another analysis compares the differential and integral-equation approaches, and happily arrives at compatible results [20]. Dow has analyzed behavior near cutoff by using an expansion about cutoff frequency [21]. Another paper covers the effects of variations in dc electron velocity in electrostatically-focused tubes [22]. The space-charge-wave noise exchanger of Sturrock has been investigated further [23]; this reduces the noise temperature of the tube.

[19] H. Sobol and J. E. Rowe, "Theoretical power output and bandwidth of traveling-wave amplifiers," IRE TRANS. ON ELECTRON DEVICES, vol. ED-7, pp. 84–94; April, 1960.
[20] J. E. Rowe, "One-dimensional traveling-wave tube analyses and the effect of radial electric field variations," IRE TRANS. ON ELECTRON DEVICES, vol. ED-7, pp. 16–21; January, 1960.
[21] D. G. Dow, "Behavior of traveling-wave tubes near circuit cutoff," IRE TRANS. ON ELECTRON DEVICES, vol. ED-7, pp. 123–131; July, 1960.
[22] W. W. Siekanowicz, "A small-RF-signal theory for an electrostatically focused traveling-wave tube," PROC. IRE, vol. 48, pp. 1888–1901; November, 1960.
[23] D. C. Forster, "Cooling of the slow space-charge wave with application to the traveling-wave tube," 1960 IRE WESCON CONVENTION RECORD, pt. 3, pp. 90–95.

Advances have also been made in new and different interaction configurations. One type, developed by Phillips, utilizes a magnetically-undulated beam reacting with the TE_{01} mode in waveguide; this is "O"-type interaction [24]. Another scheme involves a helical beam between coaxial cylinders, interacting with a TEM mode [25]. This is called an "E"-type tube. Two schemes which use cyclotron resonance interaction involve a linear-quadripole field [26] and a TE_{01} waveguide [27]. An interesting application of TWT's uses successive signal removal which converts RF to video at a number of output points and couples these into a video delay line to obtain large dynamic range [28].

[24] R. M. Phillips, "The Ubitron, a high-power traveling-wave tube based on a periodic beam interaction in unloaded waveguide," IRE TRANS. ON ELECTRON DEVICES, vol. ED-7, pp. 231–241; October, 1960.
[25] R. H. Pantell, "Small-signal analysis of the helitron oscillator," IRE TRANS. ON ELECTRON DEVICES, vol. ED-7, pp. 22–29; January, 1960.
[26] E. I. Gordon, "A transverse-field traveling-wave tube," PROC. IRE (Correspondence), vol. 48, p. 1158; June, 1960.
[27] K. K. Chow and R. H. Pantell, "The cyclotron resonance backward-wave oscillator," PROC. IRE, vol. 48, pp. 1865–1870; November, 1960.
[28] J. Kliger and E. J. Downey, "Extended-dynamic-range traveling-wave tubes," 1960 IRE INTERNATIONAL CONVENTION RECORD, pt. 3, pp. 87–94.

Research and development in hardware have produced several interesting devices. Carlile and Sensiper use ferrite-loaded coupling apertures in a re-entrant cavity chain [29]. Hollow-beam S-band tubes using periodic focusing have been investigated with electrostatic focusing appearing most advantageous [30]. A 5-mm tube with half-watt output and bandwidth of 10 Gc has also been developed [31]. The effects of transverse-beam velocities and magnetic fields have been determined by artificially introducing these into a controlled experiment [32]. Finally, three tutorial/review articles may be mentioned [33]–[35].

[29] R. N. Carlile and S. Sensiper, "A nonreciprocal-loss traveling-wave-tube circuit," IRE TRANS. ON ELECTRON DEVICES, vol. ED-7, pp. 289–296; October, 1960.
[30] C. C. Johnson, "A periodically focused backward-wave oscillator," IRE TRANS. ON ELECTRON DEVICES, vol. ED-7, pp. 274–279; October, 1960.
[31] H. L. McDowell, *et al.*, "A half-watt CW traveling-wave amplifier for the 5–6 millimeter band," PROC. IRE, vol. 48, pp. 321–328; March, 1960.
[32] L. L. Maninger, "The effects of magnetic focusing fields and transverse beam velocities on spurious oscillations in backward-wave oscillators," 1960 IRE INTERNATIONAL CONVENTION RECORD, pt. 3, pp. 67–77.
[33] E. J. Nalos, "Present state of art in high power traveling-wave tubes," *Microwave J.*, vol. 3, pp. 46–52; January, 1960.
[34] J. R. Hechtel, "Electrostatic focusing of microwave tubes," *Microwave J.*, vol. 3, pt. I, pp. 41–48, November; pt. II, pp. 81–86, December, 1960.
[35] C. L. Cuccia, "Lightweight very-wide-band integral package TWT's," *Microwave J.*, vol. 3, pp. 47–57; July, 1960.

D. Harmonic Generation and Millimeter Waves

Work has continued on unusual devices for the generation of millimeter waves. The megavolt Cerenkov device of Coleman follows the philosophy of building characteristic frequencies into the beam, rather than into the microwave structure [36]. The device has proproduced 3 w at 8 mm using the 13th harmonic. Another scheme shoots a highly-bunched beam into a high-mode cavitity (harmodotron concept) [37]. Anderson has recognized that the nonlinear volt-ampere characteristic of a Langmuir plasma probe can be utilized for harmonic generation [38]. However, with present configurations, efficiency is considerably below that of diode generators.

[36] P. D. Coleman and C. Enderby, "Megavolt electronics Cerenkov coupler for the production of millimeter and submillimeter waves," *J. Appl. Phys.*, vol. 31, pp. 1695–1696; September, 1960.
[37] E. Brannen, *et al.*, "Generation of millimeter waves by the electron beam of a microtron," *J. Appl. Phys.*, vol. 31, p. 1829; October, 1960.
[38] J. M. Anderson, "Microwave detection and harmonic generation by Langmuir-type probes in plasmas," PROC. IRE (Correspondence), vol. 48, pp. 1662–1663; September, 1960.

Most of the effort on harmonic generation has used the nonlinear properties of diodes. Hedderly uses a distributed transmission line loaded with diodes [39]. Johnson has made an analysis for the large-signal/high-harmonic case and has concluded that higher efficiencies are possible for it than for the small-signal case [40]. The theoretical conversion loss is 2.9 db$\times n$ for large n. A related analysis derives conversion efficiency for the case where some circuits are resistively terminated [41]. There are several papers on specific harmonic generators and their performance [42]–[46]. Conversion losses quoted are: 2.7 db/octave at an output of 1 Gc; 3.0 db/octave at 1 Gc; 3.9 db/octave at 1.6 Gc; and 9 db/octave at 48 Gc. From these limited data, little can be concluded except that losses increase with frequency.

[39] D. L. Hedderly, "A traveling wave harmonic generator," PROC. IRE (Correspondence), vol. 48, p. 1658; September, 1960.
[40] K. M. Johnson, "Large signal analysis of a parametric harmonic generator," IRE TRANS. ON MICROWAVE THEORY AND TECHNIQUES, vol. MTT-8, pp. 525–532; September, 1960.
[41] I. Kaufman and D. Douthett, "Harmonic generation using idling circuits," PROC. IRE (Correspondence), vol. 48, pp. 790–791; April, 1960.
[42] G. F. Montgomery, "Efficient harmonic generation," PROC. IRE (Correspondence), vol. 48, pp. 251–252; February, 1960.

[43] G. H. Heilmeier, "Millimeter wave generation by parametric methods," PROC. IRE (Correspondence), vol. 48, pp. 1326–1327; July, 1960.
[44] R. Lowell and M. J. Kiss, "Solid-state microwave power sources using harmonic generation," PROC. IRE (Correspondence), vol. 48, pp. 1334–1335; July, 1960.
[45] D. Leenov and J. W. Rood, "UHF harmonic generation with silicon diodes," PROC. IRE (Correspondence), vol. 48, p. 1335; July, 1960.
[46] G. Luettgenau, *et al.*, "High power at 1000 mc using semiconductor devices," 1960 IRE WESCON CONVENTION RECORD, pt. 3, pp. 13–26.

II. Electromagnetic Devices

A. General EM Theory

1) Energy and Reciprocity: Energy-transport processes in dispersive media are still of considerable interest: witness two important papers. Tonning identifies a "dispersion energy" and calculates energy velocity and group velocity for dispersive media [47], while Sturrock treats the negative energy of a slow wave in a moving coordinate system [48]. Two papers have appeared on reciprocity theorems for nonperiodic sources. One obtains a Lorentz integral form containing cross correlations of fields [49]; the other, using the Reaction Concept, obtains general reciprocity involving electric- and magnetic-current sources and their associated fields [50]. An interesting note shows that attenuation for common types of waveguides can be written in a quasi-separable form where separate coefficients relate dielectric loss, conductor loss, and geometry; however, the cutoff wavelength common to all prevents complete separability [51].

[47] A. Tonning, "Energy density in continuous electromagnetic media," IRE TRANS. ON ANTENNAS AND PROPAGATION, vol. AP-8, pp. 428–434; July, 1960.
[48] P. A. Sturrock, "In what sense do slow waves carry negative energy?" *J. Appl. Phys.*, vol. 31, pp. 2052–2056; November, 1960.
[49] G. Goubau, "A reciprocity theorem for nonperiodic fields," IRE TRANS. ON ANTENNAS AND PROPAGATION (Communications), vol. AP-8, pp. 339–342; May, 1960.
[50] W. J. Welch, "Reciprocity theorems for electromagnetic fields whose time dependence is arbitrary," IRE TRANS. ON ANTENNAS AND PROPAGATION, vol. AP-8, pp. 68–73; January, 1960.
[51] D. K. Gannett and Z. Szekely, "A simple general equation for attenuation," PROC. IRE (Correspondence), vol. 48, pp. 1161–1162; June, 1960.

2) Obstacles: One of the more intriguing problems has been the thermodynamic paradox associated with the single surface-wave mode in a waveguide with ferrite slab. Bresler has carefully investigated this problem and has discovered that the correct secular equation obtained as the slab is moved to the wall has a different limit than the previously obtained secular equation [52]. The correct equation admits pairs of modes representing power flow in opposite directions, thereby resolving the paradox. Another unusual problem has been solved by Forrer and Jaynes, who have shown that ghost modes are resonant modes in dielectric windows in waveguide [53]. Investigation of these has led to advances in design of high-power windows. The change in parameters produced in a gas excited by acoustic waves allows the partial reflection of incident electromagnetic energy; this has been investigated by Schmitt and Sengupta [54]. Gradual-transition absorbers constitute another partial-reflection problem. Walther solved the resulting Riccati equation by the WKB method for thick layers [55]. Other general studies have included the application of Babinet's principle to transmission lines [56]. Oliner has studied, theoretically and experimentally, symmetrical discontinuities in transmission lines [57], [58]. Spruch and Bartram, in another important paper, have applied a quantum-scattering technique to three-dimensional waveguide scattering problems wherein the usual Schwinger form gives only an upper bound [59]. This new method obtains upper and lower bounds on the principal wave phase shift. Other papers include a conformal evaluation of strip-line parameters [60] and thickness corrections for strip-line structures obtained from an exact solution using semi-infinite plates [61].

[52] A. D. Bresler, "On the TE_{n0} modes of a ferrite slab loaded rectangular waveguide and the associated thermodynamic paradox, IRE TRANS. ON MICROWAVE THEORY AND TECHNIQUES, vol. MTT-8, pp. 81–95; January, 1960.
[53] M. P. Forrer and E. T. Jaynes, "Resonant modes in waveguide windows," IRE TRANS. ON MICROWAVE THEORY AND TECHNIQUES, vol. MTT-8, pp. 147–150; March, 1960.
[54] H. J. Schmitt and D. L. Sengupta, "On the reflection of electromagnetic waves from a medium excited by acoustic waves," *J. Appl. Phys.*, vol. 31, pp. 439–440; February, 1960.
[55] K. Walther, "Reflection factor of gradual-transition absorbers for electromagnetic and acoustic waves," IRE TRANS. ON ANTENNAS AND PROPAGATION, vol. AP-8, pp. 608–621; November, 1960.
[56] G. H. Owyang and R. King, "Complementarity in the study of transmission lines." IRE TRANS. ON MICROWAVE THEORY AND TECHNIQUES, vol. MTT-8, pp. 172–181; March, 1960.
[57] A. A. Oliner, "Equivalent circuits for small symmetrical longitudinal apertures and obstacles," IRE TRANS. ON MICROWAVE THEORY AND TECHNIQUES, vol. MTT-8, pp. 72–80; January, 1960.
[58] H. M. Altschuler and A. A. Oliner, "Discontinuities in the center conductor of symmetric strip transmission line." IRE TRANS. ON MICROWAVE THEORY AND TECHNIQUES, vol. MTT-8, pp. 328–339; May, 1960.
[59] L. Spruch and R. Bartram, "Bounds on the elements of the equivalent network for scattering in waveguides," *J. Appl. Phys.*, vol. 31, "Part I: Theory," pp. 905–913; "Part II: Application to dielectric obstacles," pp. 913–917; May, 1960.
[60] T.-S. Chen, "Determination of the capacitance, inductance, and characteristic impedance of rectangular lines," IRE TRANS. ON MICROWAVE THEORY AND TECHNIQUES, vol. MTT-8, pp. 510–519; September, 1960.
[61] S. B. Cohn, "Thickness corrections for capacitive obstacles and strip conductors," IRE TRANS. ON MICROWAVE THEORY AND TECHNIQUES, vol. MTT-8, pp. 638–644; November, 1960.

B. Waveguides and Filters

1) Waveguides: Strip transmission lines and associated devices have been in use now for several years; Cohn has contributed a critical reappraisal of their merits, drawbacks, and estimated future [62]. This article also contains an excellent bibliography. Tai has demonstrated that evanescent modes in a waveguide partially filled with ferrite are members of an orthogonal set although they do not carry power [63]. Corrugated waveguides have been analyzed by replacing the periodic structure with an anisotropic quasi-homogeneous medium [64]. However, this appears to be equivalent to the transverse-resonance method and does not include the effect of all evanescent modes. Other investigations include the elliptic waveguide [65],

round waveguide with a double lining [66], [67] (for spurious mode suppression), and a superconductive coaxial line [68]. An interesting feature of the latter is that care must be exercised to avoid reflections, as the absence of loss eliminates sometimes-beneficial attenuation.

[62] S. B. Cohn, "A reappraisal of strip transmission line," *Microwave J.*, vol. 3, pp. 17–27; March, 1960.
[63] C. T. Tai, "Evanescent modes in a partially filled gyromagnetic rectangular wave guide," *J. Appl. Phys.*, vol. 31, pp. 220–221; January, 1960.
[64] G. Piefke, "A contribution to the theory of corrugated guides," *J. Res. NBS*, vol. 64D, pp. 533–555; September–October, 1960.
[65] G. R. Valenzuela, "Impedances of an elliptic waveguide (for the $_eH_1$ mode)," IRE TRANS ON MICROWAVE THEORY AND TECHNIQUES, vol. MTT-8, pp. 431–435; July, 1960.
[66] H.-G. Unger, "Round waveguide with double lining," *Bell Sys. Tech. J.*, vol. 39, pp. 161–167; January, 1960.
[67] A. P. King, "The observed 50–90 kmc attenuation of two inch improved waveguide," 1960 IRE WESCON CONVENTION RECORD, pt. 1, pp. 28–33.
[68] N. S. Nahman and G. M. Gooch, "Nanosecond response and attenuation characteristics of a superconductive coaxial line," PROC. IRE, vol. 48, pp. 1852–1856; November, 1960.

In the open waveguide area, further investigations have been made of trough waveguides by Cohn, *et al.* [69], [70]. Also, propagation constant curves have been given for a grounded dielectric slab with an air gap between the slab and ground plane [71].

[69] M. Cohn, *et al.*, "TE mode excitation on dielectric loaded parallel plane and trough waveguides," IRE TRANS. ON MICROWAVE THEORY AND TECHNIQUES, vol. MTT-8, pp. 545–552; September, 1960.
[70] M. Cohn, "TE modes of the dielectric loaded trough line," IRE TRANS. ON MICROWAVE THEORY AND TECHNIQUES, vol. MTT-8, pp. 449–454; July, 1960.
[71] J. H. Richmond, "Surface waves on symmetrical three-layer sandwiches," IRE TRANS. ON MICROWAVE THEORY AND TECHNIQUES (Correspondence), vol. MTT-8, p. 572; September, 1960.

2) Periodic Structures: An excellent review article on guiding structures has been written by Harvey [72]. The article develops the theory of dispersive structures, pass and stop bands, forward and backward waves, etc. Extensive descriptions and analyses are given of the many slow-wave structures including dielectric structures with and without metal, corrugated surfaces, ladders, coupled cavities, and helices; the bibliography contains nearly 300 references. Allen and Kino have obtained field distributions and dispersive characteristics of strongly-coupled cavities [73]. Variational principles have been developed for ω and β for periodic structures using closed-cavity modes as trial functions [74], [75]. Additional papers are a general analysis of periodic circuits [76] and an experimental description of a block-loaded guide [77].

[72] A. F. Harvey, "Periodic and guiding structures at microwave frequencies," IRE TRANS. ON MICROWAVE THEORY AND TECHNIQUES, vol. MTT-8, pp. 30–61; January, 1960.
[73] M. A. Allen and G. S. Kino, "On the theory of strongly coupled cavity chains," IRE TRANS. ON MICROWAVE THEORY AND TECHNIQUES, vol. MTT-8, pp. 362–372; May, 1960.
[74] T. J. Goblick, Jr., and R. M. Bevensee, "Variational principles and mode coupling in periodic structures," IRE TRANS. ON MICROWAVE THEORY AND TECHNIQUES, vol. MTT-8, p. 500–509; September, 1960.
[75] R. M. Bevensee, "Misconceptions about equivalent circuits for periodic microwave structures," 1960 IRE WESCON CONVENTION RECORD, pt. 1, pp. 3–10.
[76] R. N. Carlile, "General properties of the propagation constant of a nonreciprocal iterated circuit," PROC. IRE (Correspondence), vol. 48, pp. 1162–1163; June, 1960.
[77] W. B. Mims, "The block loaded guide as a slow wave structure," PROC. IRE (Correspondence), vol. 48, pp. 1176–1177; June, 1960.

3) Nonuniform and Coupled Guides: An interesting validation of coupled transmission-line theory has been provided by Bahiana and Smullin [78]. They analyzed a waveguide filled with two dielectrics by coupling the modes individually existing in each dielectric. The phase constant using this approach was found to compare favorably with that using exact theory. Cohn has derived even- and odd-characteristic impedances for closely-coupled strip lines of the type useful in coupled filters, 3-db couplers, etc. [79]; the Schwartz-Christoffel transformation was used. Other work includes a study of multi-element transmission lines by superposition of virtual two-element pairs [80], and a derivation of the higher-mode indicial equation in coaxial helices [81]. General analyses of transmission lines include a variational integral for propagation constant of a lossy line assuming only axial current [82], and an analysis of the pulse response of several hybrids in nondispersive line [83]. Finally, Sugai has attempted to fit specialized solutions of Riccati equations to the nonuniform transmission-line problem [84].

[78] L. C. Bahiana and L. D. Smullin, "Coupling of modes in uniform, composite waveguides," IRE TRANS. ON MICROWAVE THEORY AND TECHNIQUES, vol. MTT-8, pp. 454–458; July, 1960.
[79] S. B. Cohn, "Characteristic impedances of broadside-coupled strip transmission lines," IRE TRANS. ON MICROWAVE THEORY AND TECHNIQUES, vol. MTT-8, pp. 633–637; November, 1960.
[80] H. Kogo, "A study of multi-element transmission lines," IRE TRANS. ON MICROWAVE THEORY AND TECHNIQUES, vol. MTT-8, pp. 136–142; March, 1960.
[81] R. E. Hayes, "Higher order modes in coupled helices," IRE TRANS. ON MICROWAVE THEORY AND TECHNIQUES (Correspondence), vol. MTT-8, pp. 119–120; January, 1960.
[82] R. E. Collin, "A variational integral for propagation constant of lossy transmission lines," IRE TRANS. ON MICROWAVE THEORY AND TECHNIQUES, vol. MTT-8, pp. 339–342; May, 1960.
[83] W. J. Getsinger, "Analysis of certain transmission-line networks in the time domain," IRE TRANS. ON MICROWAVE THEORY AND TECHNIQUES, vol. MTT-8, pp. 301–309; May, 1960.
[84] I. Sugai, "The solutions for nonuniform transmission line problems," PROC. IRE (Correspondence), vol. 48, pp. 1489–1490; August, 1960.

C. Isotropic Devices

As might be expected in a rapidly growing hardware field, there have been many advances in components. These are grouped into six categories: switches and duplexers, mixers and modulators, filters, phase shifters, transformers and baluns, and junctions. However, several developments do not readily fit in these categories. Sooy, *et al.*, developed a microwave Meacham bridge oscillator where, in a fashion analogous to that at audio frequencies, the resonant feedback element is incorporated into a bridge circuit, thereby multiplying Q and providing exceptional stability [85]. Gradual mode transducers have been designed by determining the appropriate eigenfunction from the input and output

modes [86]. Design equations and curves for broad-band chokes have also appeared [87].

[85] W. R. Sooy, *et al.*, "A microwave Meacham bridge oscillator," PROC. IRE, vol. 48, pp. 1297–1306; July, 1960.
[86] L. Solymar and C. C. Eaglesfield, "Design of mode transducers," IRE TRANS. ON MICROWAVE THEORY AND TECHNIQUES, vol. MTT-8, pp. 61–65; January, 1960.
[87] H. E. King, "Broad-band coaxial choked coupling design," IRE TRANS. ON MICROWAVE THEORY AND TECHNIQUES, vol. MTT-8, pp. 132–135; March, 1960.

1) Switches and Duplexers: Harvey has prepared an excellent survey article covering all aspects of microwave duplexers, both ferrite and gaseous; a large bibliography is included [88]. Hill and Ichiki have developed hot-cathode gas switches [89], [90]. Two schemes have appeared for increasing average-power capabilities of gas duplexers by reducing gas volume and using silica tubes [91], [92].

[88] A. F. Harvey, "Duplexing systems at microwave frequencies," IRE TRANS. ON MICROWAVE THEORY AND TECHNIQUES, vol. MTT-8, pp. 415–431; July, 1960.
[89] R. M. Hill and S. K. Ichiki, "Microwave switching with low-pressure arc discharge," IRE TRANS. ON MICROWAVE THEORY AND TECHNIQUES, vol. MTT-8, pp. 628–633; November, 1960.
[90] S. J. Tetenbaum, *et al.*, "Arc discharge, microwave switch tube," 1960 IRE WESCON CONVENTION RECORD, pt. 3, pp. 96–102.
[91] D. W. Downton and P. D. Lomer, "A pre-TR tube for high mean power duplexing," IRE TRANS. ON MICROWAVE THEORY AND TECHNIQUES, vol. MTT-8, pp. 654–659; November, 1960.
[92] R. S. Braden, "A new concept in microwave gas switching elements," IRE TRANS. ON ELECTRON DEVICES, vol. ED-7, pp. 54–59; January, 1960.

Garver, *et al.*, have shown experimentally that germanium diodes follow the majority-carrier theory of Lawson whereas silicon diodes follow Shockley's minority-carrier theory [93]. This accounts for the switching action which is noted in germanium diodes, but is not observed in those of the silicon type. Finally, another ring waveguide switch has appeared [94].

[93] R. V. Garver, *et al.*, "Theory of the germanium diode microwave switch," IRE TRANS. ON MICROWAVE THEORY AND TECHNIQUES, vol. MTT-8, pp. 108–111; January, 1960.
[94] R. C. Johnson, *et al.*, "A waveguide switch employing the offset ring-switch junction," IRE TRANS. ON MICROWAVE THEORY AND TECHNIQUES, vol. MTT-8, pp. 532–537; September, 1960.

2) Mixers and Modulators: Advances in crystal mixers have largely been concerned with operational problems. Garver and Rosado have analyzed the equivalent circuit for a microwave diode and conclude that a three-arm circuit is needed [95]. Two papers concern the optimum operating conditions. Mohr and Okwit give curves showing the proper RF drive [96]; Staniforth and Craven indicate that a 100-μa bias and low-video load resistance give an optimum dynamic square-law range for 1N23B mixers [97]. Other papers cover a broad-band mount (with dimensions) [98], and temporary deterioration of silicon diodes due to high-power ionization at the barrier [99].

[95] R. V. Garver and J. A. Rosado, "Microwave diode cartridge impedance," IRE TRANS. ON MICROWAVE THEORY AND TECHNIQUES, vol. MTT-8, pp. 104–107; January, 1960.
[96] R. J. Mohr and S. Okwit, "A note on the optimum source conductance of crystal mixers," IRE TRANS. ON MICROWAVE THEORY AND TECHNIQUES, vol. MTT-8, pp. 622–627; November, 1960.
[97] A. Staniforth and J. H. Craven, "Improvement in the square law operation of 1N23B crystals from 2 to 11 kmc," IRE TRANS. ON MICROWAVE THEORY AND TECHNIQUES, vol. MTT-8, pp. 111–115; January, 1960.
[98] A. Staniforth, "A broad-band crystal mount 10.5 kmc to 20 kmc," IRE TRANS. ON MICROWAVE THEORY AND TECHNIQUES (Correspondence), vol. MTT-8, pp. 464–465; July, 1960.
[99] P. P. Lombardini and R. J. Doviak, "Temporary and permanent deterioration of microwave silicon crystal diodes," PROC. IRE (Correspondence), vol. 48, pp. 119–120; January, 1960.

Microwave modulators (for modulation or attenuation) have been developed. These use semiconductor wafers across the waveguide [100], [101].

[100] F. C. De Ronde, *et al.*, "The *p-i-n* modulator, an electrically controlled attenuator for mm and sub-mm waves," IRE TRANS. ON MICROWAVE THEORY AND TECHNIQUES, vol. MTT-8, pp. 325–327; May, 1960.
[101] H. Jacobs, *et al.*, "A new semiconductor microwave modulator," IRE TRANS. ON MICROWAVE THEORY AND TECHNIQUES, vol. MTT-8, pp. 553–559; September, 1960.

3) Filters: Matthaei has contributed an important paper on the theory and design of microwave filters using the insertion-loss principle [102]. This allows the designer to use either equal-ripple or maximally-flat insertion loss. Cohn has treated these two cases where isolation rather than bandwidth narrowing is desired [103]. He shows that for this case the equal-ripple design is superior to the maximally flat. Others have used an analog computer for cascading klystron cavities [104].

[102] G. L. Matthaei, "Design of wide-band (and narrow-band) band-pass microwave filters on the insertion loss basis," IRE TRANS. ON MICROWAVE THEORY AND TECHNIQUES, vol. MTT-8, pp. 580–593; November, 1960.
[103] S. B. Cohn, "Phase shift and time-delay response of microwave narrow-band filters," *Microwave J.*, vol. 3, pp. 47–51; October, 1960.
[104] A. Norris and D. M. Byck, "Analog simulation: a network method for solving microwave problems," *Microwave J.*, vol. 3, pp. 43–48; June, 1960.

In the cavity area, Kotzebue discusses broad-band circuits in coax and waveguide for a tuned filter using a YIG sphere [105]. A detailed design of temperature-compensated cavities is given by Cogdell, *et al.* [106]. Other papers include an analysis of a transmission cavity wavemeter which is treated as a lossy transmission line [107], peak fields in cavity filters [108], and the effects of refractive index variations in limiting refractometer resolution [109]. An interesting development uses two quarter-wave lines coupled together to provide a linear tuning-range resonator [110]. As one quarter-wave line is lengthened the other is shortened, so that the nonlinearities cancel.

[105] K. L. Kotzebue, "Broadband electronically-tuned microwave filters," 1960 IRE WESCON CONVENTION RECORD, pt. 1, pp. 21–27.
[106] J. R. Cogdell, *et al.*, "Temperature compensation of coaxial cavities," IRE TRANS. ON MICROWAVE THEORY AND TECHNIQUES, vol. MTT-8, pp. 151–155; March, 1960.
[107] L. Young, "Analysis of a transmission cavity wavemeter," IRE TRANS. ON MICROWAVE THEORY AND TECHNIQUES, vol. MTT-8, pp. 436–439; July, 1960.
[108] ——, "Peak internal fields in direct-coupled-cavity filters," IRE TRANS. ON MICROWAVE THEORY AND TECHNIQUES, vol. MTT-8, pp. 612–616; November, 1960.
[109] W. J. Hartman, "Limit of spatial resolution of refractometer cavities," *J. Res. NBS*, vol. 64D, pp. 65–72; January–February, 1960.
[110] B. H. Wadia and R. L. Sarda, "UHF resonator with linear tuning," IRE TRANS. ON MICROWAVE THEORY AND TECHNIQUES, vol. MTT-8, pp. 66–72; January, 1960.

4) Phase Shifters: A novel phase shifter, developed by Augustine and Cheal, consists of a helix wound of coaxial line with the portion of the outer conductor that faces inward in the helix removed [111]. Insertion of a dielectric slug produces the variable phase shift. Another scheme in this paper is a coaxial 3-db coupler with ganged shorts. This is similar to the waveguide short-slot coupler with ganged shorts that has become so popular. A related scheme terminates the coupler with diodes, thereby allowing the phase shift to be electronically controlled [112]. Wide-band phase shifters have been produced by using three half-wave anisotropic plates at appropriate angles [113], and by an iterative calculation to obtain a dispersionless dielectric quarter-wave plate [114]. Another scheme uses a feedback scheme similar to the single-sideband phase cancellation technique [115].

[111] C. F. Augustine and J. Cheal, "The design and measurement of two broad-band coaxial phase shifters," IRE Trans. on Microwave Theory and Techniques, vol. MTT-8, pp. 398–402; July, 1960.
[112] R. H. Hardin, *et al.*, "Electronically-variable phase shifters utilizing variable capacitance diodes," Proc. IRE (Correspondence), vol. 48, pp. 944–945; May, 1960.
[113] S. Adachi and E. M. Kennaugh, "The analysis of a broad-band circular polarizer including interface reflections," IRE Trans. on Microwave Theory and Techniques, vol. MTT-8, pp. 520–525; September, 1960.
[114] R. D. Tompkins, "A dispersionless dielectric quarter-wave plate in circular waveguide," Proc. IRE (Correspondence), vol. 48, pp. 1171–1172; June, 1960.
[115] A. A. Ahmed, "A wide band phase shifter," Proc. IRE (Correspondence), vol. 48, p. 945; May, 1960.

5) Transformers and Baluns: Young has derived an improved quarter-wave transformer by making the matching section less dispersive [116], [117], and has shown the relation between the quarter-wave transformer and a directly-coupled cavity [118]. Riblet considers the binomial transformer of equal quarter-wavelength steps, and derives a sort of "physical limitations" theorem stating that only minor improvement can be made without increasing the transformer length [119]. This is for monotonic, maximally-flat transformers. Another work gives the design for equal-ripple transformers in coax and in double-ridged waveguide [120].

[116] L. Young, "Optimum quarter-wave transformers," IRE Trans. on Microwave Theory and Techniques, vol. MTT-8, pp. 478–482; September, 1960.
[117] ——, "Inhomogeneous quarter-wave transformers of two sections," IRE Trans. on Microwave Theory and Techniques, vol. MTT-8, pp. 645–649; November, 1960.
[118] ——, "The quarter-wave transformer prototype circuit," IRE Trans. on Microwave Theory and Techniques, vol. MTT-8, pp. 483–489; September, 1960.
[119] H. J. Riblet, "A general theorem on an optimum stepped impedance transformer," IRE Trans. on Microwave Theory and Techniques, vol. MTT-8, pp. 169–170; March, 1960.
[120] D. J. Sullivan and D. A. Parkes, "Stepped transformers for partially filled transmission lines," IRE Trans. on Microwave Theory and Techniques, vol. MTT-8, pp. 212–217; March, 1960.

Duncan and Minerva have developed a wide-band balun where a smooth transition is made from the outer-coax conductor to one twin-line conductor [121]. This device can have impedance bandwidths of 100:1. Other work includes an impedance analysis of the split coaxial or British dipole balun [122], and two strip-line baluns which can be used with printed antennas, *e.g.*, spiral antennas [123], [124]. It has been remarked that a balun is just a hybrid with special terminations and, in fact, one of these printed baluns is just a strip-line rat race.

[121] J. W. Duncan and V. P. Minerva. "100:1 bandwidth balun transformer," Proc. IRE, vol. 48, pp. 156–164; February, 1960.
[122] H. Kogo, "Analysis of split coaxial line type balun," IRE Trans. on Microwave Theory and Techniques (Correspondence), vol. MTT-8, pp. 245–246; March, 1960.
[123] R. Bawer and J. J. Wolfe, "A printed circuit balun for use with spiral antennas," IRE Trans. on Microwave Theory and Techniques, vol. MTT-8, pp. 319–325; May, 1960.
[124] J. H. Craven, "A novel broad-band balun," IRE Trans. on Microwave Theory and Techniques (Correspondence), vol. MTT-8, pp. 672–673; November, 1960.

6) Junctions: Several interesting hybrid junction developments have appeared. Jones has developed a wide-band distributed circuit hybrid in strip-line using two coupled strip-line filters [125]; a coaxial version of this has also been in use [126]. Multiple hybrid power dividers are of interest for such applications as antenna array feeding; a multi-terminal hybrid which is a modified rat race has appeared [127]. A novel directional coupler for TE_{01} circular-electric mode in round waveguide has been developed [128]. This uses two coaxial waveguides with two bifurcations; the coupling exists in the space between the two bifurcations.

[125] E. M. T. Jones, "Wide-band strip-line magic-T," IRE Trans. on Microwave Theory and Techniques, vol. MTT-8, pp. 160–168; March, 1960.
[126] S. J. Robinson, "Broad-band hybrid junctions," IRE Trans. on Microwave Theory and Techniques (Correspondence), vol. MTT-8, pp. 671–672; November, 1960.
[127] E. J. Wilkinson, "An N-way hybrid power divider," IRE Trans. on Microwave Theory and Techniques, vol. MTT-8, pp. 116–118; January, 1960.
[128] B. Oguchi, "Circular electric mode directional coupler," IRE Trans. on Microwave Theory and Techniques, vol. MTT-8, pp. 660–666; November, 1960.

D. Plasmas

Several books could and have been written just listing references in the plasma field. From this vast science, of particular interest to the microwave area are the microwave properties of the atmosphere, and microwave diagnostic techniques.

In the first category, Bachynski, *et al.* [129], have given propagation parameters for high-temperature air for the frequency range 1 to 100 Gc with temperatures up to 12×10^3 °K. Phelps has analyzed the errors inherent in the use of an energy independent collision frequency [130]. The conductivity tensor is derived using a linear dependence of electron collision frequency on electron energy, with the result that errors are comparable to the experimental errors in ionospheric observations. Kelly and Margenau postulate by kinetic theory that the major electron loss for a moving antenna is caused by sweeping [131]. This paper gives voltage breakdown plots. Another paper investigates electron-ion recombination in water vapor [132].

[129] M. P. Bachynski, *et al.*, "Electromagnetic properties of high-temperature air," Proc. IRE, vol. 48, pp. 347–356; March, 1960.

[130] A. V. Phelps, "Propagation constants for electromagnetic waves in weakly ionized, dry air," *J. Appl. Phys.*, vol. 31, pp. 1723–1729; October, 1960.
[131] D. Kelly and H. Margenau, "High-frequency breakdown of air," *J. Appl. Phys.*, vol. 31, pp. 1617–1620; September, 1960.
[132] S. Takeda and A. A. Dougal, "Microwave study of afterglow discharge in water vapor," *J. Appl. Phys.*, vol. 31, pp. 412–416; February, 1960.

Microwave absorption for the case where collisions can be neglected has been investigated by Cullen [133]. The absorption is obtained in closed form for the extraordinary wave from electron dynamics. Other work concerns particle densities behind hypersonic shock waves [134], and on a precise definition of average electron collision frequency [135].

[133] A. L. Cullen, "Propagation of microwaves through a magnetoplasma, and a possible method for determining the electron velocity distributions," *J. Res. NBS*, vol. 64D, pp. 509–513; September–October, 1960.
[134] C. A. Roberts, *et al.*, "Theory of equilibrium electron and particle densities behind normal and oblique hypersonic shock waves in air," IRE TRANS. ON ANTENNAS AND PROPAGATION (Communications), vol. AP-8, pp. 102–103; January, 1960.
[135] J. M. Anderson, "A note on the relation between the "exact" and "simplified" theories for EM wave propagation in ionized gases," IRE TRANS. ON ANTENNAS AND PROPAGATION (Communications), vol. AP-8, pp. 337–338; May, 1960.

Diagnostic papers include plane wave reflection and scattering by a plasma sheet [136], a microwave interferometer technique [137], and a heuristic derivation of an absorption spectrum [138].

[136] R. G. Buser and P. Wolfert, "Microwave interaction with plasmas," 1960 IRE INTERNATIONAL CONVENTION RECORD, pt. 3, pp. 146–154.
[137] C. B. Wharton and D. M. Slager, "Microwave determination of plasma density profiles," *J. Appl. Phys.*, vol. 31, pp. 428–430; February, 1960.
[138] W. D. Hershberger, "Absorption and reflection spectrum of a plasma," *J. Appl. Phys.*, vol. 31, pp. 417–422; February, 1960.

III. Solid-State Devices

A. Parametric Amplifiers

1) General: An interesting history of parametric transducers is given by Mumford [139] which includes a 200-item bibliography dating from Faraday's work in 1831 to Chang's in 1959. A very complete bibliography is provided by Mount and Begg [140] which covers both parametric devices and masers.

[139] W. W. Mumford, "Some notes on the history of parametric transducers," PROC. IRE, vol. 48, pp. 848–853; May, 1960.
[140] E. Mount and B. Begg, "Parametric devices and masers: an annotated bibliography," IRE TRANS. ON MICROWAVE THEORY AND TECHNIQUES, vol. MTT-8, pp. 222–243; March, 1960.

Numerous general theoretical papers have been published including generalizations of the Manley-Rowe relations [141], [142], an important correction to the Heffner-Wade paper [143], and new formulations of the bandwidth and noise theory [144]–[149]. An important theoretical discussion of a parametric amplifier having a resonance at idler but not at the signal frequency is given by Fisher [150].

[141] C. Yeh, "Generalized energy relations of nonlinear reactive elements," PROC. IRE (Correspondence), vol. 48, p. 253; February, 1960.
[142] H. Iwasawa, "The extended theory of the Manley-Rowe's energy relations in nonlinear elements and nonlinear lossless medium," IRE TRANS. ON MICROWAVE THEORY AND TECHNIQUES (Correspondence), vol. MTT-8, pp. 459–460; July, 1960.
[143] H. Heffner and G. Wade, "Noise figure and gain of parametric converters," *J. Appl. Phys.*, vol. 31, p. 2316; December, 1960.
[144] S. T. Fisher, "Bandwidth of lower sideband parametric up-converter and parametric amplifiers," PROC. IRE (Correspondence), vol. 48, p. 946; May, 1960.
[145] S. Deutsch, "Symmetrical matrix analysis of parametric amplifiers and converters," PROC. IRE, vol. 48, pp. 1595–1602; September, 1960.
[146] D. K. Adams, "An analysis of four-frequency nonlinear reactance circuits," IRE TRANS. ON MICROWAVE THEORY AND TECHNIQUES, vol. MTT-8, pp. 274–283; May, 1960.
[147] G. Herrmann, "Idler noise in parametric amplifiers," PROC. IRE (Correspondence), vol. 48, pp. 2021–2022; December, 1960.
[148] J. C. Greene and E. W. Sard, "Optimum noise and gain-bandwidth performance for a practical one-port parametric amplifier," PROC. IRE, vol. 48, pp. 1583–1590; September, 1960.
[149] K. L. Kotzebue, "Optimum noise performance of parametric amplifiers," PROC. IRE (Correspondence), vol. 48, pp. 1324–1325; July, 1960.
[150] S. T. Fisher, "Theory of single-resonance parametric amplifiers," PROC. IRE, vol. 48, pp. 1227–1232; July, 1960.

2) Diode Type: A number of papers discuss theoretical and experimental results on various diode parametric amplifiers [151]–[153]. The highest-frequency amplifier reported is a 30-Gc degenerate amplifier by DeLoach [154]. Results of an X-band amplifier using the unique silver-bonded diode were reported by Kita and Obata [155]. Bossard, *et al.* [156] discuss a super-regenerative amplifier. The use of diodes as subharmonic oscillators [157] is well known but Kibler [158] reports on diode oscillations at frequencies higher than the pump. At low microwave frequencies the parametric up-converter is of importance and is discussed in several papers [159]–[161].

[151] M. Uenohara, "Noise consideration of the variable capacitance parametric amplifier," PROC. IRE, vol. 48, pp. 169–179; February, 1960.
[152] R. C. Knechtli and R. D. Weglein, "Low-noise parametric amplifier," PROC. IRE, vol. 48, pp. 1218–1226; July, 1960.
[153] I. Goldstein and J. Zorzy, "Some results on diode parametric amplifiers," PROC. IRE (Correspondence), vol. 48, p. 1783; October, 1960.
[154] B. C. DeLoach, "17.35 and 30-kmc parametric amplifiers," PROC. IRE (Correspondence), vol. 48, p. 1323; July, 1960.
[155] S. Kita and F. Obata, "An X-band parametric amplifier using a silver-bonded diode," PROC. IRE (Correspondence), vol. 48, pp. 1651–1652; September, 1960.
[156] B. B. Bossard, *et al.*, "X-band super-regenerative parametric amplifier," PROC. IRE (Correspondence), vol. 48, pp. 1329–1330; July, 1960.
[157] A. H. Solomon and F. Sterzer, "A parametric subharmonic oscillator pumped at 34.3 kmc," PROC. IRE (Correspondence), vol. 48, pp. 1322–1323; July, 1960.
[158] L. U. Kibler, "Parametric oscillations with point contact diodes at frequencies higher than pumping frequency," PROC. IRE (Correspondence), vol. 48, pp. 239–240; February, 1960.
[159] R. Pettai, *et al.*, "Single-diode parametric up-converter with large gain-bandwidth product," PROC. IRE (Correspondence), vol. 48, pp. 1323–1324; July, 1960.
[160] A. K. Kamal and A. J. Holub, "Gain inconsistencies in low-frequency reactance parametric up-converters," PROC. IRE (Correspondence), vol. 48, pp. 1784–1785; October, 1960.
[161] A. K. Kamal and M. Subramanian, "Gain optimization in low-frequency parametric up-converters by multidiode operation," PROC. IRE (Correspondence), vol. 48, pp. 2020–2021; December, 1960.

Several papers [162]–[164] discuss the appropriate definition of a figure of merit for a varactor diode while one paper [165] expands the capacitance coefficients in

terms of the hypergeometric function. Attention is also given to the anomalous reverse current in diodes and its effect on amplifier performance [166], [167]. Measurement techniques of diode Q are described in two papers [168], [169] while contradictory results on the frequency dependence of the equivalent series resistance are also discussed [170].

[162] R. C. Knechtli and R. D. Weglein, "Diode capacitors for parametric amplification," *J. Appl. Phys.*, vol. 31, pp. 1134–1135; June, 1960.
[163] K. E. Mortenson, "Parametric diode figure of merit and optimization," *J. Appl. Phys.*, vol. 31, pp. 1207–1212; July, 1960.
[164] C. R. Boyd, "Noise figure measurements relating the static and dynamic cutoff frequencies of parametric diodes," PROC. IRE (Correspondence), vol. 48, pp. 2019–2020; December, 1960.
[165] S. Sensiper and R. D. Weglein, "Capacitance and charge coefficients for parametric diode devices," PROC. IRE (Correspondence), vol. 48, pp. 1482–1483; August, 1960.
[166] R. D. Weglein, "Some limitations on parametric amplifier noise performance," IRE TRANS. ON MICROWAVE THEORY AND TECHNIQUES, vol. MTT-8, pp. 538–544; September, 1960.
[167] K. Siegel, "Anomalous reverse current in varactor diodes," PROC. IRE (Correspondence), vol. 48, pp. 1159–1160; June, 1960.
[168] N. Houlding, "Measurement of varactor quality," *Microwave J.*, vol. 3, pp. 40–45; January, 1960.
[169] R. I. Harrison, "Parametric diode Q measurements," *Microwave J.*, vol. 3, pp. 43–46; May, 1960.
[170] S. T. Eng and R. Solomon, "Frequency dependence of the equivalent series resistance for a germanium parametric amplifier diode," PROC. IRE (Correspondence), vol. 48, pp. 358–359; March, 1960.

Two unusual uses of parametric amplifiers as a limiter [171] and as a nonreciprocal element [172] are to be noted as well as the use of space-charge capacitors for parametric amplifiers [173]. A new development which may prove to be of importance is the "parametric mode" of operation of transistors [174] which significantly increases the amplification and oscillation frequency of transistors.

[171] A. D. Sutherland and D. E. Countiss, "Parametric phase distortionless L-band limiter," PROC. IRE (Correspondence), vol. 48, pp. 938–939; May, 1960.
[172] A. K. Kamal, "A parametric device as a nonreciprocal element," PROC. IRE, vol. 48, pp. 1424–1430; August, 1960.
[173] J. R. Macdonald, "Space-charge capacitors for parametric amplifiers," PROC. IRE (Correspondence), vol. 48, pp. 1483–1485; August, 1960.
[174] R. Zuleeg and V. W. Vodicka, "Parametric amplification properties in transistors," PROC. IRE (Correspondence), vol. 48, pp. 1785–1786; October, 1960.

3) Traveling-Wave Parametric Amplifiers: A number of theoretical papers [175]–[180] appeared giving a rigorous analysis of the traveling-wave parametric amplifier taking into account the nonlinear, parasitic, or lossy elements as well as the more usual simple time varying characteristics previously analyzed. A method for keeping the pump, signal, and idler in synchronism over a broadband is also discussed [181] in a theoretical paper. A detailed theoretical and experimental treatment of a coupled-cavity amplifier is given in two companion papers [182], [183]. Several other papers [184]–[186] present a theoretical and experimental discussion of various traveling-wave amplifiers in the UHF and S-band regions. One paper [187] describes an unusual amplifier structure using a helix.

[175] R. Landauer, "Parametric amplification along nonlinear transmission lines," *J. Appl. Phys.*, vol. 31, pp. 479–484; March, 1960.
[176] ——, "Parametric standing wave amplifiers," PROC. IRE (Correspondence), vol. 48, pp. 1328–1329; July, 1960.
[177] D. Fleri and J. Sie, "The effect of parasitic diode elements on traveling-wave parametric amplification," PROC. IRE (Correspondence), vol. 48, pp. 1330–1331; July, 1960.
[178] W. Jasinski, "Gain of a traveling-wave parametric amplifier using nonlinear lossy capacitors," PROC. IRE (Correspondence), vol. 48, pp. 2018–2019; December, 1960.
[179] K. Kurokawa and J. Hamasaki, "An extension of the mode theory to periodically distributed parametric amplifiers with losses," IRE TRANS. ON MICROWAVE THEORY AND TECHNIQUES, vol. MTT-8, pp. 10–18; January, 1960.
[180] K. K. N. Chang. "Theory of a negative-resistance transmission line amplifier with distributed noise generators," *J. Appl. Phys.*, vol. 31, pp. 871–875; May, 1960.
[181] H. Boyet and D. Fleri, "A method for broad-banding synchronism in traveling-wave parametric devices," PROC. IRE (Correspondence), vol. 48, pp. 1331–1333; July, 1960.
[182] M. R. Currie and R. W. Gould, "Coupled-cavity traveling-wave parametric amplifiers: part I—analysis," PROC. IRE, vol. 48, pp. 1960–1973; December, 1960.
[183] K. P. Grabowski and R. D. Weglein, "Coupled-cavity traveling-wave parametric amplifiers: part II—experiments," PROC. IRE, vol. 48, pp. 1973–1987, December, 1960.
[184] R. C. Honey and E. M. T. Jones, "A wide-band UHF traveling-wave variable reactance amplifier," IRE TRANS. ON MICROWAVE THEORY AND TECHNIQUES, vol. MTT-8, pp. 351–361; May, 1960.
[185] Clinton G. Shafer, "Design and operation of an S-band traveling-wave diode parametric amplifier," 1960 IRE WESCON CONVENTION RECORD, pt. 1, pp. 49–54.
[186] C. V. Bell and G. Wade, "The noise figure of iterative traveling-wave parametric amplifiers," 1960 IRE WESCON CONVENTION RECORD, pt. 1, pp. 55–60.
[187] G. Conrad, *et al.* "The diode-loaded helix as a microwave amplifier," PROC. IRE (Correspondence), vol. 48, pp. 939–940; May, 1960.

4) Electron-Beam Parametric Amplifiers: There has been apparently little experimental activity in electron-beam parametric amplifiers except for the Adler quadrupole type. Bridges and Ashkin [188] give experimental results on an Adler tube operating at 4140 Mc with 24-db gain, 67-Mc bandwidth, and 2.5-db double-channel noise figure. Possible causes of excess noise in Adler tubes are discussed [189] and analytical descriptions of various electron-beam amplifiers are given [190]–[193]. A novel dc-pumped quadrupole amplifier which needs no RF pump and has no idler is analyzed by Siegman [194]. Kino [195] gives a theoretical discussion of plasma and electron-beam parametric amplifiers.

[188] T. J. Bridges and A. Ashkin, "A microwave Adler tube," PROC. IRE (Correspondence), vol. 48, pp. 361–363; March, 1960.
[189] C. P. Lea-Wilson, "Some possible causes of noise in Adler tubes," PROC. IRE (Correspondence), vol. 48, pp. 255–256; February, 1960.
[190] C. C. Johnson, "Theory of fast-wave parametric amplification," *J. Appl. Phys.*, vol. 31, pp. 338–345; February, 1960.
[191] H. Sobol, "Extension of longitudinal-beam parametric-amplifier theory," PROC. IRE (Correspondence), vol. 48, pp. 792–793; April, 1960.
[192] B. J. Udelson, "An electrostatically focused electron beam parametric amplifier," PROC. IRE (Correspondence), vol. 48, pp. 1485–1486; August, 1960.
[193] Y. Matsuo, "New microwave tube devices 'Fawshmotron' using the fast electron wave," PROC. IRE (Correspondence), vol. 48, p. 1908; November, 1960.
[194] A. E. Siegman. "The dc pumped quadrupole amplifier—a wave analysis," PROC. IRE, vol. 48, pp. 1750–1755; October, 1960.
[195] G. S. Kino, "Parametric amplifier theory for plasmas and electron beams," *J. Appl. Phys.*, vol. 31, pp. 1449–1458; August, 1960.

5) Ferrite Amplifier: The most significant development in ferrite parametric amplifiers is Denton's [196] longitudinal-pumped magnetostatic amplifier which requires only fractional watt pump power for amplification at 4600 Mc. Thomson [197] also describes a longitudinal-pumping experiment in which subharmonic spin-wave excitation is observed. Damon and Eshbach [198] discuss the theoretical limitations to ferrite amplifier performance due to spin-wave instabilities.

[196] R. T. Denton, "A ferromagnetic amplifier using longitudinal pumping," Proc. IRE (Correspondence), vol. 48, pp. 937–938; May, 1960.
[197] A. F. H. Thomson, "Ferromagnetic amplifiers," Proc. IRE (Correspondence), vol. 48, p. 259; February, 1960.
[198] R. W. Damon and J. R. Eshbach, "Theoretical limitations to ferromagnetic parametric amplifier performance," IRE Trans. on Microwave Theory and Techniques, vol. MTT-8, pp. 4–9; January, 1960.

B. Tunnel Diodes

An excellent review of the properties, principle of operation, and applications of the tunnel diode is given by Hall [199]. Remarkable progress has been made in raising the frequency of oscillation of tunnel diodes [200] with the highest frequency reported [201] being 103 Gc. The power output varied from several milliwatts in the UHF [202] to 2 μw [201] at 90 Gc. The effect of voltage on the frequency of oscillation has also been investigated [203].

[199] R. N. Hall, "Tunnel diodes," IRE Trans. on Electron Devices, vol. ED-7, pp. 1–9; January, 1960.
[200] R. Trambarulo and C. A. Burrus, "Esaki diode oscillators from 3 to 40 kmc," Proc. IRE (Correspondence), vol. 48, pp. 1776–1777; October, 1960.
[201] C. A. Burrus, "Millimeter wave Esaki diode oscillators," Proc. IRE (Correspondence), vol. 48, p. 2024; December, 1960.
[202] D. E. Nelson and F. Sterzer, "Tunnel-diode microwave oscillators with milliwatt power outputs," 1960 IRE WESCON Convention Record, pt. 1, pp. 68–73.
[203] J. K. Pulfer, "Voltage tuning in tunnel diode oscillators," Proc. IRE (Correspondence), vol. 48, p. 1155; June, 1960.

Progress has also been made in the use of tunnel diodes in amplifiers both in attaining unusual bandwidths [204] (210–625 Mc) and in reaching 26 Gc [205]. The noise figures, however, have not yet reached an attractively low level, with reports of 7 db at 4.5 Gc [206] to 10 db at X band. The tunnel diode has also been used as a down converter with gain [207], [208]. The use of distributed tunnel diodes which lend themselves naturally to microwave applications is discussed in an important paper by Hines [209].

[204] J. S. Sie, "Absolutely stable hybrid coupled tunnel-diode amplifier," Proc. IRE (Correspondence), vol. 48, p. 1321; July, 1960.
[205] R. F. Trambarulo, "Esaki diode amplifiers at 7, 11, and 26 kmc," Proc. IRE (Correspondence), vol. 48, pp. 2022–2023; December, 1960.
[206] A. Yariv, *et al.*, "Operation of an Esaki diode microwave amplifier," Proc. IRE (Correspondence), vol. 48, p. 1155; June, 1960.
[207] K. K. N. Chang, *et al.*, "Low-noise tunnel-diode down converter having conversion gain," Proc. IRE, vol. 48, pp. 854–858; May, 1960.
[208] W. J. Robertson, "A broad-band hybrid coupled tunnel diode down converter," Proc. IRE (Correspondence), vol. 48, pp. 2023–2024; December, 1960.
[209] M. E. Hines, "High-frequency negative-resistance circuit principles for Esaki diode applications," *Bell. Sys. Tech. J.*, vol. 39, pp. 477–513; May, 1960.

Great interest [210]–[218] has also been shown in theoretical calculations of the noise performance of tunnel-diode amplifiers and in design procedures for optimizing the amplifier noise performance.

[210] K. K. N. Chang, "The optimum noise performance of tunnel-diode amplifiers," Proc. IRE (Correspondence), vol. 48, pp. 107–108; January, 1960.
[211] M. E. Hines and W. W. Anderson, "Noise performance theory of Esaki (tunnel) diode amplifiers," Proc. IRE (Correspondence), vol. 48, p. 789; April, 1960.
[212] A. van der Ziel and J. Tamiya, "Note on the noise figure of negative conductance amplifiers," Proc. IRE (Correspondence), vol. 48, p. 796; April, 1960.
[213] D. I. Breitzer, "Noise figure of tunnel diode mixer," Proc. IRE (Correspondence), vol. 48, pp. 935–936; May, 1960.
[214] A. van der Ziel, "Noise of measure of lossy tunnel diode amplifiers," Proc. IRE (Correspondence), vol. 48, pp. 1321–1322; July, 1960.
[215] J. J. Tiemann, "Shot noise in tunnel diode amplifiers," Proc. IRE, vol. 48, pp. 1418–1423; August, 1960.
[216] P. Penfield, Jr., "Noise performance of tunnel-diode amplifiers," Proc. IRE (Correspondence), vol. 48, pp. 1478–1479; August, 1960.
[217] E. G. Nielsen, "Noise performance of tunnel diodes," Proc. IRE (Correspondence), vol. 48, pp. 1903–1904; November, 1960.
[218] R. La Rosa and C. R. Wilhelmsen, "Theoretical justification for shot-noise smoothing in the Esaki diode," Proc. IRE (Correspondence), vol. 48, p. 1903; November, 1960.

The use of metal and insulator films as a tunnel-emission amplifier has been proposed [219] though not specifically for microwave applications.

[219] C. A. Mead, "The tunnel-emission amplifier," Proc. IRE, vol. 48, pp. 359–361; March, 1960.

C. Masers

Solid-state masers have received continuing attention with two papers [220], [221] discussing the progress that has been made in packaging masers and making them suitable for low-noise-system applications. In radar applications [222], conventional duplexers cannot adequately prevent degradation of maser performance due to the saturation effects of the leakage spike. However, in ruby masers, a desaturation pulsing technique is described [223] which significantly reduces the maser recovery time. Several tunable masers are described [224], [225] and a novel broad-banding technique is described [226] which makes use of the fact that a maser has a negative L and C characteristic. Another paper [227] gives a thorough discussion of the parameters entering the design of masers of the unidirectional type which do not require circulators. A 70 Gc-pulsed-field maser [228] and several titania masers are also discussed [229]–[231]. The technique of noise temperature measurement of a traveling-wave maser is described by DeGrasse and Scovil [232].

[220] H. R. Senf, "Masers for systems applications," 1960 IRE WESCON Convention Record, pt. 1, pp. 43–48.
[221] F. R. Arams and S. Okwit, "Packaged tunable L-band maser system," Proc. IRE, vol. 48, pp. 866–874; May, 1960.
[222] J. L. Carter, *et al.*, "Use of an X-band solid-state ruby maser with a conventional duplexing system," *Microwave J.*, vol. 3, pp. 43–46; July, 1960.
[223] G. K. Wessel, "Recovery technique for saturated masers," IRE Trans. on Electron Devices, vol. ED-7, pp. 297–302; October, 1960.
[224] P. D. Gianino and F. J. Dominick, "A tunable X-band ruby maser," Proc. IRE (Correspondence), vol. 48, p. 260; February, 1960.

[225] S. Okwit, *et al.*, "Electronically-tunable traveling-wave masers at L and S bands," PROC. IRE (Correspondence), vol. 48, pp. 2025–2026; December, 1960.
[226] R. L. Kyhl, "Negative L and C in solid-state masers," PROC. IRE (Correspondence), vol. 48, p. 1157; June, 1960.
[227] M. W. P. Strandberg, "Unidirectional paramagnetic amplifier design," PROC. IRE, vol. 48, pp. 1307–1320; July, 1960.
[228] L. R. Momo, *et al.*, "Pulsed field millimeter wave maser," *J. Appl. Phys.*, vol. 31, p. 443; February, 1960.
[229] S. Foner and L. R. Momo, "CW millimeter wave maser using Fe^{3+} in TiO_2," *J. Appl. Phys.*, vol. 31, pp. 742–743; April, 1960.
[230] H. J. Gerritsen and H. R. Lewis, "Operation of a chromium doped titania maser," *J. Appl. Phys.*, vol. 31, pp. 608–609; March, 1960.
[231] H. J. Gerritsen, *et al.*, "Chromium-doped titania as a maser material," *J. Appl. Phys.*, vol. 31, pp. 1566–1571; September, 1960.
[232] R. W. DeGrasse and H. E. D. Scovil, "Noise temperature measurement on a traveling-wave maser preamplifier," *J. Appl. Phys.*, vol. 31, pp. 443–444; February, 1960.

The possibility of amplifying signals at frequencies higher than the pump is described by Arams [233] who uses harmonic-spin coupling to amplify a 10,590-Mc signal using a 9595-Mc pump. Another paper [234] shows that maser action in nuclear-quadrupole systems is unlikely to result in net gain, although it is shown [235] that by applying an RF field near the frequency of the quadrupole resonance of the Al nuclei, increased gain of a ruby maser results. Proposals are also made for millimeter-wave oscillators using a beam-type gas maser [236] or Na atoms in a cavity [237]. Theoretical expressions for the emitted power and frequency pulling in an ammonia-beam maser are given [238] while the productizing of an ammonia maser as a frequency standard is also described [239]. The problem of beam formation for a gas maser is discussed in two papers [240], [241].

[233] F. R. Arams, "Maser operation with signal frequency higher than pump frequency," PROC. IRE (Correspondence), vol. 48, p. 108; January, 1960.
[234] R. E. Donovan and A. A. Vuylsteke, "On the possibility of maser action in nuclear quadrupole systems," *J. Appl. Phys.*, vol. 31, pp. 614–615; March, 1960.
[235] G. Makhov, *et al.*, "Effect of nuclear polarization on the behavior of solid state masers," *J. Appl. Phys.*, vol. 31, pp. 936–938; May, 1960.
[236] W. Gordy and M. Cowan, "Proposed molecular amplifier and coherent generator for millimeter and submillimeter waves," *J. Appl. Phys.*, vol. 31, pp. 941–942; May, 1960.
[237] S. M. Bergmann, "Submillimeter wave maser," *J. Appl. Phys.*, vol. 31, pp. 275–276; February, 1960.
[238] H. G. Venkates and M. W. P. Strandberg, "Operating characteristics of a molecular-beam maser," *J. Appl. Phys.*, vol. 31, pp. 396–399; February, 1960.
[239] S. Hopfer, "Design considerations for a self-contained ammonia maser oscillator," 1960 IRE INTERNATIONAL CONVENTION RECORD, pt. 3, pp. 78–86.
[240] J. C. Helmer, *et al.*, "Focusing molecular beams of NH_3," *J. Appl. Phys.*, vol. 31, pp. 458–463; March, 1960.
[241] J. A. Giordmaine and T. C. Wang, "Molecular beam formation by long parallel tubes," *J. Appl. Phys.*, vol. 31, pp. 463–471; March, 1960.

The most significant development in the whole field of quantum electronics is of course the first realization of the optical maser by Maiman [242]. This development opens up a whole new area of technology of great importance. Though perhaps not properly falling into the field of microwave theory and techniques, the optical maser is certainly the child of the microwave maser and can indeed profit from the application of microwave techniques as evidenced in the Fox and Li [243] paper.

[242] T. H. Maiman, "Optical maser action in ruby," *British Commun. and Electronics*, vol. 7, pp. 674–675; September, 1960. See also, R. J. Collins, *et al.*, "Coherence, narrowing, directionality, and relaxation oscillations in the light emission from ruby," *Phys. Rev.*, vol. 5, pp. 303–305; October, 1960.
[243] A. G. Fox and T. Li, "Resonant modes in an optical maser," PROC. IRE (Correspondence), vol. 48, pp. 1904–1905; November, 1960.

D. Ferrites

1) General Microwave Properties: There is a very extensive literature on fundamental investigations of ferrites, particularly on ferrimagnetic resonance, magnetostatic modes, high-power studies, magnetic structure and chemistry, and anisotropy. A good many of these papers are included in the *Proceedings of the Fifth Symposium on Magnetism and Magnetic Materials* published as a supplement to the May, 1960, *Journal of Applied Physics*. In order to make the present review of manageable size, most of the papers which deal with ferrites from the fundamental physics point of view rather than from the point of view of microwave applications are not included. It is hoped that the availability of the above *Proceedings* in the *Journal of Applied Physics* will serve as an adequate bibliographical source for those interested in the areas not covered by this review.

An excellent historical sketch of the ferrite field together with an 82-item bibliography is given by Button [244]. Button and Lax [245] have also published an outstanding three-part review paper on the microwave properties and applications of ferrites. Magnetostatic modes are reviewed by White [246], while Morgenthaler [247] gives a brief theoretical survey of ferrimagnetic resonance in ellipsoids. A review of resonance phenomena at high-power levels is given by Schlömann, *et al.* [248], who also give a detailed discussion of subsidiary absorption obtained with a microwave magnetic field applied parallel to the dc field. New methods for growing large single crystal garnets are given by Nielsen [249]. The progress made in the theory of propagation in ferrite-loaded structures has been discussed in Section II-A, 2) of the present review.

[244] K. J. Button, "Historical sketch of ferrites and their microwave applications," *Microwave J.*, vol. 3, pp. 73–79; March, 1960.
[245] B. Lax and K. J. Button, "Electromagnetic properties of ferrimagnets and their applications from UHF to millimeter waves," *Microwave J.*, vol. 3, pt. I, pp. 43–49; September; pt. II, pp. 52–62, October; pt. III, pp. 49–56, November, 1960.
[246] R. L. White, "Use of magnetostatic modes as a research tool," *J. Appl. Phys.*, vol. 31, pp. 86S–94S; Supplement to May, 1960.
[247] F. R. Morgenthaler, "Survey of ferromagnetic resonance in small ferrimagnetic ellipsoids," *J. Appl. Phys.*, vol. 31, pp. 95S–97S; Supplement to May, 1960.
[248] E. Schlömann, *et al.*, "Recent developments in ferrimagnetic resonance at high power levels," *J. Appl. Phys.*, vol. 31, pp. 386S–395S; Supplement to May, 1960.
[249] J. W. Nielsen, "Improved method for the growth of yttrium-iron and yttrium-gallium garnets," *J. Appl. Phys.*, vol. 31, pp. 51S–52S; Supplement to May, 1960.

High-power effects have been studied extensively and a representative list of papers should include the following [250]–[254]. An experimental study of the linewidth of high-anisotropy materials is given by Bady, *et al.* [255].

[250] E. Schlömann, *et al.*, "L-band ferromagnetic resonance experiments at high peak power levels," IRE TRANS. ON MICROWAVE THEORY AND TECHNIQUES, vol. MTT-8, pp. 96–100; January, 1960.
[251] J. J. Green and E. Schlömann, "High power ferromagnetic resonance at X-band in polycrystalline garnets and ferrites," IRE TRANS. ON MICROWAVE THEORY AND TECHNIQUES, vol. MTT-8, pp. 100–103; January, 1960.
[252] P. E. Seiden and H. J. Shaw, "High-power effects in ferrite devices," PROC. IRE (Correspondence), vol. 48, p. 122; January, 1960.
[253] M. T. Weiss, "High power effects on ferrimagnetic resonance," *J. Appl. Phys.*, vol. 31, pp. 778–782; May, 1960.
[254] F. C. Rossol, "Subsidiary resonance in the coincidence region in yttrium iron garnet," *J. Appl. Phys.*, vol. 31, pp. 2273–2275; December, 1960.
[255] Isidore Bady, *et al.*, "Ferrimagnetic linewidth of single crystals of barium ferrite ($B_aF_{12}O_{19}$)," PROC. IRE (Correspondence), vol. 48, p. 2033; December, 1960.

2) Ferrite Devices: For commercial purposes, the *Y* circulator has become of very great importance and a number of papers are devoted to the design of such devices [256]–[258]. *Y* circulators have now been developed in most frequency ranges from 360 Mc [259] to 140 Gc [260]. A similar device, called the three-port ring circulator [261], which makes use of nonreciprocal phase shifters, has also been developed.

[256] U. Milano, *et al.*, "A *Y*-junction strip-line circulator," IRE TRANS. ON MICROWAVE THEORY AND TECHNIQUES, vol. MTT-8, pp. 346–351; May, 1960.
[257] L. Freiberg, "Lightweight *Y*-junction strip-line circulator," IRE TRANS. ON MICROWAVE THEORY AND TECHNIQUES (Correspondence), vol. MTT-8, p. 672; November, 1960.
[258] S. Yoshida, "Strip-line *Y* circulator," PROC. IRE (Correspondence), vol. 48, pp. 1337–1338; July, 1960.
[259] ——, "*J*-band strip line *Y* circulator," PROC. IRE (Correspondence), vol. 48, p. 1664; September, 1960.
[260] J. B. Thaxter and G. S. Heller, "Circulators at 70 and 140 kmc," PROC. IRE (Correspondence), vol. 48, pp. 110–111; January, 1960.
[261] M. Grace and F. R. Arams, "Three-port ring circulators," PROC. IRE (Correspondence), vol. 48, pp. 1497–1498; August, 1960.

A detailed theoretical discussion of resonance isolators is given by Schlömann [262], while an analytical and experimental study of the field displacement isolator is presented by Comstock and Fay [263]. In the UHF region, there is a need for avoiding coincidence of main and subsidiary resonance in a resonance isolator and a method for accomplishing this is described [264].

[262] E. Schlömann, "On the theory of the ferrite resonance isolator," IRE TRANS. ON MICROWAVE THEORY AND TECHNIQUES, vol. MTT-8, pp. 199–206; March, 1960.
[263] R. L. Comstock and C. E. Fay, "Operation of the field displacement isolator in rectangular waveguide," IRE TRANS. ON MICROWAVE THEORY AND TECHNIQUES, vol. MTT-8, pp. 605–611; November, 1960.
[264] E. Stern, "Ferrite shape considerations for UHF high-power isolators," IRE TRANS. ON MICROWAVE THEORY AND TECHNIQUES (Corresponcence), vol. MTT-8, p. 565; September, 1960.

Several new ferrite switches are described including one making use of the zero-permeability condition of the ferrite as a reflective switch [265], one using ferrite toroids [266], and one using multimode propagation [267] with a 3000-Mc bandwidth at *X* band. Weiss [268], [269] describes the tetrahedral junction as a switch. This device consists of two waveguides which are mutually cross-polarized and loaded by a longitudinally-magnetized ferrite rod. The use of a quadruply-ridged waveguide in the Faraday rotators and a doubly-ridged rectangular waveguide in an isolator is described by Grimes *et al.* [270], and in a single-ridge waveguide by Chen [271]. Higher-order modes and temperature sensitivity in the Reggia-Spencer phase shifter are discussed [272] and a wide ferrite-slab phase shifter is described [273].

[265] C. M. Johnson and J. C. Wiltse, "A broad-band ferrite reflective switch," IRE TRANS. ON MICROWAVE THEORY AND TECHNIQUES (Correspondence), vol. MTT-8, pp. 466–467; July, 1960.
[266] L. Levey and L. M. Silber, "A fast-switching *X*-band circulator utilizing ferrite toroids," 1960 IRE WESCON CONVENTION RECORD, pt. 1, pp. 11–20.
[267] J. E. Tompkins, *et al.*, "Multimode propagation in gyromagnetic rods and its application to traveling-wave devices," *J. Appl. Phys.*, vol. 31, pp. 176S–177S; Supplement to May, 1960.
[268] J. A. Weiss, "The tetrahedral junction as a waveguide switch," IRE TRANS. ON MICROWAVE THEORY AND TECHNIQUES (Correspondence), vol. MTT-8, pp. 120–121; January, 1960.
[269] —, "Tetrahedral junction," *J. Appl. Phys.*, vol. 31, pp. 168S–169S; Supplement to May, 1960.
[270] E. S. Grimes, *et al.*, "Broad-band ridge waveguide ferrite devices," IRE TRANS. ON MICROWAVE THEORY AND TECHNIQUES, vol. MTT-8, pp. 489–492; September, 1960.
[271] T. S. Chen, "Nonreciprocal attenuation of ferrite in single-ridge waveguide," IRE TRANS. ON MICROWAVE THEORY AND TECHNIQUES, vol. MTT-8, pp. 247–248; March, 1960.
[272] A. Clavin, "Reciprocal ferrite phase shifters," IRE TRANS. ON MICROWAVE THEORY AND TECHNIQUES (Correspondence), vol. MTT-8, pp. 254–255; March, 1960.
[273] T. D. Geiszler and R. A. Henschke, "Broadband reciprocal ferrite phase shifters," *J. Appl. Phys.*, vol. 31, pp. 174S-175S; Supplement to May, 1960.

Two papers [274], [275] describe Faraday-rotation structures while Coale [276] discusses a novel rotating half-wave plate which uses a four-wire transmission line for generating both the rotating microwave fields and the rotating low-frequency magnetizing fields. The use of single crystal garnets in microwave filters is discussed in three papers [277], [278], [105]. Several papers [279]–[281] treat the problem of microwave generation by pulsed-magnetic fields.

[274] W. Beust and E. G. Johnson, "High average power rotator," *Microwave J.*, vol. 3, pp. 55–57; May, 1960.
[275] S. J. Lewandowski and J. Konopka, "On some problems in designing microwave Faraday-rotation devices," IRE TRANS. ON MICROWAVE THEORY AND TECHNIQUES (Correspondence), vol. MTT-8, pp. 249–251; March, 1960.
[276] F. S. Coale, "High-speed ferrite rotating half wave plate," *J. Appl. Phys.*, vol. 31, pp. 170S–171S; Supplement to May, 1960.
[277] P. S. Carter, Jr., "Magnetically tunable microwave filters employing single crystal garnet resonators," 1960 IRE INTERNATIONAL CONVENTION RECORD, pt. 3, pp. 130–135.
[278] —— and C. Flammer, "Unloaded *Q* of single crystal yttrium-iron-garnet resonator as a function of frequency," IRE TRANS. ON MICROWAVE THEORY AND TECHNIQUES (Correspondence), vol. MTT-8, pp. 570–571; September, 1960.
[279] B. J. Elliot, *et al.*, "Pulsed ferrimagnetic microwave generator," *J. Appl. Phys.*, vol. 31, pp. 400S–401S; Supplement to May, 1960.
[280] T. Schaug-Pattersen, "Growing spin waves in ferrites in unstable equilibrium," *J. Appl. Phys.*, vol. 31, pp. 372S–383S; Supplement to May, 1960.
[281] M. R. Stiglitz and F. R. Morgenthaler, "Resonance experiments with single crystal YIG in pulsed magnetic fields," *J. Appl. Phys.*, vol. 31, pp. 37S–38S; Supplement to May, 1960.

3) Ferroelectrics: Gemulla and Hall [282] review the field of ferroelectrics at microwave frequencies and point out the many problems yet to be solved before extensive applications become practical. Two other papers discuss the use of the nonlinear properties of ferroelec-

trics as microwave mixers [283] and parametric amplifiers [284].

[282] W. J. Gemulla and R. D. Hall, "Ferroelectrics at microwave frequencies," *Microwave J.*, vol. 3, pp. 47–51; February, 1960.
[283] I. Goldstein, "Interaction of two microwave signals in a ferroelectric material," PROC. IRE (Correspondence), vol. 48, p. 1665; September, 1960.
[284] Y. Aoki, "Proposed parametric amplifier utilizing ferroelectric substance," IRE TRANS. ON MICROWAVE THEORY AND TECHNIQUES, (Correspondence) vol. MTT-8, pp. 465–466; July, 1960.

IV. Measurements and Microwave Systems

A. Systems

Microwave and millimetric radiometry has again been prominent in the microwave field. An excellent review paper is by Harris [285]; Richter has described a 33-Gc radiometer [286]. The microwave aspects of particle accelerators have been covered in three articles: Barrington, *et al.*, discuss the RF system for a synchrotron [287]; Robinson discusses the Cambridge electron accelerator [288]; a review paper on linear accelerators has also appeared [289]. The problems of duplexing a ruby maser in a radar have been examined [290]. Finally, a frequency control system using a reference cavity has been patterned after an ac carrier servo by using a 100-kc crystal to modulate the reference cavity [291].

[285] D. B. Harris, "Microwave radiometry," *Microwave J.*, vol. 3, pt. I, pp. 41–46, April; pt. II, pp. 47–54, May, 1960.
[286] E. W. Richter, "Millimeter radiometers," *Microwave J.*, vol. 3, pp. 63–66; October, 1960.
[287] A. E. Barrington, *et al.*, "Model studies of a strongly coupled synchrotron RF system," IRE TRANS. ON MICROWAVE THEORY AND TECHNIQUES, vol. MTT-8, pp. 597–604; November, 1960.
[288] K. W. Robinson, "Radio-frequency system of the Cambridge electron accelerator," IRE TRANS. ON MICROWAVE THEORY AND TECHNIQUES, vol. MTT-8, pp. 593–596; November, 1960.
[289] A. E. Barrington, "Microwave engineering aspects of electron linear accelerators," *Microwave J.*, vol. 3, pt. I, pp. 35–40, April; pt. II, pp. 54–58, June, 1960.
[290] F. E. Goodwin, "Duplexing a solid-state ruby maser in an *X*-band radar system," PROC. IRE (Correspondence), vol. 48, p. 113; January, 1960.
[291] J. R. Singer, "A new automatic frequency regulation system," IRE TRANS. ON MICROWAVE THEORY AND TECHNIQUES (Correspondence), vol. MTT-8, p. 249; March 1960.

B. High-Power Resonators

Resonant ring circuits for testing of high-power components have arrived at a high degree of perfection. Tomiyasu has given curves relating ring gain, coupling, and ring attenuation [292]. Golde has presented a derivation of loaded and unloaded Q and gives parametrically the ratio of these vs gain [293]. Miller has considered, in addition, impedance mismatch effects [294]. This last paper also gives sample waveforms and includes photographs of breakdown phenomena.

[292] K. Tomiyasu "Attenuation in a resonant ring circuit," IRE TRANS. ON MICROWAVE THEORY AND TECHNIQUES (Correspondence), vol. MTT-8, pp. 253–254; March, 1960.
[293] H. Golde, "Theory and measurement of Q in resonant ring circuits," IRE TRANS. ON MICROWAVE THEORY AND TECHNIQUES, vol. MTT-8, pp. 560–564; September, 1960.
[294] S. J. Miller, "The traveling wave resonator and high power microwave testing," *Microwave J.*, vol. 3, pp. 50–58; September, 1960.

C. Dielectric Measurements

One method of measuring constitutive parameters involves filling a length of transmission line or waveguide with the dielectric material. Sharpe terminates the transmission line with a sliding short and uses a bilinear transformation to derive the constants [295]. He shows that for a TEM line the transformation leads to an immediate solution via the Smith chart. A similar technique has been used on single crystals of barium titanate, measuring transmission resonances through a section of filled waveguide [296]. Another method uses a resonant dielectric cylinder between metal plates, where the Q and two resonant frequencies are measured [297]. Culshaw has developed a Fabry-Perot interferometer at 6 mm [298].

[295] C. B. Sharpe, "A graphical method for measuring dielectric constants at microwave frequencies," IRE TRANS. ON MICROWAVE THEORY AND TECHNIQUES, vol. MTT-8, pp. 155–159; March, 1960.
[296] A. Lurio and E. Stern, "Measurements of the dielectric constant of $Ba_xTi_yO_z$ single crystals in the paraelectric region at *X*-band," *J. Appl. Phys.*, vol. 31, pp. 1805–1809; October, 1960.
[297] B. W. Hakki and P. D. Coleman, "A dielectric resonator method of measuring inductive capacities in the millimeter range," IRE TRANS. ON MICROWAVE THEORY AND TECHNIQUES vol. MTT-8, pp. 402–410; July, 1960.
[298] W. Culshaw, "High resolution millimeter wave Fabry-Perot interferometer," IRE TRANS. ON MICROWAVE THEORY AND TECHNIQUES, vol. MTT-8, pp. 182–189; March, 1960.

D. Noise Temperature

Low-noise systems have continued to be of great interest. Haun calculates single- and double-sideband noise figures for parametric amplifiers for the general case where gain is different at the two sidebands [299]. The often quoted difference of 3 db is only correct if the gain is the same at both sidebands. Hogg, in a pair of papers, has reported on investigations of sky temperature [300], [301]. At 6 Gc the sky temperature during a storm may be as high as 120°K. Extensive nonstormy data are given on sun temperature, galactic noise, atmospheric-absorption noise, etc., for a wide range of frequencies. Finally, detailed calculations for the performance of a low-noise radar at 5 Gc have been made [302].

[299] R. D. Haun, Jr., "Summary of measurement techniques of parametric amplifier and mixer noise figure," IRE TRANS. ON MICROWAVE THEORY AND TECHNIQUES, vol. MTT-8, pp. 410–415; July, 1960.
[300] D. C. Hogg and R. A. Semplak, "The effect of rain on the noise level of a microwave receiving system," PROC. IRE (Correspondence), vol. 48, pp. 2024–2025; December, 1960.
[301] D. C. Hogg and W. W. Mumford, "The effective noise temperature of the sky," *Microwave J.*, vol. 3, pp. 80–84; March, 1960.
[302] R. L. Forward and F. Richey, "Effects of external noise on radar performance," *Microwave J.*, vol. 3, pp. 73–80; December, 1960.

E. Miscellaneous Measurements

A general method for analyzing microwave measurements using flow graphs has been proposed by Hunton [303]. This procedure takes the place of the scattering matrix solution, and for some purposes it is simpler. Lerner and Wheeler measure filter bandwidths by adjusting amplitude modulation of the signal until a 45° phase shift is realized across the filter [304]. Q is then simply given by the ratio of carrier frequency to twice modulation frequency. Finnila, *et al.*, have developed a technique for measuring relative microwave phase shift

in cases where a wide difference in signal amplitudes exists [305]. They use a Serrodyne technique to translate both signals to audio, where wide differences in level can readily be handled. Another analysis compares phase-shift mismatch errors for several choices of reference wave [306]. Hu has extended the modulated dipole scatterer method for measuring electric field to the case of a modulated loop scatterer for measuring magnetic field [307]. Other devices include a calorimeter with an absorptive harmonic filter for multimode power measurements [308], and a bridge-type impedance meter [309].

[303] J. K. Hunton, "Analysis of microwave measurement techniques by means of signal flow graphs," IRE TRANS. ON MICROWAVE THEORY AND TECHNIQUES, vol. MTT-8, pp. 206–212; March, 1960.
[304] D. S. Lerner and H. A. Wheeler, "Measurement of bandwidth of microwave resonator by phase shift of signal modulation," IRE TRANS. ON MICROWAVE THEORY AND TECHNIQUES, vol. MTT-8, pp. 343–345; May, 1960.
[305] C. A. Finnila, *et al.*, "Measurement of relative phase shift at microwave frequencies," IRE TRANS. ON MICROWAVE THEORY AND TECHNIQUES, vol. MTT-8, pp. 143–147; March, 1960.
[306] G. E. Schafer, "Mismatch errors in microwave phase shift measurements," IRE TRANS. ON MICROWAVE THEORY AND TECHNIQUES, vol. MTT-8, pp. 617–622; November, 1960.
[307] M.-K. Hu, "On measurements of microwave $\bar{E}$ and $\bar{H}$ field distributions by using modulated scattering methods," IRE TRANS. ON MICROWAVE THEORY AND TECHNIQUES, vol. MTT-8, pp. 295–300; May, 1960.
[308] V. G. Price, "Harmonic calorimeter for power measurements in a multimode waveguide," 1960 IRE INTERNATIONAL CONVENTION RECORD, pt. 3, pp. 136–144.
[309] R. W. Beatty, "A microwave impedance meter capable of high accuracy," IRE TRANS. ON MICROWAVE THEORY AND TECHNIQUES (Correspondence), vol. MTT-8, pp. 461–463; July, 1960.

Several new techniques have appeared for measuring specific devices or material characteristics. In the Doppler method for measuring back scatter, the sample (in this case absorber) is nutated by means of counter-rotating eccentric disks in a ground plane [310]. This imparts an audio modulation to the scattered return, thereby allowing greater suppression of extraneous signals. A nanosecond-pulse radar has been useful in identifying internal reflections of TWT's [311]. Several papers relate to excess carrier lifetime in semiconductor materials [312]–[314]. The technique (see Section IV-C) uses a section of waveguide filled with the material; incident light pulses create excess carriers whose lifetime is determined from measurements of the microwave power absorption through the sample.

[310] E. B. McMillan, and H. J. Schmitt, "Doppler method for absorber testing," *Microwave J.*, vol. 3, pp. 64–68; November, 1960.
[311] D. O. Melroy and H. T. Closson, "Measurement of internal reflections in traveling-wave tubes using a millimicrosecond pulse radar," PROC. IRE, vol. 48, pp. 165–168; February, 1960.
[312] H. Jacobs, *et al.*, "Further consideration of bulk lifetime measurement with a microwave electrodeless technique," PROC. IRE, vol. 48, pp. 229–233; February, 1960.
[313] ——, *et al.*, "Some device aspects of multiple microwave reflections in semiconductors," 1960 IRE WESCON CONVENTION RECORD, pt. 3, pp. 42–48.
[314] H. A. Atwater, "Microwave measurement of semiconductor carrier lifetimes," *J. Appl. Phys.*, vol. 31, pp. 938–939; May, 1960.

V. Acknowledgment

M. L. Buschkotter was most helpful in assisting with the manuscript preparation.

The Short Pulse Behavior of Lossy Tapered Transmission Lines*

R. STAPELFELDT†, MEMBER, IRE, AND F. J. YOUNG†, MEMBER, IRE

Summary—**An analytic method is given which allows the design engineer to assess rapidly the short pulse characteristics of any given tapered-transmission-line type of pulse transformer. The method allows inclusion of both skin-effect losses and losses which are independent of frequency. The effects of mismatching at either end are shown to be as important as the taper function of the line itself. The results of this approximate method are expressed as simple integrals and matching terms to which it is easy to attach physical significance.**

The method is applied to the analysis of two tapered-line pulse transformers which are geometrically uniform coaxial structures with tapered dielectric constants. The line whose nominal characteristic impedance is an exponential function of electrical position is shown to have a good rise time and tilt distortion characteristics.

* Received by the PGMTT, December 6, 1960; revised manuscript received, March 15, 1961. This research was supported in part by the Office of Naval Research under Contract NONR 760(09). This paper is abstracted from a dissertation submitted by R. Stapelfeldt in partial fulfillment of the requirements for the Ph.D. degree at Carnegie Institute of Technology.

† Carnegie Institute of Technology, Pittsburgh, Pa.

Introduction

IN the already extensive literature on the tapered-transmission-line pulse transformer,[1] there has been little investigation of the pulse-distorting effects of losses in the tapered line. That such distortions must exist is evident, for even the lossy uniform line can be

[1] H. Kaufman, "Bibliography of nonuniform transmission lines," IRE TRANS. ON ANTENNAS AND PROPAGATION (Communication), vol. AP-3, pp. 218–220; October, 1955.

demonstrated to produce distortion if terminated in a pure resistance. The so-called "initial slope" distortion of the tapered transmission line which results from the high-pass nature of the ideal device would be expected to be changed to a band-pass characteristic by skin effect. A band-pass filter would, in turn, be expected to lengthen the rise time of a short pulse passing through it. This paper will concern itself with an investigation of the role of losses—primarily skin-effect losses—in lengthening the rise time and otherwise distorting the waveform of a short pulse undergoing impedance transformation by a tapered-transmission-line pulse transformer. Analytical expressions are found which relate pulse waveform distortion to the parameters of the line and to the degree of matching achieved at each end of the line. These expressions do not include the effects of multiple reflections from the ends of the line, since the effects of such additional reflections do not manifest themselves until long after the passage of pulses of practically usable length.

The problem of skin effect in the uniform transmission line has already been considered by Pélissier.[2] He has shown that skin effect can be introduced by adding a series impedance term which is proportional to the square root of frequency. The real part of this impedance is the familiar skin resistance.

The analysis is made by first introducing skin effect into the telegraph differential equations and Laplace transforming them with respect to time. A series solution for the voltage e on the lossy tapered transmission line is developed. A similar series technique is then used to find the impedance Z of the line. The boundary conditions at the generator and load ends of the tapered line are introduced through the use of transfer functions similar to the transmission coefficients of conventional uniform line analysis. An over-all transfer function which contains integrals of the tapered line's parameters over distance x is then developed as a function of s. The inverse Laplace transformation is examined for the case of a step function generator input and used to write down relatively simple expressions for the rise time, tilt, time delay and voltage multiplication ratio of the arbitrarily tapered lossy transmission-line pulse transformer driven through and terminated in arbitrary generator and load resistances. These rise time and tilt distortions are illustrated in Figs. 1 and 2 for the case of a voltage step function applied to the input of the tapered line.

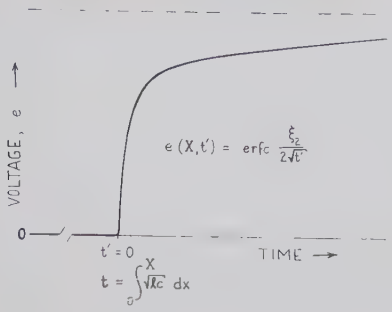

Fig. 1—Skin effect induced rounding of leading edge of pulse on a tapered transmission line.

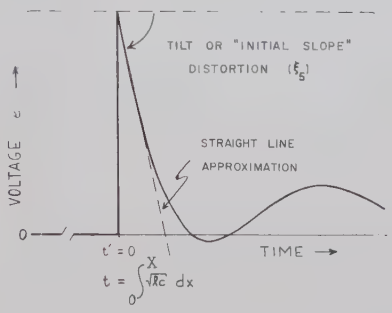

Fig. 2—The same pulse as in Fig. 1, on a greatly contracted time scale.

The Analysis

The starting point of the analysis is the pair of generalized telegraph equations Laplace transformed with respect to time.

$$\dot{e} = -\, i[Z_{\text{series}}], \tag{1}$$

where

$$\dot{e} = \frac{\partial e}{\partial x},$$

$$\dot{i} = -\, e[Y_{\text{shunt}}], \tag{2}$$

where

$$\dot{i} = \frac{\partial i}{\partial x}.$$

The series impedance per unit length Z_{series} can be expressed after Laplace transformation with respect to time as $ls+\rho\sqrt{S}+r$. The coefficients l, ρ and r are variables with respect to position x only and correspond respectively to the series inductance per unit length, skin effect coefficient per unit length, and the dc resistance per unit length. The complex skin effect impedance per unit length $\rho\sqrt{S}$ is an exact representation only for the case of plane conductors, but it can be demonstrated that the error introduced in applying this approximation to conductors with other geometries has a negligible effect on the accuracy of the total Z_{series} term when the final results of the analysis are considered.

The shunt admittance per unit length Y_{shunt} is given as the conventional $cs+g$ with both c and g being variables with respect to position only.

Solving the two telegraph equations simultaneously, one obtains a differential equation in voltage.

$$\left((l^2c)s^3+(2\rho lc)s^{5/2}+(2rlc+\rho^2c+gl^2)s^2+(2r\rho c+2\rho gl)s^{3/2}+(r^2c+2rgl+\rho^2g)s+(2rg\rho)s^{1/2}+(r^2g)\right)e$$
$$+(\dot{l}s+\dot{\rho}\sqrt{s}+\dot{r})\dot{e}-(ls+\rho\sqrt{s}+r)\ddot{e}=0. \tag{3}$$

[2] R. Pélissier, "La propagation des ondes transitoires et périodiques le long des lignes électriques," *Rev. Gén. Élec.*, vol. 59, pp. 379–399, September, 1950; pp. 437–454, October, 1950; pp. 502–512, November, 1950.

A solution to this equation is assumed of the form:

$$\frac{e(x)}{e(0)} = e^{-\Gamma_e(x,s)}. \tag{4}$$

The substitution of (4) into the differential equation in voltage yields a Riccati equation in $\dot{\Gamma}_e$.

$$(ls+\rho\sqrt{s}+r)\dot{\Gamma}_e^2+(\dot{l}s+\dot{\rho}\sqrt{s}+\dot{r})\dot{\Gamma}_e-(ls+\rho\sqrt{s}+r)\ddot{\Gamma}_e$$
$$=(l^2c)s^3+(2\rho lc)s^{5/2}+(2rlc+\rho^2c+gl^2)s^2$$
$$+(2r\rho c+2\rho gl)s^{3/2}+(r^2c+2rgl+\rho^2g)s+(2rg\rho)s^{1/2}+r^2g. \tag{5}$$

Since this type of equation cannot be solved in closed form, a series solution is found by assumption of a series expansion of $\dot{\Gamma}_e$ in decreasing powers of $s^{1/2}$. This form of asymptotic series expansion has been described by Weber and others.[3]

$$\dot{\Gamma}_e = b_1 s + b_2 s^{1/2} + b_3 + b_4 s^{-1/2} + b_5 s^{-1} + \cdots. \tag{6}$$

The b coefficients of this series are evaluated after the insertion of the series representation of $\dot{\Gamma}_e$ into (5) by a recursion process. The coefficients of the terms in the highest power of s present are equated to evaluate b_1. Then the terms in the next higher power of s are used together with b_1 to evaluate b_2. This process, when continued, will evaluate the b coefficients in sequence.

There are two independent sets of valid b coefficients corresponding to $m=+1$ and $m=-1$.

$$b_1 = m\sqrt{lc}, \tag{7}$$

$$b_2 = m\frac{\rho}{2}\sqrt{\frac{c}{l}}, \tag{8}$$

$$b_3 = -\frac{1}{4}\left(\frac{\dot{l}}{l}-\frac{\dot{c}}{c}\right)$$
$$+m\left(\frac{1}{2}r\sqrt{\frac{c}{l}}+\frac{1}{2}g\sqrt{\frac{l}{c}}-\frac{1}{8}\frac{\rho^2}{l}\sqrt{\frac{c}{l}}\right), \tag{9}$$

b_4 = all loss terms containing ρ, r and g, (10)

$$b_5 = \frac{m}{\sqrt{lc}}\left\{\frac{7\dot{l}^2}{32l^2}-\frac{5}{32}\frac{\dot{c}^2}{c^2}-\frac{1}{16}\frac{\dot{l}}{l}\frac{\dot{c}}{c}-\frac{1}{8}\left(\frac{\ddot{l}}{l}-\frac{\ddot{c}}{c}\right)\right\}$$
plus loss terms. (11)

An expression for the impedance of the lossy tapered transmission line $Z=e/i$ is found by our differentiating the defining equation for Z and inserting the values of $\dot{e}$ and $\dot{i}$ from (1) and (2).

$$Z = (cs+g)Z^2 - ls - \rho\sqrt{s} - r. \tag{12}$$

[3] E. Weber, "Linear Transient Analysis—Volume II," John Wiley and Sons, Inc., New York, N. Y., Section 7.4; 1956.

This Riccati equation can be solved by the same technique used to solve (5).

$$Z = f_1 + f_2 s^{-1/2} + f_3 s^{-1} + \cdots. \tag{13}$$

$$f_1 = m\sqrt{\frac{l}{c}} \tag{14}$$

$$f_2 = \frac{m}{2}\frac{\rho}{\sqrt{lc}} \tag{15}$$

$$f_3 = \frac{1}{4c}\left(\frac{\dot{l}}{l}-\frac{\dot{c}}{c}\right) + \text{loss terms}. \tag{16}$$

It is not necessary to assume such a simple power series solution for Z, should a different form of solution be desired. If the following series is chosen:

$$Z = m\sqrt{\frac{l}{c}}\,\epsilon^{\phi_1 s^{-1/2}+\phi_2 s^{-1}+\phi_3 s^{-3/2}+\cdots}, \tag{17}$$

another valid series representation of the high-frequency behavior of Z is obtained. In this case, the exponential must be expanded before evaluation of the ϕ coefficients, which are:

$$\phi_1 = \frac{\rho}{2l}, \tag{18}$$

$$\phi_2 = \frac{m}{4\sqrt{lc}}\left(\frac{\dot{l}}{l}-\frac{\dot{c}}{c}\right) + \text{loss terms}. \tag{19}$$

The index $m=\pm 1$ in the series solutions for e and Z results from the existence of two mathematically independent solutions which are interpreted physically as the voltages and impedances associated with a wave moving in the plus-x direction for $m=+1$ and with a wave moving in the reverse direction for $m=-1$.

For a complete solution, it is necessary to introduce the boundary conditions for the tapered transmission line at both ends of the line—at $x=0$ where the line is driven by a generator with a source resistance R_g and at $x=X$ where the line is terminated in a load resistance R_L. The method chosen for this is that of solving for a transmission coefficient or transfer function at each end of the line. Each transfer function is then considered as a "matching term" independent of the transmission characteristics of the tapered line proper.

The transfer function at the input is defined as:

$$\frac{\vec{e}(0)}{e_g} = \eta\epsilon^{g_0 s^{-1/2}+g_1 s^{-1}+\cdots}, \tag{20}$$

where

$$\eta \triangleq \frac{1}{1+\dfrac{R_g}{\sqrt{l/c}\,|_{x=0}}}, \tag{21}$$

the infinite frequency transfer function at the input.

The g coefficients are evaluated by simple circuit theory using the Z previously found and evaluating it at $x=0$ with $m=+1$ to obtain the input impedance of the line.

Similarly, the transfer function at the output is defined as

$$\frac{e_L}{\vec{e}(X)} = \lambda \epsilon^{h_0 s^{-1/2} + h_1 s^{-1} + \cdots} \tag{22}$$

where

$$\lambda \triangleq \frac{2}{1 + \dfrac{\sqrt{l/c}\,\big|_{x=X}}{R_L}}, \tag{23}$$

the infinite frequency transfer function at the output.

The choice of transfer functions containing power series in the arguments of the exponentials is a useful one since it allows the over-all transfer function of the tapered-transmission-line pulse transformer to be expressed comparatively simply.

$$\frac{e_L}{e_g} = \frac{\vec{e}(0)}{e_g} \cdot \frac{\vec{e}(X)}{\vec{e}(0)} \cdot \frac{e_L}{\vec{e}(X)}. \tag{24}$$

The three transfer functions making up the over-all transfer function are multiplied together by simply adding up terms in the arguments of the exponentials.

By use of the relationship that

$$\exp\left\{-\frac{1}{4}\int_0^X \left(\frac{\dot{l}}{l} - \frac{\dot{c}}{c}\right) dx\right\} = \sqrt{\frac{\sqrt{l/c}\,\big|_{x=X}}{\sqrt{l/c}\,\big|_{x=0}}}, \tag{25}$$

the over-all transfer function for the tapered-line pulse transformer becomes

$$\frac{e_L}{e_g} = \eta\lambda \sqrt{\frac{\sqrt{l/c}\,\big|_{x=X}}{\sqrt{l/c}\,\big|_{x=0}}}\, \epsilon^{\xi_1 s + \xi_2 s^{1/2} + \xi_3 + \xi_4 s^{-1/2} + \xi_5 s^{-1} + \cdots}, \tag{26}$$

where

$$\xi_1 = -\int_0^X \sqrt{lc}\, dx, \tag{27}$$

$$\xi_2 = -\frac{1}{2}\int_0^X \rho \sqrt{\frac{c}{l}}\, dx, \tag{28}$$

$$\xi_3 = -\int_0^X \left\{\frac{1}{2} r \sqrt{\frac{c}{l}} + \frac{1}{2} g \sqrt{\frac{l}{c}} - \frac{1}{8}\frac{\rho^2}{l}\sqrt{\frac{c}{l}}\right\} dx, \tag{29}$$

$$\begin{aligned}\xi_4 = {} & \frac{1}{2}\frac{\rho}{l}\eta R_g \sqrt{\frac{c}{l_{x=0}}} - \frac{1}{4}\frac{\rho}{l}\left\{\lambda\frac{\sqrt{l/c}}{R_L}\right\}^3_{x=X} \\ & - \frac{1}{2}\int_0^X \frac{\rho}{l}\left(\frac{1}{2}\frac{\dot{l}}{l} - \frac{1}{2}\frac{\dot{\rho}}{\rho} - \frac{1}{2} r\sqrt{\frac{c}{l}} + \frac{1}{2} g\sqrt{\frac{l}{c}} + \frac{1}{8}\frac{\rho^2}{l}\sqrt{\frac{c}{l}}\right) dx,\end{aligned} \tag{30}$$

$$\begin{aligned}\xi_5 = {} & \eta R_g \left\{\frac{1}{4l}\left(\frac{\dot{l}}{l} - \frac{\dot{c}}{c}\right) + \frac{1}{8}\frac{\rho^2}{l^2}\sqrt{\frac{c}{l}}\left(\eta R_g\sqrt{\frac{c}{l}} - 1\right) + \frac{1}{2}\frac{g}{\sqrt{lc}} - \frac{1}{2}\frac{r}{l}\sqrt{\frac{c}{l}}\right\}\Big|_{x=0} \\ & + \left[-\frac{\lambda}{8\sqrt{lc}}\left(\frac{\dot{l}}{l} - \frac{\dot{c}}{c}\right) - \frac{1}{8}\frac{\rho^2}{l}\left\{\frac{1}{2}\left(\lambda\frac{\sqrt{l/c}}{R_L}\right) - \frac{1}{2}\left(\lambda\frac{\sqrt{l/c}}{R_L}\right)^2 - \left(\lambda\frac{\sqrt{l/c}}{R_L}\right)^3 + \frac{1}{4}\left(\lambda\frac{\sqrt{l/c}}{R_L}\right)^6\right\}\right. \\ & \left. + \frac{r}{l}\left\{1 - \frac{1}{4}\left(\lambda\frac{\sqrt{l/c}}{R_L}\right)\right\} + \frac{1}{4}\frac{g}{c}\left(\lambda\frac{\sqrt{l/c}}{R_L}\right)\right]_{x=X} \\ & - \int_0^X \left\{\frac{7}{32}\frac{1}{\sqrt{lc}}\frac{\dot{l}^2}{l^2} - \frac{5}{32}\frac{1}{\sqrt{lc}}\frac{\dot{c}^2}{c^2} - \frac{1}{16}\frac{1}{\sqrt{lc}}\frac{\dot{l}}{l}\frac{\dot{c}}{c} - \frac{1}{8}\frac{1}{\sqrt{lc}}\left(\frac{\ddot{l}}{l} - \frac{\ddot{c}}{c}\right) - \frac{5}{128}\frac{\rho^4}{l^3}\sqrt{\frac{c}{l}} - \frac{1}{4}\frac{\rho^2}{l^2}\frac{\dot{l}}{l}\right. \\ & + \frac{1}{4}\frac{\rho^2}{l^2}\frac{\dot{\rho}}{\rho} - \frac{1}{8}\frac{r^2}{l}\sqrt{\frac{c}{l}} - \frac{1}{4}\frac{\dot{r}}{l} + \frac{1}{4}\frac{r}{l}\frac{\dot{l}}{l} - \frac{1}{8}\frac{g^2}{c}\sqrt{\frac{l}{c}} + \frac{1}{4}\frac{\dot{g}}{c} - \frac{1}{4}\frac{g}{c}\frac{\dot{c}}{c} + \frac{3}{16}\frac{\rho^2 r}{l^2}\sqrt{\frac{c}{l}} \\ & \left. + \frac{1}{4}\frac{rg}{\sqrt{lc}} - \frac{1}{16}\frac{\rho^2 g}{l\sqrt{lc}} + \frac{3}{16}\frac{\rho^2 r}{l^2}\sqrt{\frac{c}{l}}\right\} dx.\end{aligned} \tag{31}$$

If a step function EMF is applied at the generator, the load voltage can be found by using e_L/e_g. In this case, a physical interpretation can be assigned to each of the factors of e_L/e_g by consideration of each factor as a filter acting successively on the input step function.

$\eta\lambda\sqrt{\frac{\sqrt{l/c}\,|_{x=X}}{\sqrt{l/c}\,|_{x=0}}}$ is a distortionless multiplying factor representing the nominal voltage transformation ratio of the tapered line and its matching as would be predicted from lossless uniform line theory.

$\epsilon^{\xi_1 s}$ represents a distortionless delay of $-\xi_1$ seconds.

$\epsilon^{\xi_2 s^{1/2}}$ represents the rounding of the leading edge of the step function. The shape of this curve is shown in Fig. 1.

ϵ^{ξ_3} represents a distortionless attenuation due to losses in the line.

$\epsilon^{\xi_4 s^{-1/2}}$ represents a completely negligible modification of the delayed, attenuated and rounded-off step function (see below).

$\epsilon^{\xi_5 s^{-1}}$ represents the tilt or "initial slope" distortion discussed by Frank[4] and Young.[5] The exact inverse Laplace transformation of this term has the form:

$$e(t') = J_0[2\sqrt{-\xi_5 t'}].$$

An extremely good approximation to this is the straight line:

$$e(t') = 1 + \xi_5 t'.$$

The previous discussion has implied that the inverse Laplace transformation of the response of cascaded filters can be found by our multiplying together the time responses of the individual filters. In the general case, this is obviously incorrect and real convolution of the factors is needed. Direct multiplication of the time responses is justified only when only one factor of the complex frequency response is appreciably different from unity at a given complex frequency. This is the case here since the spectral aberration corresponding to the skin-effect-induced rounding of the leading edge of the step function occurs at frequencies which are orders of magnitude higher than those frequency response distortions determining the relatively slow tilt of the top of the step function.

The $\epsilon^{\xi_4 s^{-1/2}}$ term has a value which approaches unity with increasing frequency ($t \to 0$). At the frequencies involved in the spectra of the pulses considered here, this term can still be neglected because it is very close to unity and moreover is essentially divergent. The divergent nature of this term can be demonstrated clearly in the case of the uniform line with skin effect, in which case the contribution of this term leads to physically erroneous results. This explains why in the literature only the $\epsilon^{\xi_2 s^{+1/2}}$ term is used in computing skin effect.[2]

General Results

Other simplifications in the mathematics result when the loss terms of (26) are considered. It can be demonstrated that the presence of ρ in all terms past the ξ_2 term results from the divergent nature of the asymptotic series developed for e. Many of the other terms likewise become negligible for practical tapered-line pulse transformers.

On the basis of the preceding analysis, it is possible to write down simplified expressions of each important modification a unit step function EMF will undergo in passing through a tapered-line pulse transformer. These expressions will be valid for the duration of short pulses of usually acceptable distortion.

Time Delay

As would be expected, this delay is determined by the electrical length of the line and the speed of light.

$$\text{Time delay} = \int_0^X \sqrt{lc}\, dx \text{ (seconds)}. \tag{32}$$

Voltage Transformation

As defined here, this ratio relates the load voltage amplitude to the generator EMF and includes not only the impedance changing effect of the tapered line but also the effects of matching at each end of the line.

$$\text{Voltage transformation ratio} = \eta\lambda\sqrt{\frac{\sqrt{l/c}\,|_{x=X}}{\sqrt{l/c}\,|_{x=0}}} \cdot \exp\left\{-\frac{1}{2}\int_0^X r\sqrt{\frac{c}{l}}\,dx - \frac{1}{2}\int_0^X g\sqrt{\frac{l}{c}}\,dx\right\}. \tag{33}$$

The input and output matching terms defined in (21) and (23) are η and λ. The attenuation due to r is completely negligible for practical pulse transformers constructed of self-supporting metal conductors. The attenuation due to g will usually contribute attenuation of no more than a few per cent.

[4] I. A. D. Lewis and F. H. Wells, "Millimicrosecond Pulse Techniques," Pergamon Press, Ltd., London, England, pp. 63–93; 1954.

[5] F. J. Young, E. R. Schatz, and J. B. Woodford, "The optimum transmission-line pulse transformer," *Trans. AIEE*, vol. 79, pp. 220–223; July, 1959.

Lengthening of Rise Time

Fig. 1 shows the skin-effect-induced distortion of the voltage response to a unit step function input. The rise time of this response will be conventionally defined here as the time it takes the voltage response to rise from 10 per cent to 90 per cent of its final value.

$$\text{Rise time} = 31.45\xi_2^2 \text{ (seconds)}, \tag{34}$$

where

$$\xi_2 = -\frac{1}{2}\int_0^x \rho\sqrt{\frac{c}{l}}\,dx. \tag{35}$$

Tilt

The tilt is defined as the normalized slope of the early portion of the load voltage response to a step function input at the generator (see Fig. 2). The tilt depends on both the manner in which the transmission line is tapered and the degree of matching attained at each end of the line.

$$\begin{aligned}\text{Tilt} &= \xi_5\left(\frac{\text{volts}}{\text{volts}}\text{ per second}\right)\\ &= \eta R_0\left\{\frac{1}{4l}\left(\frac{\dot{l}}{l}-\frac{\dot{c}}{c}\right)\right\}\Big|_{x=0} - \frac{\lambda}{8\sqrt{lc}}\left(\frac{\dot{l}}{l}-\frac{\dot{c}}{c}\right)\Big|_{x=X}\\ &\quad -\int_0^x\left\{\frac{1}{\sqrt{lc}}\left(\frac{7}{32}\frac{\dot{l}^2}{l^2}-\frac{5}{32}\frac{\dot{c}^2}{c^2}-\frac{1}{16}\frac{\dot{l}}{l}\frac{\dot{c}}{c}\right.\right.\\ &\quad \left.\left.-\frac{1}{8}\left(\frac{\ddot{l}}{l}-\frac{\ddot{c}}{c}\right)\right)+\frac{1}{4}\frac{\dot{g}}{c}-\frac{1}{4}\frac{g}{c}\frac{\dot{c}}{c}\right\}dx.\end{aligned} \tag{36}$$

The four expressions just derived for time delay, voltage transformation ratio, rise time and tilt represent the simplified results of the analysis. They are valid for the duration of short pulses of usually acceptable distortion. For the special case of constant velocity of propagation or the even more special case of the exponential line where the flare constant $\gamma = \dot{l}/l = -\dot{c}/c$, the four expressions will simplify greatly.

Examples of Two Coaxial Lines with Variable Velocity of Propagation

The type of coaxial tapered line chosen for these examples is somewhat unusual in that it is assumed to be constructed of a 20-foot length of rigid $\frac{3}{4}$-inch copper water pipe and a 20-foot length of no. 25 copper wire. The impedance tapering is accomplished by tapering of the dielectric constant of the dielectric material rather than by variation of the conductor geometry. For the 4-to-1 impedance transformation ratio chosen for these examples, it is necessary to change the dielectric constant over a 16-to-1 range. One way of doing this would be to mix heavily aerated plastic and powdered sintered barium strontium titanate in differing proportions as the line is filled from one end.

Two dielectric constant taper functions will be considered so as to illustrate the effect of taper function on the over-all characteristics of the tapered-line pulse transformer. Each line will be designed to match nominally a 50-ohm generator and a 200-ohm load.

The first taper analyzed will be produced by having the dielectric constant vary linearly with physical position from $\epsilon' = 1.26$ to $\epsilon' = 20.1$.

The second taper analyzed will also have ϵ' vary between 1.26 and 20.1, but in such a manner that the nominal characteristic impedance of the line will vary exponentially with electrical position. A wavefront propagating along this line will see a change in $\sqrt{l/c}$ with time identical to that seen by a wavefront traveling along a true exponential line of the same electrical length. Since the velocity of propagation varies with position, the line will not be exponential with respect to physical position and will therefore be called "electrically exponential."

For both lines, the constant geometry implies a constant l and ρ. Only c and g will vary with position. Dielectric loss is considered proportional to dielectric constant and corresponds to a 100-Mc power factor of 0.1 per cent.

The response of each of the tapered lines to a unit step function generator EMF is determined by use of the simplified expressions (32)–(36). The results are given in Tables I–III (pp. 295 and 296).

TABLE I

Parameters of the Two Lines

	c	g	$\sqrt{l/c}$
	farads per meter	mhos per meter	ohms
Linear taper of dielectric constant	$2.99\cdot10^{-10}(1-0.1539x)$	$1.88\cdot10^{-4}(1-0.1539x)$	$\dfrac{50}{\sqrt{1-0.1539x}}$
Electrically exponential line	$\dfrac{10^{-8}}{(2.840x+5.78)^2}$	$\dfrac{6.283\cdot10^{-3}}{(2.840x+5.78)^2}$	$24.58(x+2.032)$

TABLE II
RESULTS OF THE ANALYSIS

	Delay	Voltage Transformation	Rise Time	Tilt (sec^{-1})
Linear taper of dielectric constant	60.6 nsec	0.980	0.67 nsec	$-4.7 \cdot 10^7$
Electrically exponential line	42.2 nsec	0.987	0.29 nsec	$-4.8 \cdot 10^6$

It is interesting to note the individual contributions of the three terms making up the tilt term. From (36),

$$\text{tilt} = \left(\begin{array}{c}\text{sending}\\ \text{end}\\ \text{term}\end{array}\right) + \left(\begin{array}{c}\text{load}\\ \text{end}\\ \text{term}\end{array}\right) + \left(\begin{array}{c}\text{integral}\\ \text{terms}\end{array}\right).$$

TABLE III
TILT TABULATION

	Sending End Term	Load End Term	Integral Terms	Total Tilt
Linear taper of dielectric constant	$+1.28 \cdot 10^6$	$-8.33 \cdot 10^7$	$+3.52 \cdot 10^7$	$-4.7 \cdot 10^7$
Electrically exponential line	$+8.21 \cdot 10^6$	$-8.21 \cdot 10^6$	$-4.8 \cdot 10^6$	$-4.8 \cdot 10^6$

The negative tilt is about an order of magnitude less for the nominally matched electrically exponential line than for the nominally matched line with a linear taper of dielectric constant. This is a result of the matching conditions since, as Table III indicates, the linearly-tapered line by itself contributes a positive tilt.

CONCLUSIONS

This investigation has been aimed at examining the role of skin effect in the tapered-line pulse transformer. The approximate mathematical method adopted has fortunately turned out to be general enough also to predict pulse response for time durations very much longer than the duration of the rise phenomenon alone. This has permitted a check with the pulse distortion expressions determined by other investigators for the lossless case. The method can be useful to the design engineer in predicting the entire useful response to a short pulse undergoing impedance transformation on a tapered-transmission-line pulse transformer.

As a result of this analysis, it can be concluded that:

1) The rise time of a tapered transmission line is not materially affected by resistive mismatching at either end of the line.
2) The "initial slope" or tilt of the response to a step function can be adjusted over a large range—including both negative and positive values—depending on the taper function of the line and the generator and load resistances.

This latter conclusion seems to bear out previous contentions that any "optimum" taper would have to be a function of the load and generator impedances.[5]

A Waveguide Quadruplexer System*

P. FOLDES†, MEMBER, IRE, AND T. B. THOMSON‡

Summary—**Practical design considerations are presented for a relatively simple four-channel waveguide branching system. The most important electrical characteristic of this system is an extremely low pass-band reflection coefficient (better than 1.5 per cent in 30-Mc band) which has only very small variations with the environmental conditions.**

Introduction

IN A WIDE-BAND frequency-modulated microwave communication system, the ultimate signal-to-noise ratio is usually seriously affected by the feeder distortion of the microwave transmission network [1].

The feeder distortion is the result of the time delayed reflections which are generated by the discontinuities of the long, radio-frequency line. These can be divided into end (antenna, branching system) and internal (joint) discontinuities. In this paper, one source of the end reflection, a branching system with extremely low-reflection coefficient, will be described. A newly developed low-reflection antenna [2] and waveguide system [3] for the same microwave equipment were discussed by the authors elsewhere.

The basic requirements for a modern branching system are the following:

1) low pass-band reflection coefficient,
2) high stop-band insertion loss,
3) high isolation between receiver and transmitter channels,
4) simplicity and reproducibility of fabrication,
5) small size and weight,
6) easy tuning,
7) insensitivity to the environmental conditions.

Apparently, some of the above requirements contradict each other. For instance, in the 2000-Mc band, low loss and simplicity of manufacturing implies the use of waveguide components. However, these components are relatively large and heavy. Of the known types of waveguide filter design, the direct-coupled cavity type assures the smallest over-all size [4]. At the same time, the tuning of this type of filter is relatively difficult. The independency of the filter characteristics from the transmitter output and receiver input impedance can be achieved by the insertion of ferrite isolator elements. These components, however, are temperature sensitive. With an increasing number of RF channels, the branching system becomes more and more complicated, while the pass-band reflection coefficients increase. This limits the bandwidth of the individual RF channels and reduces the over-all voice channel capacity.

The branching system to be discussed is a four-channel waveguide branching network (quadruplexer). As will be shown, this system results in a reasonable compromise between the various requirements. It also can be used as the terminal unit in a more complicated branching system, which utilizes more than four RF channels.

Principle of Operation

The basic concept of the quadruplexer arrangement is shown in Fig. 1. According to the indicated scheme, the quadruplexer is a network with five terminating reference planes. These terminating reference planes will be referred to as terminals in the following. The main, or antenna, terminal A supports all the RF channels of which two are usually transmitter channels, 1 and 2, and two are receiver channels, 3 and 4.

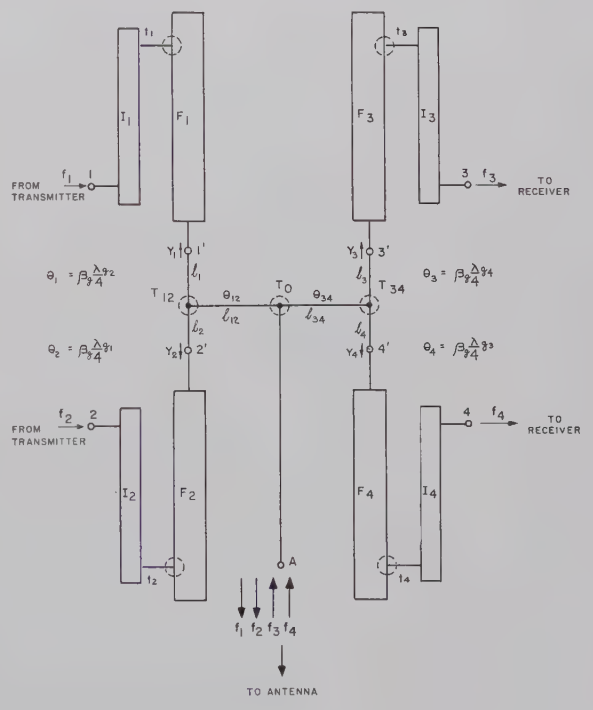

Fig. 1—Basic concept of quadruplexer arrangement.

F_1, F_2, F_3, F_4 = filter sections
I_1, I_2, I_3, I_4 = isolators
t_1, t_2, t_3, t_4 = coaxial—wg transitions
T_{12}, T_{34}, T_0 = Tee junctions.

* Received by the PGMTT, December 5, 1960; revised manuscript received, March 15, 1961.
† Tech. Products Div., RCA Victor Co., Ltd., Montreal, Canada.
‡ Computing Devices of Canada, Ltd., Montreal, Canada.

Ideally, the network connects terminals 1, 2, 3 and 4 to A without any loss in a narrow frequency band centered around f_1, f_2, f_3 and f_4, respectively, while there is no connection between the terminals at any other frequencies. Terminal A is physically connected to terminals 1, 2, 3 and 4 by means of six transmission-line sections. At f_1, f_2, f_3 and f_4 frequencies, the normalized input impedance at terminal A can be unity if the six-line sections are chosen properly and the terminating impedances of these lines have certain frequency functions; namely, they are properly-designed filter impedances. The input impedance of a wave filter depends on its terminating impedance and its internal structure. In a microwave communication system, these terminating impedances are the receiver (crystal mixer) input impedance and the transmitter (traveling-wave tube) hot output impedance. All these vary with the working and aging conditions and may change if crystals or tubes are replaced. Furthermore, different lengths of cable are usually used between the equipment and the branching system which may cause unpredictable phase changes in the receiver and transmitter reflection coefficients. Therefore, it is mandatory to use some kind of isolating attenuator. In Fig. 1 these attenuators are represented as ferrite isolators.

Factors Affecting the Pass-Band Input Reflection Coefficients

The input reflection coefficients at terminals 1, 2, 3 and 4 require less consideration. Even if the band-pass filters are only approximately tuned and terminal A is approximately matched, the generated reflections are absorbed by the ferrite isolators. Therefore, this reflection coefficient is practically determined by the ferrite components itself. Furthermore, the requirement for a low-reflection coefficient at these terminals is less severe because the length of cable between the branching system and equipment is short and the corresponding feeder distortion is low.

The reflection coefficient at terminal A is far more important. This is affected in a pass band by the following factors:

1) the reflection coefficient of the loads at the equipment end,
2) the input or output reflection coefficient of the ferrite isolators,
3) the reflection coefficient of the coaxial to waveguide transition,
4) the input impedance of the terminated band-pass filter,
5) the characteristics of the coupling line network,
6) the proximity effect caused by other filters,
7) the junction effects of the Tee connectors.

Only the most important factors will be briefly discussed here.

Terminals 1, 2 and 3, 4 are connected to the transmitters and receivers of the communication equipment at one repeater station, while at the next repeater station 1, 2 and 3, 4 are interchanged with each other.

Fig. 2(a) and 2(b) show the typical transmitter and receiver output and input reflection coefficients, respectively. These reflection coefficients are lowered by the ferrite isolators (by at least 26 db) to a 0.42 per cent average, effective terminating reflection coefficient.

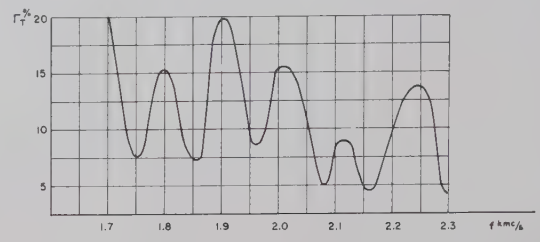

(a)

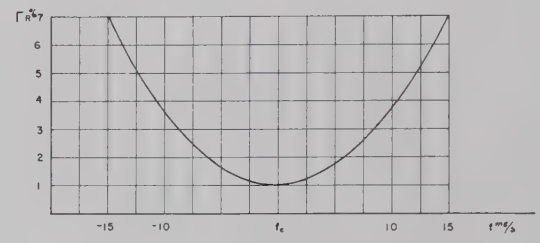

(b)

Fig. 2—(a) Typical value of the output reflection coefficient of the 7642 TW tube. $\Gamma_{T\,av} = 10.3$ per cent (contribution to the average top-channel distortion is determined by $\Gamma_{T\,av}$). (b) Average value of the receiver input reflection coefficient around the f_c carrier. $\Gamma_{R\,max} = 7$ per cent (contribution to the average top channel distortion is determined by $\Gamma_{R\,max}$).

A five-section direct-coupled filter is used as the filter building block of the quadruplexer system. The stop-band insertion-loss requirement could be fulfilled by a four-section filter. However, the five-section arrangement results in more symmetrical group-delay variations and greater flexibility in tuning.

In the accepted design six pair of inductive posts are placed approximately at equal distances along the waveguide. In the middle of the waveguide, between each pair of inductive posts, additional (coupling) screws are added which make it possible to vary the reflections generated in these cross sections. The effective line length between the reference planes of the inductive posts is made variable by other (tuning) screws placed equidistantly between the coupling screws.

Fig. 3 shows the measured input impedance curve of such a filter. The reference plane is fixed at the cross section where the effective short circuit can be measured in the input impedance at a frequency considerable higher than the center frequency of the pass band. Fig. 3(a) shows the impedance curve in the transition and stop band, while Fig. 3(b) shows the curve in the pass band.

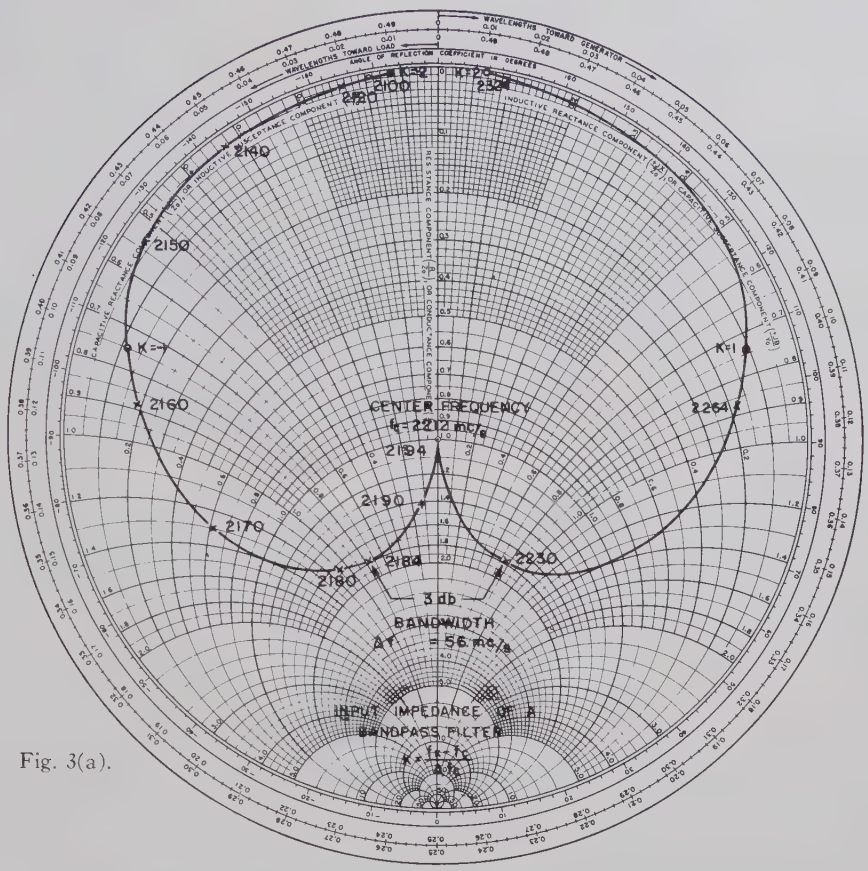
CENTER FREQUENCY
f = 2212 mc/s
3 db
BANDWIDTH
Δf = 56 mc/s
INPUT IMPEDANCE OF A
BANDPASS FILTER
K=1
K=∞
2100
2120
2140
2150
2160
2170
2180
2184
2190
2194
2230
2264

Fig. 3(a).

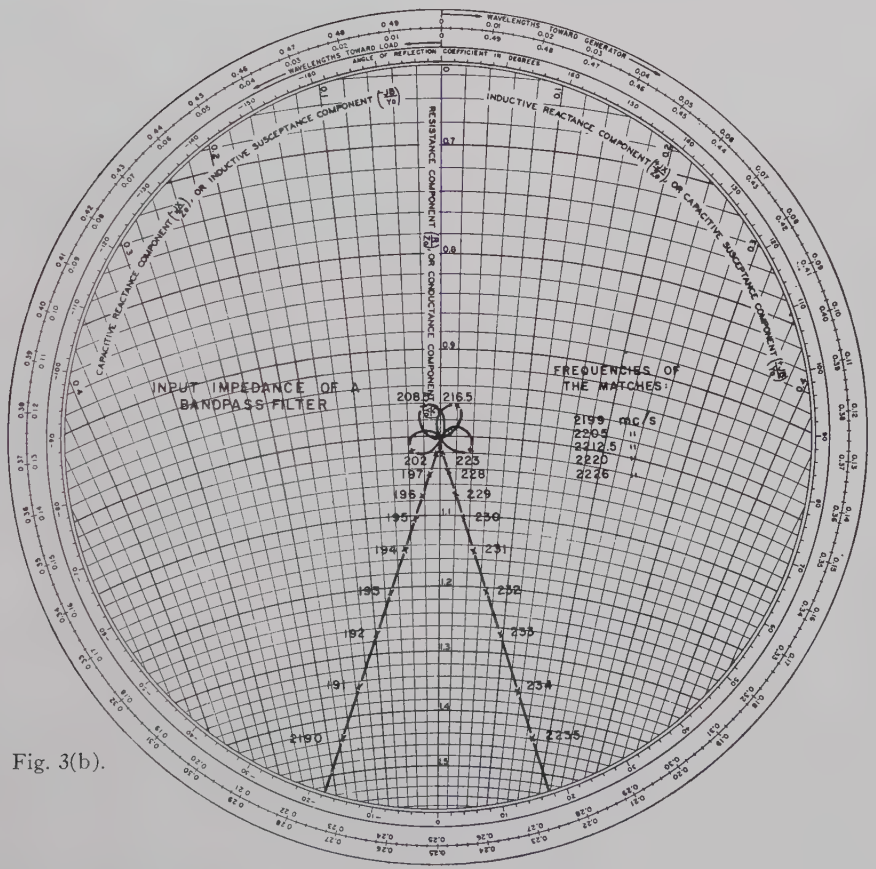
INPUT IMPEDANCE OF A
BANDPASS FILTER
FREQUENCIES OF
THE MATCHES:
2199 mc/s
2205
2212.5
2220
2226
208
202
197
195
194
193
192
191
2190
2165
223
228
229
230
231
232
233
234
2235

Fig. 3(b).

Fig. 4 indicates the reflection coefficient in the pass band, which is less than 1.5 per cent in ±15-Mc band, if the filter is properly terminated.

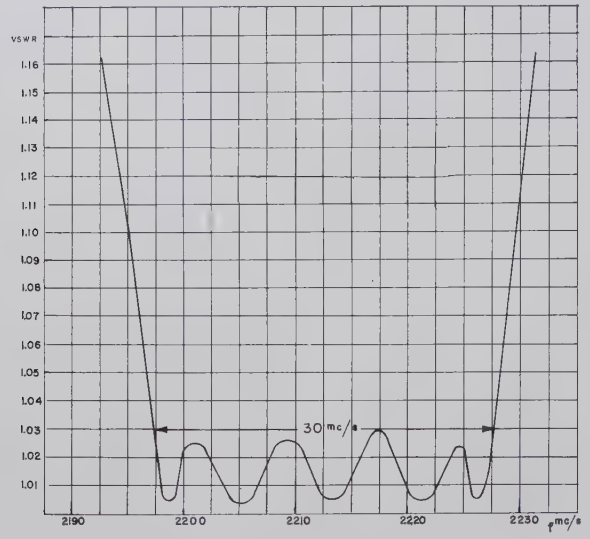

Fig. 4—Pass band reflection coefficient of a band-pass filter.

Fig. 1 shows the electrical schematics of the coupling line network. In this figure, terminal A represents a reference plane in the antenna line very close to the T_0 junction, while 1′, 2′ 3′, and 4′ represent the reference planes where the band-pass filters show their stop-band short circuit.

The line section between T_{12} and 1 is terminated with filter F_1 which has its pass band at a frequency f_1, or a wavelength λ_{g1}. Similarly, terminals 2, 3 and 4 pass the waves with λ_{g2}, λ_{g3} and λ_{g4} wavelength. According to Fig. 1, the line section between T_{12} and 2 has no effect on the junction T_{12} at a wavelength λ_{g1}, assuming that this branch line is terminated by a perfect short circuit. However, the line sections between 3 and T_{34} are not resonant at λ_{g1} wavelength (their lengths are $\lambda_{g3}/4$ and $\lambda_{g4}/4$, respectively). Consequently, a finite reactance will appear at T_{34}. The right-hand side of the network will cause the smallest effect at both λ_{g1} and λ_{g2} wavelength if the l_{34} line length is determined at $\lambda_{g12} = (\lambda_{g1}\lambda_{g2})^{1/2}$ to compensate the reactance, which would appear in T_{34} at this wavelength. The above consideration can be applied for the left-hand side of the network at $\lambda_{g34} = (\lambda_{g3}\lambda_{g4})^{1/2}$ to determine l_{12}. Assuming ideal filters with unit input impedance in their pass bands and zero input impedance in their stop bands, Table I contains the calculated input admittance values at terminal A for a typical frequency plan. The calculation neglects the junction effects.

According to Table I, the deviations from the unit admittance are small. These deviations shift the filter input admittance curve slightly. However, this effect can be easily compensated by the tuning of the band-pass filter.

In practice the values in Table I are modified by the fact that the filters are not ideal. According to Fig. 3(a), the input impedance of the band-pass filter drops rapidly from unity as K increases (K is the relative detuning of the filter expressed in 3-db bandwidth units). If $|K| \geq 2$, the filter already can be approximated by a short circuit. These conditions can be analyzed in any pass band, say in channel 4. Here, the effect of filters F_1 and F_2 are negligible, because for these filters $|K| \gg 1$. Channel 3 filter, however, is tuned in the transition band of F_4 and the two filters mutually affect each other. For instance, for $K=1$ and 2, the input impedance of F_3 will be $0.11+j0.75$ and $0.05+j0.06$, respectively. The reactive component can always be compensated by a correction of the l_3 line length, but the real component appears parallel with the F_4 filter and causes loss and mismatch.

TABLE I
CALCULATED LINE LENGTH EFFECT FOR A TYPICAL FREQUENCY PLAN

Channel	Carrier Frequency (Mc)	Normalized Input Admittance at Terminal A
1	1912.5	$1.0170-j0.0006$
2	1970.5	$0.9788+j0.0006$
3	2212.5	$1.0240-j0.0011$
4	2270.5	$0.9720+j0.0020$

CHARACTERISTICS OF THE COMPLETE BRANCHING SYSTEM

Construction

In the case of a high-quality branching network, the maintenance of the mechanical dimensions in operations is extremely important. If the desired reflection coefficient is in the order of 1 per cent, then the inside dimensions of the waveguide structure should be kept within a few thousands of an inch after the system is tuned, in order to assure a reflection coefficient variation of not more than 0.1 per cent.

The above requirement is achieved by the use of a rigid supporting frame and a nonstandard, heavy-wall waveguide.

Figs. 5 and 6 show the mechanical construction and the outside dimensions of the quadruplexer.

The microwave structure is built up from copper waveguide ($4.300'' \times 2.150''$ inside dimensions, with $0.125''$ wall thickness). Relatively large manufacturing variations

$$\begin{pmatrix} + & 0.000'' \\ - & 0.008'' \end{pmatrix}$$

are tolerated in the cross section because the tuning method of the filters automatically eliminates the effects of manufacturing variations. However, the cross-section dimensions of the waveguide at terminal A are sized to

$$4.300'' \begin{matrix} + \ 0.000'' \\ - \ 0.002'' \end{matrix} \times 2.150'' \begin{matrix} + \ 0.000'' \\ - \ 0.002'' \end{matrix}$$

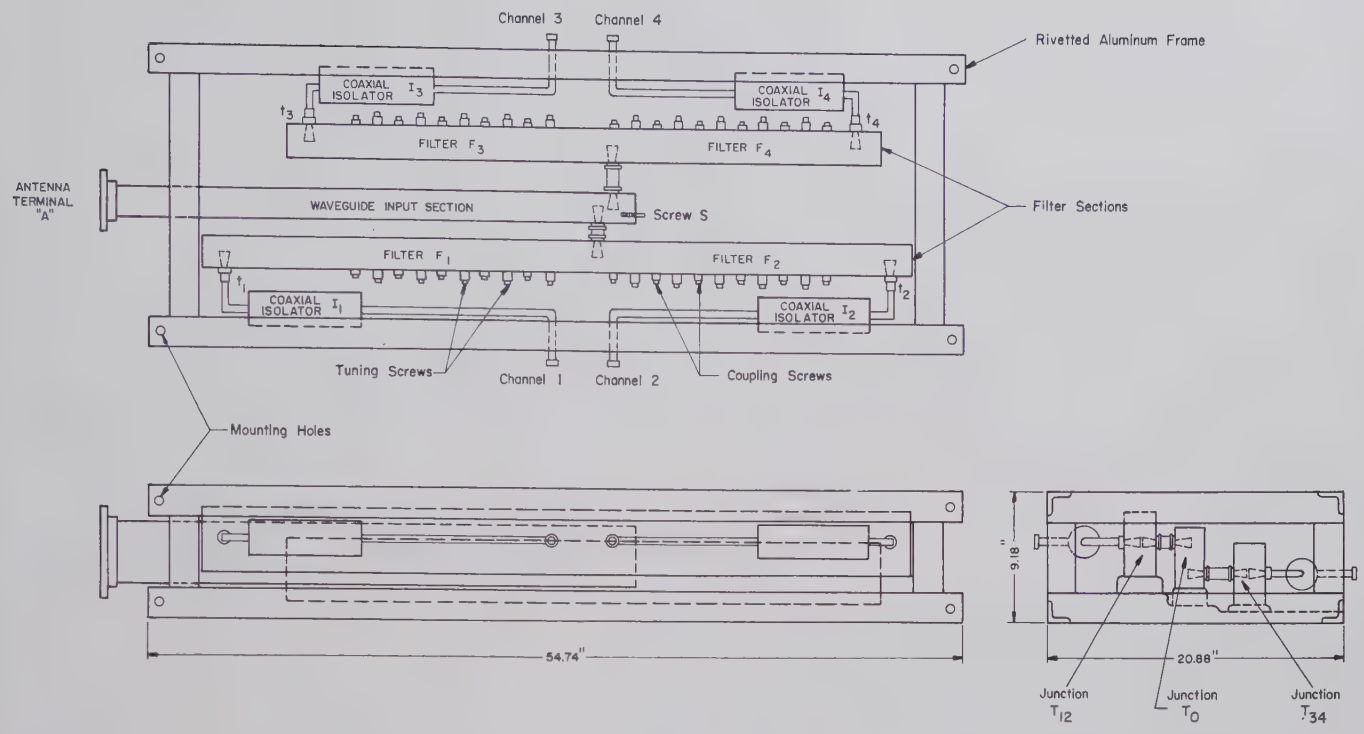

Fig. 5—Mechanical layout of the quadruplexer.

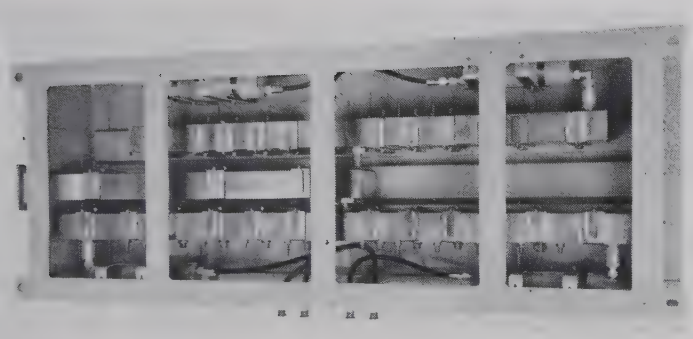

Fig. 6—Internal view of quadruplexer.

to assure a low-reflection transition between the quadruplexer and the waveguide feeder [3]. The efficiency of the joints between the various microwave components (at T_{12}, T_{34} and T_0) were the object of careful consideration. Silver-plated and rhodium-flashed metex washers are used in the flat flange joints at the ends of the coaxial coupling lines.

Tuning

As was mentioned previously, the aim of the discussed quadruplexer design was to obtain and maintain pass band reflection coefficients at terminal A in the order of a few per cent. Obviously, this specification imposes rather severe requirements on the necessary test equipments. Primarily, for tuning purposes, an intermediate power sweep generator and a high-quality waveguide directional coupler were developed. This coupler has tight coupling (approximately 7 db) to allow the detection of small reflected signals. The directivity is approximately 52 db, which is equivalent to 0.25 per cent internal coupler reflection, and thus ± 0.25 per cent error in the measurement of reflection coefficient.

The tuning procedure is reasonably straightforward. The resonant frequencies of the consecutive filter cavities follow a certain order to assure the low-reflection coefficient. The tuning procedure is based on monitoring the reflection coefficient at terminal A with an oscilloscope.

Due to the proximity effect, some interaction can be experienced between the individual filters. Therefore, it is necessary to make a second approximation in the tuning, a slight readjustment of the first cavities of the individual filters.

The tuning time of a quadruplexer is basically affected by two factors: 1) the skill of the individual operator, and 2) the reproducibility of the contact at the coupling and tuning screws.

Considerable time was spent to obtain a satisfactory design for the screw mechanism. The design requirements for such a mechanism can be summarized as follows:

1) smallness and reproducibility of the contact impedance between the screw and the waveguide wall during tuning,
2) locking facilities, which do not change the screw position after the filter tuning is completed,
3) simplicity, for quantity production.

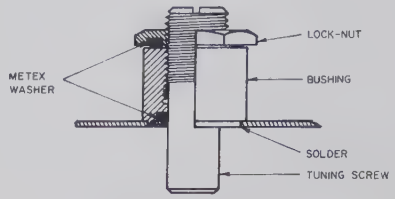

Fig. 7—Tuning mechanism.

TABLE II

ELECTRICAL AND MECHANICAL CHARACTERISTICS OF THE QUADRUPLEXER

Characteristics	Production Figure*	
	At Room Temperature	In −80 to +150 F Temperature Range
Size	54.74×20.88×9.18 inch	
Weight	200 pounds	
Tuning Range:		
Channel 1	1790–1910 Mc	
Channel 2	1890–2110 Mc	
Channel 3	2090–2210 Mc	
Channel 4	2190–2310 Mc	
Bandwidth between the 3-db insertion loss points	55–60 Mc	
Pass-band loss (at carrier frequency) including isolator loss	1.27 db	
Stop-band loss (at ±80 Mc from carrier frequency	70 db	
Minimum isolation between receiver and transmitter channels	75 db	
Average reflection coefficient in the 30-Mc pass band at terminal A†	1.3 per cent	2.1 per cent
Maximum input reflection coefficient in the 30-Mc pass band at terminal A†	1.7 per cent	2.7 per cent
Average input reflection coefficient in the 30-Mc pass band at terminal 1, 2, 3, or 4	3.8 per cent	
Maximum input reflection coefficient in the 30-Mc band at terminal 1, 2, 3 or 4.	4.5 per cent	

* Average figures based on 12 production units. † The load on terminals 1, 2, 3, 4 is as given in Fig. 2.

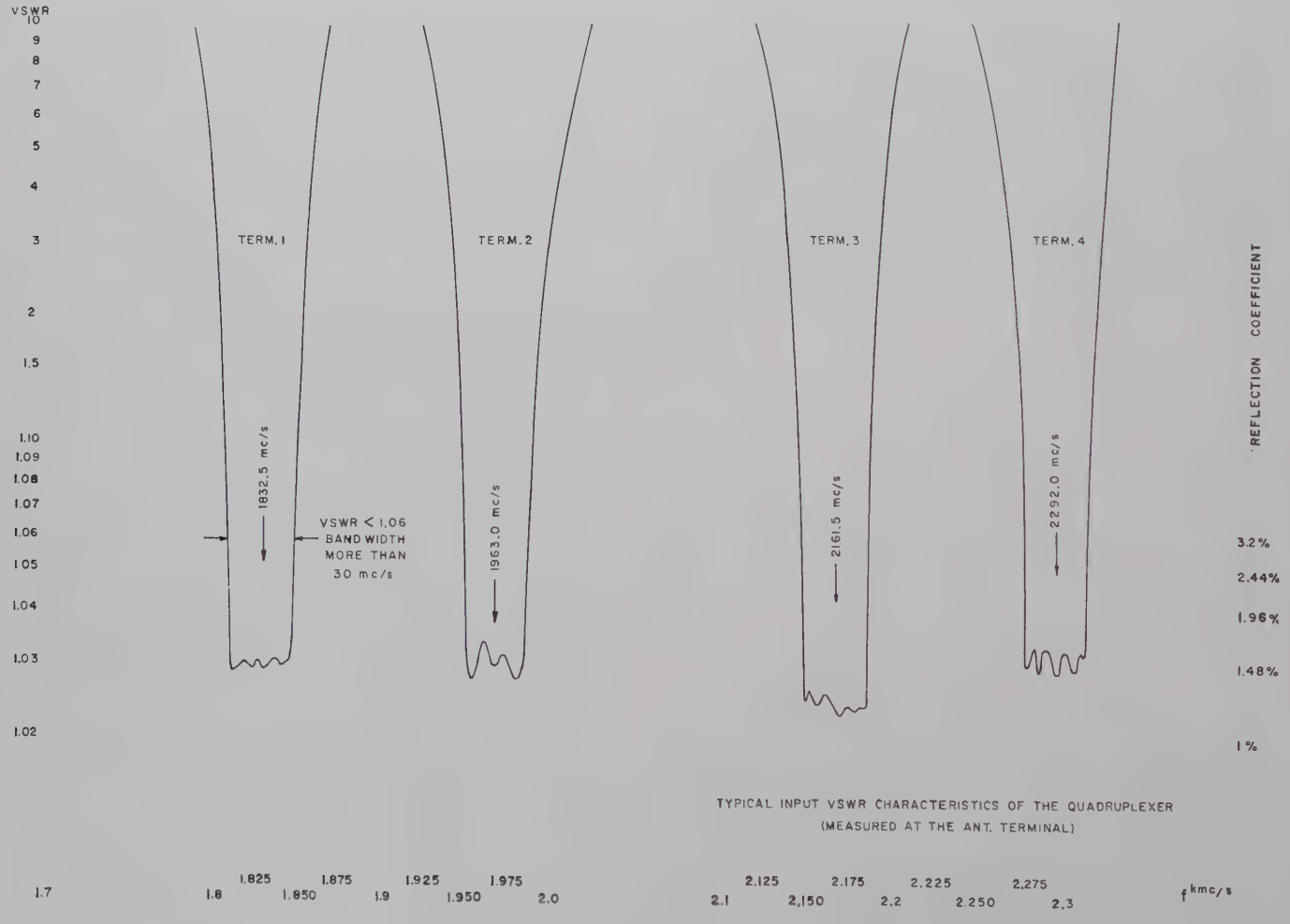

Fig. 8(a).

Three different types of screw arrangements were designed and tested. Fig. 7 shows the finally accepted version. This arrangement consists of a tuning or coupling screw with a threaded portion and a plain surface which makes contact on a metex washer firmly held in the bushing. This method provides contact between the screw and the bushing in the plain of the waveguide wall. Very exact control can be exerted over each cavity whether the locking nut is loose or tight. The lock nut also has a metex washer imbedded in its lower surface to provide locking tension. The lock nut does cause some drag on the screw when it is tightened, but this can easily be overcome by holding the screw against the thread. This method is adapted for use in the quadruplexer because the larger cost in fabrication is compensated by the saving in the tuning time.

With the above precautions, the average tuning and testing time of the completed four-channel branching system is approximately eighteen working hours.

Electrical Characteristics

The major characteristics of the quadruplexer are exhibited in Table II. The indicated figures are averages based on twelve production units. Fig. 8 (pp. 302–303) shows in more detail some of the electrical characteristics. Fig. 8(a) shows a typical input reflection coefficient characteristic at terminal A. As can be seen, each channel has approximately 1.5 per cent average reflection coefficient in a 30-Mc band while there is some variation in the shape of the pass band. Fig. 8(b) indicates the insertion-loss characteristics between terminal A and a typical output terminal. The larger part of the midband insertion loss is caused by the ferrite isolator. Fig. 8(c) represents the isolation between an adjacent transmitter and receiver channel (channels 2 and 3). It should be noted that the quadruplexer arrangement increases the transmitter-receiver isolation relative to the filter insertion loss because of the additional filter characteristics of the T_0 junction.

Effect of the Environment

General Requirement

In a long-haul microwave communication system, the radio equipment usually is installed in a more or less temperature controlled room. However, any decrease in the allowed temperature variations increases the difficulty of maintaining the performance, and a power failure of the heating equipment may cause serious deterioration in the operation. Therefore, it is advantageous to increase the useful temperature range of the individual components. A temperature range of $-80°F$ to $+150°F$ was specified for the quadruplexer.

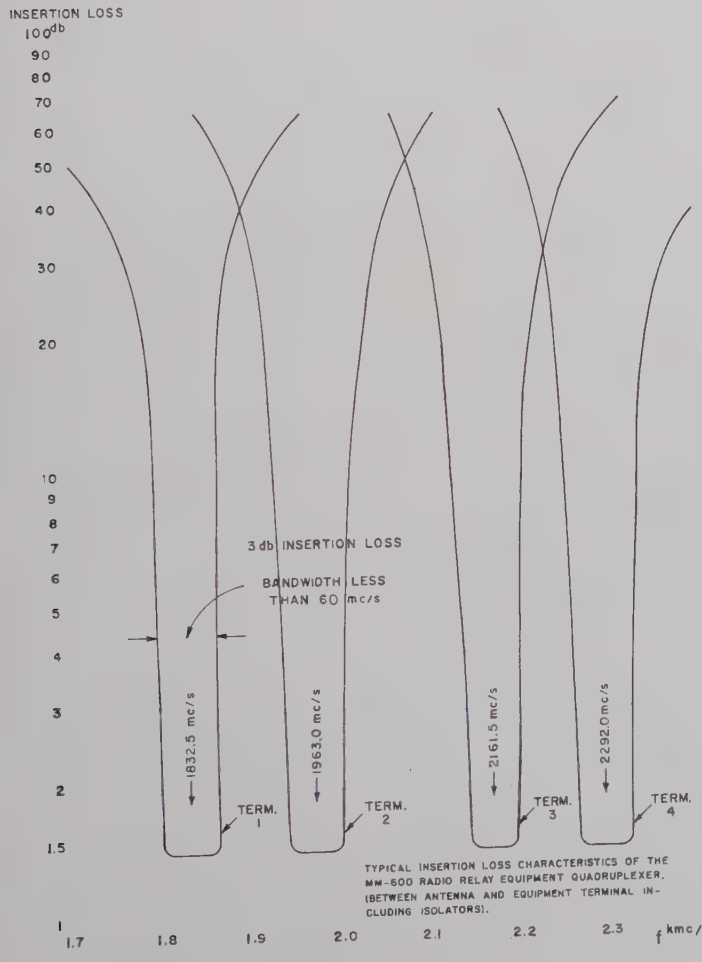

TYPICAL INSERTION LOSS CHARACTERISTICS OF THE MM-600 RADIO RELAY EQUIPMENT QUADRUPLEXER. (BETWEEN ANTENNA AND EQUIPMENT TERMINAL INCLUDING ISOLATORS).

Fig. 8(b)

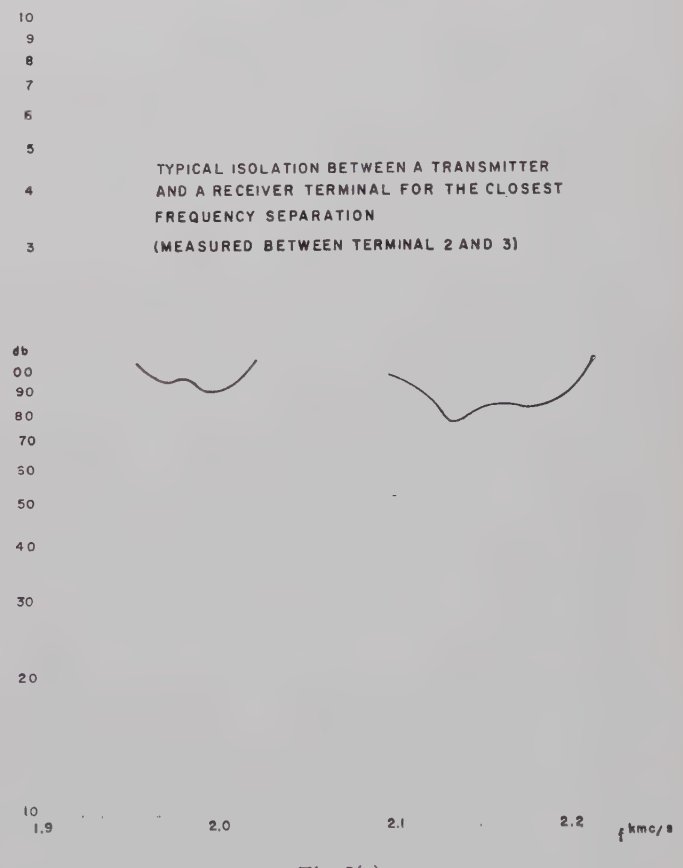

Fig. 8(c)

Among other environmental requirements, the effect of vibration and shock are of particular interest. In spite of the static-type installation of the unit, mechanical vibration may occur in the system during shipping and after installation due to the tower vibration which may be transferred through the waveguide.

Test Facilities and Methods

The temperature sensitivity of the input reflection coefficient of the quadruplexer was measured in a 300-cubic-foot stratosphere chamber. The temperature was measured in the chamber and directly on the waveguide wall of the quadruplexer. The readings were taken when the chamber temperature and the quadruplexer temperature coincided.

The vibration tests were performed on an electrodynamic vibrator with a maximum capacity of 500 pounds. The vibration test basically served to determine the effectiveness of different packing methods. The average of the input reflection coefficient in the 30-Mc pass band served as the basis of comparison. This average value was determined from the measurements performed before and after the vibration test.

Effect of the Temperature

Obviously any temperature change is most pronounced in the input reflection coefficient at terminal A. For this reason only this characteristic was measured. The input reflection coefficient may be affected by three factors:

1) thermal expansion and deformation of the microwave structure,
2) temperature variation of the contact impedance at the tuning screws,
3) temperature variation of the ferrite isolators.

The ferrite isolators were replaced by precision coaxial dummy loads to investigate the first and second factors. Fig. 9 shows the input reflection coefficient at terminal A of a typical channel (channel 3) as a function of temperature. Fig. 9(a), (b), and (c) shows the measured parameter at 75°F, 150°F and 75°F. The last curve was measured after the temperature cycle and shows that the temperature cycle had negligible permanent effect. The average reflection coefficient in the 30-Mc pass band was 0.56, 0.76 and 0.56 per cent at the respective temperatures. It can be concluded that a variation in this order is tolerable and there is no need to build up the structure using a less temperature-sensitive material (invar).

The temperature sensitivity of the individual ferrite isolators were investigated separately and then with the complete unit. Fig. 10 shows the total temperature variations of the reflection coefficient of one quadruplexer channel. This includes the effects of the various factors, but among these the temperature sensitivity of the fer-

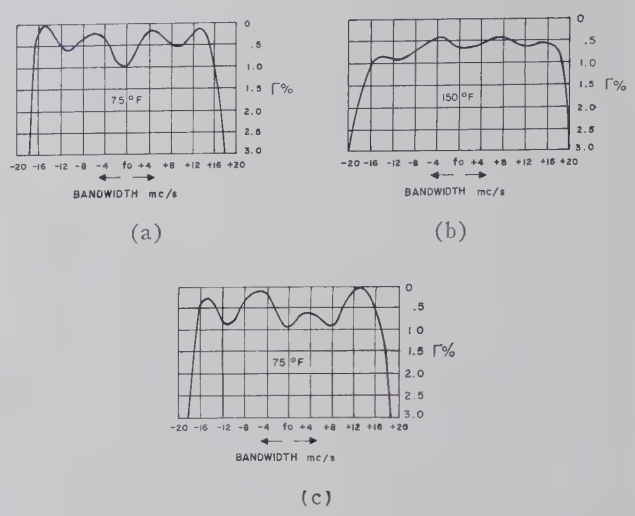

Fig. 9—Input reflection coefficient of a typical channel at terminal A, as a function of temperature (dummy load terminations). $f_0=2172$ Mc. (a) Initial tuning at temperature +75° F, $\Gamma_{AV}=0.56$ per cent. (b) At temperature +150°F, $\Gamma_{AV}=0.76$ per cent. (c) After temperature cycling. $\Gamma_{AV}=0.56$ per cent.

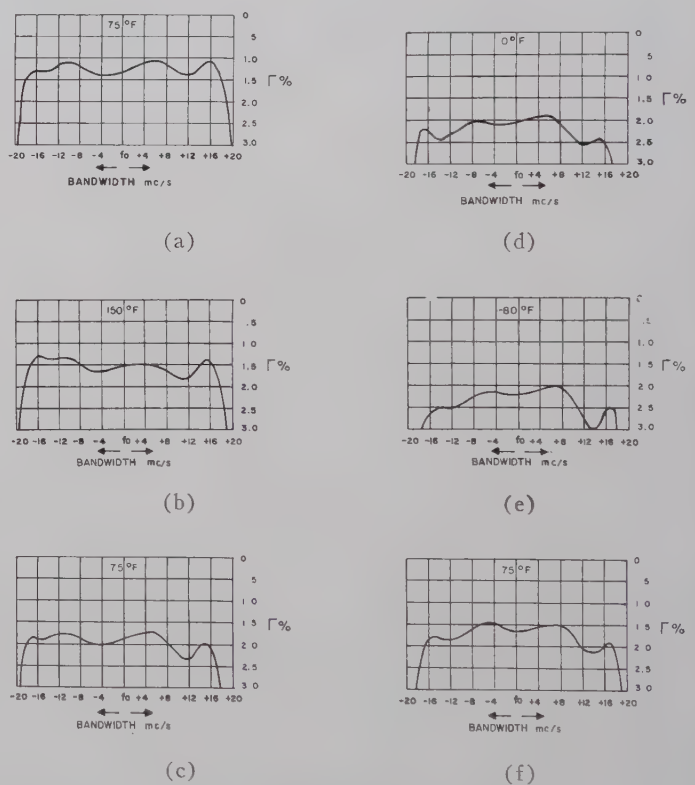

Fig. 10—Input reflection coefficient of a typical channel at terminal A, as a function of temperature (ferrite isolator terminations). $f_0=2172$ Mc. (a) Initial tuning at temperature +75° F. $\Gamma_{AV}=1.32$ per cent. (b) $\Gamma_{AV}=1.50$ per cent. (c) $\Gamma_{AV}=1.97$ per cent. (d) $\Gamma_{AV}=2.26$ per cent. (e) $\Gamma_{AV}=2.35$ per cent. (f) After temperature cycling. $\Gamma_{AV}=1.74$ per cent.

rite isolator is the dominant. In the final design, an external magnet-type isolator is employed with extremely stable electrical characteristics. The series of curves on Fig. 10 shows the temperature variation of the input reflection coefficient for a typical channel through a full temperature cycle (from +75°, +150°, 0°, −80°, +75°F). It can be seen that the variations in the pass band shape are quite tolerable for all practical purposes. Fig. 11 shows the variation of the average reflection coefficient in a 30-Mc pass band as a function of temperature. It can be seen that, in the measured case, the average reflection coefficient is 2 ± 0.7 per cent and shows a certain temperature hysteresis, *i.e.*, has different values at a given temperature depending on the previous temperature conditions of the unit.

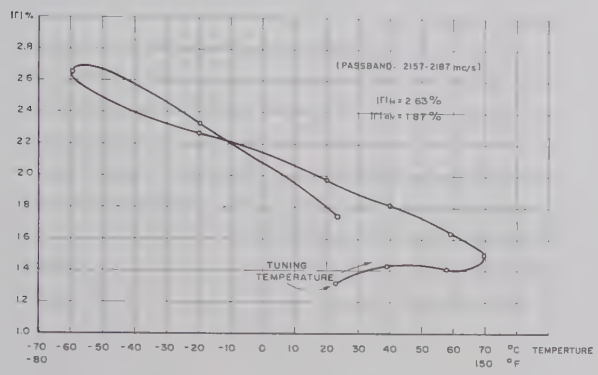

Fig. 11—Typical variation of the average reflection coefficient in one quadruplexer channel.

Vibration

A microwave communication equipment quite often has to be installed in remote areas, and careful handling during shipping cannot always be assumed. Therefore a special, reusable packing case was designed for the quadruplexer, and the effect of vibration was tested.

Fig. 12(a) shows the arrangement of the quadruplexer in the packing case, while Fig. 12(b) indicates the cross section of the packing material. The quadruplexer is lying on a number of damping rods. Each damping rod has a different self-resonant frequency in the 1- through 15-cps frequency band.

The box with the quadruplexer inside was placed and firmly held on the vibration table. The vibration amplitude was adjusted to the curve shown in Fig. 13 and was cycled for two hours. Fig. 14 show a typical filter tuning before and after vibration. Although the figure shows some deterioration in the input reflection coefficient, the change is negligible for all practical purposes. In fact, the comparison between the factory measured data (after tuning) and the field measured data (after installation) did not show any deterioration within the measurement error. These latter measurements were conducted on twelve quadruplexer units.

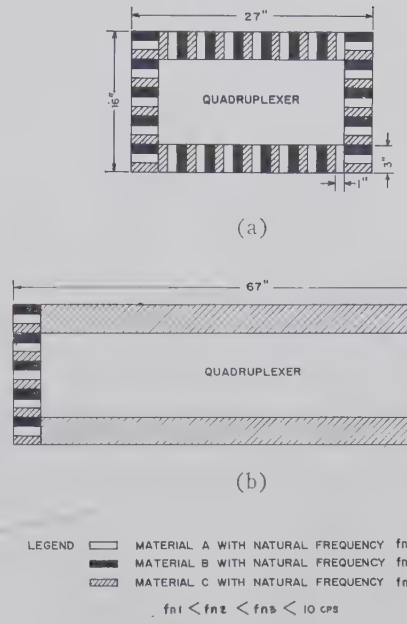

Fig. 12—Design concept of special packing case for the quadruplexer. (a) End cross section of quadruplexer packing case. (b) Longitudinal cross section of quadruplexer packing case.

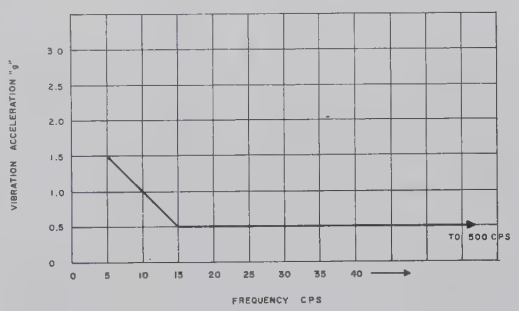

Fig. 13—Vibration acceleration vs frequency applied on quadruplexer during vibration tests on packing case.

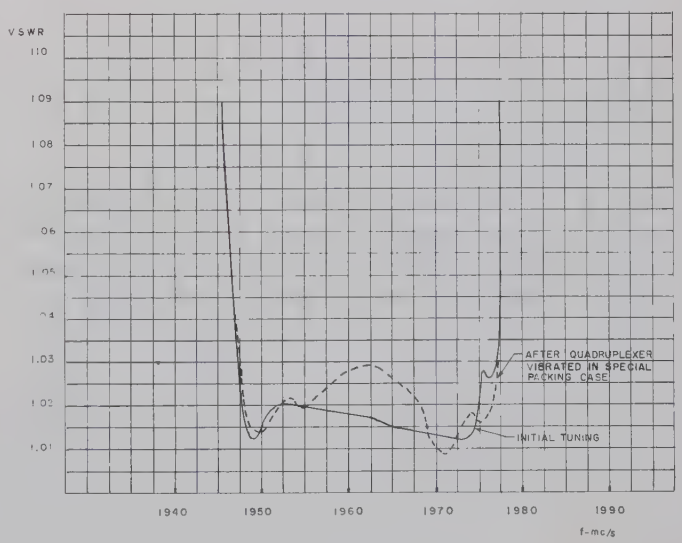

Fig. 14—Deterioration caused in filter tuning due to vibration.

Conclusion

The presented experimental data show that it is possible to connect four waveguide band-pass filters into a branching network which has an extremely low pass-band reflection coefficient. The various side effects of such a network (line length, filter proximity, junction effect) can be compensated by a proper coupling network and by the tuning possibilities of the filter sections themselves. After the basic problem is solved, the most important practical requirement for such a network is its independency from external parameters (terminal loading, temperature, vibration, shock). The elimination of these factors is possible, but requires particular design and an increase in cost relative to the conventional design.

Bibliography

[1] R. G. Medhurst, "Echo-distortion in frequency modulation," *Electronic and Radio Engr.*, pp. 253–259; July, 1959.
[2] P. Foldes and S. Komlos, "Theoretical and experimental study of wide band parabolic antenna with central reflector feed," *RCA Rev.*, vol. 21, pp. 94–116; March, 1960.
[3] P. Foldes and N. Gothard, "Synthesis of low-reflection waveguide joint systems," IRE Trans. on Microwave Theory and Techniques, vol. MTT-9, pp. 169–175; March, 1961.
[4] S. B. Cohn, "Direct-coupled-resonator filters," Proc. IRE, vol. 45, pp. 187–196; February, 1957.
[5] C. G. Montgomery, R. H. Dicke, and E. M. Purcell, "Principles of Microwave Circuits," McGraw-Hill Book Co., Inc., New York, N. Y., p. 295; 1948.

Some Recent Findings in Microwave Storage*

J. D. KELLETT†, member, ire

Summary—**This paper describes an experimental investigation of frequency memory in a recirculating amplifier storage device. The objective of the investigation was to determine what mechanism caused injected energy to shift to preferred storage frequencies. Using fast-acting crystal switches, the output energy was selectively viewed, and it was found that the energy in any circulation when viewed separately was of the input frequency. The spectrum photographs which are included in the paper show that the recirculating amplifier when operating with an open loop gain greater than unity does not oscillate at preferred frequencies.**

Introduction

ALTHOUGH a complete historical search on the origin of RF storage has not been conducted, it appears that much of the early work can be attributed to L. M. Field, W. A. Edson, R. W. DeGrasse, and T. B. Warren of Stanford University. The work at Stanford resulted in memory devices capable of storing frequency for considerable periods of time. The need for such devices in military systems prompted continued development, and as a result, broad-band storage devices capable of reasonable storage times have been built.

The basic storage device, consisting of an amplifier and a delay line in a closed loop with appropriate input and output coupling devices, operates on a recirculating principle. An instruction pulse applied at the input is amplified by a TWT, delayed and attenuated by the delay line, and reamplified by the TWT. The TWT also supplies the limiting and suppression characteristics necessary for storage operation. Limiting is obtained by operating the TWT in the region of saturation where the gain vs power-in curve exhibits a negative slope; suppression is obtained from that characteristic of a saturated TWT or other limiter which in the presence of a strong signal exhibits a lower value of gain for a weaker signal than for the strong signal. Thus, when the storage system is operating with an open loop gain greater than unity, the limiting characteristic prevents the signal from increasing to an infinite magnitude and the suppression characteristic retards the build-up of unwanted signals such as noise.

The basic storage system as described above suffers two major limitations:

1) Storage time, the length of time an input signal can be stored before noise build-up takes over, is limited if very large bandwidths are considered.
2) Frequency accuracy, the amount of energy at the instruction frequency as compared to total energy in the system, may be low.

This report deals exclusively with the frequency-accuracy limitation. The treatment is limited to short storage times, 10 microseconds or less, and it is assumed that TWT and microwave component parameters are such that the necessary storage time is obtainable. Consistent with these assumptions, the reported data has

* Received by the PGMTT, December 13, 1960; revised manuscript received, March 16, 1961.
† Sylvania Electronic Systems, Commun. Lab., Amherst, N. Y.

been taken at frequencies for which the system exhibited reasonable storage times. It will be shown that exact frequency storage can be achieved if the output energy is properly extracted from the loop.

Frequency Accuracy of a Storage Device

To be useful in most applications, a storage device must be capable of memorizing the frequency of the received signal. The advantages of a system capable of storing equally well all frequencies within the band of operation over a system capable of storing only at discrete frequencies is readily apparent. Thus, frequency accuracy when defined as the per cent of total output power within a given bandwidth centered about the input frequency can be used as a figure of merit for storage devices.

It has previously been thought that such a storage system as represented in Fig. 1 was capable of storing only at discrete frequencies.[1–3] This device, often described as a multimode oscillator when having an open loop gain greater than unity, operates on a recirculation principle. An instruction pulse applied at the input is amplified by the TWT, delayed and attenuated in the delay network and reapplied to the TWT input. If the instruction pulse width is made equal to the delay time of the delay network and the frequency is such that the total electrical length of the loop is an integral number of wavelengths, then each circulation is in phase and a concentration of energy at the input frequency is seen at the output. A typical spectrum photograph for this condition is shown in Fig. 2.

Next, consider that the instruction pulse width is again made equal to the delay time of the delay unit, but the input frequency is such that the total electrical length of the loop is an odd number of half wavelengths. Each circulation is now π radians out of phase with its neighboring circulation, and a spectrum photograph of such a condition (Fig. 3) shows the output energy to have shifted and to be concentrated at the frequencies for which the electrical length of the loop is an even number of half wavelengths.

For frequencies intermediately between the two cases sighted above, observations of the output always show a concentration of energy at those frequencies for which all circulations are in phase, with the greatest concentration of energy at the nearest such frequency. The frequencies at which the energy is concentrated are called preferred frequencies or preferred modes. The frequency spacing between preferred frequencies is determined by the delay in the loop and is given by $\Delta f = 1/\tau_0$, where τ_0 is the total delay time around the loop. It is generally interpreted that the system is oscillating at one or more of the preferred modes, and the output energy is concentrated at preferred frequencies.

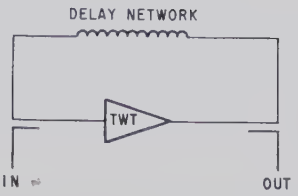

Fig. 1 Basic storage loop.

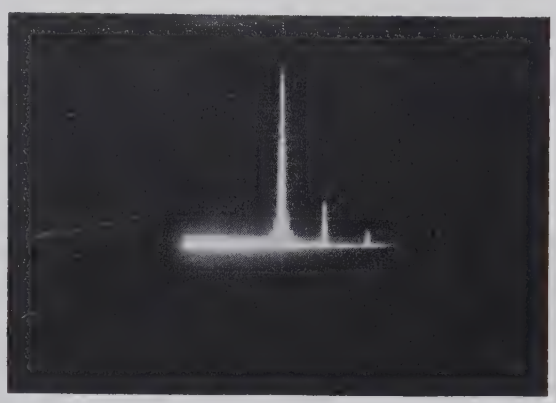

Fig. 2—Typical spectrum of 2 μsec of storage on a preferred frequency.

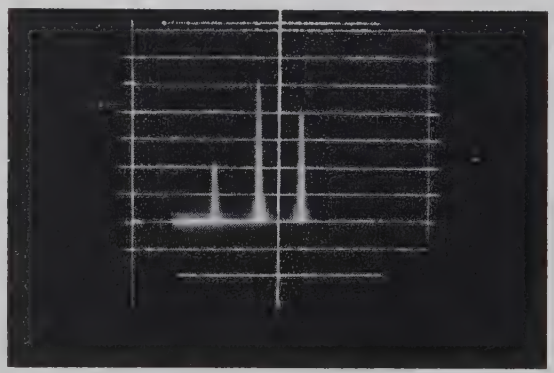

Fig. 3—Typical spectrum of 2 μsec of storage midway between preferred frequencies.

Adopting the viewpoint that a recirculating amplifier when operating with an open loop gain greater than unity oscillates at the nearest frequency for which a favorable phase shift exists (electrical length of loop an integral number of wavelengths), brings up some interesting questions. If the instruction pulse width is slightly less than the delay time of the delay network such that the circulations do not overlap each other, what mechanism causes oscillations to occur at preferred frequencies? How long after initiation of the instruction pulse do oscillations first appear? Does the energy at the instruction frequency shift suddenly or gradually to the preferred modes?

[1] W. A. Edson, "Frequency Memory in Multi-Mode Oscillators," Electronics Res. Lab., Stanford University, Stanford, Calif., Tech. Rept. No. 16; July 19, 1959.
[2] R. W. DeGrasse, "Stability of Multi-Mode Oscillatory Systems," Electronics Res. Lab., Stanford University, Stanford, Calif., Tech. Rept. No. 18; August 9, 1954.
[3] H. C. Lee, "Linear Analysis of Multi-Mode Oscillatory Systems," Electronics Res. Lab., Stanford University, Stanford, Calif., Tech. Rept. No. 20; July 26, 1954.

In view of recent improvements in high-speed crystal switches, it was felt that the answers to these questions could be obtained most readily from an experimental study of an actual storage device incorporating high-speed crystal switches.

Experimental Setup

Fig. 4 shows a block diagram of the experimental storage device used in this investigation. The storage loop consists of a TWT, a delay line, a crystal switch, input and output directional couplers, and a variable attenuator. Delay lines of both coaxial and waveguide variety were used as delay networks. The specific delay line used in the various tests will be noted.

The "loop gate" crystal switch, capable of rise and fall times of less than 10 nanoseconds, is used to gate the storage loop on for the desired storage time. The variable attenuator is used to adjust the loop loss and thus select the operating point of the TWT.

The instruction pulse is obtained by gating the output of a CW signal source with fast-rise time crystal switches. The output energy extracted by the 3-db directional coupler is passed through an "out gate" crystal switch and then fed to a spectrum analyzer, a narrow-band receiver, or a broad-band detector. The "out gate" switch is controlled in both its "on time" and its "time position" relative to the instruction pulse. Thus, any circulation can be viewed separately, or any number of circulations can be viewed together. Repetitive operation of the storage system, necessary for visual display, is obtained using the 1-kc sync source. The narrow-band receiver is used to monitor storage time within a fixed bandwidth about the instruction frequency, while the broad-band detector shows the energy in the entire bandwidth of the system as a function of time.

Experimental Findings

Using a waveguide delay line, an instruction pulse of width equal to the delay time of the loop was injected into the storage loop at a "preferred" frequency. With the "loop gate" adjusted for 10 microseconds of storage and the "out gate" adjusted for 2 microseconds (several circulations) of viewing, the spectrum photograph of Fig. 5 was obtained.

Next, using the same waveguide delay line, an instruction pulse of width equal to the delay time of the loop was injected into the storage loop at a frequency midway between two preferred frequencies. With the "loop gate" again adjusted for 10 microseconds of storage and the "out gate" again adjusted for 2 microseconds of viewing, the spectrum photograph of Fig. 6 was obtained.

To determine how the energy in the system shifted to the preferred mode, the "out gate" switch was adjusted to allow viewing of a single circulation. By moving the time position of the "out gate" switch through the storage period, it was observed that the energy in any circulation was always at the input frequency. Fig. 7 compares the spectrum of the first with the 47th circulation and the combination of the first, second, and third with the combination of the 45th, 46th and 47th circulations for the condition of instruction pulse width equal to the loop delay and input frequency midway between preferred frequencies. Fig. 8 shows the spectra

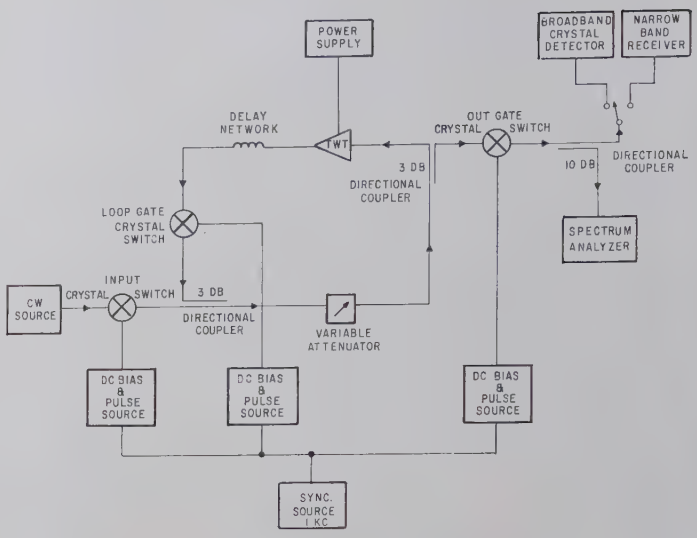

Fig. 4—Block diagram of experimental storage device.

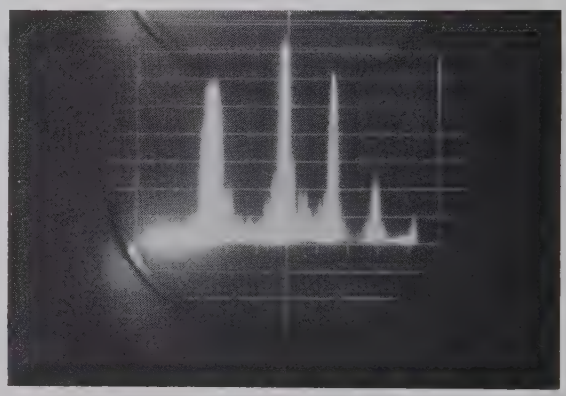

Fig. 5—Spectrum of 2 μsec of storage on a preferred frequency using waveguide delay line.

Fig. 6—Spectrum of 2 μsec of storage between preferred frequencies using waveguide delay line.

(a)

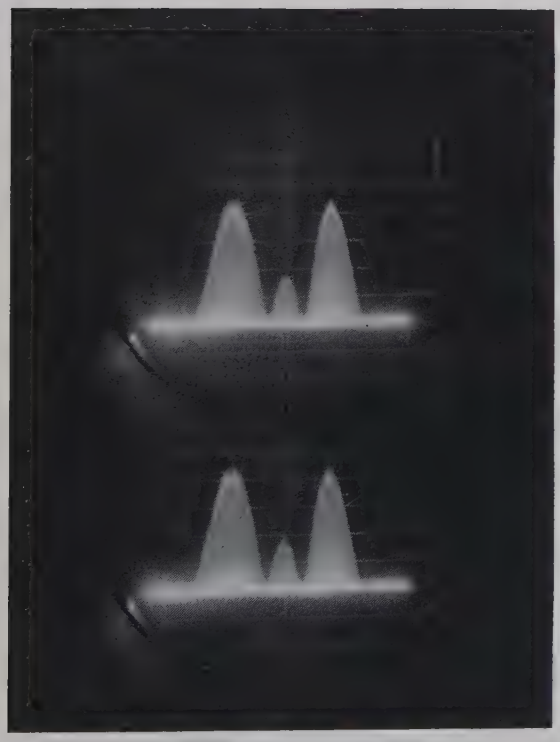

(b)

Fig. 7—Spectra showing various circulations during storage.

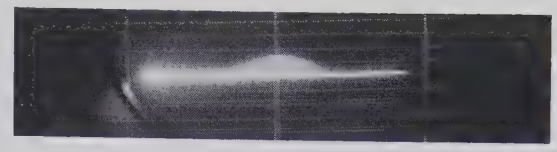

(a)

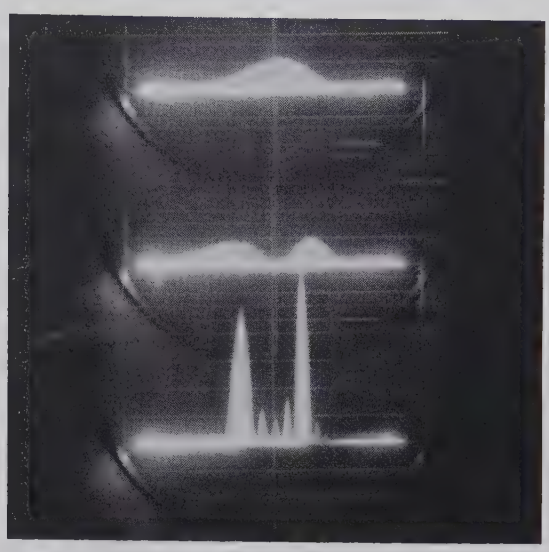

(b)

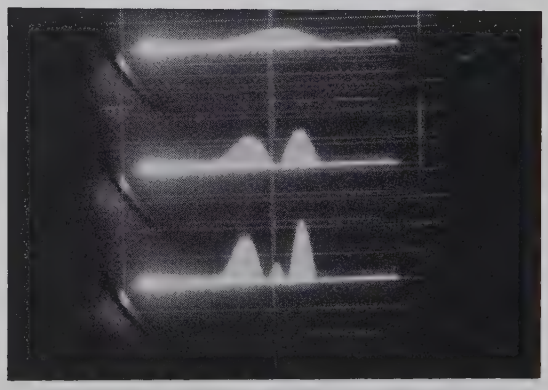

(c)

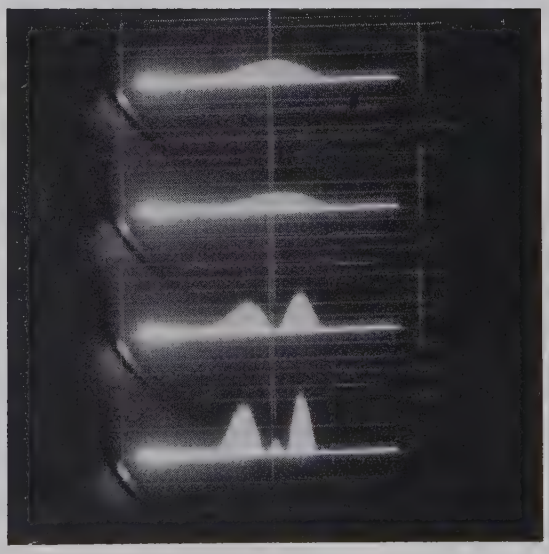

(d)

Fig. 8—Spectra showing various combinations of "out gate" width and time position.

obtained for various combinations of "out gate" width and time position again for the condition of the input frequency being midway between preferred frequencies. Fig. 8(a) shows the input signal; 8(b) the 1st circulation, 1st and 2nd, 1st through 5th; 8(c) the 7th circulation, 7th and 8th, 7th through 9th; 8(d) input signal, 14th circulation, 14th and 15th, 14th through 16th.

The waveguide delay line was replaced by a coaxial delay line. Further tests were conducted, and the results are shown in the following figures.

Fig. 9 shows the spectrum of a circulation 2 microseconds after initiation of storage tracking smoothly as the input frequency is varied. Fig. 10 shows a similar condition except the circulation being viewed is at 8 microseconds after initiation of storage.

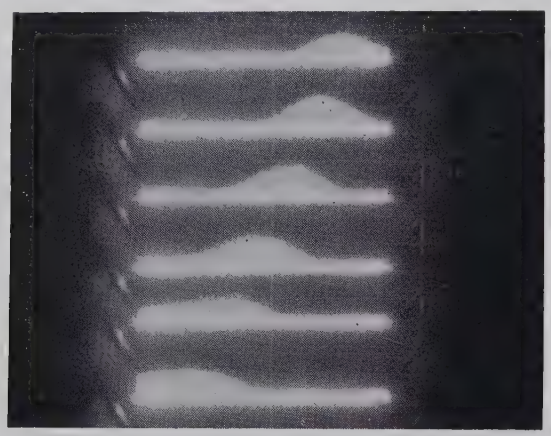

Fig. 9—Spectrum of a single circulation 2 μsec after initiation of storage.

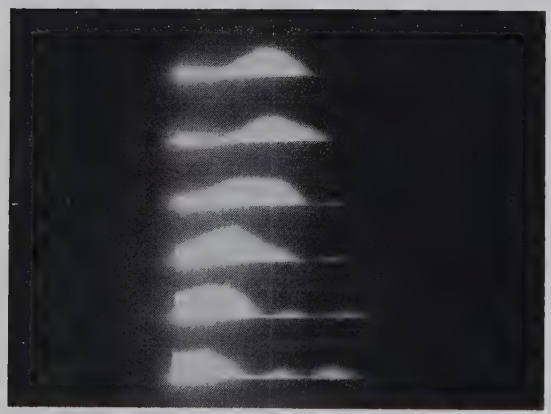

Fig. 10—Spectrum of a single circulation 8 μsec after initiation of storage.

Fig. 11 shows the spectrum of a single circulation viewed at 2, 4, 6, and 8 microseconds after initiation of storage for the condition of input frequency midway between preferred frequencies. Bottom spectrum shows input signal.

The effect of viewing two adjacent circulations under the condition of input frequency midway between preferred frequencies is shown in Fig. 12. Spectra from bottom to top are: input, 1st and 2nd, 3rd and 4th, 5th and 6th, 21st and 22nd. The circulations, both of fre-

Fig. 11—Spectrum of single circulation at various times in the storage cycle.

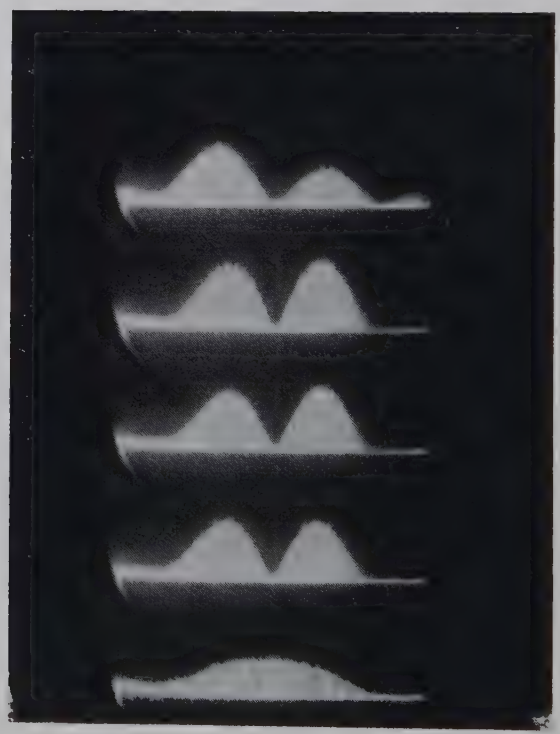

Fig. 12—Spectrum of two circulations.

quency f_0, are π radians out of phase with each other and when summed in the spectrum analyzer, produce a concentration of energy at frequency $f_0 \pm (3/8)1/\tau_0$, where τ_0 is the total time delay of the loop. Notice that there is no energy at the input frequency f_0. Since these results, especially the $\pm(3/8)1/\tau_0$ spacing, were other than expected, a Fourier analysis was conducted. In the analysis, given in the Appendix, a Fourier integral formulation is used to obtain the envelope of the power spectrum. The power spectrum obtained from the analysis displays peaks at $\pm(3/8)1/\tau_0$, as shown in Fig. 13, and thus verifies the experimental findings.

Since the viewing of two circulations gave $(3/4)1/\tau_0$ separation between power spectrum peaks, and the viewing of several circulations resulted in a $1/\tau_0$ separation between peaks, an additional test was conducted to observe the intermediate steps. As can be seen in Fig. 14, as more circulations are viewed, the peaks of energy concentration move outward to the $1/\tau_0$ spacing.

It is interesting to note that although there is no energy at the input frequency when an even number of circulations are viewed, as in Fig. 14, there is energy at the input frequency when an odd number of circulations are viewed, as shown in Figs. 7 and 8.

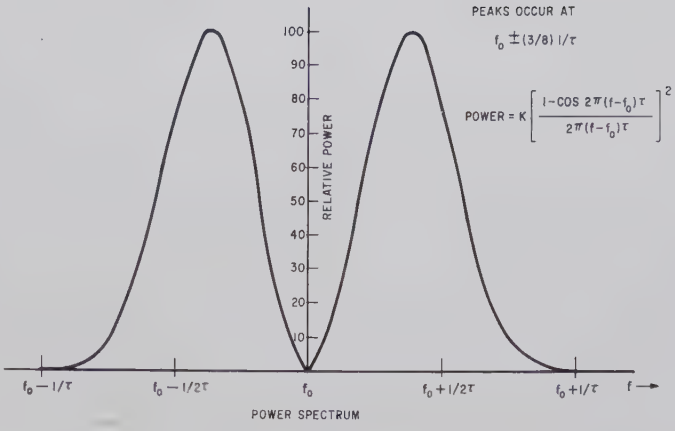

Fig. 13—Power spectrum obtained by Fourier analysis.

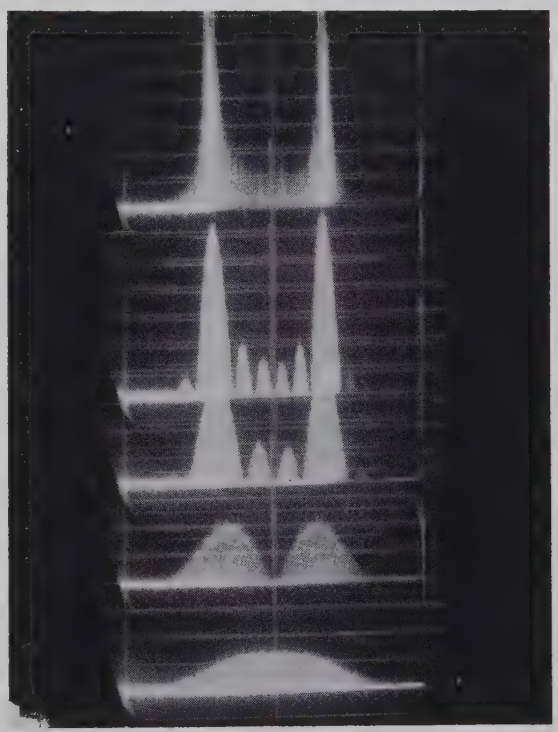

Fig. 14—Spectra showing peaks of energy concentration moving from $(3/4)\ 1/\tau_0$ to $1/\tau_0$ separation.

Conclusions

After examining the experimental results, it can be concluded that the RF storage system described in this report does not oscillate in the true sense of the word, but rather operates on a recirculating amplifier principle. The concentration of energy at the preferred frequencies results only from the summing process in the receiver of the spectrum analyzer when several circulations of various phases are viewed. Thus, a short-time RF storage system consisting of a fixed delay line, a TWT, and appropriate input and output coupling devices is capable of exact frequency storage *if the output energy is properly extracted.*

It can also be concluded that pulse spreading, known to occur in the TWT and delay line, although a possible cause for multimode oscillations in a long-time storage device, is not of sufficient magnitude to disturb the short-time storage of a recirculating amplifier.

Appendix

Fourier Analysis

The following analysis was performed to obtain the power spectrum and, in particular, the frequency separation between power peaks for a train of pulses where a single pulse has the waveform shown in Fig. 15. The waveform is made up of two sine waves of carrier frequency f_0 but differing in phase by π radians.

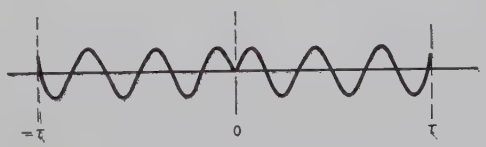

Fig. 15.

The function is described by:

$$f(t) = -A \sin \omega_0 t \qquad -T \leq t \leq 0$$
$$f(t) = A \sin \omega_0 t \qquad 0 \leq t \leq T$$
$$f(t) = 0 \qquad |t| > T.$$

The envelope of the harmonics of the train of pulses is readily obtained from a Fourier integral formulation of a single pulse.

The Fourier transform of the function $f(t)$[4,5] is given by

$$g(\omega) = \frac{1}{2\pi}\int_{-\infty}^{\infty} f(t)e^{-j\omega t}dt, \tag{1}$$

where $g(\omega)$ describes the spectral density of the waveform. Substituting $f(t)$ for the waveform shown above, (1) becomes

$$g(\omega) = -\frac{1}{2\pi}\int_{-\tau}^{0} A \sin \omega_0 t e^{-j\omega t}dt + \frac{1}{2\pi}\int_{0}^{\tau} A \sin \omega_0 t e^{-j\omega t}dt. \tag{2}$$

Substituting $e^{-j\omega t}=\cos \omega t - j \sin \omega t$ and integrating yields

$$g(\omega) = \frac{A}{2\pi}\left[\frac{1-\cos(\omega_0-\omega)\tau}{(\omega_0-\omega)} + \frac{1-\cos(\omega_0+\omega)\tau}{(\omega_0-\omega)}\right]. \tag{3}$$

[4] J. A. Stratton, "Electromagnetic Theory," 1st ed., McGraw-Hill Book Co., Inc., New York, N. Y.; 1941.
[5] L. A. Pipes, "Applied Mathematics for Engineers and Physicists," 2nd ed., McGraw-Hill Book Co., Inc., New York, N. Y.; 1958.

Eq. (3) can be simplified by neglecting the term containing $(\omega_0+\omega)$ in the denominator and defining a new term α by $\omega=\omega_0\pm\alpha$ where $\alpha \ll \omega_0$. Thus (3) becomes

$$g(\omega) = \frac{A}{2\pi}\frac{1-\cos(\pm\alpha)\tau}{(\pm\alpha)}. \tag{4}$$

The power spectrum is given by

$$(g(\omega))^2 = \left[\frac{A}{2\pi}\right]^2\left[\frac{1-\cos(\pm\alpha)\tau}{(\pm\alpha)}\right]^2. \tag{5}$$

Multiplying numerator and denominator by τ, (5) becomes

$$(g(\omega))^2 = \left(\frac{A\tau}{2\pi}\right)^2\left[\frac{1-\cos(\pm\alpha)\tau}{(\pm\alpha)\tau}\right]^2. \tag{6}$$

Eq. (6) displays power peaks at $\alpha \approx \pm 3/4\pi/\tau$, as shown in Fig. 13. While actual differentiation of (6) yields power peaks at $\alpha = \pm 0.741\ \pi/\tau$, for purposes of this report, the approximation of $3/4\pi/\tau$ will be used.

Acknowledgment

The author would like to thank R. Stickney and D. Khouri for their effort in obtaining the experimental data, S. N. Miller for his initial investigation into the pulse analysis, and Dr. C. E. Faflick for valuable suggestions and supervision.

Excess Noise in Microwave Detector Diodes*

J. J. FARIS†, MEMBER, IRE, AND J. M. RICHARDSON†, SENIOR MEMBER, IRE

***Summary*—The dependence of available excess noise in type 1N26 microwave crystal-diode rectifiers on applied microwave power was measured. This may be approximated by a power law with constants characteristic of the particular crystal. As a consequence of the dependence of both excess noise and dc rectified power on input-power level, there is a level which minimizes the ratio of these quantities. Similarly, in the case of a modulated microwave carrier there is an input level which minimizes the ratio of excess noise to demodulated power, and so provides optimum detection of small modulation.**

I. Introduction

THE NOISE in excess of kT_0B resulting from application of microwave power to a crystal detector is important in many applications of microwaves. It is interesting in itself to know the functional dependence of the excess noise on the input microwave power and the variation of excess noise with change in the various parameters that may be varied. Furthermore, in order to determine operating conditions that result in optimum video detection of signals of specified RF power and modulation factor, it is necessary to know the dependence of both detected signal and excess noise on these parameters. These considerations find direct application in systems dealing with small amplitude, low-frequency modulation on relatively large microwave signals—for example, in detection of Zeeman or Stark modulation in microwave spectroscopy and parmagnetic resonance, or in certain stabilization systems for microwave oscillators in which error modulation is placed on a microwave signal by a stabilizing element such as a reference cavity.

When a crystal diode is used as a detector of microwave power, the average operating point $(\bar{e}, \bar{i})$ that results is a point in the current voltage plane that cannot be reached by application of dc voltages to the crystal. Thus, the excess noise produced by application of microwave signals on a crystal detector cannot be

* Received by the PGMTT, January 9, 1961; revised manuscript received, March 16, 1961.
† National Bureau of Standards, Boulder, Colo.

inferred from dc measurements. In another study,[1] the notation of which is adopted here, measurement techniques were developed that permit measurement of excess video output noise voltage resulting from microwave excitation of crystal detectors. These techniques essentially involved a two-channel detector system in which detected klystron noise common to both channels was rejected by out-of-phase cancellation, permitting the observation of excess noise to lower levels than otherwise. By also measuring the video impedance of the crystal, which varies with the various operating conditions used in the noise measurements, it is possible to express these results in terms of the total available noise power, $S_0 = kT_0B + S_{\text{excess}}$, which in turn may be expressed as a noise temperature, $T = T_0 + T_{\text{excess}}$, through the relation $S_0 = kTB$ for bandwidth B and standard noise temperature T_0.

II. Experimental

Measurements were made on three 1N26 crystal detectors assumed typical, using two values of load resistance in the rectified crystal current return path, 2000 ohms and 10,000 ohms. The pass band of the measurement system would pass the same power from a white-noise spectrum as a square pass band of width 8 cps; however, the data presented have been reduced to a bandwidth of 1 cps. For all of the measurements reported here, this pass band was centered on 270 cps, where the excess noise predominated over the Johnson and shot noise because of its approximate $1/f$ spectral distribution. The microwave power impressed on the crystal under test was varied from about 10 μw to 100 mw when the 10,000-ohm biasing resistor was used and from 10 μw to 1 mw with the 2000-ohm bias.

The data obtained are shown in Fig. 1 (next page). These curves indicate, for the range investigated, that below a critical input microwave power, the available excess-noise power can be approximated by an expression of the form

$$S_{\text{excess}} = CP_1^n, \tag{1}$$

where P_1 is the input microwave power, and both C and n are parameters which depend on the particular crystal under test. The $1/f$ dependence probably can be contained in C. The critical input power above which this expression no longer holds is also a characteristic of the individual crystal. It is interesting to note that for the three crystals tested, the value of C is less with the 2000-ohm bias than with the 10,000-ohm; however, the value of n seems to be essentially independent of bias resistance.

Approximate values for these two parameters are shown in Table I for the three crystals tested.

The noise power S_0 is related to fluctuations in the rectified voltage. A measure of the severity of these fluctuations is an equivalent noise modulation factor m_0, defined by the general relationship.

$$m_0^2 = 2S_0/P_0, \tag{2}$$

where P_0 is the available rectified power from the detector.[2] Fig. 2 shows measured values of m_0^2 plotted as a function of P_1 for the crystals used in this study. It is interesting to note that m_0 has a definite minimum value for a power input of a few db below 1 mw. This is readily understandable, since square-law detection applies at low powers. Thus P_0 varies as P_1^2 while S_0 varies as P_1^n, where $n<2$ from Table I. At high powers the detector law becomes linear or even less strong because of incipient saturation, while S_0 continues to rise approximately linearly because of excess noise. This modulation on the rectified dc output places a lower limit on the smallest detectable RF modulation.

Finally, it is interesting to consider an RF signal of power level P_1 with a small modulation m_{1s} impressed on it. It is desirable to adjust the signal level before detection by attenuation (or by amplification with negligible addition of noise) to a value that will maximize the ratio of available detected signal power S_{0s} to available noise power S_0. We designate the signal sideband power on the RF carrier S_{1s}; thus $S_{1s} = \frac{1}{2}m_{1s}^2P_1$. We further define a small signal demodulation efficiency $G = S_{0s}/S_{1s}$. For any particular crystal, G may be obtained from the slope of the curve of available rectified power vs input power and is a function of P_1. Thus the ratio of demodulated signal power to noise power is

$$S_{0s}/S_0 = GS_{1s}/S_0 = \tfrac{1}{2}Gm_{1s}^2P_1/S_0. \tag{3}$$

The least value of the ratio S_{0s}/S_0 that results in a detectable signal depends on the method of observation used. However, we will adopt the commonly used criterion of detectability that a signal is detectable if the ratio

$$\frac{S_{0s}}{S_0} \geqq 1.$$

Thus we can define a critical value of m_{1s}, which we will label M_{1s}, that produces a signal at the limit of detectability. Hence

$$\tfrac{1}{2}GM_{1s}^2P_1/S_0 = 1, \tag{4}$$

or

$$M_{1s}^2 = 2S_0/GP_1. \tag{5}$$

Fig. 3 displays M_{1s}^2 as a function of P_1. The character of the curves is readily understood, since at low powers square-law detection applies and G is roughly proportional to P_1, so that M_{1s}^2 falls with increasing P_1. At high powers, G becomes constant or even decreases, while S_0 continues to increase so that M_{1s}^2 rises again.

[1] J. M. Richardson and J. J. Faris, "Excess noise in microwave crystal diodes used as rectifiers and harmonic generators," IRE Trans. on Microwave Theory and Techniques, vol. MTT-5, pp. 208–212; July, 1957.

[2] For sinusoidal amplitude modulation of a carrier, it is well known that the total sideband power is $S = m^2P/2$. This relation is easily generalized by defining an effective modulation factor so as to apply to a complex modulating waveform synthesized from several frequencies. The same relationship holds even for zero carrier frequency, so that we identify the dc component of the rectified output with P_0 and the fluctuating component with S_0 in (2).

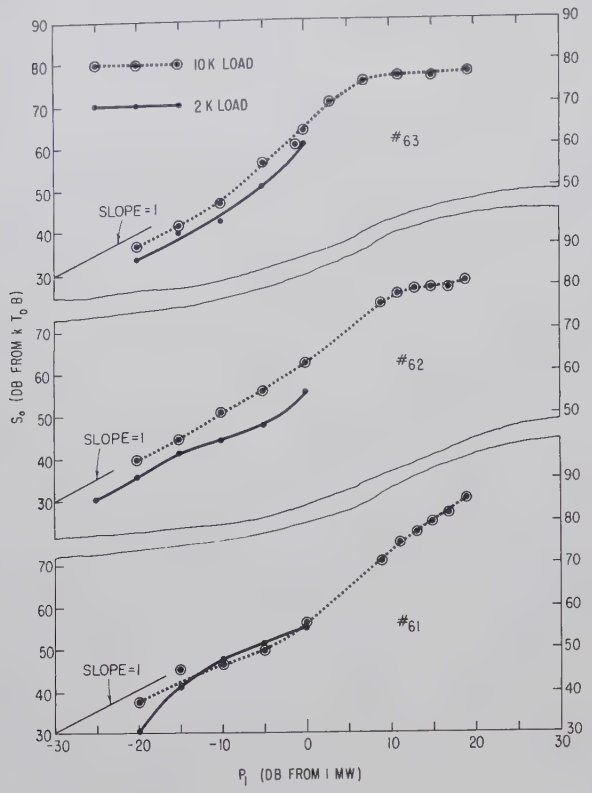

Fig. 1—Available noise power for unit bandwidth at 270 cps as a function of input microwave power; 1N26 detector crystals.

TABLE I
CONSTANTS FOR EQUATION (1)

Crystal No.	n	C (watts)$^{-(n-1)}$	
		2 K load	10 K load
61	0.9	1.25×10^{-12}	1.25×10^{-12}
62	1.0	1.25×10^{-12}	5.0×10^{-12}
63	1.5	1.12×10^{-10}	2.5×10^{-10}

The range of M_{1s}^2 may be several orders of magnitude. These data demonstrate that there is a signal level which minimizes M_{1s}^2 and thus leads to optimum detection of a small modulation on the RF signal.

III. Conclusions

We have demonstrated that the available excess noise power in a microwave crystal detector can be approximated by the expression

$$S_{\text{excess}} = CP_1^n,$$

where both C and n depend on the characteristics of the particular crystal.

We have further shown that if the excess noise present on the dc rectified output from the crystal studied is represented as a modulation on the dc carrier, there is a signal level that minimizes the modulation coefficient.

Finally we conclude that there is a signal level that results in a maximum ratio of available detected modulation power to available noise power, for small modulation. This signal level provides optimum detection of a small modulation on an RF signal.

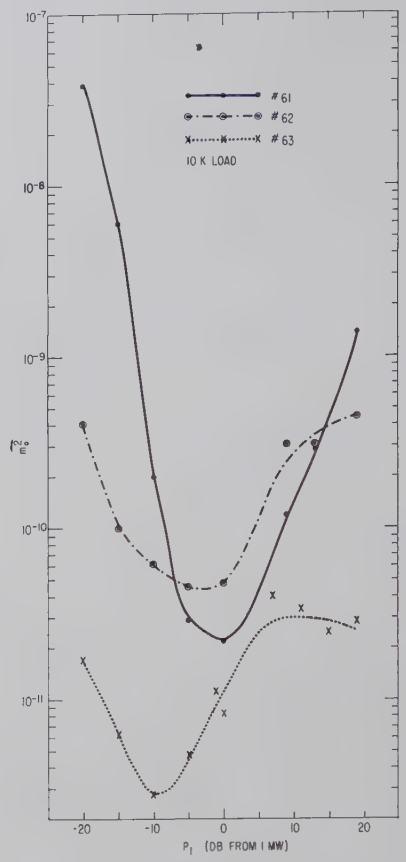

Fig. 2—Square of equivalent noise modulation factor for unit bandwidth at 270 cps as a function of input microwave power.

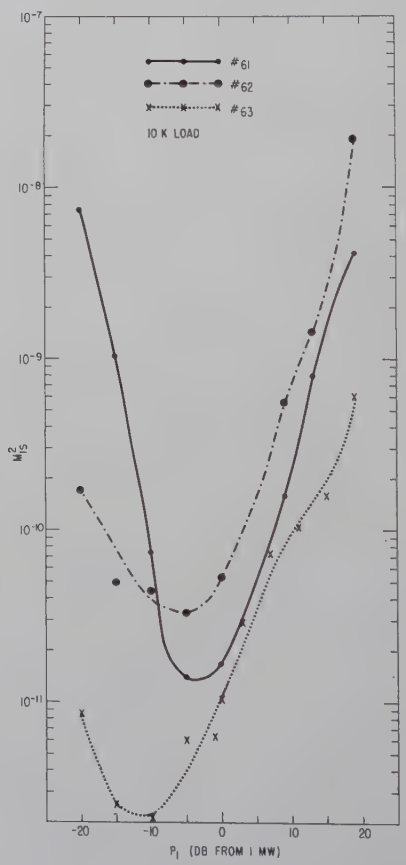

Fig. 3—Square of critical modulation factor to produce demodulated signal power equal to noise power in unit bandwidth at 270 cps.

Quantum Fluctuations in Microwave Radiometry*

L. P. BOLGIANO, JR.†, MEMBER, IRE

Summary—This paper assesses the possible significance of the quantum nature of electromagnetic radiation in limiting the measurement accuracy attainable with a microwave radiometer. Analogies are shown to exist between the form of a formula describing fluctuations in the radiometer output, and both a formula describing the radiometer input signal, and also, a formula describing the output of a photocell detector. Detailed quantum mechanical consideration of the processes of amplification and detection are circumvented by considering how the formula for fluctuations in the radiometer output might be modified so as to make it consistent with the measurement precision implied by these other formulas. A modified formula is suggested which includes a quantum fluctuation whose magnitude depends on signal power.

I. Introduction

THE development of microwave radiometers with very low noise figures and very wide bandwidths has been steadily decreasing the average number of photons per unit time-bandwidth represented by the minimum perceptible signal. It is, therefore, of interest to consider whether the quantum nature of electromagnetic radiation might be significant in limiting the measurement accuracy attainable in microwave radiometry.

Weber[1] and Strandberg[2] have computed the ultimate limit on sensitivity set by spontaneous emission noise for both maser and vacuum tube amplifiers. The equivalent temperature of this noise is only hf/k for a maser and $hf/2k$ for a vacuum tube amplifier. Perhaps of more immediate significance for microwave radiometry is the possibility of a quantum fluctuation dependent on signal power analogous to the random counting rate of a photon counter. Gabor[3,4] has demonstrated mathematically that it is not possible to extract more information from a signal with electron tube apparatus capable of measuring both amplitude and phase than with photon counters. Accordingly, quantum mechanics should place similar restrictions on the degree to which fluctuations can be reduced in optical and microwave radiometry. Recently, wave and particle fluctuations have been measured simultaneously in the outputs of optical photocell detectors.[5,6] In Section II, we shall show that wave and particle fluctuations also coexist in the description statistical mechanics gives for the input signal to a microwave radiometer. In Section III, we show that the usual formula for the fluctuations in the output of a microwave radiometer has an analogous form to the portion associated with wave effects of both the formula found in Section II and also a formula describing the wave and particle fluctuations in the output of a photocell detector. In Section IV, we show how the microwave radiometer formula might be modified to include a particle fluctuation term of the form suggested by these analogies. In Section V, we compare the magnitude of this particle fluctuation with that of the classical wave fluctuation.

II. Fluctuations in a Radio Signal

In this section, we shall deduce a formula describing fluctuations in the input signal of a wide-band microwave radiometer. If the input signal consists of thermal radiation, it may be described by the Planck radiation formula. In its most familiar form the Planck radiation formula is written as the product of two factors. One factor, $8\pi f^2 V df/c^3$, specifies the number of standing-wave modes between frequencies f and $f+df$ in a large, three-dimensional volume V. The other factor, $hf/(\exp hf/kT-1)$, gives the energy associated with each mode. For a long one-dimensional microwave transmission line of length L, for which only one field polarization is possible, the first factor becomes instead $(2L/c)df$. This gives it the frequency independence necessary for radiative equilibrium with the Johnson noise of a resistive termination. In the language of statistical mechanics, each standing-wave mode corresponds to a quantum state, and the Bose-Einstein distribution $1/(\exp hf/kT-1)$ is regarded as specifying the number of quanta of energy hf in the quantum state associated with the mode of frequency f. Our interest will be in the time fluctuation which the Bose-Einstein probability distribution implies in the number of quanta occupying a group of adjacent quantum states. From a communication theory viewpoint these fluctuations in numbers of quanta constitute energy fluctuations within the frequency bandwidth corresponding to these quantum states.

This fluctuation may be computed by quantum statistics. We shall describe the relationship of this theory to electromagnetic theory only in sufficient detail to permit stating the computation of the fluctuation as given by Landau and Lifschitz[7] who give an extensive discussion of fluctuations in statistical mechanics. In the classical Rayleigh-Jeans wave theory of thermal

* Received by the PGMTT, December 13, 1960; revised manuscript received, March 22, 1961. This work was supported by the Ballistic Research Labs., Aberdeen Proving Ground, Md., under U. S. Army Contract DA-36-034-509-ORD27.

† Dept. of Elec. Engrg., University of Delaware, Newark, Del.

[1] J. Weber, "Maser noise considerations," *Phys. Rev.*, vol. 108, pp. 537–541; November 1, 1957.

[2] M. W. P. Strandberg, "Inherent noise of quantum mechanical amplifiers," *Phys. Rev.*, vol. 106, pp. 617–620; May 15, 1957.

[3] D. Gabor, "Communication theory and physics," *Phil. Mag.*, vol. 41, pp. 1161–1187; November, 1950.

[4] D. Gabor, "Der Nachrichtengehalt eines elektromagnetischen Signals," *Archiv der Elektrischen Ubertragung*, vol. I, pp. 95–99; February, 1953.

[5] R. Q. Twiss and A. G. Little, "The detection of time-correlated photons by a coincidence counter," *Australian J. Phys.*, vol. 12, pp. 77–93; January, 1959.

[6] M. O. Harwit, "Measurement of Radiation Fluctuations from a Source in Thermal Equilibrium," Research Lab. of Electronics, M.I.T., Cambridge, Quart. Prog. Rept., pp. 23–26; April 15, 1960.

[7] L. D. Landau and E. M. Lifschitz, "Statistical Physics," Addison-Wesley Publishing Co., Inc., Reading, Mass.; 1958. See especially p. 358. (Translated from the Russian by E. and R. F. Peierls.)

radiation, equal energy was accorded each standing-wave mode. In the quantum statistical description, the total energy is assumed distributed among all the modes in the most probable way consistent with the constraint that the energy of each mode be an integral multiple of hf. This gives particle properties to the radiation since the computation parallels the classical particle mechanics computation of the most probable distribution of gas particles among cells in phase space, such that all particles in a given cell have equal kinetic energy. In fact, the only essential difference is the lack of an equivalent for the possibility which exists with classical particles of imagining them individually labelled so that one can speak of which particle is in which cell. This has no equivalent in the quantum statistical theory where only the total number of quanta associated with each standing-wave mode or quantum state need be specified to completely describe a possible energy distribution. The quantum statistical theory may thus be regarded alternatively as describing waves with quantized energies or, equivalently, particles which are intrinsically indistinguishable from one another.

This intrinsic indistinguishability of particles must be assumed for gas particles, in general, in order to obtain a correct quantum mechanical description, and so is not a peculiar property of massless photons. The photon distribution formula $1/(\exp hf/kT-1)$ may thus be regarded as a special case of the general Bose-Einstein distribution formula applicable to gas particles not subject to the Pauli exclusion principle. This formula may also be used to compute the mean number of particles in a single quantum state, in which case it may be written as

$$\overline{n_s} = \frac{1}{e^{(E_s-\mu)/kT} - 1} \tag{1}$$

where E_s is the kinetic energy, equal to hf for photons, and μ is the chemical potential, equal to zero for photons.

Since this mean is associated with a thermal equilibrium, the precise number of particles in the state will fluctuate about $\overline{n_s}$ with time. The mean-square fluctuation may be computed by the general formula[7]

$$\overline{(\Delta n_s)^2} = kT\frac{\partial \overline{n_s}}{\partial \mu} \tag{2}$$

which describes the fluctuation in number of particles in a portion of a gas at constant temperature and volume. Applying this to (1) gives

$$\overline{(\Delta n_s)^2} = \frac{e^{(E_s-\mu)/kT}}{(e^{(E_s-\mu)/kT} - 1)^2} = \overline{n_s} + \bar{n}_s^2 \tag{3}$$

for all Bose-Einstein particles and for photons in particular. The statistical independence of the quanta permits summing over a group of N adjacent quantum states containing altogether $n=\Sigma n_s$ quanta to obtain for the mean-square fluctuation in the number of quanta associated with N adjacent quantum states

$$\overline{(\Delta n)^2} = N(\overline{n_s} + \bar{n}_s^2) = N\overline{n_s} + \frac{(N\overline{n_s})^2}{N} = \bar{n} + \frac{\bar{n}^2}{N}. \tag{4}$$

The corresponding fluctuation in energy E obtained by multiplying by $(hf)^2$ is

$$\overline{(\Delta E)^2} = hf\overline{E} + \overline{E}^2/N. \tag{5}$$

This expression is interesting because, as first shown by Einstein and Lorentz,[8] it gives the total fluctuation as the sum of two terms which separately correspond to either classical particle or classical wave phenomena. The first term by itself is the $\sqrt{\bar{n}}$ rms fluctuation kinetic theory gives for the fluctuation in the number of classical particles in a small region of a large gas. The second term by itself is identifiable with the rms energy fluctuation proportional to squared amplitude which results from beats between random classical waves and is normally the only fluctuation considered in communication theory.

In order to evaluate the number of quantum states N associated with a portion of the radiometer input signal, we need a correspondence between the equilibrium quantum states we have associated with the Planck radiation law and the received signal. The needed correspondence is implicit in the previous statement that the number of standing-wave modes or quantum states between frequencies f and $f+df$ in a line of length L is $(2L/c)\Delta f$. The length of line per quantum state obtained by dividing the number of states into L is $\Delta x = 2c/\Delta f$. Halving the number of degrees of freedom to correspond to the fact that we are interested in propagation in only one direction gives $\Delta x \Delta f = c$. In terms of the particle momentum $p=hf/c$, this is equivalent to the usual association of quantum states with cells of area $\Delta x \Delta p = h$ in two-dimensional phase space. Alternatively, since a wave propagated at velocity c advances a distance $c\Delta t = \Delta x$ in time Δt, one may say that quantum states correspond to cells of area $\Delta t \Delta f = 1$ on the time-frequency or information plane. This correspondence was first introduced by Gabor[3] and has been used by Stern[9] to analyze the information handling capabilities of a discrete photon channel. It permits one to say that the number of quantum states in a duration Δt of signal extending over a frequency range Δf is the

[8] H. A. Lorentz, "Les Theories Statistiques en Thermodynamic," Teubner Verlag, Leipzig and Berlin, Germany; 1916.

[9] T. E. Stern, "Some quantum effects in information channels," IRE TRANS. ON INFORMATION THEORY, vol. IT-6, pp. 435–440; September, 1960.

number of cells of unit area in the rectangle on the information plane representing the time-bandwidth product, $\Delta t\Delta f$.

A microwave radiometer accepts only the signal power in a bandwidth Δf set by its reception filter and averages this power over an integrating time Δt set by its final smoothing filter. Accordingly, the portion of input signal energy of significance in determining fluctuations may be regarded as that included in the time-bandwidth $\Delta t\Delta f$. Since this time-bandwidth product also equals the number of quantum states in the corresponding portion of signal, it may be taken as the appropriate value of N in (4) and (5). Thus, the mean-square energy fluctuation or equivalently the mean-square fluctuation in power integrated over time Δt in the radiometer input signal is:

$$\overline{(\Delta E)^2} = hf\bar{E} + \bar{E}^2/\Delta t\Delta f, \tag{6}$$

and the mean-square fluctuation in the quanta contained in this portion of the signal is

$$\overline{(\Delta n)^2} = \bar{n} + \frac{\bar{n}^2}{\Delta t\Delta f}. \tag{7}$$

The first term in these formulas is a consequence of the quantum nature of the radiation and has no equivalent in classical wave theory. The second term corresponds to the usual wave fluctuation associated with a random radio signal. In Appendix II we show that the fluctuation in the energy of random waves along a transmission line is given by a formula of this form. Rice[10,11] has computed the mean-square fluctuation in a random current. The formula he obtains for the mean-square fluctuation is of similar form to (29) of Appendix II and, as explained there, it may be transformed into the form $\bar{E}^2/\Delta t\Delta f$ by a change of variables.

III. Analogies Between Fluctuation Formulas

Purcell[12] and Mandel[13] find for the mean-square fluctuation in the average number of photoelectrons produced in time Δt in a photocell illuminated by Gaussian random waves from a spectral line of width Δf

$$\overline{(\Delta n)^2} = \bar{n} + \alpha\frac{\bar{n}^2}{\Delta t\Delta f}. \tag{8}$$

[10] S. O. Rice, "Mathematical analysis of random noise," in "Selected Papers on Noise and Stochastic Processes," N. Wax, Ed., Dover Publications, Inc., New York, N. Y., p. 227; 1954. (Reprinted from *Bell Sys. Tech. J.*, vol. 23, pp. 282–322, July, 1944; vol. 24, pp. 47–156, January, 1945.)

[11] S. O. Rice, "Filtered thermal noise-fluctuation of energy as a function of interval length," *J. Acoust. Soc. Am.*, vol. 14, pp. 216–227; April, 1943.

[12] E. M. Purcell, "The question of correlation between photons in coherent light rays," *Nature*, vol. 178, pp. 1449–1450; December 29, 1956.

[13] L. Mandel, "Fluctuations of photon beams and their correlations," *Proc. Phys. Soc.*, vol. 71, pp. 1037–1048; December, 1958.

The first term corresponds to the usual $\sqrt{\bar{n}}$ rms fluctuation in counting rate associated with all particle counters. The second term results from the added assumption of wave fluctuations in the light illuminating the photocell. α is a constant of the order of unity. Since a similar constant would be required in (7), had we not tacitly assumed integrating time and bandwidth definitions such as to make the minimum Fourier integral uncertainty product $\Delta t\Delta f$ precisely unity, the form of (8) may be regarded as similar to that of (7).

The usual expression for the mean-square fluctuation in the output of a microwave radiometer may be written in the general form[14]

$$\overline{(\Delta z)^2} = \frac{\bar{z}^2}{\Delta t\Delta f} \tag{9}$$

where $\bar{z}$ denotes the mean output meter deflection, Δf the reception filter bandwidth, and Δt the smoothing filter integrating time. $\sqrt{\overline{(\Delta z)^2}}$ is the rms fluctuation in output meter deflection occasioned by the random character of both signal and system noise.

As in (7), the absence of a factor of proportionality of the order of unity in (9) depends on the choice of definitions for integrating time and bandwidth. Dicke,[15] for example, gives this proportionality factor as $\pi^{3/2}/8$. The significant point for the qualitative discussion intended here is that this formula for the fluctuation at the receiver output is of similar form to the terms representing classical wave effects in both (6), which describes fluctuations at the receiver input, and (8), which describes fluctuations in the output of a photoelectric detector.

IV. Modification of Radiometer Formula

In this section, we shall show how (9) might be modified so as to include a quantum fluctuation term. For a receiver which contributes no noise of its own, the mean deflection $\bar{z}$ is directly proportional to signal power. For this limiting case, (9), like (6), (7), and (8) may be regarded as representing signal fluctuations. However, as stated in Section I, Gabor has shown that no greater measurement accuracy should be possible with radio equipment than for the measurements to which (6), (7), and (8) apply. Formula (9) differs in form from these formulas only by the lack of a term associated with particle fluctuations. Formula (7) may be written as

$$\overline{(\Delta n)^2} = \left(\frac{\Delta t\Delta f}{\bar{n}} + 1\right)\frac{\bar{n}^2}{\Delta t\Delta f}. \tag{10}$$

Thus, a modified fluctuation formula for a microwave radiometer with unity noise figure equivalent to (9) at

[14] R. S. Colvin, "Faint signal limitations of radiometers," 1959 IRE WESCON Convention Record, pt. 8, pp. 52–58.

[15] R. H. Dicke, "The measurement of thermal radiation at microwave frequencies," *Rev. Sci. Instr.*, vol. 17, pp. 268–275; July, 1946.

high intensities, and of similar form to (6), (7), and (8) is

$$\overline{(\Delta z)^2} = \left(\frac{\Delta t \Delta f}{\bar{n}} + 1\right)\frac{\bar{z}^2}{\Delta t \Delta f} \tag{11}$$

where $\bar{n}$ denotes the mean number of photons received in the integrating time Δt.

The assumption of an ideal receiver which adds negligible noise to the signal prevents the usual interpretation of the mean-square fluctuation given by (9) as the minimum perceptible signal. This usual interpretation is based on the opposite assumption that for a weak signal the output meter deflection is mainly due to receiver noise. Then the fluctuation in meter deflection is primarily a fluctuation in system noise, indistinguishable from an incremental deflection representing a weak signal unless it exceeds this fluctuation. In the limit considered here of no receiver noise, the mean output meter deflection is proportional to mean signal strength alone and the fluctuation in deflection is a fluctuation in measured signal strength. This fluctuation does determine the accuracy with which the mean signal strength can be measured. It does not, however, limit the minimum signal which can be detected, since the mean-square fluctuation decreases with signal strength according to either the unmodified formula (9), or the modified formula (11).

Gabor[4] concludes that quantum mechanics prevents measuring an electromagnetic signal in steps smaller than the square root of the number of quanta it contains with electron tube apparatus. The mean-square fluctuation given by (11) differs from the purely wave fluctuation of (9) by an amount $\bar{z}^2/\bar{n}$. The corresponding rms relative fluctuation $\sqrt{\overline{(\Delta z)^2}}/\bar{z}$ equals $1/\sqrt{\bar{n}}$. Thus, the quantum fluctuation in (11) is the minimum fluctuation consistent with Gabor's general result.

V. Comparison of Wave and Particle Fluctuations

Since the rms particle fluctuation may be regarded as a fractional fluctuation of $1/\sqrt{\bar{n}}$ in signal power, its absolute magnitude increases with signal power. Whether it is likely to be of consequence in a particular radiometer measurement is, therefore, likely to depend on its size relative to the wave fluctuation whose magnitude increases even more rapidly with signal power.

The ratio of the mean-square wave fluctuation to the mean-square particle fluctuation in (11) equals the mean number of quanta per quantum state. Thus, if this ratio is denoted as R,

$$R = \bar{n}/\Delta t \Delta f. \tag{12}$$

If $\bar{n}$ is estimated as signal power P times integrating time Δt divided by the mean quantum energy expressed as the product of Planck's constant h and the mean signal frequency $\bar{f}$, so that $\bar{n} = (P\Delta t)/h\bar{f}$, then the ratio of the mean-square fluctuations may be written in the equivalent form

$$R = \frac{P\Delta t}{h\bar{f}} \div \Delta t \Delta f = \frac{P}{h\bar{f}\Delta f}. \tag{13}$$

$h\bar{f}\Delta f$ is the minimum sensitivity set by spontaneous emission noise for a maser amplifier since the equivalent temperature[2] of this noise $T = hf/k$ corresponds to a minimum power $kT\Delta f = h\bar{f}\Delta f$. From this, it is apparent that these formulas can have no significance unless R is greater than unity. Such a limit is to be expected since many particle statistics were used to derive (4).

VI. Conclusions

Analogies have been shown to exist between the dependence of output meter deflection fluctuations of a microwave radiometer on bandwidth and integrating time, and the term representing wave fluctuations in two formulas which include quantum effects and describe, respectively, fluctuations in a radiometer input signal and fluctuations in a photocell output current. It is shown that a particle fluctuation dependent on signal power results if the usual formula for the mean-square fluctuation in the output of a microwave radiometer with unity noise figure is modified to have the same form as these other formulas. Although the form of the modified formula is inferred by analogy, the modification is required by Gabor's general theorem which denies the possibility of greater signal measurement accuracy with electron tube apparatus than with particle counters.

Appendix I

Effect of Antenna

In this appendix, we shall consider how the operation of the antenna system of the receiver is related to the fluctuations.

Purely wave considerations are adequate to describe the coupling which an antenna effects between degrees of freedom in three-dimensional space and a one-dimensional transmission line. In fact, if the antenna did not couple equal numbers of degrees of freedom, a line terminated by a matched load at one end and at the other by an antenna in an enclosure of the same temperature as the line and matched load, could not be in thermal equilibrium simultaneously at all frequencies.[15] Thus, in Section II, we were able to compute the number of degrees of freedom involved by simply counting the number of possible standing-wave modes for the transmission line. Since the statistical mechanics computation required only a knowledge of this number, specific consideration of the antenna was unnecessary.

It may not be entirely evident that this computation of degrees of freedom using purely wave concepts is adequate to account for the particle as well as the wave nature of the radiation. In order to clarify this fact, we shall give an alternative computation based on

particle considerations. This computation leads to the same association of quantum states with information cells of area $\Delta t\Delta f=1$ as we found using only wave concepts. This shows that the particle nature of the radiation in no way modifies the result and that classical wave theory is completely adequate to describe the guiding of the radiation into the transmission line by the antenna. In as much as from a wave theory viewpoint the antenna may be regarded as a suitable aperture to create a desired diffraction pattern, it is interesting to compare this situation with X-ray diffraction. The X-ray diffraction pattern created by a calcite crystal can similarly be computed from purely wave considerations even when the intensity is so weak that the photons "guided by" the diffraction pattern are counted only one at a time.

We now consider how the coupling of the radiation field in space to a transmission line may be considered using particle statistics. The radiation in three-dimensional space will be considered to consist of a photon gas. As is usual in gas theory, quantum states will be associated with cells of volume h^3 in the phase space associated with the gas particles which are in this case photons, and where h is Planck's constant. In order to determine the portion of signal corresponding to one quantum state, we shall relate the volume of one of these cells in the six-dimensional phase space associated with three-dimensional real space to the area of a corresponding cell in the two-dimensional phase space associated with the one-dimensional antenna feed line.

To do this, we note that an antenna with an effective aperature of width a will have a beam angle of approximately λ/a radians were λ signifies the wavelength. From a particle point of view, one says instead that there is an uncertainty in the direction of arrival of a photon. If the usual momentum $p=hf/c$ is associated with a photon, the corresponding uncertainty in either transverse components of momentum is $(hf/c)\sin(\lambda/a)$ or for small angles approximately $(hf/c)(\lambda/a)=h/a$, corresponding to the Heisenberg uncertainty relation $\Delta p\Delta x\geq h$ with $\Delta x=a$. A similar uncertainty in the forward component of momentum of magnitude $h\Delta f/c$ might result from a receiver bandwidth Δf. Thus, since the volume of a cell in phase space is h^3 we have

$$\begin{aligned} h^3 &= \Delta x\Delta y\Delta z\Delta p_x\Delta p_y\Delta p_z \\ &= \Delta x\Delta y\Delta z(h/a)(h/a)(h\Delta f/c) \end{aligned} \tag{14}$$

making the volume in real space corresponding to a cell in phase space

$$\Delta x\Delta y\Delta z=\frac{a^2c}{\Delta f}\cdot \tag{15}$$

Putting $\Delta x=\Delta y=a$ gives the length in the antenna feed line corresponding to one cell as

$$\Delta z=c/\Delta f. \tag{16}$$

In time Δt, the radiation will travel a distance $\Delta z=c\Delta t$, if the transmission line has propagation velocity c. Hence, we can also say that the quanta received in a time

$$\Delta t=\frac{1}{\Delta f} \tag{17}$$

may be regarded as belonging to the same phase-space cell. The portion of signal in a one-dimensional transmission line which the antenna associates with a cell in six-dimensional phase space may thus be associated alternatively with cells of area $\Delta z\Delta p_z=(c/\Delta f)(h\Delta f/c)=h$ in the two-dimensional phase space of the photons in the transmission line or cells of area $\Delta t\Delta f=1$ in a two-dimensional time-frequency or information plane. The precise values of these uncertainty products, of course depend on the definitions used for angular beamwidth, frequency bandwidth, and effective antenna aperture.

Appendix II

Wave Fluctuation in a Transmission Line

In this appendix, we compute an appropriate wave-theory formula for the mean-square energy fluctuation in a one-dimensional black body consisting of a transmission line with matched terminations at both ends such as used, for example, in the Nyquist derivation of the Johnson noise formula. The method of derivation and notation will be chosen to emphasize the similarity of this computation both to Lorentz's computation for the equivalent three-dimensional case[8] and to Rice's computation of the fluctuation in a random current.[10,11]

We assume that the current along the line has statistical properties permitting the representation

$$I_N(z,t)=\sum_{n=-N}^{N}C_n\cos(\omega_nt+\beta_nz+\phi_n) \tag{18}$$

where the ϕ_n are random angles. If the fundamental radian frequency is denoted by $\Delta\omega$ and the constant phase velocity by c, $\omega_n=|n|\Delta\omega$ and $\beta_n=n(\Delta\omega/c)=n\Delta\beta$. That is, frequency is always considered positive, but positive and negative wave numbers are associated respectively with waves traveling in negative and positive directions. We let C_n equal the actual current amplitude multiplied by the square root of the inductance per unit length so that C_n^2 is the average energy per unit line length in the electromagnetic fields of a single traveling wave.

The energy per unit line length is then

$$\begin{aligned} I_N^2(z,t) &= \sum_{n=-N}^{N}C_n^2\cos^2(\omega_nt+\beta_nz+\phi_n) \\ &\quad+2\sum_{n=-N}^{N-1}\sum_{m=n+1}^{N}C_nC_m\cos(\omega_nt+\beta_nz+\phi_n) \\ &\quad\cdot\cos(\omega_mt+\beta_mz+\phi_m). \end{aligned} \tag{19}$$

Integrating over z gives the energy in a length L of the line as

$$E = \int_{-L/2}^{L/2} I_N^2(z, t)dz$$

$$= L\left\{\frac{1}{2}\sum_{n=-N}^{N} C_n^2 + \frac{1}{2}\sum_{n=-N}^{N} C_n^2 P_n \cos(2\omega_n t + \phi_n) + \sum_{n=-N}^{N-1}\sum_{m=n+1}^{N} Q_{nm}C_nC_m \cos[(\omega_n + \omega_m)t + (\phi_n + \phi_m)] + \sum_{n=-N}^{N-1}\sum_{m=n+1}^{N} R_{nm}C_nC_m \cos[(\omega_n - \omega_m)t + (\phi_n - \phi_m)]\right\}, \quad (20)$$

where

$$P_n = \frac{\sin \beta_n L}{\beta_n L}, \quad Q_{nm} = \frac{\sin[(\beta_n + \beta_m)(L/2)]}{(L/2)(\beta_n + \beta_m)},$$

$$R_{nm} = \frac{\sin[(\beta_n - \beta_m)(L/2)]}{(L/2)(\beta_n - \beta_m)}.$$

We shall compute the mean energy in length L and its mean-square fluctuation by averaging over-all possible values of the ϕ_n. These averages may be easily computed using the fact that a cosine function with random phase averages zero and also that its square averages $\frac{1}{2}$.

The mean energy is given by the first term

$$\overline{E} = (1/2)L\sum_{n=-N}^{N} C_n^2. \quad (21)$$

The remaining terms give the difference ϵ between the mean energy and the total energy. Since this difference accounts for the fluctuation we wish to compute, we can compute the mean-square fluctuation in energy by calculating the mean value of the square of these remaining terms.

This computation is facilitated by the following considerations. With the aid of trigonometric identities all of the cross-product terms may be readily shown to average zero. We can neglect the sum containing P since if N is large, the sums containing Q and R will contain many more terms. If we also replace the cosine squared terms by their average values we have left

$$\overline{\epsilon^2} = L^2\sum_{n=-N}^{N-1}\sum_{m=n+1}^{N}\frac{C_n^2C_m^2}{2}[Q_{nm}^2 + R_{nm}^2]. \quad (22)$$

Before completing the computation, it is convenient to replace the summations by equivalent integrations. A suitable representation may be obtained by writing the mean energy as an equivalent integration over a continuous energy spectrum

$$\overline{E} = (1/2)L\sum_{n=-N}^{N} C_n^2$$

$$= L\sum_{n=-N}^{N} W(\beta_n)\Delta\beta \to L\int_{-\infty}^{\infty} W(\beta)d\beta. \quad (23)$$

In order to effect a corresponding transformation of the expression for $\overline{\epsilon^2}$, we note that including also the N terms with $n=m$ represents a negligible percentage increase in the total number of terms which permits us to write

$$\overline{\epsilon^2} = L^2\sum_{n=-N}^{N}\sum_{m=-N}^{N}\frac{C_n^2C_m^2}{4}[Q_{nm}^2 + R_{nm}^2], \quad (24)$$

which transforms into

$$\overline{\epsilon^2} = L^2\int_{-\infty}^{\infty} W(\beta)\int_{-\infty}^{\infty} W(\beta')\left(\frac{\sin[(\beta+\beta')(L/2)]}{(\beta+\beta')(L/2)}\right)^2 d\beta' d\beta + L^2\int_{-\infty}^{\infty} W(\beta)\int_{-\infty}^{\infty} W(\beta')\left(\frac{\sin[(\beta-\beta')(L/2)]}{(\beta-\beta')(L/2)}\right)^2 d\beta' d\beta. \quad (25)$$

The first integrand will have an appreciable value only if β' is nearly equal to $-\beta$. The second integrand will have an appreciable value only if β' is nearly equal to β. Thus, we can make the substitutions $W(\beta') = W(-\beta)$ and $W(\beta') = W(\beta)$ in the respective integrands obtaining

$$\overline{\epsilon^2} = L^2\int_{-\infty}^{\infty} W(\beta)W(-\beta)\int_{-\infty}^{\infty}\left(\frac{\sin[(\beta+\beta')(L/2)]}{(\beta+\beta')(L/2)}\right)^2 d\beta' d\beta + L^2\int_{-\infty}^{\infty} W^2(\beta)\int_{-\infty}^{\infty}\left(\frac{\sin[(\beta-\beta')(L/2)]}{(\beta-\beta')(L/2)}\right)^2 d\beta' d\beta. \quad (26)$$

Each integral over β' equals $2\pi/L$ and the bidirectional symmetry of the problem makes $W(\beta) = W(-\beta)$. Thus,

$$\overline{\epsilon^2} = L^2\int_{-\infty}^{\infty} W^2(\beta)\left[\frac{2\pi}{L} + \frac{2\pi}{L}\right]d\beta = 4\pi L\int_{-\infty}^{\infty} W^2(\beta)d\beta. \quad (27)$$

Since $w(\beta) = w(-\beta)$, the integrals in the expressions for both $\overline{E}$ and $\overline{\epsilon^2}$ may be written as twice integrals from zero to infinity. We can then make the substitutions $\beta = 2\pi f/c$ valid for $\beta > 0$ and $4\pi W(\beta) = w(f)$. Defining $w(f)$ as 4π times $W(\beta)$ gives $w(f)$ the significance of energy per cycle for $0 < f < \infty$ since $W(\beta)$ signifies energy per radian for $-\infty < \beta < \infty$. Formulas (23) and (27) then become

$$\overline{E} = \frac{L}{c}\int_0^{\infty} w(f)df \quad \text{and} \quad \overline{\epsilon^2} = \frac{L}{c}\int_0^{\infty} w^2(f)df. \quad (28)$$

If we are interested in these mean values for only a limited frequency range $f_a < f < f_b$, write $T = L/c$ for the time required for a wave to propagate the length L of the line, and assume that the spectral density function $w(f)$ has a uniform value w_0 between f_a and f_b (as it does by even the quantum mechanical form of the Nyquist noise formula up to nearly the highest microwave frequencies in current use):

$$\overline{E} = Tw_0(f_b - f_a) \quad \text{and} \quad \overline{\epsilon^2} = Tw_0^2(f_b - f_a). \tag{29}$$

Eliminating w_0 by substituting the first of these formulas into the second and redesignating T as Δt and $f_b - f_a$ as Δf gives

$$\overline{\epsilon^2} = \frac{\overline{E}^2}{\Delta t \Delta f}. \tag{30}$$

Rice[10,11] obtains for the mean energy dissipated in a one-ohm resistor by a noise current with uniform spectral density w_0 during time T in bandwidth $f_b - f_a$

$$\overline{E} = Tw_0(f_b - f_a), \tag{31}$$

and for the mean-square energy fluctuation

$$\overline{\sigma_T^2} = w_0^2 T(f_b - f_a). \tag{32}$$

By similarly eliminating w_0 between these formulas, this mean-square fluctuation formula can also be converted to the characteristic form $\overline{E}^2/\Delta t \Delta f$.

ACKNOWLEDGMENT

The author takes pleasure in thanking Professor W. M. Gottschalk of the University of Delaware for his encouragement, suggestions, and helpful discussions.

On the Resolution of a Class of Waveguide Discontinuity Problems by the Use of Singular Integral Equations*

L. LEWIN†

Summary—**It is shown that a considerable number of solutions of rectangular waveguide problems appearing in the literature are all special cases of a general treatment focused around the known solution of a singular integral equation. In terms of this a number of typical results are re-examined. The method is then applied to four new configurations, and the range of application and the limitations are examined.**

I. INTRODUCTION

THE number of waveguide problems capable of exact solution is limited to a few very simple shapes, even when the common approximations of ideal geometry and infinite wall conductivity are made. A class of problems recently amenable to exact treatment has involved configurations in which the discontinuity has separated the space into two uniform regions, $z<0$ and $z>0$. Examples are the radiation into free space of a semi-infinite length of guide, a bifurcation of the waveguide, and, exceptionally, a diaphragm halfway across the guide. The solutions involve the setting up of an integral equation for the field along the guide axis, or some other equivalent axis, the integral equation taking a different form on either side of the discontinuity. It is then solved by the Wiener-Hopf technique, the waveguide parameters being readily obtainable from the solution.

This method gives a rigorous result for the limited number of configurations to which it can be applied. It is not successful, however, in the majority of those cases in which the discontinuity takes the form of a variation over the cross section of the waveguide, such as, for example, diaphragms, strips, change of guide cross section, etc. Nor is it applicable to configurations in which the propagation medium changes at the discontinuity, *e.g.*, if there is a dielectric or ferrite insert.

For such cases it is more satisfactory to take the field over the cross section as the unknown variable, and a different type of integral equation can be set up for this class of problems. The Wiener-Hopf technique is no longer usuable, but the equation can be solved to various quasi-static degrees of approximation in some particular cases. This has been done by Schwinger and co-authors[1] for waveguide diaphragms, and by Lewin[2,3] for un-

* Received by the PGMTT, March 8, 1961.
† Standard Telecommunication Laboratories, Harlow, Essex, England.

[1] N. Marcuvitz, "Waveguide Handbook," M.I.T. Rad. Lab. Ser., McGraw-Hill Book Co., Inc., New York, N. Y., p. 147; 1951.
[2] L. Lewin, "The impedance of unsymmetrical strips in rectangular waveguides," *Proc. IEE*, vol. 99, pt. 4, pp. 168–176, Monograph No. 29; 1952.
[3] L. Lewin, "A ferrite boundary value problem in a rectangular waveguide," *Proc. IEE*, vol. 106, pt. B, pp. 559–563; November, 1959.

symmetrical waveguide strips, and for a ferrite-loaded guide section. Schwinger[4] has also used conformal transformation methods to obtain expressions for the waveguide parameters without obtaining in explicit form the integral equation solution. This last method is very powerful, and its results include those for some of the diaphragm configurations, otherwise obtainable by the direct solution of the quasi-static integral equation.

However, not all such configurations can be catered for in this way; and it appears that a direct solution of the quasi-static integral equation is necessary for unsymmetrical inductive configurations, changes of propagation medium, reactive strips, and others.

It is with this latter class of discontinuities that this paper is concerned. The equations have occurred sporadically in the literature and have been solved by *ad hoc* methods. It is now realized that they are all particular cases of a general treatment which has a wide, albeit limited, field of applicability. The paper outlines first the known examples mentioned above, as particular cases of the general treatment, and finishes with a few new examples and an indication of the types of configuration to which the method should be successful. It does not, of course, displace the earlier treatments; rather it extends the range of problems that can, to the various quasi-static degrees of approximation chosen, be rigorously solved.

II. Inductive Diaphragm

Fig. 1 shows an inductive diaphragm in a rectangular waveguide. A wave in the dominant mode, $E_x = \sin(\pi y/a)e^{-ik'z}$, is incident from $z = -\infty$ and sets up a reflected wave, a transmitted wave, and a train of evanescent modes on both sides of the diaphragm. The field in the aperture, $E(y)$, is as yet unknown, but in terms of it, by a Fourier expansion, the amplitudes of the various modes can be expressed. The continuity of tangential magnetic field over the aperture leads to an equation containing the mode amplitudes, and if these be expressed, as above, in terms of $E(y)$ an integral equation for $E(y)$ results. This equation can be simplified by an integration by parts, and, in terms of the unknown diaphragm susceptance, B, takes the form[5]

$$B \sin(\pi y/a) \int F(\eta) \cos(\pi\eta/a)\,d\eta = -\sum_{2}^{\infty} (\lambda_G/a)(1-\delta_n) \int F(\eta) \sin(n\pi y/a) \cos(n\pi\eta/a)\,d\eta. \quad (1)$$

Here $F(\eta) = E'(\eta)$, the variable of integration, η, ranging only over the aperture, which is also the range of y over which (1) has to hold. The quantity $\delta_n = 1 - (1 - k^2a^2/n^2\pi^2)^{1/2}$ is a small quantity, vanishing for high-mode number, n, and is a measure of the departure of the nth mode from its quasi-static value. As a first approximation it can be neglected. As a second, the first one or two coefficients are retained, with a corresponding higher-order solution resulting. The retention of these higher-order terms does not affect the method of solution, though it complicates it. They will therefore not be considered here, though their inclusion at any point is relatively straightforward.

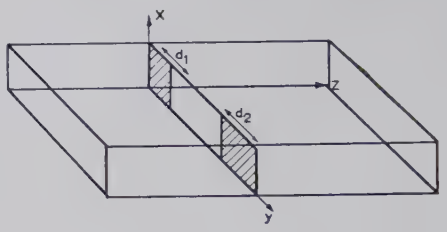

Fig. 1—Inductive diaphragm in rectangular waveguide.

In order to solve (1) with δ_n neglected, we add and subtract the first term of the infinite series, summing it via the known result

$$\sum_{1}^{\infty} \frac{\cos(n\pi y/a)\cos(n\pi\eta/a)}{n} = -\tfrac{1}{2}\log 2\,|\cos(\pi\eta/a) - \cos(\pi y/a)|.$$

On differentiation with respect to y this gives

$$\sum_{1}^{\infty} \sin(n\pi y/a)\cos(n\pi\eta/a) = \frac{\tfrac{1}{2}\sin(\pi y/a)}{\cos(\pi\eta/a) - \cos(\pi y/a)}, \quad (2)$$

and substituting into (1) gives

$$(2 + 2aB/\lambda_0) \int F(\eta)\cos(\pi\eta/a)\,d\eta = -\int \frac{F(\eta)\,d\eta}{\cos(\pi\eta/a) - \cos(\pi y/a)}, \quad (3)$$

where, as before, the range of both y and η is the diaphragm aperture.

Now the whole of the left-hand side is some constant, C, independent of y. If we take new variables $X = \cos(\pi\eta/a)$, $Y = \cos(\pi y/a)$ and put $F(\eta)d\eta = G(X)dX$ then (3) becomes

$$\int_A^B \frac{G(X)dX}{X - Y} = -C \qquad A < Y < B. \quad (4)$$

Here A and B are the new limits for X corresponding to the aperture limits for η. The inclusion of higher-order terms would add a polynomial in Y to the right-hand side; otherwise the form of (4) is unaltered.

The principal value of the integral in (4) is to be understood. Hence (4) is a singular integral equation, and we can appeal to the theory of these equations for its solution. A convenient reference is Tricomi,[6] where

[4] Marcuvitz, *op. cit.*, p. 156.

[5] L. Lewin, "Advanced Theory of Waveguides," Iliffe and Sons, London, England, p. 47; 1951.

[6] F. G. Tricomi, "Integral Equations," Interscience Publishers, New York, N. Y., pp. 173–188; 1957.

we find the solution of

$$f(X) = \frac{1}{\pi}\int_{-1}^{1} \frac{\phi(Y)}{Y - X}\, dY \tag{5}$$

is given by

$$\phi(X) = -\frac{1}{\pi}\int_{-1}^{1} \sqrt{\frac{1 - Y^2}{1 - X^2}}\, \frac{f(Y)}{Y - X}\, dY + \frac{K}{\sqrt{1 - X^2}}. \tag{6}$$

K is of the nature of an integration constant. To apply this result to (4) it is necessary to change the range of integration from (A, B) to $(-1, 1)$. This is easily done by taking new variables

$$X' = \frac{2(X - A)}{B - A} - 1 \tag{7}$$

with a similar form for Y' in terms of Y. This is precisely equivalent to Schwinger's transformation[1] $\cos(\pi y/a) = c + s\cos\theta$ which is the "trick" by means of which such equations as (3) have been treated hitherto. Now K in (6) is

$$\frac{1}{\pi}\int_{-1}^{1} \phi(X)dX$$

which, in the case of (4), reduces to

$$\int G(X)dX = \int F(\eta)d\eta = E(\eta).$$

For physical reasons this vanishes at both limits; thus $K = 0$ and the additional term in (6) vanishes. $f(Y)$ is a constant in the present case, and since

$$\int_{-1}^{1} \frac{\sqrt{1 - Y^2}\, dY}{Y - X} = -\pi X,$$

the solution to (4) follows at once. Corresponding solutions are obtained if the right-hand side of (4) is replaced by a finite polynomial so that higher-order solutions are readily obtained without any *ad hoc* guessing at the necessary forms.

The details of these expressions do not concern us here. The important thing is the realization that (3) can be reduced to a special case of (5) by means of a simple change of variable. It is the constant reappearance of the singular integral equation in various forms that is the key to the extension of the method to a wider range of configurations.

III. The Unsymmetrical Capacitive Strip

The setting up of the integral equation follows a similar route to that of the previous case except that the current on the strip rather than the aperture field is the unknown to be evaluated. (A similar type of expression results when the current rather than the aperture field is used in the diaphragm cases.) The quasi-static integral equation can be put in the form[2]

$$x + C = 2\sum_{1}^{\infty} \int \sin(n\pi x/b)\cos(n\pi\xi/b)I(\xi)d\xi, \tag{8}$$

where C is a constant, $I(\xi)$ is proportional to the unknown current in the strip, and the range of both x and ξ is over the strip.

This equation, on using (2) to effect the summation, and on putting $\cos(\pi x/b) = X$, $\cos(\pi\xi/b) = Y$, $I(\xi)d\xi = F(Y)dY$ becomes

$$\frac{C + \dfrac{b}{\pi}\cos^{-1} X}{\sqrt{1 - X^2}} = \int \frac{F(Y)dY}{Y - X}. \tag{9}$$

The change of variable of (7) at once reduces this to the form (5) and the solution, apart from the rather awkward integration, follows. Integration constants, which enter in this problem, are determined by setting the tangential electric field zero at the strip edge.

In the original paper[2] (8) was solved through the use of Schwinger's transformation, assuming an infinite Fourier series for $I(\xi)$. This was eventually summed, leading to the same result as the solution to (9). The details, together with the final integrations, are given in the reference.

The point to be noted here is the reappearance of the singular integral equation in (9), albeit in a more complicated form than in (4).

IV. Ferrite-Loaded Waveguide

The arrangement consists of a rectangular waveguide filled with a medium of dielectric constant ϵ for $-\infty < z < 0$, and transversely magnetized ferrite for $0 < z < \infty$. The reason that this arrangement gives rise to anything more involved than simple reflected and transmitted waves is that the ferrite supports a magnetic field distribution which differs, on account of the tensor permeability, from that in the plain guide. Hence an infinite series of modes is needed, on both sides of the boundary, to satisfy continuity conditions. The details are given in Sharpe and Heim's paper.[7] In Lewin[3] the integral equation derived is of the form

$$C = MF(Y) + \frac{jK}{\pi}\int_{-1}^{1} \frac{F(X)}{X - Y}\, dX, \tag{10}$$

where C, M and K are constant, and $F(X)$ is related to the field at the junction across the ferrite face.

This is a singular integral equation, but of a different sort from (5). In the reference it was solved partly by guesswork; but it is a particular case of Carleman's equation[6]

$$a(x)\phi(x) - \lambda\int_{-1}^{1} \frac{\phi(y)}{y - x}\, dy = f(x), \tag{11}$$

[7] C. B. Sharpe and D. S. Heim, "A ferrite boundary-value problem in a rectangular waveguide," IRE Trans. on Microwave Theory and Techniques, vol. MTT-6, pp. 42–46; January, 1958.

with the solution

$$\phi(x) = \frac{a(x)f(x)}{a^2(x) + \lambda^2\pi^2} + \frac{\lambda e^{\tau(x)}}{\sqrt{a^2(x) + \lambda^2\pi^2}} \cdot \left[\int_{-1}^{1} \frac{e^{-\tau(y)}f(y)}{\sqrt{a^2(y) + \lambda^2\pi^2}} \frac{dy}{y - x} + \frac{c}{1 - x}\right], \quad (12)$$

where

$$\tau(x) = \frac{1}{\pi}\int_{-1}^{1} \frac{\theta(t)}{t - x}\, dt, \qquad \theta(t) = \tan^{-1}\frac{\lambda\pi}{a(t)}.$$

All the integrals involved are principal values.

Eq. (12) contains (5) as the special case $a(x) = 0$. Eq. (10) is the case $a(x) = M$, $f(x) = C$: higher-order mode solutions replace C by a simple polynomial, with no change in the character of the solution.

Although solutions have, in the past, been obtained, partially by guesswork, the formulation of the explicit form (11) and its solution (12), with (5) and (6) as a special case, is the central feature around which this paper is written. Some new extensions of existing configurations follow.

V. Ferrite-Loaded Waveguide with Inductive Diaphragm

Although the solution of the ferrite-loaded waveguide of Section IV is quite a formidable task, it is not, in fact, much more difficult to combine it with an inductive diaphragm. The arrangement is shown in Fig. 2, the diaphragm being located at the ferrite face.

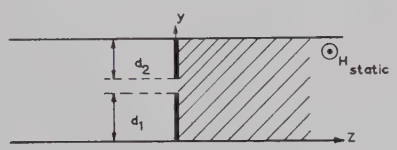

Fig. 2—Inductive diaphragm in ferrite-loaded guide.

If the process of setting up the integral equation is repeated, with the addition of the metallic diaphragm at the boundary, it is seen that the only changes occasioned by the alteration is a reduction of the range of integration, and of the independent variable in the integral equation, to the new aperture. Hence, the new equation is

$$C = MF(y) + j\frac{K}{\pi}\int_{\alpha}^{\beta} \frac{F(x)}{x - y}\, dx, \quad (13)$$

where $-C = 1 + KX$ and the normalized reactance, X, is

$$jX = \frac{2}{\pi}\int_{\alpha}^{\beta} yF(y)dy. \quad (14)$$

These forms are taken from Lewin.[3] Moreover, $F(y)$ must satisfy

$$\int_{\alpha}^{\beta} F(y)dy = 0.$$

If d_1 and d_2 are the diaphragm inserts, then the values of α and β are given by $-\cos(\pi d_2/a)$ and $\cos(\pi d_1/a)$. The transformation (7) gives new limits $(1, -1)$ with

$$\frac{dx}{x - y} = \frac{dx'}{x' - y'}.$$

Hence the equation transforms unaltered into (10), and the only eventual change is that (14) for jX becomes multiplied by the factor $f^2 = \frac{1}{4}(\beta - \alpha)^2$ from the contribution of ydy on changing variables. From (33) of Lewin[3] we accordingly get the equation

$$X = -\frac{4C}{K}p(1 - p)f^2 \text{ instead of } -\frac{4C}{K}p(1 - p),$$

which, together with $-C = 1 + KX$ gives, eventually,

$$X = -\frac{1}{K}\left\{1 + \frac{\pi^2}{f^2L^2 + \pi^2(f^2 - 1)}\right\}, \quad (15)$$

where

$$L = \frac{1}{\pi}\log\frac{K + M}{K - M}$$

(see (35) of Lewin[3]). The factor f can be put in the form $\sin(\pi d/2a)\ \sin(\pi y_0/a)$ where $d = a - d_1 - d_2$ is the aperture opening and $y_0 = \frac{1}{2}(a + d_1 - d_2)$ is the coordinate of its center. Eq. (15) reduces to (35) of Lewin[3] when $f = 1$ (no diaphragm inserts) and gives $X = 0$, as it must, for $f = 0$ (diaphragm completely across the guide).

VI. Rectangular Waveguide Bifurcation (*H*-plane)

Fig. 3 shows an H-plane bifurcation of a rectangular waveguide, in which two guides of width a join at $z = 0$ into a single guide of width $2a$.

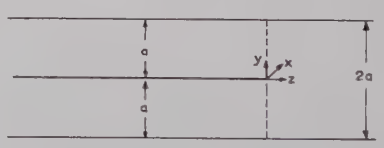

Fig. 3—H-plane bifurcation in rectangular waveguide.

This arrangement in it simplest form is solvable rigorously by the Wiener-Hopf technique.[8] The justification of treating it here by the quasi-static integral equation method is that a number of variants are possible which yield only to the latter method of attack. Thus, a different dielectric material can be used on either side of the junction, or an arrangement of diaphragm or strips can be incorporated there, or both of these can be used together. These variants are foreign to the Wiener-Hopf approach, which, nevertheless, has its own field of applicability, *e.g.*, to bifurcation with unequal guides. It just so happens that the two approaches overlap in the simple arrangement of Fig. 3.

[8] Marcuvitz, *op. cit.*, p. 383.

Two basic modes can be supported by Fig. 3, symmetrical and antisymmetrical. Any method of feeding the two guides from the left can be resolved into a sum of these two. Moreover, since the antisymmetrical mode is just the natural second-order mode in the broad guide, there is no change of field at the junction—the field propagates without reflection.

Hence only the symmetrical mode needs to be considered, and we confine our attention to the upper part of the figure, $0<y<a$.

For $z<0$ we have

$$E_x = (e^{-ik'z} + Re^{ik'z}) \sin(\pi y/a) + \sum_2^\infty R_n e^{\gamma_n z} \sin(n\pi y/ \tag{16}$$

$$Z_0 H_y = (e^{-ik'z} - Re^{ik'z})(k'/k) \sin(\pi y/a) + j \sum_2^\infty R_n(\gamma_n/k) e^{\gamma_n z} \sin(n\pi y/a), \tag{17}$$

where $Z_0 = 120\pi$, $k' = 2\pi/\lambda_g$ and $\gamma_n = \sqrt{n^2\pi^2/a^2 - k^2} \sim n\pi/a$ for large n. The reflection coefficient R and the mode amplitudes R_n have yet to be determined.

For $z>0$, bearing in mind the symmetrical feeding,

$$E_x = T_1 e^{-jK'z} \cos(\pi y/2a) + \sum_1^\infty T_{2m+1} e^{-\Gamma_{2m+1} z} \cos(\sqrt{2m+1}\,\pi y/2a) \tag{18}$$

$$Z_0 H_y = T_1(K'/k) e^{-jK'z} \cos(\pi y/2a) - j \sum_1^\infty T_{2m+1}(\Gamma_{2m+1}/k) e^{-\Gamma_{2m+1} z} \cos(\sqrt{2m+1}\,\pi y/2a). \tag{19}$$

Here $K' = 2\pi/\Lambda_g$ with $\Lambda_g = \lambda/\sqrt{1-(\lambda/4a)^2}$ and

$$\Gamma_{2m+1} = \sqrt{(2m+1)^2\pi^2/4a^2 - k^2} \sim (2m+1)\pi/2a \text{ for large } m.$$

If $E(\pi y/a)$ is the as yet unknown field in the aperture $(0<y<a)$, then the various mode amplitudes can be expressed in terms of it as follows:

$$1 + R = \frac{2}{a}\int_0^a E(\pi\eta/a) \sin(\pi\eta/a) d\eta = \frac{2}{\pi}\int_0^\pi E'(\theta) \cos\theta d\theta \tag{20}$$

on putting $\pi\eta/a = \theta$ and integrating by parts. (The integrated part vanishes at both limits because of the vanishing of the tangential electric field at the metal boundaries.) Similarly,

$$R_n = \frac{2}{\pi n}\int_0^\pi E'(\theta) \cos n\theta d\theta \tag{21}$$

$$T_{2m+1} = \frac{-4}{\pi(2m+1)}\int_0^\pi E'(\theta) \sin(\sqrt{2m+1}\,\theta/2) d\theta. \tag{22}$$

These values can be substituted in (17) and (19). We replace γ_n and Γ_{2m+1} by their dominant forms and a remainder term, and write $\pi y/a = \phi$ as a conplementary variable to θ. The summations are affected via (2), there being some simplification of terms. The equation expressing continuity of tangential magnetic field over the aperture is obtained by equating (17) to (19) for $0<y<a$.

$$A \sin\phi + B \cos(\phi/2) = \int_0^\pi \frac{E'(\theta) \cos(\phi/2) d\theta}{2[\sin(\theta/2) - \sin(\phi/2)]} + S, \tag{23}$$

where

$$A = -\tfrac{1}{2} jk'a(1-R) - \int_0^\pi E'(\theta) \cos\theta d\theta,$$

$$B = (1 - j2aK'/\pi)\int_0^\pi E'(\theta) \sin(\theta/2) d\theta.$$

S is a remainder term giving the effect of the differences of the higher-order mode attenuation constants from their quasi-static values.

$$S = \sum_1^\infty \left(\frac{2a\Gamma_{2m+1}}{\pi(2m+1)} - 1\right)\int_0^\pi E'(\theta) \sin(\sqrt{2m+1}\,\theta/2) \cdot \cos(\sqrt{2m+1}\,\phi/2) d\theta - \sum_2^\infty \left(\frac{a\gamma_n}{n\pi} - 1\right)\int_0^\pi E'(\theta) \sin(n\phi) \cos(n\theta) d\theta. \tag{24}$$

To solve (23) to the quasi-static approximation, neglect S and change variables by putting $\sin(\theta/2) = \tfrac{1}{2}(1+x)$, $\sin(\phi/2) = \tfrac{1}{2}(1+y)$. A common factor $\cos(\phi/2)$ can be cancelled in (23) which becones, on putting $E'(\theta)d\theta = F(x)dx$,

$$A(1+y) + B = \int_{-1}^1 \frac{F(x)dx}{x-y}. \tag{25}$$

This is of the form (5), giving as solution,

$$F(x) = \frac{1}{\pi^2\sqrt{1-x^2}}[C + \pi x(A + B + Ax)]. \tag{26}$$

In order to determine C, we note that

$$\int_{-1}^1 F(x)dx = \int_0^\pi E'(\theta)d\theta = E(\pi) - E(0) = 0,$$

since E vanishes at the limits. Finally, therefore,

$$F(x) = \frac{1}{\pi\sqrt{1-x^2}}[Ax^2 + (A+B)x - \tfrac{1}{2}A]. \tag{27}$$

From (20), together with the two equations defining A and B, we get three relations from which A and B can be eliminated. These give the following expression for the normalized quasi-static impedance at the junction,

$$Z = \frac{1+R}{1-R} = j\frac{k'a}{\pi}\,\frac{35\pi + j2K'a}{13\pi + j30K'a}. \tag{28}$$

If only one waveguide is fed from the left we have to add an antisymmetrical mode of unit amplitude to cancel the wave in the other guide. Hence the incident mode amplitude is now 2 so that in this case the *relative* reflection coefficient is $\frac{1}{2}R$ with R still given by (28).

Improvements on (28) can be obtained by retaining early terms in the series (24). Thus the first term to deviate appreciably from zero is the term in Γ_3. If we retain it, (25) is augmented to

$$A(1+y) + B + C(y^2+2y) = \int_{-1}^{1} \frac{F(x)}{x-y}\,dx, \tag{29}$$

where

$$C = \Delta_3 \int_0^{\pi} E'(\theta)\sin(3\theta/2)d\theta, \qquad \Delta_3 = \frac{2a\Gamma_3}{3\pi} - 1.$$

The appropriate solution of (29) is

$$F(x) = \frac{1}{\pi\sqrt{1-x^2}}\left\{Cx^3 + (A+2C)x^2 + (A+B-\tfrac{1}{2}C)x - (\tfrac{1}{2}A + C)\right\}. \tag{30}$$

If this is substituted in (20), and also into the expressions defining A, B and C, and the latter eliminated, an equation analogous to (28) appears, in which the small quantity $d = 3\Delta_3/(64+28\Delta_3)$ indicates the order of departure from (28)

$$\frac{1+R}{1-R} = j\frac{k'a}{\pi}\,\frac{35\pi + j2K'a - d(119\pi + j18K'a)}{13\pi + j30K'a + d(135\pi - j14K'a)}. \tag{31}$$

It is a straightforward matter to include different dielectric media in the solution. Thus, if the guides on the left have a dielectric constant ϵ, instead of the value unity so far assumed, (16) and (17) hold except that k' becomes $(2\pi/\lambda)\sqrt{\epsilon-(\lambda/2a)^2}$ and γ_n becomes $\sqrt{n^2\pi^2/a^2 - k^2\epsilon}$. The analysis is otherwise unaltered, and the results (28) or (31) are valid with the new values of the constants. Similarly, the dielectric on the right can be varied.

Another configuration which is similarly solvable without much further trouble is the case of the bifurcated waveguide with diaphragms at the junction. In order to maintain symmetry the diaphragm in the lower half is the mirror image of that in the upper. There is no complication, either, to accept arbitrary dielectrics in the different guides.

The effect of the diaphragm first appears in (20), wherein the limits of integration become as in Section V. The solution leads directly to (25), but with the altered limits. The change of variable of (7) then restores the range to -1, 1 and the solution proceeds as before. We shall not, however, pursue the matter any further here, as the example given in Section V is typical of the method of solution obtained.

VII. Inductive Diaphragm and Strip

As a further example we shall examine an obstacle in a rectangular waveguide consisting of the combination of a symmetrical diaphragm with a central strip. Only the inductive case will be examined, as the capacitive case is obtainable from the known result[2] for an unsymmetrical capacitive strip, by the method of images.

The arrangement is shown in Fig. 4. It is apparent that there is a double aperture and a triple metallic obstacle, either method of description being permissible. In order to reduce the problem to one involving a single unknown function we note that, because of the symmetry, a single aperture distribution function suffices,

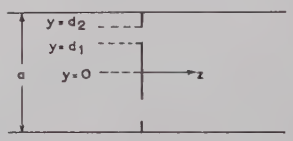

Fig. 4—Inductive diaphragm and strip in rectangular waveguide.

the same for each aperture. Hence we set up the equations from this point of view. As in the previous section, we could allow for different dielectric materials on either side of the discontinuity, but this is an unnecessary complication which will be omitted here.

The field to the left of the obstacle can be written

$$E_x = (e^{-ik'z} + Re^{ik'z})\cos(\pi y/a) + \sum_1^{\infty} R_{2n+1}e^{\gamma_{2n+1}z}\cos(\sqrt{2n+1}\,\pi y/a) \tag{32}$$

$$Z_0H_yk = k'(e^{-ik'z} - Re^{ik'z})\cos(\pi y/a) + j\sum_1^{\infty} R_{2n+1}\gamma_{2n+1}e^{\gamma_{2n+1}z}\cos(\sqrt{2n+1}\,\pi y/a), \tag{33}$$

with

$$\gamma_{2n+1} = \sqrt{(2n+1)^2\pi^2/a^2 - k^2} \sim (2n+1)\pi/a \text{ for large } n.$$

To the right a similar form is obtained, except that the first term for E_x is $(1+R)e^{-ik'z}\cos(\pi y/a)$, the magnitude coming from the equality of E_x on the two sides of the boundary. The sign of z in the exponentials is reversed, and this changes the sign of j in the series for H_y. Only odd-order modes appear in the various summations on account of the symmetry of the arrangement.

If the field in the upper aperture is represented by $E(\pi y/a)$, then Fourier analysis gives

$$1 + R = \frac{4}{a}\int_{d_1}^{d_2} \cos(\pi y/a)E(\pi y/a)dy$$

$$= -\frac{4}{\pi}\int_{\pi d_1/a}^{\pi d_2/a} E'(\theta)\sin\theta d\theta \qquad (34)$$

on changing variable and integrating by parts. As previously, the integrated part vanishes at the limit because of the physical requirements on E at the edges of the metal inserts.

Similarly for the higher mode coefficients

$$R_{2n+1} = -\frac{4}{\pi}\frac{1}{2n+1}\int_{\pi d_1/a}^{\pi d_2/a} E'(\theta)\sin(\overline{2n+1}\,\theta)d\theta.$$

The equation resulting from equating the tangential magnetic fields on the two sides of the boundary can be written

$$ak'R\cos\phi = -4j\sum_1^\infty \frac{a\gamma_{2n+1}}{\pi(2n+1)}\int E'(\theta)\sin(\overline{2n+1}\,\theta)\sin(\overline{2n+1}\,\phi)d\theta, \qquad (35)$$

The solution of the integral equation is

$$F(y) = \frac{A}{\pi\sqrt{1-y^2}}(y + C). \qquad (39)$$

In order to determine C we note that, from the vanishing of $E(\theta)$ at the limits,

$$0 = \int_{\pi d_1/a}^{\pi d_2/a} E'(\theta)d\theta = -\beta\int_{-1}^{1}\frac{F(y)dy}{\sin\theta}, \text{ hence}$$

$$\int_{-1}^{1}\frac{y+C}{\sqrt{1-y^2}}\frac{dy}{\sqrt{1-\alpha-\beta y}} = 0. \qquad (40)$$

The determination of C from this relation is given in Appendix I.

From (34) and (37) we can now calculate the reflection at the aperture, and hence the normalized reactance X representing the discontinuity. In terms of C we have

$$X = -\frac{a}{\lambda_g}\frac{\beta C}{1+\beta C}.$$

This relation can be put in various forms. Perhaps the simplest is

$$X = \frac{a}{\lambda_g}\left\{-1 + \frac{K}{2\sin^2(\pi d_2/a)E + [\cos^2(\pi d_2/a) - \sin^2(\pi d_1/a)]K}\right\}, \qquad (41)$$

where the integration and the range of the variable $\phi = \pi y/a$ is over the upper aperture $\pi d_1/a \leq \phi, \theta \leq \pi d_2/a$. From the symmetry of the problem correct conditions are maintained in the lower half of the guide. Now

$$\frac{a\gamma_{2n+1}}{\pi(2n+1)} = 1 - \delta_{2n+1},$$

where $\delta \to 0$ for large n. For the quasi-static solution we ignore δ completely (as previously, the first few terms could be retained to give an improved solution).

On adding the first term of the series to each side, summing and simplifying, (35) can be written

$$A\cos\phi = \int_{\pi d_1/a}^{\pi d_2/a}\frac{E'(\theta)\sin\theta\cos\phi d\theta}{\cos 2\phi - \cos 2\theta}, \qquad (36)$$

where

$$A = jak'R/4 + \int_{\pi d_1/a}^{\pi d_2/a} E'(\theta)\sin\theta d\theta. \qquad (37)$$

To solve this equation, put $\cos 2\phi = \alpha + \beta x$, $\cos 2\theta = \alpha + \beta y$ and $E'(\theta)\sin\theta d\theta = \beta F(y)dy$. The factor $\cos\phi$ cancels and (36) becomes

$$A = \int_{-1}^{1}\frac{F(y)dy}{y-x}, \text{ provided that}$$

$$\alpha + \beta = \cos(2\pi d_1/a) \text{ and } \alpha - \beta = \cos(2\pi d_2/a). \qquad (38)$$

where the modulus of the complete elliptic functions K and E is given by

$$k = \sqrt{1 - \sin^2(\pi d_1/a)\operatorname{cosec}^2(\pi d_2/a)}. \qquad (42)$$

This may be compared to Lewin,[5] (p. 62) to which it reduces when $d_2 = \frac{1}{2}a$.

VIII. Unsymmetrical H-Plane Step

Fig. 5 shows a waveguide filled with a medium ϵ_1, μ_1 (relative values) from $z = -\infty$ to $z = 0$. At $z = 0$ the guide side $y = a$ is stepped to give a guide of width $2a$ for $z > 0$. This region is filled with medium ϵ_2, μ_2. A wave with electric field $E_x = e^{-jk'z}\sin(\pi y/a)$ is incident from the left, with the propagation constant given by

$$k' = k(\epsilon_1\mu_1 - \lambda^2/4a^2)^{1/2}. \qquad (43)$$

The modes which can propagate for $z > 0$ depend on the values of ϵ_2 and μ_2. In particular, if both media are the same, at least two modes can propagate in the wider guide, the dominant mode and the second. They are of the form, respectively,

$$e^{-jK'z}\sin(\pi y/2a) \quad \text{and} \quad e^{-jK_2z}\sin(\pi y/a),$$

with

$$K' = k(\epsilon_2\mu_2 - \lambda^2/16a^2)^{1/2}$$

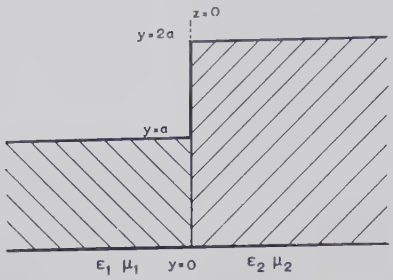

Fig. 5—Change of cross section and of medium in H-plane of rectangular waveguide.

and

$$K_2 = k(\epsilon_2\mu_2 - \lambda^2/4a^2)^{1/2}. \tag{44}$$

When the media are the same, K_2 is the same as k'.

In order to treat the most general case, the loading to these two modes at $z>0$ must be considered. If the second guide is completely matched, there is no reflection in either mode. In general there will be reflections of amplitude R_1' and R_2', with phases dependent on the positioning of the reflecting loads. If these loads are referred to the plane $z=0$, we can define admittances

$$Y_1 = (1 - R_1')/(1 + R_1')$$

and

$$Y_2 = (1 - R_2')/(1 + R_2'), \tag{45}$$

which determine the effects of the reflections. These admittances are relative to the wave-admittances in the second guide, the relevant admittance being that of the respective mode.

The equations for the electric and magnetic fields can now be set up. For $z<0$ we have

$$E_x = (e^{-jk'z} + Re^{jk'z}) \sin(\pi y/a) + \sum_2^\infty R_n e^{\gamma_n z} \sin(n\pi y/a) \tag{46}$$

$$\mu_1 k Z_0 H_y = k'(e^{-jk'z} - Re^{jk'z}) \sin(\pi y/a) + j\sum_2^\infty R_n\gamma_n e^{\gamma_n z} \sin(n\pi y/a), \tag{47}$$

where

$$\gamma_n = (n^2\pi^2/a^2 - k^2\epsilon_1\mu_1)^{1/2} \sim n\pi/a \text{ for large } n. \tag{48}$$

For $z>0$,

$$E_x = \frac{T_1}{1 + R_1'}(e^{-jK'z} + R_1'e^{jK'z}) \sin(\pi y/2a) + \frac{T_2}{1 + R_2'}(e^{-jK_2z} + R_2'e^{jK_2z}) \sin(\pi y/a) + \sum_3^\infty T_n e^{-\Gamma_n z} \sin(n\pi y/2a) \tag{49}$$

$$\mu_2 k Z_0 H_y = \frac{K'T_1}{1 + R_1'}(e^{-jK'z} - R_1'e^{jK'z}) \sin(\pi y/2a) + \frac{K_2T_2}{1 + R_2'}(e^{-jK_2z} - R_2'e^{jK_2z}) \sin(\pi y/a) - j\sum_3^\infty T_n\Gamma_n e^{-\Gamma_n z} \sin(n\pi y/2a), \tag{50}$$

where

$$\Gamma_n = (n^2\pi^2/4a^2 - k^2\epsilon_2\mu_2)^{1/2} \sim n\pi/2a \text{ for large } n. \tag{51}$$

In putting the equations in this form the coefficients of the first two modes have been written so as to exhibit fully the effect of the loading in the second guide. Thus, T_1 alone is simply the transmission coefficient in the absence of mismatch in the dominant mode.

At $z=0$ the electric field is taken to be $E(\pi y/a)$ for $0<y<a$, and 0 for $a<y<2a$. At $y=0$, a, it is zero at the metal walls. Otherwise the form of E is as yet undetermined. It will be convenient to take a dummy variable of integration η instead of y, and also to change variables from $\pi\eta/a$ to θ and $\pi y/a$ to ϕ. Then the various coefficients can be determined by Fourier analysis in terms of the as yet unknown E. For example,

$$1 + R = \frac{2}{a}\int_0^a E(\pi\eta/a) \sin(\pi\eta/a)d\eta.$$

If we integrate by parts, taking the integrated part zero because of the vanishing of E at the limits, and change from η to θ as explained above, we get

$$1 + R = \frac{2}{\pi}\int_0^\pi E'(\theta) \cos\theta d\theta. \tag{52}$$

Similarly

$$R_n = \frac{2}{\pi n}\int_0^\pi E'(\theta) \cos n\theta d\theta \tag{53}$$

and

$$T_n = \frac{2}{\pi n}\int_0^\pi E'(\theta) \cos\tfrac{1}{2}n\theta d\theta. \tag{54}$$

Inserting these values in the equations for the magnetic field, putting $z=0$, and equating the two fields over the aperture, gives

$$\tfrac{1}{2}\pi\mu_2k'(1 - R) \sin\phi + j\sum_2^\infty \mu_2(\gamma_n/n)\int_0^\pi E'(\theta) \cos n\theta d\theta \cdot \sin n\phi = \mu_1K'Y_1 \sin\tfrac{1}{2}\phi\int_0^\pi E'(\theta) \cos\tfrac{1}{2}\theta d\theta + \tfrac{1}{2}\mu_1K_2Y_2 \sin\phi\int_0^\pi E'(\theta) \cos\theta d\theta - j\sum_3^\infty \mu_1(\Gamma_n/n)\int_0^\pi E'(\theta) \cos\tfrac{1}{2}n\theta d\theta \cdot \sin\tfrac{1}{2}n\phi. \tag{55}$$

In order to obtain the quasi-static equation we now replace γ_n by $n\pi/a$ and Γ_n by $n\pi/2a$. If desired, a finite number of early terms could be retained in their exact form: this has, in fact, been done with the second-order mode, which happens, in this problem, to be a propagating mode. The series are then extended down to $n=1$ by adding and subtracting terms, and summed using the formula

$$\sum_1^\infty \cos(nu)\sin(nv) = \tfrac{1}{2}\sin v/(\cos u - \cos v).$$

We introduce two constants as follows:

$$A = (j4/\pi^2)(j\pi + 2K'aY_1)\int_0^\pi E'(\theta)\cos\tfrac{1}{2}\theta d\theta \tag{56}$$

$$B = (-j8/\pi)[k'a(1-R)\mu_2/\mu_1 - \tfrac{1}{2}(1+R)(j\pi + K_2aY_2 + j\pi\mu_2/\mu_1)]. \tag{57}$$

Then (55) becomes, after expressing the trigonometrical terms in terms of their half angles,

$$\frac{1}{\pi}\int_0^\pi E'(\theta)\left[\frac{1}{\sin\frac{1}{2}\theta - \sin\frac{1}{2}\phi} - \frac{1}{\sin\frac{1}{2}\theta + \sin\frac{1}{2}\phi}\right]\cdot[\cos\tfrac{1}{2}\theta + \cos\tfrac{1}{2}\phi(1+2\mu_2/\mu_1)]d\theta = A\sin\tfrac{1}{2}\phi + B\sin\tfrac{1}{2}\phi\cos\tfrac{1}{2}\phi \qquad 0<\phi<\pi. \tag{58}$$

Now $E(\theta)$, qua function of θ can be considered to be an odd function. It goes to zero linearly at $\theta=0$. In fact, the alternative problem of a symmetrical waveguide step, fed by the *second*-order mode, and obviously having antisymmetrical features, is converted into the present one by placing a metal wall along the center where the electric field is null. Thus (58), which is obtained only for $0<\phi<\pi$, is in fact still valid for $-\pi<\phi<0$. This can also be seen by putting $-\phi$ for ϕ and $-\theta$ for θ, when the equation is seen to transform into itself, on using the symmetry properties of $E(\theta)$. In order to see this, and at the same time simplify the equation, we note that, if in the second term only, on the left, we write $-\theta$ for θ, it takes the form of the first term, but with limits 0 and $-\pi$. Hence, the left hand side becomes

$$\frac{1}{\pi}\int_{-\pi}^\pi E'(\theta)\frac{\cos\frac{1}{2}\theta + \cos\frac{1}{2}\phi(1+2\mu_2/\mu_1)}{\sin\frac{1}{2}\theta - \sin\frac{1}{2}\phi}d\theta,$$

which obviously has the symmetry properties stated.

Finally we change variable again, putting $x=\sin\frac{1}{2}\theta$ and $y=\sin\frac{1}{2}\phi$. (This use of x and y in this section will not be confused with their earlier use as coordinates.) Instead of $E'(\theta)$ we introduce a function $F(x)$ such that $E'(\theta)d\theta = F(x)dx$.

The quantity $1+2\mu_2/\mu_1$ which occurs repeatedly from here on will be denoted by α^2

$$\alpha^2 = 1 + 2\mu_2/\mu_1 (=3 \text{ for equal media}). \tag{59}$$

Eq. (58) becomes

$$\frac{1}{\pi}\int_{-1}^1 \frac{F(x)}{x-y}[(1-x^2)^{1/2} + \alpha^2(1-y^2)^{1/2}]dx = Ay + By(1-y^2)^{1/2} \qquad -1<y<1, \tag{60}$$

with the additional requirement

$$\int_0^1 F(x)dx = \int_0^\pi E'(\theta)d\theta = E(\pi) - E(0) = 0. \tag{61}$$

Eq. (60) is considerably more involved than the simple singular integral equation which it at first sight appears to be. If the term in α^2 were absent it would be a straightforward equation with $(1-x^2)^{1/2}F(x)$ as unknown. Similarly, if the term in $(1-x^2)^{1/2}$ were absent it would become, on dividing by $(1-y^2)^{1/2}$, a simple equation in $F(x)$. The *general* equation, in which two arbitrary functions appear, would seem to be not solvable by known techniques. However, the particular case (60), and quite a range of other equations, can be solved by a technique outlined in Appendix II. We will here quote only the final results. The solution to (60) which also satisfies (61) is

$$F(x) = \frac{A\sec\pi\beta}{2(1+\alpha^2)}\left[X^\beta\left(\frac{2\beta}{1-x}-1\right) + X^{-\beta}\left(\frac{2\beta}{1+x}-1\right)\right] - \frac{B\operatorname{cosec}\pi\beta}{2(1+\alpha^2)}\left[X^\beta\left(x+2\beta-\frac{2\beta^2}{1-x}\right) + X^{-\beta}\left(-x+2\beta-\frac{2\beta^2}{1+x}\right)\right], \tag{62}$$

where

$$X = (1-x)/(1+x)$$

and

$$\beta = \frac{1}{\pi}\tan^{-1}(\alpha)\ (=1/3 \text{ for equal media}). \tag{63}$$

A relation between the constants A and B can now be obtained by insertion into (56),

$$A = \frac{4B}{3\alpha}\cdot\frac{\beta(1-\beta)(1-2\beta)(1-j2K'aY_1/\pi)}{1-(1-2\beta)^2(1-j2K'aY_1/\pi)}. \tag{64}$$

Finally, if these results are inserted into (52) and (57), an equation results for $(1-R)/(1+R)$, the input admittance relative to the wave admittance of the first waveguide

$$Y_{in} = \frac{1}{2}\frac{\mu_1}{\mu_2}\frac{1}{k'a}\left\{Y_2K_2a + j\pi\alpha^2\left[1 - \frac{9}{16\beta^2(1-\beta)^2}\frac{1-(1-2\beta)^2(1-j2K'aY_1/\pi)}{9-(1-2\beta)^2(1-j2K'aY_1/\pi)}\right]\right\}. \quad (65)$$

In the case $\mu_2 \gg \mu_1$ this gives $\beta \to \frac{1}{2}$ and $Y_{in} \sim 0$, an open circuit, as is to be expected.

Eq. (62) can be integrated to give the electric field across the aperture, since

$$E(\theta) = \int_0^\theta E'(\theta)d\theta = \int_0^x F(x)dx.$$

$$E(\theta) = \frac{A \sec \pi\beta}{1+\alpha^2}\left[\frac{X^{1-\beta} - X^\beta}{1+X}\right] - \frac{B \operatorname{cosec} \pi\beta}{1+\alpha^2}\left[\frac{X^{1-\beta} - X^{1+\beta}}{(1+X)^2} - \beta\frac{X^{1-\beta} - X^\beta}{1+X}\right]. \quad (66)$$

Herein we must take $x = \sin \frac{1}{2}\theta$ giving $X = \tan^2(\pi - \theta/4)$.

Now, for equal media we have $\beta = \frac{1}{3}$, whilst for $\mu_2 \gg \mu_1$, $\beta = \frac{1}{2}$. β is always the smallest of the various exponents of X. Hence, near the sharp corner, where $\theta \to \pi$, the electric field is seen to vary as X^β or $(\pi-\theta)^{2\beta}$. This can now be expressed in terms of the coordinate y across the aperture,

$$E \sim (a-y)^{2\beta} \quad \text{as} \quad y \to a. \quad (67)$$

Expressing the exponent in terms of α through (63), and hence in terms of μ_1 and μ_2, we get

$$2\beta = \frac{2}{\pi}\tan^{-1}(1 + 2\mu_2/\mu_1)^{1/2}. \quad (68)$$

For equal media this exponent is $\frac{2}{3}$. In prior calculations of this sort of problem it has been usual to conformally map the boundary by the Schwartz-Christoffel transformation, and the exponent has arisen from a consideration of the geometry of the boundary surface at the re-entrant corner. Eq. (68) on the other hand, exhibits the exponent in terms of electrical parameters with a value which varies according to the changes in the media. This result appears to be new. In particular, with $\mu_2 \gg \mu_1$, the first guide is open-circuited, and (68) gives $2\beta = 1$, corresponding to the normal sinusoidal waveguide mode going to zero linearly at the guide wall.

IX. Range of Applicability

The present method is applicable, so far as is known, only to rectangular waveguides, including infinite parallel plate arrangements. When the obstacle is inductive a change of dielectric constant on either side of the boundary can be accommodated. Similarly, when the obstacle is capacitive a change in permeability of the media can be met. But the analysis may sometimes be more involved, apparently, the other way round. The method can be used for any finite number of feeding modes, and can be used to calculate the electric fields, the reflection coefficient, transmission coefficient, or the mode conversion. The quasi-static solution can be augmented by the retention of a finite number of higher-order modes, the solution of the relevant integral equation being not appreciably more complicated thereby. However, each new mode introduces an additional constant into the solution, whose elimination is complicated if too many modes are retained.

The method has not yet been successfully applied in those cases in which guides of different dimensions are involved, except where integrally related, nor in cases in which an axial extension of an obstacle needs to be taken into account. It is believed that at least the first limitation may be eventually removed, but success will depend on new methods of dealing with the special types of singular integral equations that arise.

Appendix I

In (40) put $y = -\cos 2\theta$.

$$0 = \int_0^{\pi/2} \frac{C - 1 + 2\sin^2\theta}{\sqrt{1-\alpha+\beta-2\beta\sin^2\theta}}d\theta.$$

Multiply through by $\sqrt{1-\alpha+\beta}$ and put $k^2 = 2\beta/(1-\alpha+\beta)$.

$$0 = \int_0^{\pi/2} \frac{(C-1+2/k^2) - (1-k^2\sin^2\theta)2/k^2}{\sqrt{1-k^2\sin^2\theta}}d\theta$$

where

$$C = 1 + \frac{E-K}{\frac{1}{2}Kk^2} \bmod \sqrt{2\beta/(1-\alpha+\beta)}.$$

On simplifying the various terms this leads to (41) and (42) of the text.

Appendix II

Following Tricomi[6] we introduce the transform operator T_y operating on a function $\phi(x)$

$$T_y[\phi(x)] = \frac{1}{\pi}\int_{-1}^{1}\frac{\phi(x)}{x-y}dx. \quad (69)$$

The principal value of the integral is to be understood. Where no confusion of the variables is likely to exist we shall write this simply $T(\phi)$. Eq. (60) is a particular case of the equation

$$aT(F) + T(bF) = f, \quad (70)$$

with

$$a = \alpha^2(1 - y^2)^{1/2}, \qquad b = (1 - x^2)^{1/2},$$
$$f = Ay + By(1 - y^2)^{1/2} \tag{71}$$

and subject to $0 = \int_{-1}^{1} F(x)dx$, an alternative form of (61) for $F(x)$ even. The similar problem, but with the addition of inductive diaphragms, would give, after renormalization, a like equation, but with the radicals replaced by the form $[1-(c+dy)^2]^{1/2}$ throughout. In the absence of a general solution of (70), this latter problem so far remains unsolved. Eq. (70) can, however, be solved in a large number of special cases, including $a=b$, $ab=C(1-x^2)$ and many others. But we shall here concentrate only on the analysis which leads to the solution of the problem in hand.

Tricomi gives a number of useful results. A convolution theorem is

$$T[\phi_1 T(\phi_2) + \phi_2 T(\phi_1)] = T(\phi_1)T(\phi_2) - \phi_1\phi_2. \tag{72}$$

The solution of $T(\phi) = \psi$ is

$$\phi = (1 - y^2)^{-1/2}\{-T_y[(1 - x^2)^{1/2}\psi(x)] + C\}, \tag{73}$$

where C is a constant.

The solution of Carleman's equation

$$a(x)\phi(x) - T_x[\phi(y)] = g(x)$$

is

$$\phi(y) = \frac{a(y)g(y)}{1 + a^2(y)} + A(y)\left\{T_y\left[\frac{e^{-\tau(x)}g(x)}{[1 + a^2(x)]^{1/2}}\right] + \frac{C}{1 - x}\right\}, \tag{74}$$

where

$$\tau(x) = T_x\,[\tan^{-1} 1/a(y)] \qquad (0, \pi)$$

and

$$A(x) = e^{\tau(x)}[1 + a^2(x)]^{-1/2}$$

Using these formulas we return to (70) and ask under what circumstances, if at all, it can be reduced to an example of Carleman's equation, whose solution we know.

Let us start with the equation

$$cF + eT(dF) = h, \tag{75}$$

where c, d, e and h are all functionals at our disposal. Operating with T, and using (72) to express $T[eT(dF)]$ in other terms, we get

$$T(h) = T(cF) - edF + T(e)T(dF) - T[dFT(e)]. \tag{76}$$

Let us choose $T(e) = K$, a constant, so that, from (73)

$$e = K(x - C)(1 - x^2)^{-1/2}, \tag{77}$$

with C as yet arbitrary.

Then (76) simplifies to

$$T(h) = T(cF) - edF. \tag{78}$$

From (75) and (78), on eliminating the untransformed terms in F,

$$T(h) + edh/c = T(cF) + (e^2 d/c)T(dF). \tag{79}$$

Choose $c = x - C$, $d = (1-x^2)^{1/2}$, so that $ed/c = K$. Now

$$T(cF) = \frac{1}{\pi}\int_{-1}^{1} \frac{x - C}{x - y} F(x)dx$$
$$= \frac{1}{\pi}\int_{-1}^{1} \frac{x - y + y - C}{x - y} F(x)dx$$
$$= (y - C)T(F) \text{ since } \int_{-1}^{1} F(x)dx = 0 \text{ by (61).}$$

Putting $K = 1/\alpha$, and substituting these results in (79) gives finally

$$\alpha^2(1 - y^2)^{1/2}T(F) + T[(1 - x^2)^{1/2}F] = \frac{\alpha^2(1 - y^2)^{1/2}}{y - C}[T(h) + h/\alpha]. \tag{80}$$

If now we choose h such that

$$T(h) + h/\alpha = \alpha^{-2}(y - C)(1 - y^2)^{-1/2}f(y), \tag{81}$$

then (80) becomes equivalent to (70) and (71).

From (78) with h given by (81)

$$T[(x - C)F] - (y - C)F/\alpha = \tfrac{1}{2}[T(h) - h/\alpha] + \tfrac{1}{2}\alpha^{-2}(y - C)(1 - y^2)^{-1/2}f(y).$$

If we put $(y-C)F(y) = \frac{1}{2}H(y) + \frac{1}{2}h(y)$, then H is given by

$$T(H) - H/\alpha = \alpha^{-2}(y - C)(1 - y^2)^{-1/2}f(y), \tag{82}$$

an equation differing from (81) for h only by the sign of α. These two equations, both of Carleman's type, can now be solved for h and H, and $F(y)$ is given in terms of them by

$$F(y) = \frac{H(y) + h(y)}{2(y - C)}. \tag{83}$$

In writing down the solution it becomes apparent that the integration diverges at $x=1$ unless the so far arbitrary constant C is given the value unity. This feature determines the constant, and the solution takes the form

$$F(y) = \frac{1}{2\pi(1 - y)(1 + \alpha^2)}\left\{Y^{1-\beta}\int_{-1}^{1} \frac{X^{\beta-1/2}}{y - x} f(x)dx + Y^{\beta}\int_{-1}^{1} \frac{X^{1/2-\beta}}{y - x} f(x)dx\right\}, \tag{84}$$

where $Y = (1-y)/(1+y)$ and X is a similar function of x. The constant β is related to α by $\beta = (1/\pi)\tan^{-1}\alpha$.

In view of the requirement of the integrability of $F(y)$ at $y=1$ no complementary functions along the lines indicated in (74) appear in this problem.

The integrations in (84) are straightforward when X is taken as a new variable. If we write

$$y_n = \int_0^\infty X^p(1+X)^{-n}dX,$$

then $y_1 = -\pi \operatorname{cosec} \pi p$, and the recurrence relation $y_n = y_{n-1}(n-2-p)/(n-1)$ is readily obtained. The integral

$$\int_0^\infty \frac{X^p}{X-Y}dX = -Y^p\pi \cot \pi p$$

on taking $\xi = X/Y$ as new variable. These results suffice to integrate (84) when $f(x)$ is of the form specified in (71) and p is suitably chosen.

It is readily verified that $\int_{-1}^{1} F(x)dx$ is zero, confirming the absence of any other complementary function.

The integrations involved in the determination of A and $1+R$ involve the integrals

$$x_n = \int_0^\infty X^p(1-X)^n(1+X)^{-n-2}dX$$

which can be shown to satisfy

$$(n+1)x_n + 2px_{n-1} - (n-1)x_{n-2} = 0$$

x_0 and x_1 are readily expressed in terms of y_2 and y_3 of the previous paragraph, whence the value of x_n follows.

Finally, (62) of the text for $F(x)$ is found on collection of terms, Its integration to give $E(\theta)$ is elementary.

The solution to (70) with completely arbitrary functions $a(x)$ and $b(x)$ has not yet been determined by this method, and it is possible that in this general case more powerful mathematical tools are required. In particular, it has not been possible to find the solution when the radical takes the more complicated form appropriate to the presence of a diaphragm, except in the very special case $\alpha = 1 (\mu_2 = 0)$.

A Dielectric Surface-Wave Structure: the V-Line*

P. DIAMENT†, S. P. SCHLESINGER†, MEMBER, IRE, AND A. VIGANTS†

Summary—**Properties of the V-line, a wedge-shaped surface-wave structure comprising a cylindrical dielectric binding medium of sectorial cross section supported by two conducting plates, are considered in terms of its higher-order hybrid modes of propagation. Practical modifications of the ideal structure are emphasized.**

Design curves and equations are presented to determine various propagation parameters and their significance is discussed. Experimental verification of the theory is described.

Introduction

An analysis of surface-wave propagation on dielectric cylinders of sectorial cross section bounded by conducting plates, as in Fig. 1, leads to the usual set of low-order transverse modes and higher-order hybrid modes. In cases of practical interest, however, the prototype structure, here designated "V-line," will be modified in that the plates will be insulated at the apex, whereupon the transverse modes are eliminated and consideration of high-order hybrid modes is required. This modification of the V-line enhances its versatility; in particular, it facilitates the excitation of the modes and permits the application of biasing potentials between the conducting plates. With the use of ferroelectric cylinders, such bias fields may provide convenient electronic control of propagation characteristics.

Although the angle included by the plates is, in principle, unrestricted, for simplicity it will be taken to be an aliquot portion of a semicircle, *i.e.*, π/n radians, where the integer n designates the order of the mode. For such angles, the modes that may be supported by the V-line may propagate on full circular dielectric cylinders as well. The latter waveguide has undergone extensive analysis with respect to its dominant modes.[1–6]

* Received by the PGMTT, August 16, 1960; revised manuscript received, April 26, 1961. This work is based on studies undertaken pursuant to Contract AF 19(604)3879 with the AF Res. Div.

† Dept. of Elec. Engrg., Columbia University, New York, N. Y.

[1] R. E. Beam, *et al.*, "Dielectric Tube Waveguides," Northwestern University, Evanston, Ill., Report A.T.I. 94929, ch. 5; 1950.

[2] S. A. Schelkunoff, "Electromagnetic Waves," D. Van Nostrand Co., Inc., New York, N. Y., p. 427; 1943.

[3] A. Sommerfeld, "Electrodynamics," Academic Press, Inc., New York, N. Y., pp. 177–193; 1952.

[4] H. Wegener, "Ausbreitungsgeschwindigkeit, Wellenwiderstand, und Dampfung electromagnetischer Wellen an dielektrischen Zylindern," Forschungbericht Nr. 2018, Deutsch Luftfahrtforschung. Vierjahresplan-Inst. für Schwingungsforschung, Berlin, Germany; August 26, 1944. (CADO Wright-Patterson AF Base, Dayton, Ohio, Document No. ZWB/FB/Re/2018.)

[5] C. H. Chandler, "An investigation of dielectric rod as waveguide," *J. Appl. Phys.*, vol. 20, pp. 1188–1192; December, 1949.

[6] W. M. Elsasser, "Attenuation in a dielectric circular rod," *J. Appl. Phys.*, vol. 20, pp. 1193–1196; December, 1949.

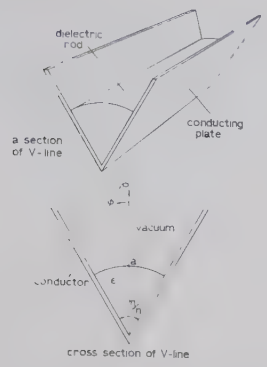

Fig. 1—Geometry and coordinate system for the V-line.

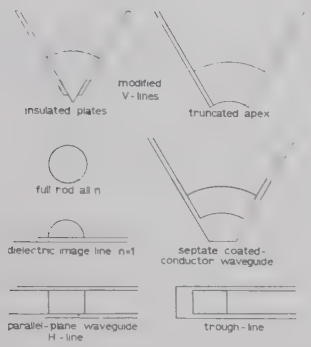

Fig. 2—Modifications of the V-line and some related structures.

The modes of interest for the modified V-line correspond to the higher-order hybrid modes of circular cylinders, which have received only modest attention in the literature.[2,7–9] It will be demonstrated that such higher-order hybrid modes can propagate on a V-line with insulated plates or truncated apex (see Fig. 2) with negligible perturbation.

Structures closely related to the V-line are shown in Fig. 2 and include the septate coated-conductor waveguide,[10] which may be considered a truncated V-line with the apex replaced by a conductor. The dielectric image line[11,12] corresponds to a V-line with $n=1$. The parallel-plane waveguide[13,14] has insulated conducting plates that permit biasing of the binding medium and has fields on both sides of the dielectric. The trough-line[15] has a unilateral field pattern and a continuous conducting boundary. The V-line, as modified at the apex, combines the features of confining the fields to one side of the dielectric and permitting biasing potentials across the binding medium.

Following a brief review of the theory of propagation on the V-line, design curves will be presented for the principal modes of orders two and six for a variety of dielectric constants. Graphs obtained by numerical solution of the equations will be given to illustrate some theoretical results. Experimental work verifying the existence of the high-order modes and their characteristics will be described, together with a discussion of the effects of the separation of the plates.

Theoretical Results

The V-line is a surface-wave structure comprising two conducting plates of infinite extent forming the sides of a wedge and containing within the "V" a sectorial section of dielectric circular cylinder of relative permittivity ϵ, from the apex out to a radius a, with free space in the region beyond the cylinder (see Fig. 1). The line is taken to be infinitely long and is assumed lossless.

With n integral, the modes of propagation on the V-line are also those of a full round rod. For the latter waveguide the HE_{11} mode is dominant, but it can not propagate on a V-line for which $n>1$. The TM_0 mode with axial electric fields is clearly precluded by the longitudinal plates of the V-line. It would appear, then, that the TE_0 mode is the principal mode for the V-line. However, this mode requires the plates to be joined at the apex to accommodate the radial current flow, while practical forms of the V-line have insulated plates or even a truncated apex (see Fig. 2). Thus, the principal mode for the modified V-line is a hybrid mode, in fact, the HE_{n1} mode.

The derivation of the electromagnetic fields for the circular symmetry of the V-line is straightforward.[2,7,8] The axial fields have a sinusoidal angular variation and a Bessel function radial dependence of the form $J_n(p\rho/a)$ inside the dielectric cylinder and $K_n(q\rho/a)$ outside, where the eigenvalues p and q are related to the free-space wavelength λ_0, by

$$p^2 + q^2 = R^2, \qquad R = (2a/\lambda_0)\pi(\epsilon - 1)^{1/2}. \tag{1}$$

The boundary conditions provide another relation between p and q through the characteristic equation involving Bessel functions and their derivatives given by Schelkunoff and others.[2,1,4]

The eigenvalues p and q conveniently characterize the mode of propagation, not only by supplying the arguments of the Bessel function factors in the field equations, but by yielding much direct information.

[7] S. P. Schlesinger, P. Diament, and A. Vigants, "On higher-order hybrid modes of dielectric cylinders," IRE Trans. on Microwave Theory and Techniques, vol. MTT-8, pp. 252–253; March, 1960.

[8] P. Diament, S. P. Schlesinger, and A. Vigants, "A Dielectric Surface Wave Structure: The V-Line," Columbia University, New York, N. Y., Tech. Rept. No. 3, Contract No. AF 19(604)3879; July 1, 1960.

[9] E. Snitzer, American Optical Co., Southbridge, Mass., personal communication.

[10] R. Notvest, "Septate Coated-Conductor Waveguide," Northwestern University, Evanston, Ill., Final Rept. on Wave Propagation in Dielectric Tubes, Army Signal Corps Contract No. DA 36-039 sc-5397 (R. E. Beam, Tech. Dir.); ch. 2; October, 1952.

[11] D. D. King, "Dielectric image line," *J. Appl. Phys.*, vol. 23, pp. 699–700; June, 1952.

[12] S. P. Schlesinger and D. D. King, "Dielectric image lines," IRE Trans. on Microwave Theory and Techniques, vol. MTT-6, pp. 291–299; July, 1958.

[13] F. J. Tischer, "The *H*-guide, a waveguide for microwaves," 1956 IRE Convention Record, pt. 5, pp. 44–47.

[14] M. Cohn, "Propagation in a dielectric-loaded parallel plane waveguide," IRE Trans. on Microwave Theory and Techniques, vol. MTT-7, pp. 202–208; April, 1959.

[15] M. Cohn, "TE modes of the dielectric loaded trough line," IRE Trans. on Microwave Theory and Techniques, vol. MTT-8, pp. 449–454; July, 1960.

Thus, the guide wavelength λ_g is given by

$$p^2 + \epsilon q^2 = U^2 R^2, \qquad U = \lambda_0/\lambda_g. \tag{2}$$

These equations permit mathematical characterizations of physical phenomena. Cutoff of a mode, with equality of guide and free-space wavelengths, *i.e.*, $U=1$, translates into $q=0$ by combining relations (1) and (2). The limiting guide wavelength, $\lambda_g=\lambda_0\epsilon^{-1/2}$ or $U^2=\epsilon$, is describable by $q\to\infty$ from (2) for finite p. The range of q from 0 to ∞, hence, corresponds to the physical range of guide wavelength from λ_0 to $\lambda_0\epsilon^{-1/2}$ on the V-line. Thus, an analysis of the characteristic equation relating p and q with ϵ and n as parameters is indicated.

A convenient form of the characteristic equation, from which derivatives of Bessel functions are absent, is

$$(J^+ + K^+)(\epsilon J^- - K^-) + (J^- - K^-)(\epsilon J^+ + K^+) = 0 \tag{3}$$

where

$$J^- = \frac{J_{n-1}(p)}{pJ_n(p)}, \qquad J^+ = \frac{J_{n+1}(p)}{pJ_n(p)},$$

$$K^- = \frac{K_{n-1}(q)}{qK_n(q)}, \qquad K^+ = \frac{K_{n+1}(q)}{qK_n(q)}.$$

The cutoff values of p are obtainable by letting $q\to 0$ in this equation. Using the appropriate limiting process, the solutions are, for $n>1$, the cutoff equations

$$J^- = \frac{1}{(n-1)(\epsilon+1)} \tag{4}$$

$$J_n(p) = 0, \qquad p \neq 0. \tag{5}$$

Eq. (4) was given by Schelkunoff[2] and (5) was reported by the authors.[7,8]

A mathematical analysis of the above characteristic and cutoff equations is available.[7,8] Numerical results will presently be given, for which purpose it will be sufficient to abstract some salient results of the theory.

For $n>1$, the V-line supports a doubly-infinite set of hybrid modes, designated HE_{nm} and EH_{nm}, with cutoff given by (4) and (5), respectively. While q may assume any positive value, increasing with closer binding of the energy to the rod, the range of p for a given mode is confined to that between the roots of $J_{n-2}(p)$ and of $J_{n-1}(p)$ for HE_{nm} modes, and that from the roots of $J_n(p)$ to those of $J_{n+1}(p)$ for EH_{nm} modes. The successive intervals of p defined by these limits correspond to modes of increasing rank m, beginning with the "principal mode" for which $m=1$.

The property of the higher-order hybrid modes of greatest interest here is their negligible field intensity in the vicinity of the apex of the rod. This suggests that the two conducting plates may be insulated at the apex, or the apex truncated, with no appreciable perturbation of the field configuration inside the rod, as will be shown quantitatively.

Numerical Results

The V-line's parameters of interest are the order of the mode n, the permittivity of the rod ϵ, the radial eigenvalues p and q, the diameter-to-wavelength ratio $2a/\lambda_0$, and the free space-to-guide wavelength ratio $U=\lambda_0/\lambda_g$. These are related through (1)–(3). The cutoff values of p and $2a/\lambda_0$ are of importance and are given by (4), (5), and (1). Properties of interest are cutoff, field extent and effects of truncation of the V-line. Theoretical curves, representing solutions of the characteristic equation (3), coupled with relations (1) and (2), are now presented to relate and compare the above characteristics.

Fig. 3 relates p and q according to (3) for the HE_{21} mode for a wide range of ϵ, including the limiting case of $\epsilon=1$ (no rod). While the full range of p is included, only the low values of q, the range of interest for propagation of a pure principal mode, are covered. The asymptote for all curves is the dashed line at the top. Fig. 4 gives the corresponding curves for the HE_{61} mode. The dashed line is again the asymptote for all curves, although the curves for high ϵ do not begin to approach it in the narrow range of q presented.

Fig. 5 relates the parameters $1/U=\lambda_g/\lambda_0$ and $2a/\lambda_0$ for the HE_{21} and HE_{61} modes for various ϵ, and includes the HE_{11} mode for $\epsilon=2.56$ and 8 for comparison. The asymptotes are $\lambda_g/\lambda_0\to\epsilon^{-1/2}$. The striking contrast in the slopes of the curves for large ϵ is noteworthy; it indicates that large changes in guide wavelengths for small changes in frequency are obtainable near cutoff, or that frequency stability is of increasing importance with increasing ϵ.

The cutoff values of p and $2a/\lambda_0$ for the HE_{21} and HE_{61} modes as functions of ϵ are plotted in Fig. 6. The two curves are related by $(2a/\lambda_0)_c=p_c/\pi(\epsilon-1)^{1/2}$, where the subscript c designates cutoff.

Comparative information on the field extent in V-lines of different angles may be obtained from Fig. 7, which indicates the attenuation in db of the field intensity, relative to that at the surface of the rod, at different distances above the rod. The attenuation ratio is $K_n(q\rho/a)/K_n(q)$. It is clear that the binding of the energy to the rod is greater, the larger the value of n. Proper sizes for the supporting plates of the V-line may also be determined from Fig. 7, which will yield an estimate of the radial extent to which the boundary condition provided by the conducting plates is required.

The possibility of truncating a sizable portion of the V-line without seriously affecting the theory of the full V-line is indicated by Fig. 8. The argument of the Bessel functions in the expressions for the field intensities inside the rod is $p\rho/a$. The 100 per cent curve gives the values of this argument at which maximum intensities are attained. The other curves then give the arguments up to which the intensities are less than the indicated percentage of the maximum intensity. Thus, the curves

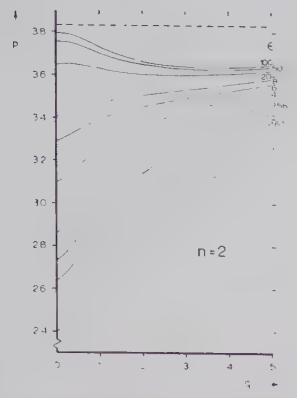

Fig. 3—Solutions of characteristic equation for HE_{21} mode.

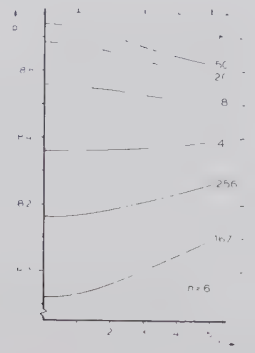

Fig. 4—Solutions of characteristic equation for HE_{61} mode.

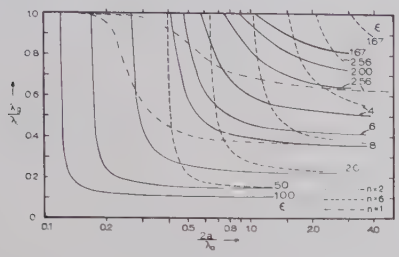

Fig. 5—Dependence of λ_g/λ_0 on $2a/\lambda_0$ for HE_{11}, HE_{21}, and HE_{61} modes for various ϵ.

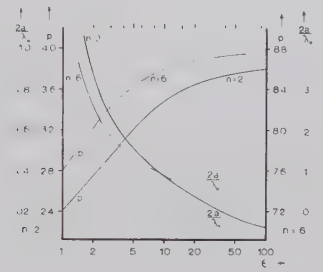

Fig. 6—Cutoff values of p and $2a/\lambda_0$ vs ϵ for HE_{21} and HE_{61} modes.

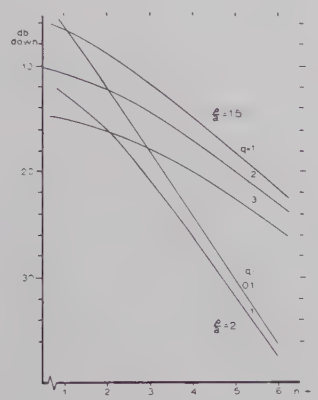

Fig. 7—Field extent vs order of mode. Attenuation in db down from field intensity at surface of rod.

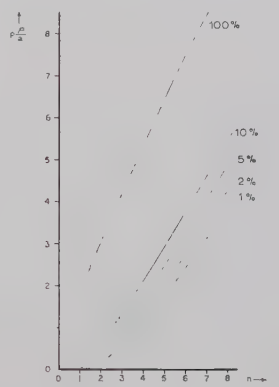

Fig. 8—Truncation of V-line. Radial extent of negligible field intensity vs order of mode. Normalized radius to indicated percentage of maximum field intensity inside rod.

indicate, for example, that for an $n=6$ V-line, as much as 2.42/7.50, or about 30 per cent, of the full radius of the rod may be truncated with loss of field intensity of no more than 1 per cent of the maximum intensity within the rod. The above assumes that the point at which the Bessel functions reach their maximum value is within the rod, *i.e.*, that the operating value of p is greater than the value of pp/a indicated by the 100 per cent curve. If this is not so, the curves must be modified in an obvious way to take account of the maximum field intensity actually attained within the rod. It is evident that V-lines of larger n permit the truncation of larger portions of the rod in which the field intensities are negligible. The significance of this is that the two plates supporting the rod may be separated at the apex without seriously affecting the field configuration of the V-line.

It should be emphasized that the curves discussed above, obtained with the aid of an IBM 650 computer, represent only the principal modes of the indicated orders. Similar information for higher-rank modes may be obtained through a more complete solution of the characteristic equation.

Experimental Results

Experimental verification of the theory of propagation of higher-order modes of dielectric cylinders on a V-line was obtained for the HE_{21} mode. The purpose of the experiments was to verify the existence of the

higher-order modes, to launch and identify these modes, to measure such properties of the V-line as field extent and insertion loss, and to demonstrate that the modified V-line eliminates the lower-order transverse modes while sustaining the higher-order modes of the dielectric rod waveguide.

The scheme used to verify the existence of, and identify, the HE_{21} mode was to construct the V-line in the form of a resonator,[12] *i.e.*, with transverse conducting plates at both ends of the line, and to predict from the geometry of the V-line the frequencies at which the cavity would be resonant. Several rod sizes and materials were used and various methods of launching and detecting the modes were tried. Experiments were carried out at 3-cm wavelengths.

Theory and experiment were correlated successfully in the case of the 90° V-line with the HE_{21} mode. An effective means of transition from rectangular waveguide to V-line was found in a vertical probe penetrating a short distance into the rod at the apex of the upward-opening V, the supporting plates being separated at the bottom to accommodate the probe at the center of the V-line cavity. The perturbation introduced by insulating the plates at the apex was investigated and compared with the effects on the transverse TE_0 mode. Work is continuing on the excitation of higher-order modes on the V-line, particularly in the case of the HE_{61} mode.

The HE_{21} mode was launched on a 90° V-line with a polystyrene rod ($\epsilon=2.56$) of radius 0.635 in. The resonator was 23.59 in long, *i.e.*, about 25 guide wavelengths long at X band. Coupling to the V-line was through an iris in the resonator end-plate with a tapered transition-piece of the rod inserted into the rectangular waveguide. The resonant frequencies were predicted by determining at which frequencies the length L of the line would be an integral number of half-wavelengths, *i.e.*, when $(L/a)(2a/\lambda_0)U$ is an integer. The results are presented in Table I.

The field extent was checked against the theory by introducing a short probe through a number of holes in one end-plate at various heights above the rod surface in order to compare the axial field intensities. The results of this test are included in Table I.

The experiment was repeated, with some refinements, for a rod of smaller radius ($a=0.507$ in). The results of the resonance tests are plotted in Fig. 9 semilogarithmically in order to segregate the physical dimensions of the V-line from the theoretical parameters; that is, an error in the measurement of L/a would appear on the plot as a shift of the experimental curve parallel to the theoretical curve, since it is a simple factor in $L/(\lambda_g/2)=(L/a)(2a/\lambda_0)U=$integer. The field extent measurements for this case, given in Table II, show poorer agreement with theory, the wave being more loosely bound than was predicted.

To verify the theoretical indications that a separation of the plates at the apex would perturb high-order modes only negligibly while effectively eliminating the transverse electric zero-order mode, the effects of such separation on the resonances of the HE_{21} and TE_{01} modes in a V-line resonator were compared. Virtually no effect was observed upon the HE_{21} resonances throughout X band, while radical changes in the resonant frequencies occurred when the TE_{01} mode was preferentially launched and the conductivity of the apex destroyed. This confirms that the modified V-line is incapable of supporting the transverse electric mode, while the conductivity of the apex is relatively inconsequential for higher-order modes.

TABLE I

EXPERIMENTAL VERIFICATION OF RESONANCES AND FIELD EXTENT IN V-LINE RESONATOR

Rod:	$n=2$	$\epsilon=2.56$	$a=0.635$ in

Resonant Frequencies

Predicted (kMc)	Experimental (kMc)
9.243	9.244
9.375	9.373
9.508	9.502
9.64	9.639

Field Extent $2a/\lambda_0=1.037$

Probe Position (Reference)	Attenuation	
	Predicted (db)	Experimental (db)
1	0	0
2	12	14.2
3	21.9	23.1

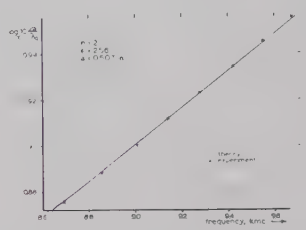

Fig. 9—Verification of support of HE_{21} mode on 90° V-line resonator with polystyrene rod ($\epsilon=2.56$, radius $=0.507$ in). Theoretical and experimental guide wavelength vs frequency.

TABLE II

VERIFICATION OF FIELD EXTENT IN V-LINE RESONATOR

Rod:	$n=2$	$\epsilon=2.56$	$a=0.507$ in $2a/\lambda_0=0.761$

Field Extent

Probe Position (Reference)	Attenuation	
	Predicted (db)	Experimental (db)
1	0	0
2	5.8	3.5
3	9.9	6.5
4	13.6	10.7

Conclusions

This work has demonstrated the feasibility of the V-line as a surface-wave guiding structure supporting higher-order hybrid modes of propagation. Various characteristics of such modes have been discussed qualitatively on the basis of algebraic solutions of the characteristic equation and, more quantitatively, on the basis of numerical solutions obtained for a variety of orders and dielectric constants.

Experimental confirmation of the theory has been successful qualitatively and quantitatively for the second-order principal mode. Verification has been obtained for the exclusion of the transverse electric mode from the V-line with insulated plates, thereby confirming that it is the high-order hybrid modes rather than the simpler low-order transverse modes that are of interest for operation with disjoint plates. The evitability of joining the plates affords distinct advantages in launching and detecting the modes and in the versatility of the V-line.

The V-line configuration with separated plates or truncated apex appears well suited to convenient electronic control of propagation characteristics through the use of a ferroelectric binding medium. The plates serve as supports for the structure, as image surfaces for the guided wave, and as electrodes for the application of bias potentials. The V-line is distinguished from some other configurations that permit bias fields across a binding medium in that it confines the propagating or radiating fields to one side of the dielectric. The region of the apex remains available for auxiliary structures, such as exciting or detecting mechanisms.

Wave Propagation in a Medium with a Progressive Sinusoidal Disturbance*

A. HESSEL†, MEMBER, IRE, AND A. A. OLINER†, FELLOW, IRE

Summary—**A recent paper by Simon derives approximate results, employing only three space harmonics, for the propagation characteristics of an electromagnetic wave traveling in a medium possessing a progressive sinusoidal disturbance. A rigorous result is presented here for this same problem, taking into account all of the space harmonics; also, a sufficiency condition for the convergence of this solution is discussed. This sufficiency condition is not satisfied in a particular case treated by Simon. It is shown that his analysis of this case is in error, and that the total field is singular there. The singular nature of the field is associated with "supersonic" effects in the medium containing the progressive disturbance.**

Introduction

A STIMULATING, recent paper[1] by Simon presents solutions for the propagation characteristics of an electromagnetic wave traveling in a medium possessing a progressive sinusoidal disturbance. This disturbance is expressed in terms of a time-varying dielectric constant, in the form

$$\epsilon = \epsilon_0 + \epsilon_1 \cos(\omega_1 t - k_1 z), \tag{1}$$

using the notation employed by Simon. The electromagnetic field is then expanded in terms of spatial harmonics and a relation is found between the amplitudes of these space harmonics. This relation is essentially a system of infinite homogeneous equations with an infinite number of unknowns. Simon then points out that in problems of interest ϵ_1 is very small, and that a rigorous solution to this system of equations is not simple to obtain. He, therefore, adopts a perturbation approach, and retains only the lowest three of the infinite number of space harmonics. With this approximation, he obtains a determinantal equation for the propagation constants, solves this equation for several interesting special cases, and then obtains the corresponding space-harmonic amplitudes.

A major contribution of Simon's paper lies in the stress he places on the interrelation between physical concepts in different disciplines. For example, while it has long been known that a stop band for electromagnetic waves in a periodic structure corresponds to Bragg reflection in crystals, Simon relates the Doppler effect produced in a stop band associated with a moving disturbance to parametric amplification phenomena. The conditions for both up-conversion and down-conversion are considered in some detail, and approximate expressions are presented for the propagation constants and the fields. An additional so-called "triple root" case is also treated in some detail, but the results are of questionable value, for reasons presented below.

* Received by the PGMTT, January 16, 1961; revised manuscript received, May 1, 1961. The work described in this paper was conducted at the Microwave Res. Inst. of the Polytechnic Inst. of Brooklyn, N. Y., under Contract AF-19(604)-2031 under the sponsorship of the Air Force Cambridge Res. Labs., Air Res. and Dev. Command.

† Microwave Research Inst., Polytechnic Inst. of Brooklyn, Brooklyn, N. Y.

[1] J. C. Simon, "Action of a progressive disturbance on a guided electromagnetic wave," IRE TRANS. ON MICROWAVE THEORY AND TECHNIQUES, vol. MTT-8, pp. 18–29; January, 1960.

In this note we wish to:

1) present a *rigorous* result to the problem treated by Simon, taking into account *all* of the space harmonics, rather than only three,
2) present a "*sufficiency condition*" between the various physical quantities which, if satisfied, insures the validity of any space-harmonic type of solution, and
3) apply this "sufficiency condition" to the various cases considered by Simon, and indicate the ranges of parameter values to be excluded from his solutions. Particular stress is laid on his triple root case, which does *not* satisfy this condition. Both physical and mathematical reasoning is presented in verification.

Rigorous Result

Over most of the range of frequency and wavenumber values, the perturbation solution of Simon is completely adequate for very small values of ϵ_1. In particular regions, however, the perturbation solution is invalid. For example, as pointed out by Simon, his solution cannot apply to regions corresponding to the higher-order stop bands, or Bragg reflections. It is desirable, therefore, to have available a rigorous solution.

Let us first review, for the sake of clarity, the basic steps involved in the development of such a rigorous solution. We are concerned with the propagation of electromagnetic waves in an infinite medium possessing a fixed permeability μ_0 and a time-varying dielectric constant $\epsilon(z, t)$ of the form given by (1). Such a medium is created by the presence of a traveling disturbance; examples of the source of such a disturbance could be an electromagnetic "pump" wave or an acoustic wave, the latter constituting an example of microwave-phonon interaction. The assumption (1) regarding the properties of the medium thus linearizes the basically nonlinear interaction problem.

Let us restrict the development below to TEM mode propagation in a direction parallel or antiparallel to the moving disturbance. (Simon initially considers a slightly more general case, but he immediately thereafter reduces his relations to those for TEM modes.) Under these conditions, the wave equation for the electric field $E(z, t)$ becomes

$$\frac{\partial^2 E(z,t)}{\partial z^2} = \mu_0 \frac{\partial^2 D(z,t)}{\partial t^2}, \tag{2}$$

with

$$D = \epsilon E, \tag{3}$$

and ϵ given by (1). A representation of the electric field in the disturbed medium is then taken in the form

$$E(z, t) = E_0 e^{-j(\omega t - kz)} P(\omega_1 t - k_1 z), \tag{4}$$

where ω is the angular frequency of the applied signal, k is the macroscopic wavenumber of the wave propagating in the z direction, ω_1 and k_1 are, respectively, the "pump" angular frequency and propagation wavenumber, and P represents a periodic function of its argument with a period of 2π. The notation employed in (4) follows that of Simon. The objective in this development is to obtain a rigorous dispersion relation expressing k as a function of ω and the parameters of the medium.

The right-hand side of (4) is essentially a Floquet representation of the electric field in the moving coordinate system. Let us next expand P into a Fourier series, *i.e.*,

$$P(\omega_1 t - k_1 z) = \sum_{n=-\infty}^{\infty} a_n e^{-jn(\omega_1 t - k_1 z)}. \tag{5}$$

When the series (5) is substituted, along with (4), (1) and (3), into (2), one obtains the following three-term recursion formula for the desired propagation wavenumber k and the unknown electric-field space-harmonic amplitudes a_n:

$$\frac{\epsilon_1}{2\epsilon_0} a_{n+1} + D_n a_n + \frac{\epsilon_1}{2\epsilon_0} a_{n-1} = 0, \tag{6}$$

where

$$D_n = 1 - \left(\frac{\omega}{k_0}\right)^2 \left(\frac{k + nk_1}{\omega + n\omega_1}\right)^2, \tag{7}$$

$$n = 0, \pm 1, \pm 2, \cdots; \qquad k_0 = \omega\sqrt{\epsilon_0 \mu_0}.$$

Relations (6) and (7) are identical with Simon's relation (10), except for his π^2/b^2 term which he drops soon after. Simon then solves (6) and (7) by a perturbation technique which includes only three space harmonics. We present below a rigorous solution which takes into account all of the space harmonics. Relations (6) and (7) are also given by Slater[2] as (20); while Slater then also proposes a perturbation approach employing only three space harmonics, $n = 0, \pm 1$, he does not continue with the detailed analysis and interpretation presented by Simon.

In a recent paper,[3] the writers have treated, by a technique commonly employed in the solution of Mathieu-type equations, an infinite set of equations very similar to (6) but with a different expression for D_n. A rigorous solution was obtained in the form of a rapidly convergent continued fraction. Following the

[2] J. C. Slater, "Interaction of waves in crystals," *Rev. Mod. Phys.*, vol. 30, p. 203; January, 1958.

[3] A. A. Oliner and A. Hessel, "Guided waves on sinusoidally-modulated reactance surfaces," IRE Trans. on Antennas and Propagation, vol. AP-7, pp. S201–S208; December, 1959.

derivation presented there, we obtain from (6) the equation:

$$D_0 - \left(\frac{\epsilon_1}{2\epsilon_0}\right)^2 \left[\frac{1}{D_1 - \dfrac{(\epsilon_1/2\epsilon_0)^2}{D_2 - \dfrac{(\epsilon_1/2\epsilon_0)^2}{D_3 - \cdots}}} + \frac{1}{D_{-1} - \dfrac{(\epsilon_1/2\epsilon_0)^2}{D_{-2} - \dfrac{(\epsilon_1/2\epsilon_0)^2}{D_{-3} - \cdots}}} \right] = 0 \tag{8}$$

for the propagation wavenumber k. The small parameter $\epsilon_1/2\epsilon_0$ is explicitly exhibited in (8); D_n is defined by (7). When (8) is taken to the first order only, it is identical with Simon's relation (15). Expression (8) is rigorous and is rapidly convergent almost everywhere, so that k can be computed to any desired degree of accuracy.

The corresponding electric-field amplitudes can be shown to be given rigorously by:

$$\frac{a_n}{a_{n-1}} = \frac{-(\epsilon_1/2\epsilon_0)}{D_n - \dfrac{(\epsilon_1/2\epsilon_0)^2}{D_{n+1} - \dfrac{(\epsilon_1/2\epsilon_0)^2}{D_{n+2} - \cdots}}}, \qquad n \geq 1 \tag{9}$$

$$\frac{a_n}{a_{n+1}} = \frac{-(\epsilon_1/2\epsilon_0)}{D_n - \dfrac{(\epsilon_1/2\epsilon_0)^2}{D_{n-1} - \dfrac{(\epsilon_1/2\epsilon_0)^2}{D_{n-2} - \cdots}}}, \qquad n \leq -1, \tag{10}$$

and

$$\frac{a_n}{a_0} = \frac{a_n}{a_{n-1}} \cdot \frac{a_{n-1}}{a_{n-2}} \cdots \frac{a_1}{a_0}, \qquad n \geq 1 \tag{11}$$

$$\frac{a_n}{a_0} = \frac{a_n}{a_{n+1}} \cdot \frac{a_{n+1}}{a_{n+2}} \cdots \frac{a_{-1}}{a_0}, \qquad n \leq -1. \tag{12}$$

Hence, after k is found from (8), the D_n values are known and the amplitude ratios, relative to a_0, say, are obtained from relations (9)–(12). To the first order in $\epsilon_1/2\epsilon_0$, (9) and (10) reduce to

$$\frac{a_1}{a_0} = -\frac{\epsilon_1}{2\epsilon_0} \frac{1}{D_1} \tag{13}$$

$$\frac{a_{-1}}{a_0} = -\frac{\epsilon_1}{2\epsilon_0} \frac{1}{D_{-1}}, \tag{14}$$

in agreement with (14) and (12), respectively, of Simon.

Sufficiency Condition for a Space-Harmonic Form of Solution

It can be shown[4] from the theory of three-term recursion formulas, that if the condition

$$|D_n| > \frac{\epsilon_1}{\epsilon_0} \tag{15}$$

is satisfied for all $n > N$, then relations (8) and (9)–(12) converge absolutely and uniformly. A space-harmonic representation of the solution will also converge provided that (15) is satisfied. If (15) is not satisfied, the convergence is not assured, and a perturbation solution in such a range is, at the very least, highly suspect.

A physical interpretation of condition (15) is obtained by considering it in the limit of high n. Thus, as $n \to \infty$,

$$|D_\infty| = \left|1 - \left(\frac{k_1 \omega}{k_0 \omega_1}\right)^2\right| = \left|1 - \left(\frac{v_0}{v_1}\right)^2\right|, \tag{16}$$

where $v_1 = \omega_1/k_1$ and $v_0 = \omega/k_0$ are the phase velocities of the progressive disturbance (pump wave) and the unperturbed electromagnetic wave, respectively. Condition (15) then becomes

$$\left|1 - \left(\frac{v_0}{v_1}\right)^2\right| > \frac{\epsilon_1}{\epsilon_0}, \tag{17}$$

and is satisfied except when the two velocities are almost equal. Simon's triple-root case corresponds exactly to the equality of the two velocities, and thus violates (17). This case is discussed further below.

Double-Root Cases

Simon's double-root cases correspond physically to stop bands, Bragg reflection situations, or parametric conversion regions, depending on the point of view adopted. Only the two lowest stop bands are considered, differing in that for one band the progressive disturbance and the electromagnetic wave propagate in opposite directions, while for the other they travel in the same direction, corresponding to parametric up-conversion and down-conversion, respectively.

[4] J. Meixner and F. W. Schäfke, "Mathieusche Funktionen und Sphäroidfunktionen," Springer Verlag, Berlin, Germany, pp. 89–93; 1954.

For the up-conversion case, the following relation holds:

$$\frac{k_1}{k_0} = -2 - \frac{\omega_1}{\omega}. \tag{18}$$

Substituting (18) into the sufficiency condition (15) for $n \to \infty$, one obtains

$$4\frac{\omega}{\omega_1}\left(\frac{\omega}{\omega_1} + 1\right) > \frac{\epsilon_1}{\epsilon_0}, \tag{19}$$

indicating that one should avoid values of ω/ω_1 that are too small. This conclusion is also borne out in Simon's (18), which loses its meaning when ω/ω_1 becomes extremely small.

For the down-conversion case, one finds the relation

$$\frac{k_1}{k_0} = 2 - \frac{\omega_1}{\omega}, \tag{20}$$

so that condition (15) becomes

$$4\frac{\omega}{\omega_1}\left|\frac{\omega}{\omega_1} - 1\right| > \frac{\epsilon_1}{\epsilon_0}. \tag{21}$$

As above, one should avoid values of ω/ω_1 that are too small but now, in addition, a region around $\omega = \omega_1$. These results are again in accord with Simon's (29)–(32) which become meaningless in these extremes. The $\omega = \omega_1$ region may also be seen via (20) to be a special case of the triple-root case, which is considered below.

The application of condition (15) to the double-root cases bears out the validity of the solutions to these cases. The same considerations apply to the higher-order stop bands, about which we can briefly comment in view of the availability of the rigorous solutions (8)–(12). The mth-order stop band occurs when D_m becomes small, and the solution is characterized by the presence of two principal space harmonics whose amplitudes a_0 and a_m are both of the same order. Upon inspection of (9) and (11), one sees that

$$\frac{a_m}{a_0} \approx \frac{(-1)^m(\epsilon_1/2\epsilon_0)^m}{D_m \cdot D_{m-1} \cdot D_{m-2} \cdots D_1}, \tag{22}$$

since all values of D_n except that for $n = m$ are not small. Outside of the stop band, the ratio a_m/a_0 is small; it becomes of the order of unity only when D_m becomes sufficiently small. One can see from (9) that this occurs only over a limited range of ω; one may conclude from this that the width of the stop band in ω is proportional to $(\epsilon_1/2\epsilon_0)^m$, and that for high values of m the stop bands become very narrow.

It may be added that Epsztein has independently recognized the parametric up-conversion behavior associated with such stop bands and has proposed[5] a device for producing millimeter waves based on this principle. He has suggested the use of a higher-order stop band so that the frequency conversion ratio may be large, but this introduces practical difficulties because of the very narrow stop band that would be present.

[5] B. Epsztein, "Millimeter Waves," Microwave Res. Inst., Polytechnic Inst. of Brooklyn, N. Y., Rept. No. 840–60, pp. 8–9; July 25, 1960.

Triple-Root Case

Simon's perturbation solution assumes the existence of only three space harmonics, and his triple-root case corresponds to that condition for which all three of his space harmonics must be considered, since none of them is small in amplitude. If the complete solution involving an infinite number of space harmonics is considered, it is seen that the triple-root condition

$$\frac{k_1}{\omega_1} = \frac{k_0}{\omega} \tag{23}$$

implies that none of the infinite number of space harmonics is small in amplitude, and that therefore *all* of them must be considered. This statement becomes clear by considering (6) for any n, and realizing that condition (23) results in *every* D_n being small when solutions in the range k near k_0 are examined. Such a space-harmonic expansion may thus result in a divergent total field. Any solution that includes only three of the space harmonics, and ignores the non-neglectable infinite remainder, must evidently be highly suspect.

From (16) and (17) it is seen that relation (23) clearly violates the sufficiency condition for a space-harmonic form of solution, and that, as Simon recognizes (23) corresponds to equal propagation velocities for the unperturbed electromagnetic wave and the progressive disturbance. As is shown in the Appendix, this effect is analogous to that of a material body passing through the sonic barrier.

The singular nature of the total field is also brought out by considering the asymptotic behavior of the space-harmonic amplitudes. In the range for which (17) is violated, (6) becomes for sufficiently high n

$$\frac{\epsilon_1}{2\epsilon_0} a_{n+1} + D_\infty a_n + \frac{\epsilon_1}{2\epsilon_0} a_{n-1} \cong 0, \tag{24}$$

so that

$$a_n \sim (-1)^n e^{\pm jn\theta}, \tag{25}$$

where

$$\cos\theta = \frac{\epsilon_0}{\epsilon_1} D_\infty, \tag{26}$$

and θ is *real*. Thus, the sum of the squares of the absolute values of the coefficients a_n need not converge. More detailed considerations are presented in the Appendix, where it is shown that a space-harmonic form of expansion will diverge in this range for real values of k, all of which are solutions of (8) or an equivalent determinantal equation.

Further physical and mathematical insight into the singular nature of the solution is afforded by considering

certain properties of the original differential equation. In the Appendix, it is shown via a transformation to a moving coordinate system that a singularity in the differential equation occurs whenever the phase velocity v_1 of the moving disturbance is equal to the *local* phase velocity v_L of the electromagnetic wave in the disturbed medium. This equality, which is thus a condition for the appearance of a singularity in the equation, is exactly the complement of (17), which is the sufficiency condition for the solution to be convergent. It is also seen, that if this equality is satisfied there will exist values of the phase u of the progressive disturbance for which v_1 is "supersonic" or "subsonic" with respect to v_L. The Appendix also shows that in the moving coordinate system solutions of the differential equation admit discontinuities in $\partial^2 E/\partial u^2$ across sonic lines, *i.e.*, lines of constant u for which $v_L = v_1$. On each side of such a sonic line a different solution will exist in general, neither of which can be analytically continued across the sonic line.

It is clear from the above discussion that Simon's harmonic expansion treatment of his triple-root case has no meaning in this context. We have not attempted in this paper to consider under what circumstances, if any, his treatment may be of value.

We have attempted here to enhance the value of Simon's interesting paper by presenting a rigorous solution and a sufficiency condition for the convergence of the solution, and by applying this condition to indicate that the treatment of Simon's triple-root case is in error.

Appendix

A. Convergence of the Space-Harmonic Expansion

We prove below that in the range

$$-1 < \frac{\epsilon_0}{\epsilon_1} D_\infty < 1,$$

where

$$D_\infty = \lim_{n \to \infty} D_n,$$

there exists for any real value of k a solution of the difference equation (6) for which the infinite determinant of the system vanishes, and for which the sum

$$\sum_{n=-\infty}^{\infty} |a_n|^2,$$

of the magnitude squared of the coefficients of the space-harmonic expansion diverges.

The existence of solutions of (6), consistent with the vanishing of the infinite determinant, for every real value of k can be demonstrated by a theorem of Weyl.[6] The possible existence of corresponding solutions with complex k was not investigated.

[6] F. Riesz and B. S. Nagy, "Functional Analysis," Frederick Ungar Co., New York, N. Y., p. 367; 1955.

The convergence of the above-mentioned sum can be determined from the asymptotic behavior of the coefficients a_n. To this end, let us write a general linear homogeneous difference equation of the nth order in the form

$$\sum_{i=0}^{n} p_i(x) u(x+i) = 0. \tag{27}$$

We shall assume that the coefficients $p_i(x)$ admit the following expansion, valid for sufficiently large values of x:

$$p_i(x) = p_i^{(0)} + p_i^{(1)} x^{-1} p_i^{(2)} x^{-2} + \cdots. \tag{28}$$

If now the so-called characteristic equation

$$p_n^{(0)} t^n + p_{n-1}^{(0)} t^{n-1} + \cdots + p_1^{(0)} t + p_0^{(0)} = 0 \tag{29}$$

possesses n different roots t_i, $1 \leq i \leq n$, then there exist n independent solutions of the difference equation (27) which are asymptotically represented in the form[7]

$$u_j(x) \sim (t_j)^x x^{r_j} \left(1 + \frac{b_{1j}}{x} + \frac{b_{2j}}{x^2} + \cdots\right), \quad 1 \leq j \leq n. \tag{30}$$

One determines the characteristic exponent r_j and the coefficients b_j by substitution of (30) into (27) and equating the sum of the coefficients of equal powers of x to zero.

Let us apply the above general result to the specific equation

$$a_{n+1} + \frac{2\epsilon_0}{\epsilon_1} D_n a_n + a_{n-1} = 0, \qquad n = 0, \pm 1, \cdots, \tag{31}$$

with D_n expressed in the form (valid for n sufficiently large)

$$D_n = D_\infty + \frac{d_1}{n} + \frac{d_2}{n^2} + \cdots. \tag{32}$$

The characteristic equation (29) now becomes

$$t^2 + \frac{2\epsilon_0}{\epsilon_1} D_\infty t + 1 = 0, \tag{33}$$

which has solutions

$$t_{1,2} = -e^{\pm i\theta}, \tag{34}$$

with $\cos\theta = (\epsilon_0/\epsilon_1) D_\infty$, as in (26). Hence, one finds that

$$a_{nj} \sim t_j^n n^{r_j} \left(1 + \frac{b_{1j}}{n} + \frac{b_{2j}}{n^2} + \cdots\right), \quad j = 1, 2. \tag{35}$$

[7] G. D. Birkhoff, "General theory of linear difference equations," *Trans. Am. Math. Soc.*, vol. 12, pp. 243–284; 1911.

J. Horn, "Zur Theorie der linearen Differenzengleichungen," *Math. Ann.*, vol. 53, pp. 177–192; 1900. Also, "Über das Verhalten der Integrale linearer Differenzen- und Differentialgleichungen für grosse Werte der Veränderlichen," *J. Reine angew. Math.*, vol. 138, pp. 159–191; 1910.

Substituting (35) into (31), we obtain

$$-l_j\left(1+\frac{1}{n}\right)^{r_j}\left(1+\frac{b_{1j}}{n\left(1+\frac{1}{n}\right)}+\cdots\right)$$
$$+\left(D_\infty+\frac{d_1}{n}+\cdots\right)\left(1+\frac{b_{1j}}{n}+\frac{b_{2j}}{n^2}+\cdots\right)$$
$$-(l_j)^{-1}\left(1-\frac{1}{n}\right)^{r_j}\left(1+\frac{b_{1j}}{n\left(1-\frac{1}{n}\right)}+\cdots\right)=0. \quad (36)$$

Equating to zero the coefficient of $(1/n)^0$, one has

$$\cos\theta=\frac{\epsilon_0}{\epsilon_1}D_\infty,$$

which agrees with (26) while equating to zero the coefficient of $(1/n)^1$, and using (34), one obtains the relation

$$r_{1,2}=\mp j\frac{d_1}{2\sin\theta}. \quad (37)$$

Therefore, it follows from (35) that

$$(a_n)_{1,2}=(-1)^n e^{\pm jn\theta}e^{\mp jd_1\ln n/2\sin\theta}\left[1+0\left(\frac{1}{n}\right)\right]. \quad (38)$$

In the range of parameters for which

$$-1<\frac{\epsilon_0}{\epsilon_1}D_\infty<1, \quad (39)$$

i.e., for which θ is real, and for d real, which corresponds to k real, as seen from (7) and (32), one finds

$$a_n-(-1)^n e^{\pm j\left[n\theta\mp(d_1\ln n/2\sin\theta)\right]}=0\left(\frac{1}{n}\right). \quad (40)$$

It is clear that under these conditions the sum

$$\sum_{n=-\infty}^{\infty}|a_n|^2$$

does not converge. This follows since the right-hand side of (40) is square-summable, and hence the left-hand side must be also. However, because the second term on the left-hand side is not square-summable, a_n cannot be. The divergence of this sum indicates the presence of a non-square-integrable singularity in the solution of the differential equation and, therefore, does not permit a harmonic expansion in this range.

B. Differential Equation Considerations and Sonic Lines

Further physical and mathematical insight into the singular nature of the solution in the range $(\epsilon_0/\epsilon_1)|D_\infty|\leq 1$ is afforded by considering the always hyperbolic differential equation

$$\frac{\partial^2 E(z,t)}{\partial z^2}-\mu_0\frac{\partial^2}{\partial t^2}\left[\epsilon(z,t)E(z,t)\right]=0, \quad (41)$$

where $\epsilon(z,t)$ is given by (1). Let us introduce the following transformation of variables appropriate to a moving coordinate system:

$$u=k_1z-\omega_1t;\qquad t'=t. \quad (42)$$

One obtains from (41) and (42) the transformed differential equation

$$(k_1^2-\mu_0\epsilon_0\omega_1^2-\mu_0\epsilon_1\omega_1^2\cos u)\frac{\partial^2E(u,t')}{\partial u^2}$$
$$+2\omega_1(\mu_0\epsilon_0+\mu_0\epsilon_1\cos u)\frac{\partial^2E}{\partial u\partial t'}-(\mu_0\epsilon_0+\mu_0\epsilon_1\cos u)\frac{\partial^2E}{\partial t'^2}$$
$$+2\mu_0\epsilon_1\omega_1^2\sin u\frac{\partial E}{\partial u}-2\omega_1\mu_0\epsilon_1\sin u\frac{\partial E}{\partial t'}$$
$$-\mu_0\epsilon_1\omega_1^2\cos uE=0. \quad (43)$$

Upon recognizing that

$$v_1=\frac{\omega_1}{k_1}$$

and

$$v_0=\frac{\omega}{k_0}=\frac{1}{\sqrt{\mu_0\epsilon_0}}$$

are the phase velocities of the progressive disturbance (pump wave) and the electromagnetic wave in the unperturbed medium, respectively, and that the local phase velocity of the electromagnetic wave in the disturbed medium is

$$v_L=\frac{\omega}{k_0\sqrt{1+(\epsilon_1/\epsilon_0)\cos u}}. \quad (44)$$

(43) can be rewritten in the form

$$\left(1-\frac{v_1^2}{v_L^2(u)}\right)\frac{\partial^2E}{\partial u^2}+\frac{2v_1}{k_1}\frac{1}{v_L^2(u)}\frac{\partial^2E}{\partial u\partial t'}$$
$$-\frac{1}{k_1^2}\frac{1}{v_L^2(u)}\frac{\partial^2E}{\partial t'^2}-2v_1^2\frac{d}{du}\left[\frac{1}{v_L^2(u)}\right]\frac{\partial E}{\partial u}$$
$$+2\frac{v_1}{k_1}\frac{d}{du}\left[\frac{1}{v_L^2(u)}\right]\frac{\partial E}{\partial t'}-v_1^2\left(\frac{1}{v_L^2(u)}-\frac{1}{v_0^2}\right)E=0. \quad (45)$$

In the range

$$\frac{\epsilon_0}{\epsilon_1}|D_\infty|\leq 1, \quad (46)$$

for which the sufficiency condition is not satisfied, there will always exist a real value $u=u_0$ for which the co-

efficient of $\partial^2 E/\partial u^2$ in (43) vanishes, *i.e.*,

$$k_1^2 - \mu_0\epsilon_0\omega_1^2 - \mu_0\epsilon_1\omega_1^2 \cos u_0 = k_1^2\left(1 - \frac{v_1^2}{v_L^2(u_0)}\right) = 0. \quad (47)$$

The existence of real u_0 in this range is seen by rewriting (47) as

$$\cos u_0 = \frac{\epsilon_0}{\epsilon_1}\left[\frac{k_1^2/\omega_1^2}{\mu_0\epsilon_0} - 1\right]; \quad (48)$$

hence, u_0 is real if

$$\frac{\epsilon_0}{\epsilon_1}\left|\frac{(k_1/\omega_1)^2}{\mu_0\epsilon_0} - 1\right| \leq 1, \quad (49)$$

or

$$\frac{\epsilon_0}{\epsilon_1}\left|D_\infty\right| \leq 1,$$

which is identical with (46).

The vanishing of the coefficient of $\partial^2 E/\partial u^2$, however, gives rise to a singularity of the differential equation (45). The singularity arises because even though the values of E and $\partial E/\partial u$ are given on the line $u = u_0$ for all t', the values of $\partial^2 E/\partial u^2$ are not determined by the differential equation (45), and $\partial^2 E/\partial u^2$ may jump across the line $u = u_0$. Hence, the "sonic lines," for which $v_1^2 = v_L^2(u_0)$, are singular lines of the differential equation (45). On each side of such a sonic line a different solution will exist, neither of which can be analytically continued across the sonic line. The sufficiency condition (17), therefore, eliminates the occurrence of such a singularity and guarantees the existence of square-integrable solutions of (45).

Acknowledgment

The authors wish to thank Prof. H. Kurss of the Polytechnic Institute of Brooklyn for helpful discussions regarding the question of convergence.

A New Broad-Band Absorption Modulator for Rapid Switching of Microwave Power*

FRANK REGGIA†, SENIOR MEMBER, IRE

Summary—This paper describes a new technique for obtaining a broad-band absorption modulator for high-speed switching or amplitude modulation of microwave power. This ferrite modulator, an outgrowth of the longitudinal-field rectangular-waveguide phase shifter,[1] has electrical characteristics particularly desirable in a microwave switch. These include a zero-field insertion loss of approximately 0.5 db in the ON state, an isolation of greater than 60 db in the OFF state which is nearly independent of the magnetic control field in this state, and a nearly matched input impedance for all values of applied field. These electrical characteristics are nearly constant over a 30 per cent bandwidth at *X* band. Also, it is possible to design the amplitude modulator to have negligible phase shift at the desired operating frequency.

Other characteristics of this ferrite modulator include small physical size, magnetic control fields of less than 50 oersteds, operating temperatures up to 150°C, and a capability of less than one μsec switching time.

* Received by the PGMTT, March 9, 1961; revised manuscript received, May 3, 1961.

† Diamond Ordnance Fuze Labs., Washington, D. C.

[1] F. Reggia and E. G. Spencer, "A new technique in ferrite phase-shifting for beam scanning of microwave antennas," PROC. IRE, vol. 45, pp. 1510–1517; November, 1957.

Introduction

In its most general form, the relationship between the induced RF flux density $\boldsymbol{b}$ and the internal RF magnetic field $\boldsymbol{h}$ in an arbitrarily magnetized polycrystalline-ferrite medium is a permeability tensor given by

$$\begin{bmatrix} b_x \\ b_y \\ b_z \end{bmatrix} = \begin{bmatrix} \mu_{xx} & \mu_{xy} & \mu_{xz} \\ \mu_{yx} & \mu_{yy} & \mu_{yz} \\ \mu_{zx} & \mu_{zy} & \mu_{zz} \end{bmatrix} \begin{bmatrix} h_x \\ h_y \\ h_z \end{bmatrix}. \quad (1)$$

From this expression, Rado[2] has shown that for an unsaturated ferrite medium at microwave frequencies and a dc magnetic field applied in the z direction, the permeability tensor reduces to

$$[\mu] = \begin{bmatrix} \mu & -jK & 0 \\ +jK & \mu & 0 \\ 0 & 0 & \mu_z \end{bmatrix}, \quad (2)$$

[2] G. T. Rado, "Electromagnetic characterization of ferromagnetic media," IRE TRANS. ON ANTENNAS AND PROPAGATION, vol. AP-4, pp. 512–525; July, 1956.

where μ, K, and μ_z are the components in the three mutually perpendicular directions and are complex quantities. Thus,

$$\begin{aligned} b_x &= \mu h_x - jKh_y \\ b_y &= jKh_x + \mu h_y \\ b_z &= \mu_z h_z. \end{aligned} \tag{3}$$

As seen from the first two equations of (3), an RF magnetic field h_x in the x-direction induces a component of the RF flux density b_x which is proportional to μ and, due to the electron spins precessing about the direction of the dc magnetizaton, also induces a component b_y in the y-direction proportional to K. The operation of the absorption modulator which will be described later depends primarily upon the variation of this latter permeability component K with applied magnetic field.

By making certain approximations, valid only for a low-loss ferrite medium at microwave frequencies and for applied magnetic fields below magnetic saturation, the real part of K is given in terms of the magnetic properties of the medium by

$$K' = -\frac{4\pi M\gamma}{\omega}, \tag{4}$$

where M is the dc magnetization in the direction of the applied magnetic field, $\gamma = 2.8$ Mc/sec-oersteds is the gyromagnetic ratio of the electron for a ferrite medium and ω is the operating angular frequency.

This expression agrees very well with experimental results,[3] shown in Fig. 1, which were obtained at 9340 Mc for a low-loss MgMn ferrite[4] vs the internal dc magnetic field below magnetic saturation. Only the real parts are shown, the imaginary parts are small in comparison. These results were obtained by microwave-cavity perturbation techniques, and the measurements of M vs the applied magnetic field H were obtained by standard ballistic galvanometer techniques.

As seen in Fig. 1, the coupling coefficient K' is zero when no external magnetic field is applied. Since $\mu' = \mu_z' = 0.76$ for this case, the ferrite medium exhibits a scalar permeability with no dispersion to the microwave energy. This intitial permeability of less than unity at X-band is due to the gyromagnetic resonance of electron spins in the internal crystalline anisotropy field of the ferrite.

When the dc biasing field is applied to this ferrimagnetic medium, K' increases to approximately 0.67 at magnetic saturation, at which time the other two components approach unity. It is this variation of K' with applied magnetic field which accounts for the transfer of the incident microwave energy of one polarization to another perpendicular wave in a magnetized ferrite medium. If this perpendicular RF field, which is generated inside a magnetized ferrite, could be attenuated without appreciable loss to the microwave energy which exists in the medium when unmagnetized, it would be possible to design an amplitude modulator with an attenuation characteristic similar to the curve shown for K'. This was done[5] by placing a very thin resistive film inside a relatively large ferrite rod used in the rectangular-waveguide absorption modulator which follows.

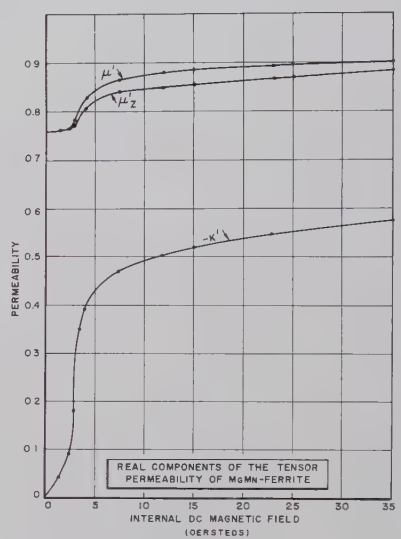

Fig. 1—The three components of the tensor permeability at 9340 Mc vs applied magnetic field below magnetic saturation for a low-loss MgMn ferrite.[4]

Broad-Band Absorption Modulator

A cross-sectional view of the absorption modulator (or microwave switch) making use of the gyromagnetic phenomena described above is shown at the left of Fig. 2. It consists of a low-loss MgMn ferrite rod (split along its length) centrally located inside a standard rectangular-waveguide section excited in its fundamental TE_{01} mode. Both the ferrite rod and the polyfoam dielectric support make use of linear tapers at both ends for impedance matching. A thin resistive film, placed between the sections of the split rod and in a plane perpendicular to the input RF electric field, is used to attenuate the perpendicular component of this field generated in the magnetized ferrite rod. A low-current solenoid, wound around the rectangular-waveguide section, is used to supply the longitudinal magnetic control field.

An early model[5] of the modulator made use of a rectangular ferrite rod (0.280×0.300 inch) and an attenuating element consisting of a thin layer of

[3] R. C. LeCraw and E. G. Spencer, "Intrinsic Tensor Permeabilities of Ferrites Below Magnetic Saturation," DOFL TR-345; May, 1956.

[4] Ferramic R-1 ferrite, manufactured by General Ceramic Corp., has a dielectric constant (ϵ') of 13.6 and saturation magnetization ($4\pi M_s$) of approximately 2000 gauss.

[5] J. E. Tompkins, F. Reggia, and L. Joseph, "Multimode Propagation in Gyromagnetic Rods and its Application to Traveling Wave Devices," DOFL TR-861; Sept. 21, 1960.

aquadag (or carbon) on a 0.0002-inch thick mylar sheet. The low-current solenoid supplying the longitudinal control field was wound around the $\frac{1}{2}\times 1$-inch rectangular-waveguide section. The total length of the absorption modulator was 4 inches.

The isolation characteristics and input VSWR of the above model at 9250 Mc vs applied magnetic field are shown in Fig. 3. The width and length of the attenuating element were the same as those of the ferrite rod. Nearly constant electrical characteristics were obtained with this model over the frequency range of 7500 Mc to 10,500 Mc with the ferrite rod dimensions given in the figure. These electrical characteristics are reciprocal—that is, they do not depend upon the direction of propagation or magnetic control field.

As seen in Fig. 3, when the ferrite switch is operating in the OFF state, an isolation greater than 40 db is obtained, and this isolation is nearly independent of the magnitude of the magnetic control field. This characteristic is especially desirable in high-speed microwave switches. It is also interesting to note the similarity between this curve and the variation of the permeability component K' with applied field shown in Fig. 1. Thus, the simplified analysis leading to (4) gives a qualitative insight into the behavior of the ferrite rod in the absorption modulator.

The zero-field insertion loss is 0.5 db and the input VSWR remains less than 1.20 for all values of applied

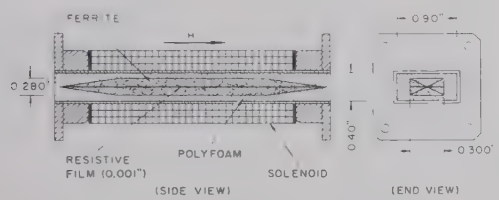

Fig. 2—Cross-sectional views of the ferrite absorption modulator.

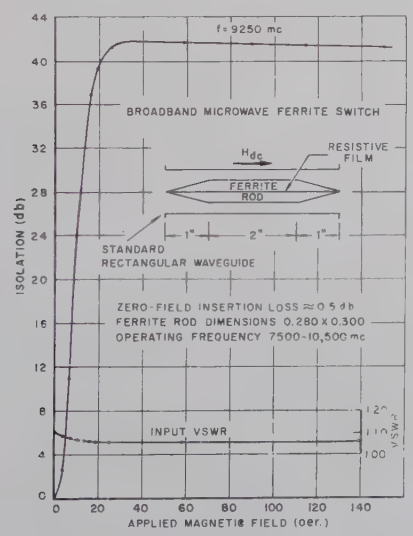

Fig. 3—Typical electrical characteristics vs applied longitudinal magnetic field. An aquadag resistive film on mylar was used as the attenuator element.

field over the operating frequency range. The total length of the modulator and the MgMn ferrite rod (including the impedance matching tapers) is 4 inches, and the dc power required to operate the modulator as a switch is approximately 2 watts.

Improved Isolation-Bandwidth Characteristics

Because the resistivity of the aquadag film on the mylar sheet was not known and because its reproducibility and temperature characteristics were not good, a new type of attenuating element was devised which consisted of a specially selected mica sheet (0.001-inch thick) upon which was deposited a very thin film of pure metal. The resistivity of these attenuating elements was accurately known and could be adjusted over a wide range. Their temperature and frequency characteristics were also very good.

The first of these new attenuator elements which were used had a resistivity of 65 ohms per square. Beginning with these elements, an attempt was first made to optimize the isolation-bandwidth characteristics of the absorption modulator by adjusting the height and width of the ferrite rod. These results are shown in Figs. 4 and 5 for a number of MgMn ferrite rods in standard X-band rectangular waveguide (0.400×0.900-inch inside dimensions). The length of the ferrite rods and rectangular-waveguide sections was 4 inches.

Beginning with the ferrite rod dimensions given in Figs. 2 and 3 and making use of a metallized-mica attenuating element with a resistivity of 65 ohms per square, the maximum isolation of the absorption-modulator switch in the OFF state was measured from 7000 Mc to 11,000 Mc for a number of ferrite-rod heights and widths. The applied magnetic field used for these measurements was approximately 100 oersteds.

The measured data shown in Fig. 4(a) were obtained for three 0.300-inch wide ferrite rods with heights ranging from 0.280 inch to 0.300 inch. Only a slight improvement in the isolation characteristics is seen to occur at the low-frequency end. However, each of these rods was capable of giving an isolation of greater than 60 db over at least a 2000-Mc bandwidth. By optimizing the geometry of the attenuator element, isolations in excess of 70 db over a relatively narrow bandwidth (centered around 9500 Mc) were obtained with a rectangular ferrite rod having a height and width of 0.290 inch and 0.300 inch, respectively. The zero-field insertion loss of the above rods was approximately 0.5 db over the frequency range shown.

Further improvements in the isolation-bandwidth characteristics of the absorption modulator are shown in Fig. 4(b). Here we see the results for three ferrite rods, 0.320 inch wide, with heights also varying from 0.280-inch to 0.300 inch. A marked improvement in the isolation characteristics with height at the low-frequency end and a slight deterioration at the high-frequency end of the bandwidth are observed. The

increased isolation at the low-frequency end is due to an increase in the microwave energy concentration in the larger ferrite rods, while the dropping off of the isolation characteristics at the high-frequency end is due to higher-order modes propagating out of the attenuating region. Undulations in the isolation characteristics were also observed at the lower field values when operating at frequencies above 10,500 Mc.

Similar results obtained over the same frequency range are shown in Fig. 5 for several ferrite rods, each having a height of 0.300 inch. This time the width was taken as the parameter, increasing from 0.300-inch to 0.340-inch. No improvement was observed in the isolation characteristics by increasing the rod width above 0.320 inch. Thus, a ferrite rod 0.300 inch high and 0.320 inch wide was considered optimum over this frequency range. For this particular ferrite rod, the isolation in the OFF state was greater than 60 db over a bandwidth in excess of 2500 Mc and more than 55 db isolation was obtained over a 3500-Mc bandwidth. These characteristics can be extended to a higher frequency range by making use of techniques similar to

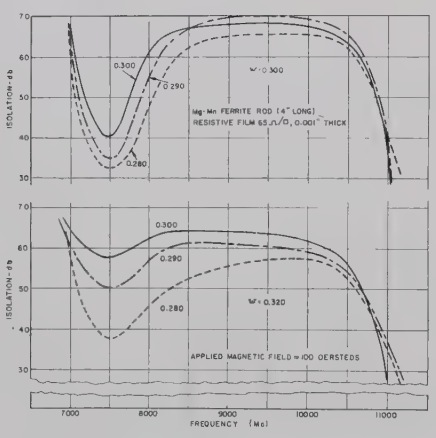

Fig. 4—Isolation-bandwidth characteristics of absorption modulator. Parameter was the ferrite rod height. (a) Rod width is 0.300 inch. (b) Rod width is 0.320 inch.

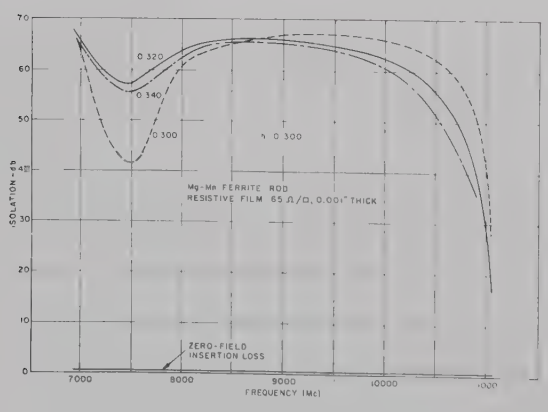

Fig. 5—Isolation-bandwidth characteristics using ferrite rods 0.300-inch high. The applied field was 100 oersteds and the rod widths varied from 0.300 to 0.340-inch.

that used with the rectangular-waveguide phase modulator,[1] *i.e.*, making use of a rectangular waveguide and ferrite rod with smaller cross-sectional dimensions. The zero-field insertion loss (approximately 0.5 db) is shown for comparison at the bottom of the figure.

The length and width of the attenuating elements which were used for the above measurements were the same as those of the particular ferrite rod used in the absorption modulator. It was found that attenuating elements which were wider and narrower than the ferrite rod resulted in higher zero-field insertion losses and narrower operating bandwidths, respectively. However, attenuator elements having a width slightly less than that of the ferrite rod are capable of isolations greater than that shown here.

The isolation characteristics from 8500 Mc to 9500 Mc of the rectangular-waveguide absorption modulator versus the applied magnetic field are shown in Fig. 6. These results were obtained with a 4-inch long rectangular ferrite rod, including 7/8-inch tapers at both ends, having a height and width of 0.300 inch and 0.320 inch, respectively. A metallized-mica attenuating element (0.001-inch thick) having a resistivity of 65 ohms per square was used between the split sections of the ferrite rod. As seen in the figure, the isolation characteristics did not vary greatly over this bandwidth, reaching a maximum value in excess of 60 db. Similar results, not shown, were obtained at 8000 Mc and 10,000 Mc. The input VSWR of this modulator at 9000 Mc, shown at the bottom of the figure, remained below 1.15 for all values of applied field. The solenoid current required to obtain the necessary magnetic-field strength is shown at the top of the figure. Approximately 2 watts of dc power were required to obtain a field strength of 40 oersteds.

Although (4) shows the permeability component K' to vary inversely with frequency, it is also true that the amount of energy concentrated in the ferrite rod ($\epsilon' = 13.6$) increases with frequency—one tending to cancel the effect of the other. Other factors contributing to the broad-band characteristics of the absorption modulator include the length and cross section of the ferrite rod, the thickness and width of the attenuating element, and, to a lesser degree, the resistivity of the attenuating element.

The ferrite modulator of Fig. 6 was subjected, in the OFF state, to an input CW power of 5 watts for a period of 3 hours. Very little change was observed in its isolation characteristics at this power level. In this state, essentially all the microwave power was dissipated in the metallized-mica attenuating element. Some deterioration of the polyfoam dielectric was observed at this power level, but this was corrected by using a low-loss silicone-foam dielectric. The peak power-handling capability of this ferrite modulator is approximately 5 kilowatts.

Data, shown in Fig. 7, were also taken at 9300 Mc to determine the isolation characteristics vs applied magnetic field of the absorption modulator for a number of ferrite-rod lengths and attenuator-element resistivities. These results were also used to determine the minimum length of the ferrite modulator necessary to obtain approximately 60 db isolation in the OFF state.

The curves in Fig. 7(a) show the isolation characteristics of the absorption modulator for several MgMn rods with lengths varying from $2\frac{1}{2}$ inches to 4 inches, including the impedance matching tapers at both ends. These rods had a cross-sectional dimension of 0.300 inch by 0.320 inch, and the resistivity of the attenuator element used for these measurements was 60 ohms per square. As seen in the figure, the maximum isolation obtainable increases rapidly with rod length up to 4 inches, and the effect of the demagnetizing field decreases with increasing rod length.

The curves in Fig. 7(b) were taken with a single ferrite rod, with dimensions given at the bottom, as the resistivity of the attenuator element was increased from 10 ohms to 80 ohms per square. Here we see that the maximum isolation which can be obtained increases rapidly until the resistivity reaches approximately 50 ohms per square, and decreases again as the resistivity is increased above this value. It is thus important to select the correct value of resistivity if good isolation characteristics are to be obtained. The value of resistivity chosen for a particular operating frequency also determines the phase-shift characteristics of the ferrite modulator.

Small discrepancies in the results shown here with those in preceding figures are probably due to differences in the taper lengths of the rods used, attenuating elements, and possibly even due to some variations in the ferrite material itself.

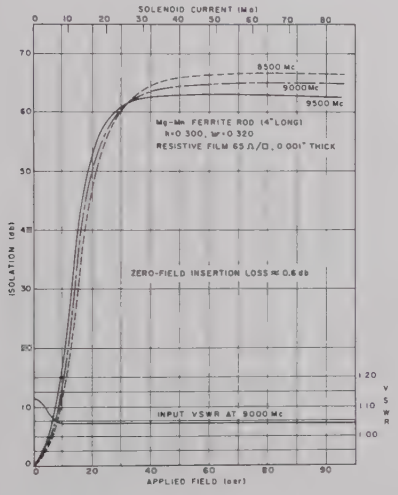

Fig. 6—Isolation characteristics of improved absorption modulator vs applied magnetic field.

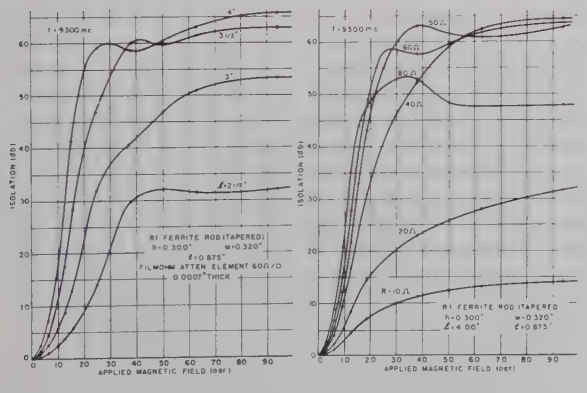

(a) (b)

Fig. 7—Isolation characteristics vs applied field for various ferrite-rod lengths and resistivities of attenuating element. (a) Parameter is rod length. (b) Parameter is attenuator-element resistivity (ohms per square).

Phase-Shift Characteristics

A final refinement of the absorption modulator is to adjust the resistivity of the attenuator element used with an optimum rod such that nearly zero phase shift occurs at the desired operating frequency. This has been accomplished at a number of frequencies between 8000 Mc and 9500 Mc.

The phase-shift characteristics of the absorption modulator at 9200 Mc for various values of resistivity of the attenuator element with a rectangular ferrite rod ($h = 0.300$ inch, $w = 0.320$ inch) are shown in Fig. 8. The metallized-mica attenuating elements between the split sections of the ferrite rod were 0.0006-inch thick, and their widths were the same as that of the rod. The magnitude of the applied magnetic field, not shown, increases from left to right along each of the phase-shift curves.

As seen in the figure, attenuator elements with very large values of resistivity give large phase shifts (lag) with applied magnetic field, similar to that which is obtained with the rectangular-waveguide phase modulator.[1] As the resistivity of the attenuator element is decreased, the phase shift obtained becomes small, ap-

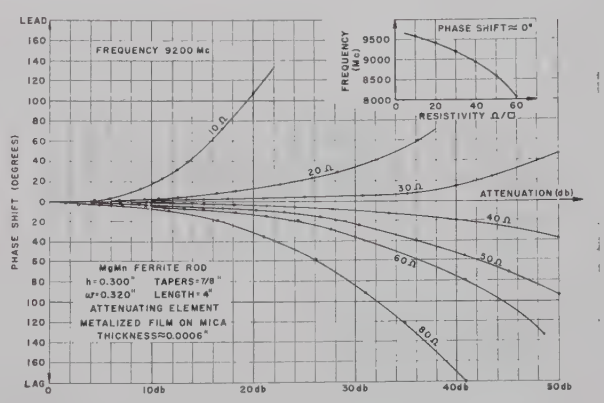

Fig. 8—Phase-shift characteristics of modulator using a 4-inch long ferrite rod (0.300×0.320 inch). Parameter is resistivity of attenuator element.

proaching zero for a resistivity of approximately 35 ohms per square. As the resistivity of the attenuator element is decreased below this value, the phase shift again begins to increase, but now a phase lead is obtained. As the resistivity is decreased to 10 ohms per square or less, the phase shift increases rapidly again, but the maximum insertion loss (or isolation) deteriorates very rapidly. This decrease in maximum isolation for large and small values of resistivity was also shown in Fig. 7.

The small insert at the top right of Fig. 8 shows the approximate resistivity of the attenuator element needed for a particular ferrite rod if nearly zero phase shift is to be obtained in the frequency range from 8000 to 9500 Mc. The most important region is from 20 ohms to 60 ohms per square. Thus, amplitude modulation with negligible phase modulation is possible with the above ferrite modulator. The length and width of the attenuator elements which were used for these measurements were the same as those of the ferrite rod, and their thickness was less than 0.001 inch.

Isolation Characteristics vs Temperature

The isolation characteristics of the rectangular-waveguide absorption modulator at 9350 Mc as a function of applied magnetic field are shown in Fig. 9 for a number of equilibrium temperatures from 33°C to 200°C. This modulator made use of a tapered ferrite rod (4 inches long), whose width and height were 0.320 and 0.300 inch, respectively. A silicone dielectric was used to support the rod at these high temperatures, and a 50-ohm per square resistive-attenuator element (0.001 inch thick) was used to dissipate the microwave energy in the OFF state. The dimensions of the attenuator element (approximately the same as that of the ferrite rod) were optimized for the 9000- to 10,000-Mc frequency range.

As seen in the figure, the isolation characteristics showed little deterioration with applied magnetic field for temperatures up to 100°C, reaching a maximum isolation in excess of 70 db. At 150°C, isolations greater than 60 db were still possible, but higher values of applied magnetic field were required. Above this temperature, however, the isolation characteristics deteriorate rapidly until the Curie temperature (290°C) is reached, at which time the ferrite medium becomes paramagnetic. These results are consistent with the known deterioration of the saturation magnetization of the ferrite material with temperature. The zero-field insertion loss of the absorption modulator remained nearly constant at 0.4 db for all temperatures up to 200°C.

Standard techniques were used to make the temperature measurements. An aluminum-constantan thermocouple was attached to the brass housing of the absorption modulator, which was placed in a 2-foot long electric oven. The EMF generated by the thermocouple was then measured as a function of temperature with a precision potentiometer. The modulator remained at each of the equilibrium temperatures shown in the figure for one hour before its isolation characteristics were determined.

A photograph of an early model of the absorption modulator described above is shown in Fig. 10. The two sections of the split ferrite rod and their dielectric supports are clearly seen in the foreground. The thin attenuator element, having the same length and width as that of the ferrite rod, is lying on top of the ferrite section nearest the modulator housing. Both ends of the ferrite rod and polyfoam dielectric supports are tapered for impedance matching.

As seen in the photograph, the ferrite modulator has axial symmetry which is necessary for reciprocal microwave characteristics. The low-current solenoid supplying the longitudinal magnetic control field is wound around the $\frac{1}{2}\times 1$-inch rectangular-waveguide section and is potted in an Epon resin. The total length of the modulator is 4 inches.

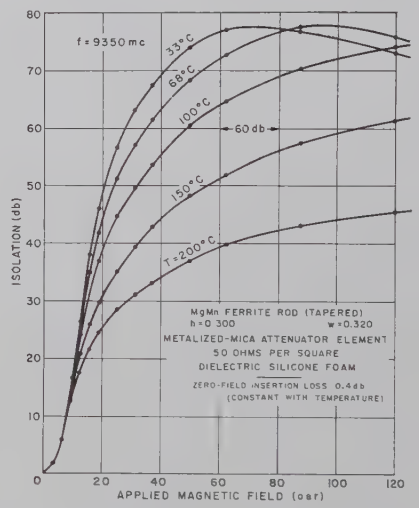

Fig. 9—Isolation characteristics of the absorption modulator vs ambient temperature from 33°C to 200°C.

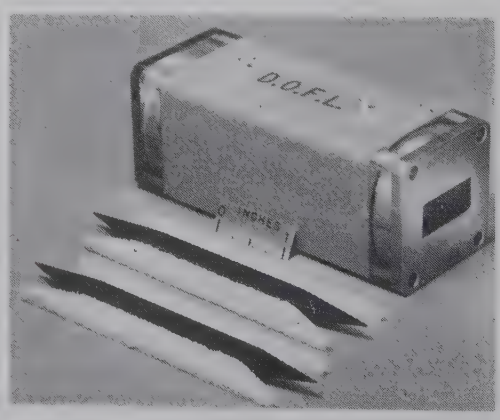

Fig. 10—Photograph of broad-band absorption modulator. Total length of modulator is 4 inches.

Conclusion

A new ferrite absorption modulator has been developed for high-speed switching of microwave power. This high-speed amplitude modulator makes use of a longitudinally magnetized ferrite rod (split along its length) centrally located inside a standard rectangular waveguide excited in its fundamental TE_{01} mode. A thin resistive film, placed between the sections of the split ferrite rod and perpendicular to the input RF electric field, is used to attenuate the perpendicular mode generated in the magnetized ferrite rod.

Several fiber-glass waveguide models of this absorption modulator, with a 0.0005-inch thick silver plating on the inside, have been designed for sine-wave modulation frequencies up to 100 kc. These units make use of a modulating solenoid (with ferrite-rod loading) which is self-resonant at the desired modulating frequency. Because of the small electrical inertia associated with its low-field solenoid, these ferrite modulators can be designed for switching microwave energy in less than 1 μsec with noncritical magnetic control fields.

Other important applications of the absorption modulator described above include an electrically controlled variable attenuator for automatically stabilizing the amplitude of FM oscillators, pulse shaping of the microwave energy and high-speed TR switching in microwave radar systems.

Rectangular Waveguide Theoretical CW Average Power Rating*

H. E. KING†, SENIOR MEMBER, IRE

Summary—**A theoretical CW average power rating, limitation imposed by a temperature rise resulting from power dissipation within the rectangular waveguide walls, can be determined by predicting the rise in temperature. Formulas for the evaluation of the CW average power rating have been developed and are presented here, and the power rating curves are given for the WR-2300 waveguide (320 Mc) through the WR-19 waveguide (60 kMc).**

Localized hot spots, associated with a standing wave on a mismatched waveguide, require a derating factor. The axial flow of heat from these high current spots has been considered in calculating and plotting this derating factor.

I. Introduction

THE major power rating consideration in present waveguide designs, using the TE_{10} mode, has been the limitation imposed by voltage breakdown (peak power rating). However, with the advent of high average power microwave systems, the average power rating of waveguides should be considered for future designs. The average power rating is determined by imposing a specified temperature rise in the conducting wall of the waveguide. High average RF power can be obtained by systems using high power generators or an array of generators united through a power combiner.

This paper presents formulas and curves that can be used to determine the average power rating of rectangular waveguides.[1] The rating is defined by choosing an arbitrary limit for the temperature rise with the waveguide in an environment of still air. (The average power rating can be raised, if desired, by choosing a higher temperature limit and using forced cooling.)

High current points, associated with a voltage-standing wave, on a mismatched waveguide cause additional increases in temperature. Therefore, a derating factor as a function of the standing wave ratio (VSWR) has been plotted. This derating factor takes into account the axial flow of heat from the high current point.

II. Theory

A. Power Rating of a Waveguide

The approach to determining the average power rating is to find the attenuation per unit length. With the attenuation known, the dissipated power in the walls of the matched waveguide may be found where a given power is being transmitted through it. The dissipated

* Received by the PGMTT, December 13, 1961; revised manuscript received, May 4, 1961. A portion of the work reported in this article was performed under U. S. Air Force Contract AF 04(647)-619.

† Aerospace Corp., Los Angeles, Calif.; formerly with Space Technology Labs., Inc., Los Angeles.

[1] The average power rating of coaxial cable has been treated by W. W. Macalpine, "Heating of radio frequency cables," *Elec. Commun.*, vol. 25, pp. 84–89; March, 1948.

power is then related to the rate of heat transfer from the waveguide walls to obtain the power rating of the waveguide.

The formula for the attenuation[2] of an air-filled copper rectangular waveguide (TE_{10} mode) at a temperature of 20°C is

$$\alpha = \frac{12.68(10^{-5})\dfrac{\lambda}{\lambda_c}\left[\dfrac{a}{2b}+\left(\dfrac{\lambda}{\lambda_c}\right)^2\right]}{\lambda^{3/2}\sqrt{1-\left(\dfrac{\lambda}{\lambda_c}\right)^2}} \text{ db/ft}, \tag{1}$$

where

a = the wide inner dimension of the waveguide in meters,
b = the narrow inner dimension of the waveguide in meters,
λ = the wavelength in meters, and
$\lambda_c = 2a$.

The attenuation, in terms of the power levels in the waveguide, is

$$\alpha = 4.34\frac{P_l}{P_1} \text{ db/unit length}, \tag{2}$$

where

P_1 = power input, or the power rating of the waveguide, and
P_l = power loss in the unit length of waveguide.

P_l is equivalent to the rate of heat transfer, q (Btu/hr[3]) from a unit length of the waveguide, and is related by $P_l = 0.293\ q$. Thus, the average power rating of the waveguide is

$$P_1 = \frac{1.271q}{\alpha}. \tag{3}$$

Neglecting transfer of heat by conduction, the rate of heat transfer is the sum of heat transferred by thermal convection and by thermal radiation, or

$$q = q_c + q_r \text{ Btu/hr}. \tag{4}$$

In the Appendix, Section B, the convection term is found to be

$$q_c = (\Delta T)^{5/4}\left[\frac{0.708A_b}{b'^{1/4}}+\frac{0.717A_a}{a'^{1/4}}\right] \text{Btu/hr/ft} \tag{5}$$

and the radiation term is found to be

$$q_r = 5.19(10^{-10})A_t(T_w^4 - T_a^4) \text{ Btu/hr/ft} \tag{6}$$

[2] G. L. Ragan, "Microwave Transmission Circuits," M.I.T. Rad. Lab. Ser., McGraw-Hill Book Co., Inc., New York, N. Y., vol. 9, p. 55; 1948.
[3] 1 Btu/hr = 0.293 watt.

where

ΔT = temperature differential = $T_w - T_a$ in °F,
T_w = wall temperature of the waveguide in °R,
T_a = ambient temperature of the waveguide in °R,
a' = outer wide dimension of the waveguide in ft,
b' = outer narrow dimension of the waveguide in ft, and
$A_t = 2(A_a + A_b)$ = total outer surface area of 1 ft of waveguide in sq ft.

Eqs. (5) and (6) use the empirical heat transfer coefficients, and are theoretically valid for a rectangular waveguide. Also, the wave guide b dimension is in the horizontal position as illustrated in Fig. 1; the waveguide is in still air at sea level; and the thermal radiation factor or emissivity of the guide wall is equal to 0.3 (a black surface has an emissivity = 1). An additional assumption is that the dissipation of power per unit area in the waveguide walls is uniform for all walls.[4]

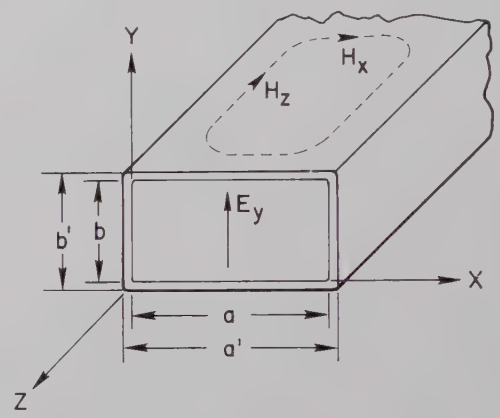

Fig. 1—Position of waveguide for determining heat transfer relations.

Eq. (4) gives the heat transfer by convection and by radiation, computed separately. In many practical cases, the treatment of convection and radiation as a single combined process is desirable. Using only a first-power equation, the heat transmission is

$$q = h_{rc}A_t(T_w - T_a) \text{ Btu/hr}, \tag{7}$$

where h_{rc} = the combined radiation and convection conductance, and can be found theoretically by equating (4) and (7), or h_{rc} can be found empirically.

B. Derating Factor for a VSWR on Waveguide

The power rating as determined from (4) is based on a matched waveguide. However, in many cases a VSWR exists on the waveguide. In the Appendix, the equation for temperature rise resulting from a reflecting termination is developed as a function of distance along the waveguide. Because high-current points exist on a mismatched waveguide, the heat at the hot spots will be conducted axially by virtue of the temperature dif-

[4] See Appendix, Section A.

ference. If the power rating of the waveguide is defined by a maximum permissible temperature rise, the temperature at the high-current points will be the limiting factor.

Two cases should be considered when discussing the derating factor for a VSWR on the waveguide. Case 1 represents the derating factor for a condition where the same amount of power is delivered to either the mismatched or to the matched loads. Case 2 is the derating factor for a condition where the incident wave is equal regardless of the load impedance. Case 1 is useful when a transmitter is delivering equal power to either a matched antenna or a mismatched antenna, and Case 2 is used in a balanced duplexer circuit or a power equalizer circuit[5] where the reflected wave does not disturb the loading of the transmitter. For example, in a duplexer circuit the net power delivered to the mismatched load (TR tube) approaches zero when the duplexer is in the transmit condition.

Case 1—Equal Power Delivered to Either Matched or Mismatched Loads: The general equation in terms of VSWR (see Appendix) for the waveguide temperature rise at the high-current point on the waveguide is

$$\Delta T_{\rho 1} = q\left[\frac{1}{h_{rc}A_t}\,\frac{\rho^2+1}{2\rho} + \frac{1}{kA_c\left(\frac{4\pi}{\lambda}\right)+h_{rc}A_t}\,\frac{\rho^2-1}{2\rho}\right], \quad (8)$$

where

q = heat transmission with a matched line,
h_{rc} = the combined radiation and convection conductance in Btu/(hr)(sq ft) °F,
A_t = total outer surface area of one foot length of waveguide, in square feet
A_c = cross-sectional area of waveguide in square feet,
k = heat conductivity of waveguide wall in

(Btu)(ft)/(hr)(sq ft) °F,

ρ = VSWR, and
λ = wavelength in feet.

The term $kA_c(4\pi/\lambda)$ represents the heat transfer by conduction in the axial direction. Should the wall of the waveguide be composed of several laminated materials, such as copper-clad steel or metallic plating on fibreglas, the composite heat conductivity can be treated in the same manner as electrical conductivity; that is,

$$kA_c = k_1A_{c1} + k_2A_{c2} + \cdots,$$

where the subscript numbers refer to the different materials of the waveguide wall.

[5] R. W. Masters, "A power-equalizing network for antennas," Proc. IRE, vol. 37, pp. 735–738; July, 1949.

If $k=0$, then (8) reduces to

$$\Delta T_{\rho 1} = \frac{q\rho}{h_{rc}A_c}. \quad (9)$$

Eq. (9) indicates that, if no axial heat flow is involved and the same amount of power is delivered for both the mismatched load and the matched load cases, the temperature rise would be proportional to the VSWR. In most of the practical applications, the wall of the guide is copper, aluminum, or brass. Thus,

$$kA_c\left(\frac{4\pi}{\lambda}\right) \gg h_{rc}A_t,$$

and (8) reduces to

$$\Delta T_{\rho 1} \approx q\left[\frac{1}{h_{rc}A_t}\,\frac{\rho^2+1}{2\rho} + \frac{1}{kA_c\left(\frac{4\pi}{\lambda}\right)}\,\frac{\rho^2-1}{2\rho}\right]. \quad (10)$$

Eq. (10) represents the temperature rise (Case 1) at the high-current point of a waveguide with any VSWR on the line, if the waveguide wall is constructed of a relatively high thermal conductive material.

Case 2—Equal Incident Wave for Either Matched or Mismatched Loads: The general equation in terms of VSWR (see Appendix) for the waveguide temperature rise at the high-current point on the waveguide is

$$\Delta T_{\rho 2} = q\left[\frac{2}{h_{rc}A_c}\,\frac{(\rho^2+1)}{(\rho+1)^2} + \frac{2}{kA_c\left(\frac{4\pi}{\lambda}\right)+h_{rc}A_c}\left(\frac{\rho-1}{\rho+1}\right)\right], \quad (11)$$

where again q equals heat transmission with a matched line and the other symbols are defined under (8). The axial heat conductivity term kA_c has the same significance in Case 2 as in Case 1. If $k=0$, then (11) reduces to

$$\Delta T_{\rho 2} = \frac{q}{h_{rc}A_c}\,\frac{4\rho^2}{(\rho+1)^2}. \quad (12)$$

Eq. (12) indicates, that for a very high VSWR, the derating factor is asymptotic to 4. This value of 4 is reasonable, considering that, for a given incident voltage on a matched waveguide, the maximum voltage on the waveguide for a reflection coefficient of unity will be doubled. However, in Case 2 (unlike Case 1) the power delivered to the mismatched load is less than the power delivered to the matched load. As the VSWR increases, the power delivered to the load approaches zero.

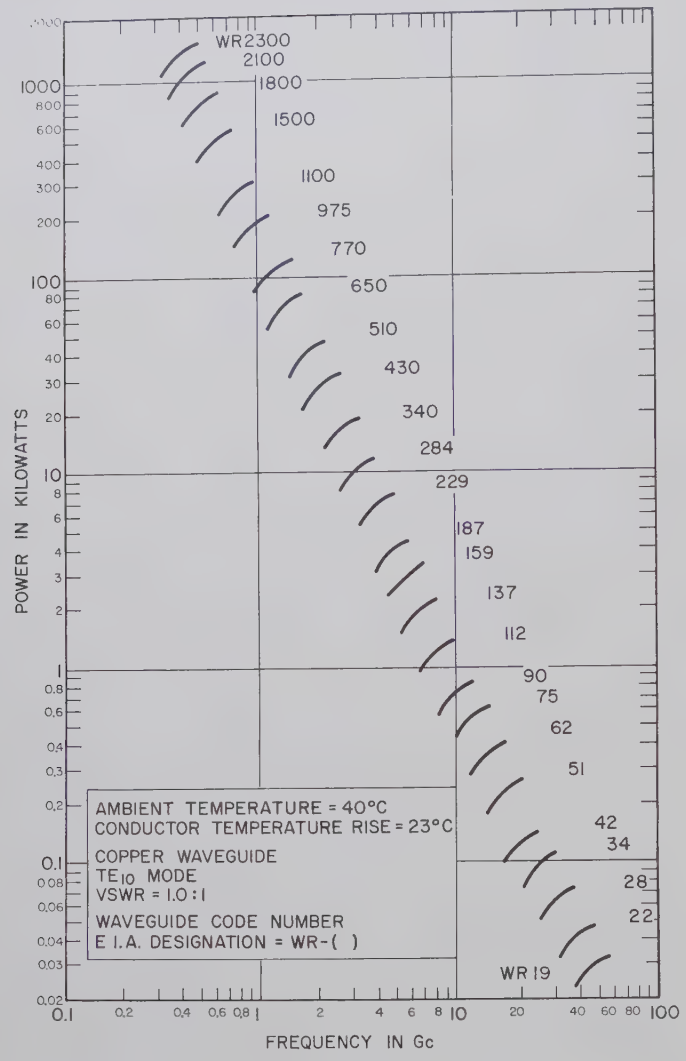

Fig. 2—Theoretical curves of the average power rating for copper rectangular waveguide (conductor temperature rise of 23°C).

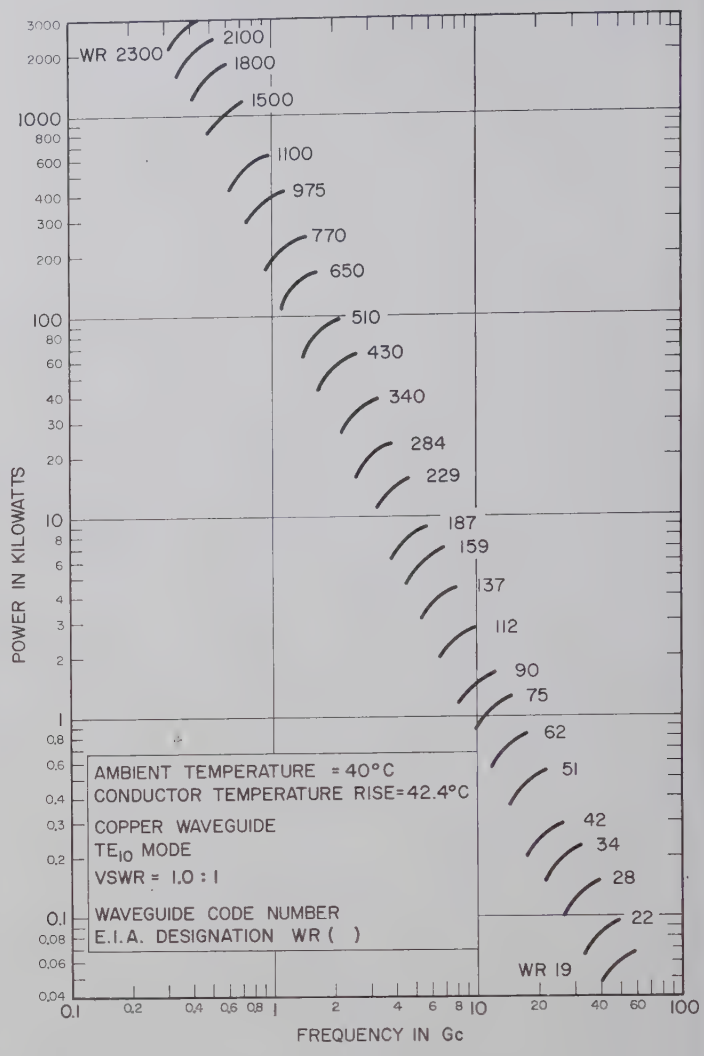

Fig. 3—Theoretical curves of the average power rating for copper rectangular waveguide (conductor temperature rise of 42.4°C).

Considering most of the practical cases where the wall of the guide is copper, aluminum, or brass, (11) reduces to

$$\Delta T_{\rho 2} \approx 2q\left[\frac{1}{h_{rc}A_c}\,\frac{(\rho^2+1)}{(\rho+1)^2}+\frac{1}{kA_c\left(\frac{4\pi}{\lambda}\right)}\left(\frac{\rho-1}{\rho+1}\right)\right]. \quad (13)$$

The derating factor (DF), because of the VSWR on the waveguide, is then

$$\mathrm{DF}=\frac{\Delta T}{\Delta T_{\rho 1}} \quad \text{or} \quad \frac{\Delta T}{\Delta T_{\rho 2}}, \quad (14)$$

where ΔT = temperature rise of the matched waveguide.

III. Description of Curves

A. Power Rating of Standard Rectangular Waveguides

Upon calculating the attenuation with (1), the heat transfer by convection and radiation is calculated for various temperature rises using (4). Then α and q are substituted into (3), giving the power ratings of the waveguide. Figs. 2–5 are curves for chosen temperature rises of 23°C, 42.4°C, 62°C, and 110°C, respectively, and represent the theoretical average power ratings of standard rectangular copper waveguide in an ambient temperature of 40°C. Eq. (1), the attenuation, has to be modified for the elevated waveguide wall temperatures of 63°C, 82.4°C, 102°C, and 150°C to determine the final power rating.

The theoretical peak power rating of standard waveguides (limitation due to voltage breakdown) with a dry air and unpressured environment is also plotted in Fig. 5. A comparison of the two curves in this figure will show that the CW power handling limitation is a function of the temperature rise, rather than the limitation imposed by voltage breakdown.

Figs. 2–5 can be modified for other ambient temperatures by referring to the ambient correction factor curves of Fig. 6. The correction factor is approximately the same for small or large size waveguides.

Experimental confirmation of the theoretical average power rating has been reported by Gould.[6] In recent

[6] L. Gould, Microwave Associates, Inc., private communication; September 19, 1960.

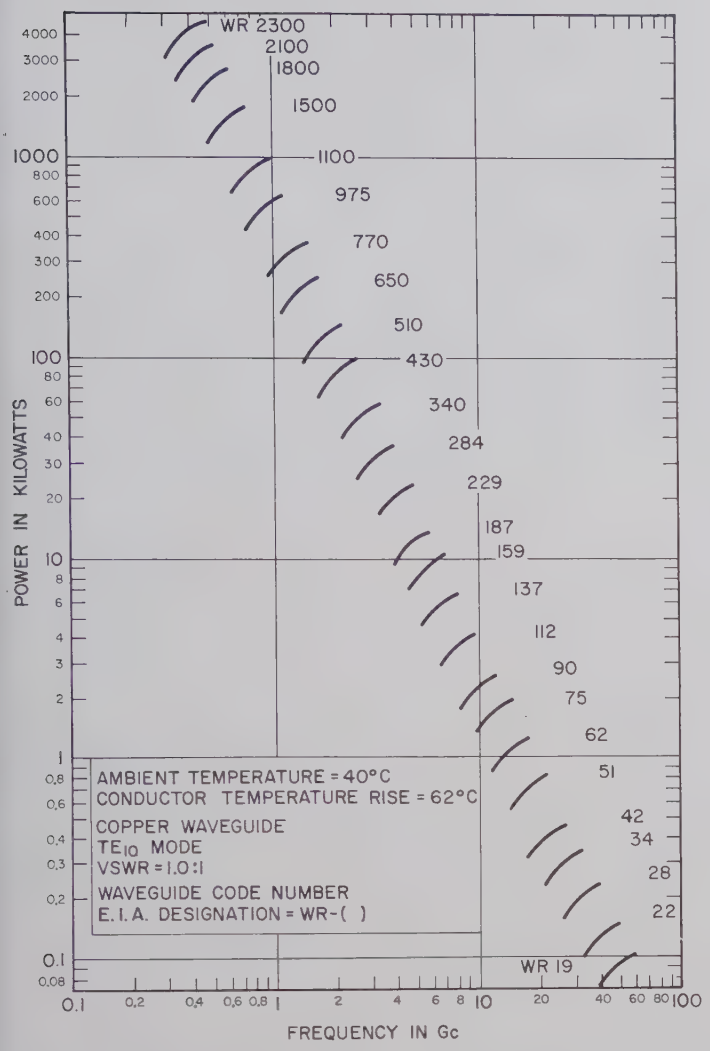

Fig. 4—Theoretical curves of the average power rating for copper rectangular waveguide (conductor temperature rise of 62°C).

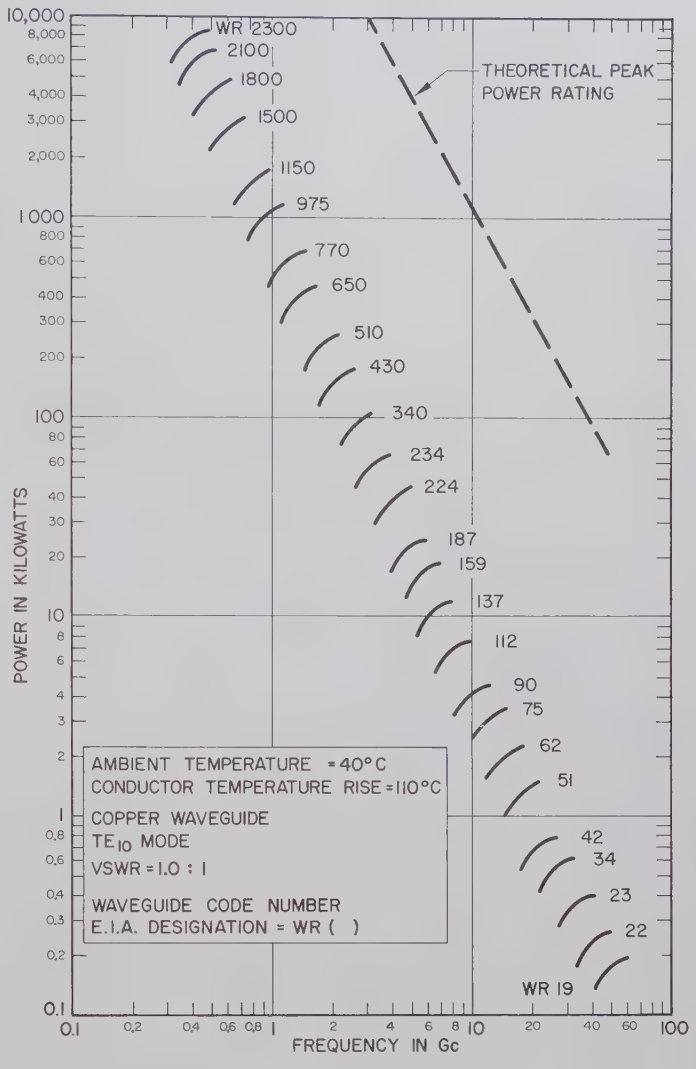

Fig. 5—Theoretical curves of the average power rating for copper rectangular waveguide (conductor temperature rise of 110°C).

Fig. 6—Correction factor curve for average power rating of rectangular waveguide for various ambient temperatures and conductor wall temperatures.

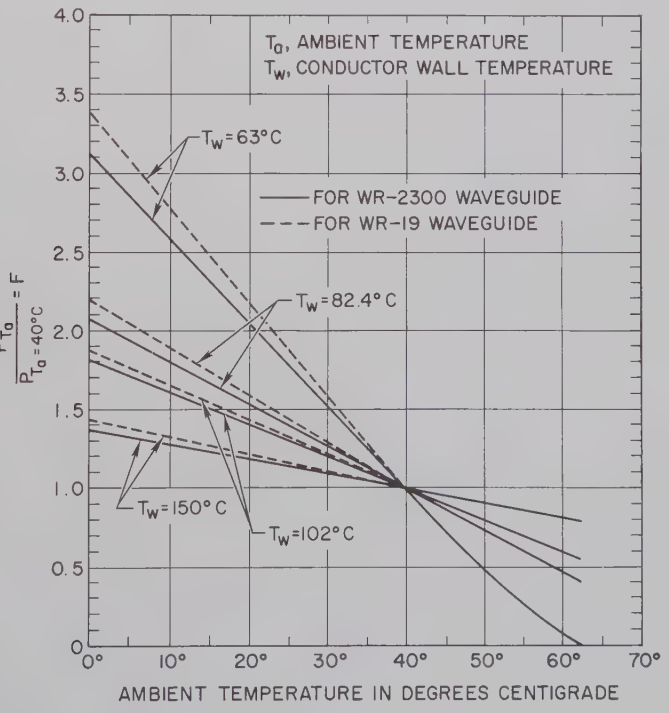

high-power tests at 30 kw average power at 3000 Mc, Gould reports that the test yielded a waveguide conductor temperature rise of 60°C above room temperature, as compared to a theoretical value of 62.4°C. The comparison can be made by studying Fig. 3—the power rating curve for an ambient temperature of 40°C and a temperature rise of 42.4°C—and the ambient temperature correction curve of Fig. 6.

B. Combined Radiation and Convection Conductance

Often, it is desirable and convenient to use the combined radiation and convection conduction term. The h_{rc} is determined by using (7) with q equal to the heat calculated from (4). Fig. 7 is a plot of h_{rc} for various temperature differentials and waveguide sizes.

C. Derating Factor Caused by VSWR

Case 1—Equal Power Delivered to Load Regardless of Load Impedance: Fig. 8 plots the derating factor for a copper waveguide as a function of VSWR. The thermal conductivity term, k, for copper is 220 [Btu (ft)/(hr) (sq ft) °F]. Fig. 8 also shows the curve of the derating factor for $k=0$, the condition when the derating factor is proportional to the VSWR.

Case 2—Equal Incident Wave Regardless of Load Impedance: Fig. 9 is a plot of a copper waveguide derating factor as a function of the VSWR, when the incident wave remains the same amount for all values of VSWR. Fig. 9 also shows the derating factor curve for $k=0$, where $\Delta T_{\rho 2}$ is calculated from (12).

For all practical purposes, in Cases 1 and 2, brass and aluminum waveguides yield the same results as the copper waveguide. Eqs. (8) and (13) should be used whenever the wall of the waveguide is made of a low conductivity material.

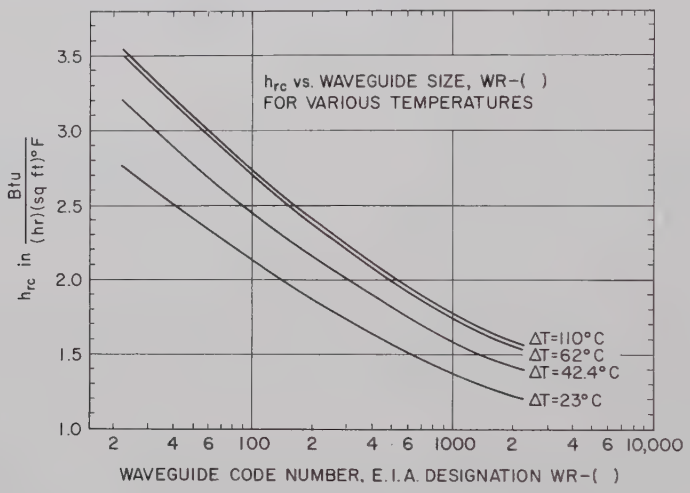

Fig. 7—Combined thermal radiation and convection conductance term as a function of waveguide size and temperature.

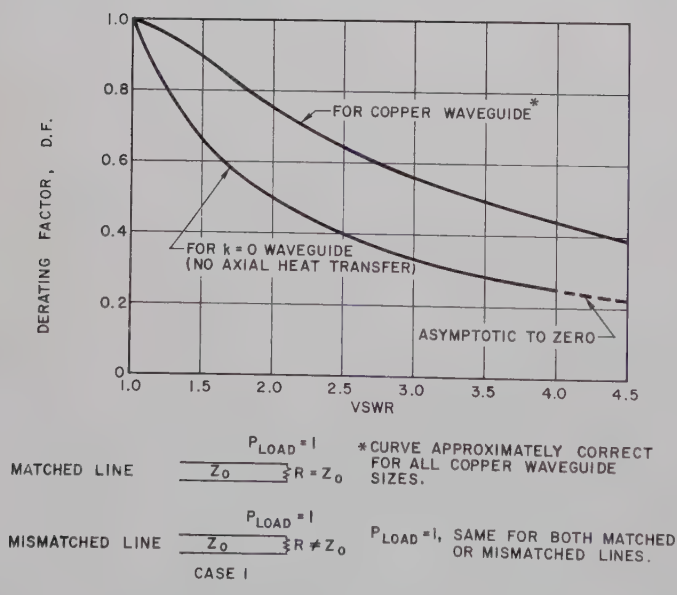

Fig. 8—Power derating factor caused by a standing wave on waveguide for Case 1.

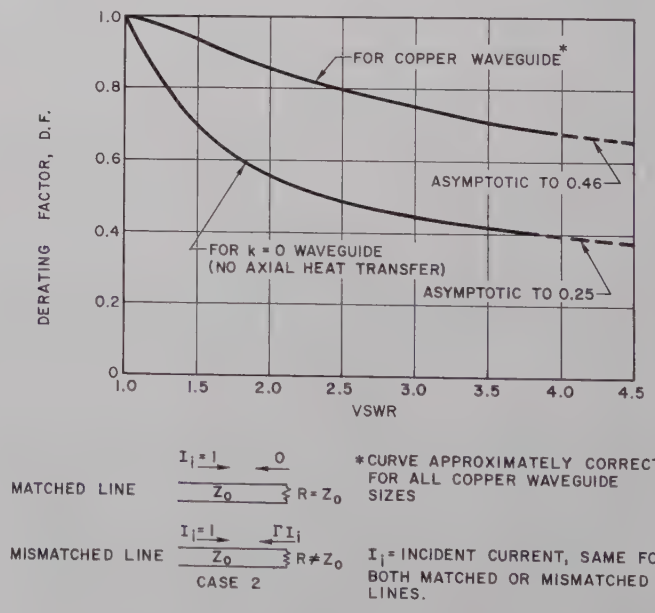

Fig. 9—Power derating factor caused by a standing wave on waveguide for Case 2.

IV. Conclusions

The CW average power rating of a rectangular waveguide is dictated by the permissible temperature rise above ambient of the waveguide wall. The theoretical power rating has been determined by calculating the convection, radiation, and conduction rate of heat transfer for both a mismatched load and a matched load on the waveguide. When a given power is delivered to a waveguide with a specified VSWR, the waveguide wall temperature rise along the axial direction can be predicted.

With the data presented in this paper, waveguide guide designers can determine, in advance, whether forced cooling will be necessary and can establish CW average power ratings for future designs.

Appendix

A. Losses in Waveguide

It is interesting to compare the relative power loss in the side walls with the loss in the top and bottom walls.

The average power absorbed by the walls of a waveguide may be found by integrating over a unit area the component of the Poynting vector that is directed into the waveguide walls. The current flow in the guide walls of low-loss waveguides may be determined in the same manner as in the ideal waveguide; *i.e.*, the current is equal, by the $\bar{n}\times\bar{H}$ rule, to the tangential magnetic fields at the boundary.

The power lost per unit length for the side walls of an air-filled waveguide[7] is

$$W_b = \frac{1}{2} R_s \int_0^b |H_z|^2 dy = \frac{R_s E^2}{2} \frac{\pi^2 b}{\eta^2 \beta^2 a^2}, \qquad (15)$$

and for the top and bottom walls is

$$W_a = \frac{1}{2} R_s \int_0^a (|H_x|^2 + |H_z|^2) dx = \frac{R_s E^2}{2} \frac{a}{2\eta^2}, \qquad (16)$$

where

R_s = surface resistivity of the conducting walls,

$$|H_z| = \frac{\pi E}{\eta \beta a} \cos \frac{\pi x}{a},$$

$$|H_x| = \frac{\sqrt{1 - \left(\frac{\lambda}{2a}\right)^2}}{\eta} E \sin \frac{\pi x}{a},$$

$$\beta = \frac{2\pi}{\lambda}, \text{ and}$$

$$\eta = \sqrt{\frac{\mu_0}{\epsilon_0}}.$$

[7] For waveguide field expressions, see, for example, S. Ramo and J. R. Whinnery, "Fields and Waves in Modern Radio," John Wiley and Sons, Inc., New York, N. Y., p. 370; 1953.

The total power loss per unit length of waveguide is

$$P_l = W_a + W_b = \frac{R_s E^2}{2\eta^2}\left[1 + \frac{2b}{a}\left(\frac{\lambda^2}{2a}\right)\right]. \qquad (17)$$

The first term in the bracket is associated with losses on the top and bottom walls, and the last term is associated with losses in the side walls.

For conventional rectangular waveguide ($b/a \approx 1/2$), the ratio of power loss in the side walls to the loss in the top and bottom walls at approximately the mid-band frequency of the TE_{10} mode is

$$\frac{W_b}{W_a} \approx \frac{1}{2}.$$

Thus, the power dissipated in the waveguide per unit area is approximately the same in the top and bottom walls as in the side walls.

B. Heat Transfer Convection and Radiation Term[8]

The position of the rectangular waveguide for determining the heat transfer is shown in Fig. 1. The rates of heat transfer for both the convection and radiation terms from the four walls of the waveguide are treated separately, and the resulting temperature rises are added together. The convection and radiation flowrate expressions may be approximated by a linear temperature difference so the superposition theorem can be applied.

The thermal convection rate equation,

$$\frac{q}{A} = h_c(T_w - T_a) \frac{\text{Btu}}{\text{hr (sq ft)}}, \qquad (18)$$

states that the thermal convection per unit transfer area q/A is proportional to the temperature difference $(T_w - T_a)$, the temperature of the waveguide wall less that of the external ambient temperature. The proportionality factor is known as the unit thermal convective conductance in

$$\frac{\text{Btu}}{\text{hr (sq ft) °F}}.$$

The thermal convection of the four walls of the waveguide is added to yield the total waveguide convection heat transfer, or

$$q_c = [2\,{}_N h_c A_b + {}_T h_c A_a + {}_B h_c A_a](T_w - T_a), \qquad (19)$$

where

A_a = the top or bottom area of 1-ft length of waveguide (outer dimensions) in sq ft, and

A_b = the side or narrow area of 1-ft length of waveguide (outer dimensions) in sq ft.

[8] "Heating Ventilating Air Conditioning Guide," Am. Soc. Heating, Refrigerating and Air-Conditioning Engrs.; 1960.

The unit convective conductance for the four walls of the waveguide can be found in the literature.[9] For the side walls, or the narrow dimension of the guide.

$$_{N}h_c = 0.354\left(\frac{T_w - T_a}{b'}\right)^{1/4};$$

for the top wall,

$$_{T}h_c = 0.478\left(\frac{T_w - T_a}{a'}\right)^{1/4};$$

and for the bottom wall,

$$_{B}h_c = 0.239\left(\frac{T_w - T_a}{a'}\right)^{1/4}.$$

The dimensions a' and b' are, respectively, the wide and narrow dimensions in feet of the waveguide outer walls. With the conductances substituted into (19), the rate of convection heat transfer for a rectangular waveguide is expressed by (5).

C. Derating Factor Caused by VSWR

With a reflecting termination on the waveguide, the standing wave pattern (Fig. 10) is the sum of the incident and reflected waves. The resultant current, neglecting losses, is

$$|I|^2 = |I_i|^2(1 + |\Gamma|^2 - 2|\Gamma| \cos(\psi - 2\beta z)), \quad (20)$$

where

$|I_i|$ = incident current,
Γ = reflection coefficient = $|\Gamma| < \psi$, and
z = distance along the waveguide.

The power loss P_l in a unit length of waveguide is proportional to I^2R; thus $P_l = q$ Btu/hr/unit length of waveguide. Therefore the standing wave pattern can be expressed in terms of the heat transfer, or

$$\begin{aligned} q &= q_i(1 + |\Gamma|^2 - 2|\Gamma| \cos(\psi - 2\beta z)) \\ &= q' - q'' \cos(\psi - 2\beta z), \end{aligned} \quad (21)$$

where q_i is defined as the "incident" heat, Btu/hr/unit length,

$$q' = q_i(1 + |\Gamma|^2) \text{ and}$$
$$q'' = 2q_i|\Gamma|.$$

The factor q' is independent of z, and no heat flows in the axial direction. The temperature rise above ambient temperature caused by q' is

$$\theta' = \frac{q'}{h_{rc}A_t}, \quad (22)$$

where h_{rc} = combined radiation and convection thermal conductance.

Ibid., ch. 5, Table 2.

The part of (21) which is a function of z represents sinusoidal heating and cooling of the waveguide, relative to the heating, caused by q'. The temperature rises above ambient, represented by each portion of (21), θ' caused by q' and θ'' caused by $q''\cos(\psi - 2\beta z)$, can be added, since the superposition theorem is assumed to be valid. That is, the temperature rise

$$\Delta T_p = \theta' + \theta''. \quad (23)$$

To find θ'', the following analysis is presented. Fig. 11 illustrates the summation of heat in a section Δz of the waveguide. The heat generated in the elemental section Δz of the guide, plus the heat flowing along the guide into the section, plus the heat from the surrounding air, is equal to zero[10] or

$$kA_c\frac{d^2\theta''}{dz^2} - h_{rc}A_t\theta'' - 2q_i|\Gamma| \cos\xi = 0, \quad (24)$$

where

$\theta'' = \theta''(z) = T_w(z) - T_a$ = temperature rise above ambient temperature,
k = thermal conductivity of waveguide wall,
A_c = cross-sectional area of waveguide,
A_t = total outer surface area of a unit length of waveguide, and
$\xi = \psi - 2\beta z$.

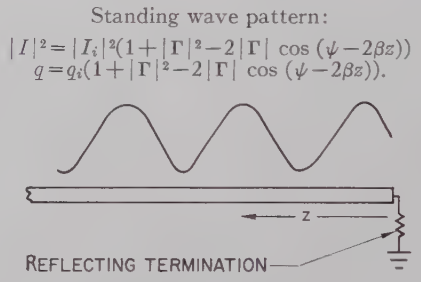

I = Current distribution
q = Heat distribution

Fig. 10—Standing-wave pattern on a mismatched transmission line.

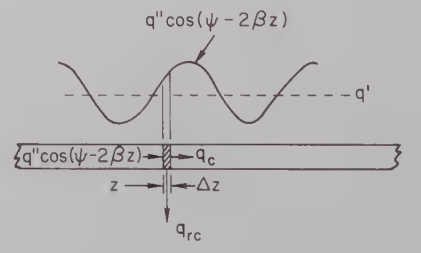

q_{rc} = combined radiation and convection heat transfer.
q_c = heat transfer by conduction.
$q''\cos(\psi - 2\beta z)$ = input heat.

Fig. 11—Sinusoidal heat transfer relations of a mismatched transmission line.

[10] Refer to M. Jakob and G. A. Hawkins, "Elements of Heat Transfer," John Wiley and Sons, Inc., New York, N. Y., p. 157; 1957.

f the variable[11] of (24) is changed into

$$\frac{d^2\theta''}{dz^2} = \left(\frac{d\xi}{dz}\right)^2 \frac{d^2\theta''}{d\xi^2} = \left(\frac{4\pi}{\lambda}\right)^2 \frac{d^2\theta''}{d\xi^2}, \tag{25}$$

he temperature distribution θ'' along the waveguide can be determined by

$$kA_c\left(\frac{4\pi}{\lambda}\right)^2 \frac{d^2\theta''}{d\xi^2} - h_{rc}A_t\theta'' - 2q_i|\Gamma| \cos\xi = 0. \tag{26}$$

Eq. (26) is a nonhomogenous linear equation with the complementary function, or the transient term, equal to zero. The complementary function is zero, since the waveguide is assumed to be immersed in a uniform medium and is infinitely long.

A particular solution of (26) may be found[12] by assuming a particular integral and verifying by substitution. Thus,

$$\theta'' = \frac{-2q_i|\Gamma| \cos(\psi - 2\beta z)}{kA_c\left(\frac{4\pi}{\lambda}\right)^2 + h_{rc}A_t}. \tag{27}$$

Case 1—Equal Power Delivered to Either Matched or Mismatched Loads: A matched or a mismatched waveguide, having the same power W delivered to the load, has the following relations as derived from the transmission line equations:[1]

$$W = I^2_{\text{match}}Z_0 = I_{\max}I_{\min}Z_0 \tag{28}$$

$$\frac{I_{\max}}{I_{\min}} = \frac{I\sqrt{\rho}}{\frac{I}{\sqrt{\rho}}} = \rho = \text{VSWR}, \tag{29}$$

$$I_i = \frac{I}{2}\left[\sqrt{\rho} + \frac{1}{\sqrt{\rho}}\right]. \tag{30}$$

The "incident heat" q_i is proportional to $|I_i|^2$. If q_i is substituted into (22) and (27) with the reflection coefficient expressed in terms of VSWR, (8) expresses the waveguide maximum temperature rise corresponding to the high-current point on the mismatched waveguide with equal power dissipated in the load.

Case 2—Equal Incident Wave for Either Matched or Mismatched Loads: A mismatched waveguide having the same incident current as a matched load on the waveguide, or $I_{\text{match}} = I_i$ for various ρ, will have a derating factor for temperature rise different from Case 1. If (22) and (27) are expressed as a function of VSWR instead of the reflection coefficient, (11) expresses the waveguide temperature rise at the high temperature point resulting from a mismatched termination; however, (11) is valid, in this instance, only when the incident signal I_i for various $\rho = I_{\text{match}}$.

ACKNOWLEDGMENT

The author would like to thank L. Nelson for computing the average power rating of the rectangular waveguides.

[11] W. W. Macalpine, *op. cit.*, (25A).
[12] For example, M. Morris and O. E. Brown, "Differential Equations," Prentice-Hall, Inc., New York, N. Y., p. 91; 1942.

Correspondence

Wave Propagation in Coaxial-Cylindrical Slow-Wave Systems*

Introduction

Recent interest in E-type traveling-wave tubes,[1] in which a ribbon-shaped electron beam is caused to follow a circular path by balancing the centrifugal force of the particle against a steady radial electric field force, has led to an investigation of wave propagation in azimuthally reentrant and nonreentrant coaxial-cylindrical slow-wave structures. The study is facilitated by the simplifying approximation that the actual azimuthally-periodic slow-wave circuit, situated along the inner conductor, can be replaced by a smooth dielectric cylinder. While such a dielectric cylinder would probably not be employed in the construction of an actual tube, because of its small value of surface impedance, it serves as a convenient model in determining the general forms of functional dependence for the field equations.

The Field Equations

Although the first exhaustive study of wave propagation in azimuthally reentrant coaxial-cylindrical transmission systems appears to have been given by Kalahne,[2] in 1905, the problem has since been widely treated.[3–5] In addition, Buchholz[6] has studied the related problem of wave propagation around a circular bend in a rectangular waveguide, and Waldron[7] has investigated the characteristics of wave propagation in helical waveguides of square cross section.

When the analysis is extended to the case involving periodic structures situated along the center conductor to produce azimuthally slow waves, the boundary conditions are altered to include the periodic variation of the inner conductor radius with the spatial angle θ. This change of shape leads to an infinite number of azimuthal space harmonic components, each one of which is characterized by a particular circular propagation constant. The amplitudes and phases of these harmonic components are determined by satisfying the conditions imposed on the fields by the periodic boundaries of the circuit.

Though the procedure can, in principle, be applied to any azimuthally-periodic boundary, the method becomes involved for any but the simplest structures. Moreover, each time the geometry is changed the evaluation must be repeated, so that practical considerations tend to restrict the analysis to a small number of potentially important configurations. Despite these difficulties, certain general properties of azimuthally periodic slow-wave structures can be inferred from a study of typical situations. Thus, when the circuit is reentrant, or when the spatial period of the structure is such that the fields would be undisturbed by making it reentrant, the azimuthal space harmonics form a countably infinite set of integral values. When the nature of the structure is such that the fields would be disturbed by making it reentrant, the space harmonics form a countably infinite set of rational fractional, or general nonintegral, order values. Either of these situations involves a discrete summation over the associated circular propagation constants in order to obtain the field expressions. It follows that the general expressions for the electric and magnetic field intensities have the form

$$E_z = \mathrm{Re} \sum_{n,\beta_0} A_{n\beta_0} V_{\beta_0}(k_n r) \cos\left(\frac{n\pi}{L} z\right) e^{j(\omega t - \beta_0 \theta)}, \tag{1}$$

$$H_z = \mathrm{Re} \sum_{n,\beta_0} jB_{n\beta_0} V_{\beta_0}(k_n r) \sin\left(\frac{n\pi}{L} z\right) e^{j(\omega t - \beta_0 \theta)}, \tag{2}$$

$$E_r = \mathrm{Re} \sum_{n,\beta_0} \left\{ A_{n\beta_0} \left(\frac{-n\pi}{k_n L}\right) V_{\beta_0}'(k_n r) + B_{n\beta_0} \left(\frac{-j\omega\mu_0\beta_0}{k_n^2 r}\right) V_{\beta_0}(k_n r) \right\} \sin\left(\frac{n\pi}{L} z\right) e^{j(\omega t - \beta_0 \theta)}, \tag{3}$$

$$E_\theta = \mathrm{Re} \sum_{n,\beta_0} \left\{ A_{n\beta_0} \left(\frac{jn\pi\beta_0}{k_n^2 r L}\right) V_{\beta_0}(k_n r) + B_{n\beta_0} \left(\frac{-\omega\mu_0}{k_n}\right) V_{\beta_0}'(k_n r) \right\} \sin\left(\frac{n\pi}{L} z\right) e^{j(\omega t - \beta_0 \theta)}, \tag{4}$$

$$H_r = \mathrm{Re} \sum_{n,\beta_0} \left\{ A_{n\beta_0} \left(\frac{\omega\epsilon_0\beta_0}{k_n^2 r}\right) V_{\beta_0}(k_n r) + B_{n\beta_0} \left(\frac{jn\pi}{k_n L}\right) V_{\beta_0}'(k_n r) \right\} \cos\left(\frac{n\pi}{L} z\right) e^{j(\omega t - \beta_0 \theta)}, \tag{5}$$

$$H_\theta = \sum_{n,\beta_0} \left\{ A_{n\beta_0} \left(\frac{-j\omega\epsilon_0}{k_n}\right) V_{\beta_0}'(k_n r) + B_{n\beta_0} \left(\frac{n\pi\beta_0}{k_n^2 r L}\right) V_{\beta_0}(k_n r) \right\} \cos\left(\frac{n\pi}{L} z\right) e^{j(\omega t - \beta_0 \theta)}, \tag{6}$$

where

μ_0 = free-space permeability in henries per meter,
ϵ_0 = free-space permittivity in farads per meter,
β_0 = circular propagation constant in electrical radians per spatial radian,
ω = electrical angular velocity of the RF wave in electrical radians per second,
L = height of the waveguide parallel to the cylindrical axis in meters,
r = radial coordinate variable in meters,
θ = azimuthal coordinate variable in radians,
z = axial coordinate variable in meters,
t = time in seconds,
$k_n = \sqrt{(n\pi/L)^2 - \omega^2\mu_0\epsilon_0}$ electrical radians per meter,
$A_{n\beta_0}$ = a quantity depending on β_0 and n, which is a measure of the space harmonic amplitude of the associated E-mode wave,
$B_{n\beta_0}$ = a quantity depending on β_0 and n, which is a measure of the space harmonic amplitude of the associated H-mode wave,
$V_{\beta_0}(k_n r) = I_{\beta_0}(k_n r) K_{\beta_0}(k_n r_s) - K_{\beta_0}(k_n r) I_{\beta_0}(k_n r_s)$,
$Y_{\beta_0}(k_n r) = I_{\beta_0}(k_n r) K_{\beta_0}'(k_n r_s) - K_{\beta_0}(k_n r) I_{\beta_0}'(k_n r_s)$,
$I_{\beta_0}(k_n r)$, $K_{\beta_0}(k_n r)$ = hyperbolic Bessel functions of the first and second kinds, respectively, of order β_0 and argument $k_n r$,
r_s = radius of the inside surface of the outer conductor (in an electron beam device this corresponds to the sole radius) in meters.

The primes appearing in the foregoing expression indicate differentiation of the associated functions with respect to $k_n r$. The terminology of Morse and Feshback[8] is used in referring to the Bessel functions as "hyperbolic" rather than "modified," since these expressions are related to the corresponding Bessel functions of real argument in a manner similar to that of the more elementary trigonometric and hyperbolic functions.

The transition from the Bessel functions of real argument, which accompany higher-mode *propagating* waves in coaxial-cylindrical transmission systems, to the hyperbolic Bessel functions employed here results from the premise that the fringing circuit fields, which permeate the interaction space, could not exist in the absence of the slow-wave circuit. The introduction of a lossless dielectric cylinder surrounding the center con-

* Received by the PGMTT, October 17, 1960; revised manuscript received, February 24, 1961. Supported by the Diamond Ordnance Fuze Labs., under Contract No. DA-49-186-502-ORD-720.

[1] W. M. Nunn, Jr., "A Small-Signal Analysis of E-Type Traveling-Wave Devices," Electron Phys. Lab., Elec. Engrg. Dept., The University of Michigan, Ann Arbor, Tech. Rept. No. 38; August, 1960.

[2] A. Kalähne, "Electrical oscillations in ring-shaped metal tubes," *Annalen der Physik*, vol. 18, pp. 92–127, 1905; vol. 19, pp. 80–115; 1906.

[3] S. Ramo and J. R. Whinnery, "Fields and Waves in Modern Radio," John Wiley and Sons, Inc., New York, N. Y., 2nd ed.; 1953.

[4] J. A. Stratton, "Electromagnetic Theory," McGraw-Hill Book Co., Inc., New York, N. Y.; 1941.

[5] N. Marcuvitz, "Waveguide Handbook," MIT Rad. Lab. Ser., McGraw-Hill Book Co., Inc., New York, N. Y., vol. 10; 1951.

[6] H. Buchholz, "Effect of curvature of rectangular hollow conductors on the phase constant of ultra-short waves." *Elektrische Nachrichtentech.*, vol. 16, pp. 73–85; March, 1939.

[7] R. A. Waldron, "Theory of the helical waveguide of rectangular cross-section," *J. Brit. IRE*, vol. 17, pp. 577–592; October, 1957.

[8] P. M. Morse and H. Feshback, "Methods of Theoretical Physics," McGraw-Hill Book Co., Inc., New York, N. Y., pts. 1, 2; 1953.

ductor (which is assumed to be homogeneous and isotropic), as a replacement for the actual slow-wave circuit, implies the presence of both axial and azimuthal slowing, although only the latter is of importance in E-type devices. A limitation inherent in the use of the dielectric cylinder arises from the fact that the dielectric is perfectly smooth, so that analyses based on this model indicate the presence of only one of the infinite number of possible space harmonics produced in the actual structure. However, the constraint is not serious so long as the conditions are such that the electron beam effectively interacts with only one space-harmonic component of the RF field.

A Further Examination of the Field Relations

A study of the field equations leads to some interesting conclusions concerning the characteristics of the transmission system described above. It is convenient in this study to regard the entire cross-sectional area of the system as being divided into the "slow-wave region," containing the periodic RF structure, and the "interaction space" which surrounds the slow-wave region. Thus, in the slow-wave region the radial propagation constant k_{2n} is given by

$$k_{2n}^2 = \left[\omega^2\mu_0\epsilon_2 - \left(\frac{n\pi}{L}\right)^2\right], \tag{7}$$

where ϵ_2 is the permittivity associated with the dielectric cylinder in farads per meter. It is apparent that k_{2n}^2 must be greater than zero, for otherwise wave propagation would be cut off in the slow-wave region, and therefore in the entire system. It follows that the radial variation of all field components in the slow-wave region must exhibit the real argument (rather than the imaginary argument) Bessel function behavior. The cutoff condition for axial propagation in the slow-wave region, $k_{2n}^2 \equiv 0$, leads to

$$|n| \leqq \frac{\omega L}{\pi}\sqrt{\mu_0\epsilon_2}, \tag{8}$$

as shown in Fig. 1. It may be noted that the allowed range of axial eigenvalues, corresponding to the integer n values, increases with frequency, with the height of the waveguide parallel to the cylindrical axis, and with the dielectric constant.

Since only the cutoff modes were assumed to be present in deriving the field relations given above, then the radial propagation constant appropriate to the interaction space k_n yields, for the condition $k_n^2 = 0$,

$$\left|\frac{\omega L}{\pi}\sqrt{\mu_0\epsilon_0}\right| < |n| < \infty,$$

as shown in Fig. 2. Thus, a finite and bounded set of axial eigenvalues associated with wave propagation in the slow-wave region leads to a pair of sets of infinite eigenvalues associated with the cutoff modes permeating the interaction region. It is apparent, however, that if the guide height L or the operating frequency is sufficiently increased to permit E- or H-wave *propagating* modes to exist in this space, then the elements of the periodic structure act as sources of radiation that excite strong fields in the region surrounding the RF circuit. The *propagating-wave* axial eigenvalues then

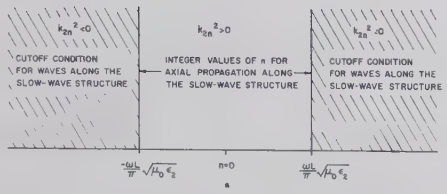

Fig. 1—Graphical representation of the range of n in the slow-wave region.

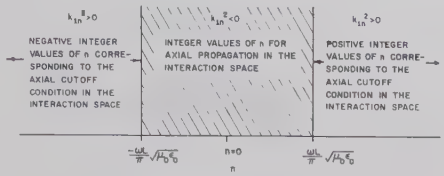

Fig. 2—Graphical representation of the range of n in the interaction space.

lie in the shaded area of Fig. 2, and the radial variation of all field components now take on the real-argument Bessel function variation.

Since the Hankel functions of the first and second kinds are linearly related to the two types of Bessel functions of real argument, it may be shown that radially propagating waves accompany axially propagating waves, and that radially attenuating functions accompany axially cutoff modes. The fields on the slow-wave structure must always be associated with radially and axially propagating modes, since operation below the cutoff frequency of the RF circuit suppresses electromagnetic radiation in the entire system. The fields in the interaction space may be associated either with radially and axially propagating or attenuating waves, depending on the relation of the operating frequency to the cutoff frequency of the interaction space.

The lowest E-mode field occurs for $n=0$, because E_z has the axial variation

$$\cos\left(\frac{n\pi}{L}z\right),$$

while the lowest H-mode field occurs for $n=1$, because H_z has the axial variation

$$\sin\left(\frac{n\pi}{L}z\right).$$

However, since E_θ possesses the same axial variation as H_z, it follows that the lowest mode, for which effective electron-wave interaction in E-type devices is possible, occurs when $n=1$.

In contrast to the "permitted sets" of axial eigenvalues, all field components possess an azimuthal variation of the form $e^{-j\beta_0\theta}$. A study of this function leads to the interesting physical intepretation that, as far as azimuthal variations are concerned, the waves may be regarded as propagating in a Riemann space.[9] Each *spatial* excursion of θ corresponding to 2π electrical radians of $\beta_0\theta$ causes the waves to encounter a "new leaf" of this surface, so that the total number of leaves required to provide a closed domain of electrical angular values of the fields is equal to the circular propagation constant. Thus, β_0 is a measure of the number of leaves encompassed in completing a spatial excursion of 2π radians. The order of the real and hyperbolic Bessel functions which specify the radial behavior of all fields are therefore determined by the number of Riemann leaves involved.

W. M. Nunn, Jr.
Electron Physics Lab.
Elec. Engrg. Dept.
The University of Michigan
Ann Arbor, Mich.

[9] S. A. Schelkunoff, "Electromagnetic Waves," D. Van Nostrand Co., Inc., New York, N. Y.; 1953.

Ring Network Filter*

A filter circuit comprising two ring networks which are connected by two quarter-wavelength lines is described. This circuit has one output with a relatively wide pass band and a second output with a sharp rejection band. A printed microstrip version designed for 1-Gc operation is shown in Fig. 1. Input is at terminal 1, band-pass output at terminal 3, and rejection band output at terminal 2.

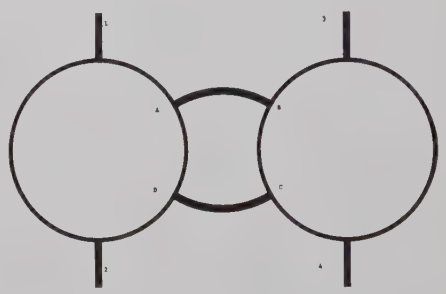

Fig. 1—1-Gc filter on $\frac{1}{16}$- inch teflon fiberglass.

A heuristic explanation of circuit action at the center frequency is as follows: Current entering arm 1 tends to divide equally between terminals A and 2 of the first ring network. A portion of the current entering terminal A travels around the loop $ABCD$, arriving at terminal D. Here one-half of the current goes to terminal 2 and one-half to terminal A. The part going to terminal A arrives in-phase while the part going to terminal 2 arrives antiphase with the currents flowing directly from terminal 1. The resultant partial cancellation at terminal 2 forces more current to enter arm AB, which in turn reduces the output from terminal 2 even more. Equilibrium is reached when the net current at terminal 2 is zero and all current into terminal 1 leaves by terminal 3. For zero circuit losses, cancellation of currents at terminal 2 would be complete, and there would be zero insertion loss between terminal 1 and terminal 3. Rejection occurs for a narrow band of frequencies at or near which the loop $ABCDA$ is one-wavelength long.

* Received by the PGMTT, March 10, 1961.

Ideally, all current entering the second ring network at terminal B flows out at terminals 3 and C. Terminal 4 is inherently isolated from terminal B and therefore from terminal 1 because no current enters the second ring network at terminal C. The isolation between terminals 1 and 4 can be no better than the intrinsic isolation between alternate terminals of either ring network.

The circuit of Fig. 1 is printed on $\frac{1}{16}$-inch teflon fiberglass with a copper backing. No effort is made to conserve space. The characteristic impedance of the printed lines used for the terminals 1-2-3-4 and coupling arms is 50 ohms, while the characteristic impedance of printed lines in the rings is approximately 70 ohms.

Characteristics for a single filter section designed for 1 Gc are shown in Fig. 2. These include VSWR of the input to arm 1 and isolation (or insertion loss) of the filter between terminal 1 and each of the other three terminals with unused terminals terminated in 50 ohms. Fig. 3(a) shows the isolation for two units cascaded into a band-pass filter, while Fig. 3(b) shows isolation for the same two units cascaded into a rejection filter. The two peaks in the rejection curve of Fig. 3(b) are due to a 10-Mc separation of the peak rejection frequencies of the individual sections.

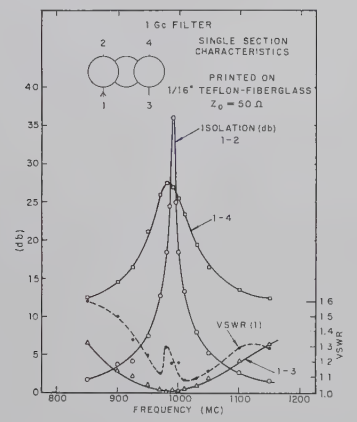

Fig. 2.

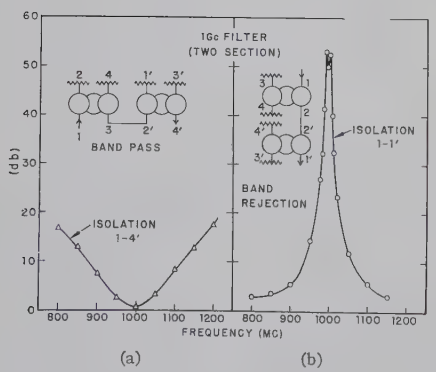

(a) (b)

Fig. 3.

J. A. Kaiser
Microwave Branch
Ordnance Corps.
Diamond Ordnance Fuze Labs.
Washington, D. C.

A Technique for Obtaining DC Isolation in Coaxial Cable RF Transmission Lines*

Introduction

In many applications involving microwave tubes it is desirable to monitor the voltages and currents of the various tube elements. This is particularly true of experimental tubes. The situation may be illustrated by a high voltage pulsed traveling-wave tube in which the collector and body are operated at or near ground level with the cathode at a negative potential. In order to observe current pulses at collector and body it is necessary to ground these points through a series resistor. Since the RF terminals of the device are generally fixed to the body, some form of dc isolation is required on the input and output transmission lines. If the ports are of waveguide construction, one method commonly employed is to place a thin teflon or polyethylene window between two cover flanges which are held together with nylon insulating screws. Tubes with coaxial connectors are usually adapted to waveguide and the above procedure is followed. The technique described below has been developed for obtaining dc isolation quite simply in coaxial cable.

The basic idea is to sever the outer conductor or shielding braid of the coaxial line, in this case a cable of the RG-9B/U type. A sever presents an open circuit to the DC path but permits transmission of the RF. It is noted that a capacitive coupling on the center conductor would not be satisfactory for this application. Most attempts to cut the braid with a sharp knife or other instrument will result in some damage to the dielectric underneath. An alternate approach might be to lift each strand individually and snip with electricians scissors, but this is a rather lengthy procedure. However, a very satisfactory method is described in the section below.

Description of Technique

The cable is first cut to the desired length and the outer protective covering removed for a distance of two or three inches near the middle. A strip of electrical tape about one-sixteenth of an inch wide is then wrapped circumferentially about the exposed braid at the position selected for the sever. It is necessary to keep the sever small with respect to cable wavelength in order to prevent excessive radiation. A narrow opening also minimizes the effect of the discontinuity presented to the TEM traveling-wave. The remaining braid is then completely covered with a layer of melted paraffin. After the wax has hardened a wedge-shaped cut is made at the severing point and the wax removed until the band of tape is uncovered. The tape is then peeled off leaving a narrow strip of exposed braid [Fig. 1(a)]. The careful application of concentrated nitric acid by means of a cotton swab rapidly etches away the silvered-copper braid. This operation should be performed under a hood. The paraffin protects the remaining braid [Fig. 1(b)] and the polyethylene dielectric does not react with nitric acid. The acid residue can be rinsed away with water and the paraffin removed by gentle heating or scraping. A very thin coating of paraffin left on the braid will prevent the loose strands from fraying throughout the rest of the procedure. It is important that all the frayed ends lie flat so that they do not puncture the insulating sleeve that follows.

The braid is then wrapped with thin teflon, polyethylene or electrical tape. An outer sleeve of braid is placed over this wrapping in contact with just one end of the outer conductor. The open end should overlap the sever by about a quarter wavelength in order to reduce radiation losses. A final covering with electrical tape keeps the outer sleeve snugly in place and presents a neat finished appearance. The desired cable connectors are then placed on the ends.

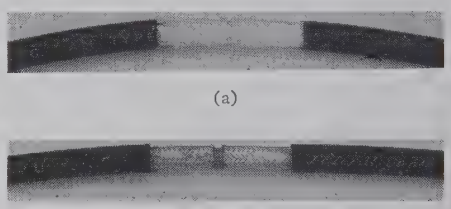

(a)

(b)

Fig. 1—(a) Before etching. (b) After etching.

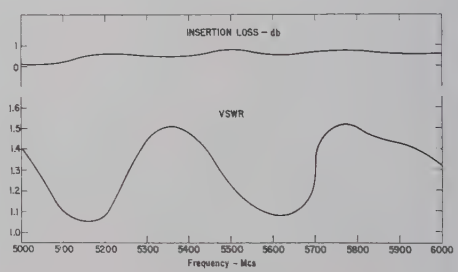

Fig. 2.

Results

An experimental cable was obtained and the technique described above was carried out. A continuity check of the assembled cable indicated an open circuit between the ends of the outer conductor. A further confirmation was obtained by applying a potential of five hundred volts with no arcing or current reading. To prevent possible contact at the sever, the gap may be wrapped with electrical tape during the procedure. Measurement of the RF characteristics showed that a VSWR of 1.5 or less and an insertion loss of about 0.5 db could be expected over the band from 5000 to 6000 Mc (Fig. 2). Considering the load and connector characteristics, these results are comparable to an unsevered cable.

The experimental data indicate that this technique provides the dc isolation and RF transmission required for this type of application.

R. A. Sparks
Appl. Phys. Lab.
The Johns Hopkins University
Silver Spring, Md.

* Received by the PGMTT, March 16, 1961.

Push-Pull Tunnel Diodes*

Presented in this note is a discussion of the advantages of using a pair of tunnel diodes arranged parallel to the signal and in series to the dc power supply. Large improvements are shown to exist in both dynamic range and large signal stability.

Tunnel-diode microwave amplifiers have at present the reputation of being small-signal devices. The noise figure of the devices, while not being as low as may be obtained with a well-designed reactance amplifier, is still quite competitive in the low-noise field. When a tunnel-diode preamplifier is used before a system, signals within very few db of noise may be amplified to a level well above the noise of the succeeding stages, so that the noise figure of the system will be essentially that of the preamplifier. However, in most microwave systems proper handling of small signals is not enough. Large signals must also be faithfully reproduced. The tunnel-diode amplifier will show marked change in gain at input signal levels of the order of -35 dbm.

It is the object here to point out an arrangement for using two tunnel diodes which, it is estimated, should improve the dynamic range of the amplifier by a factor of approximately 20 db so that, with germanium units, the point at which saturation begins will be approximately -15 dbm (for an assumed gain of 15 db).

Consider the pair of tunnel diodes connected in a circuit as shown in Fig. 1. The diodes are connected in shunt with the transmission line for the ac signal. The line as shown would represent a coaxial or parallel-plate transmission line system.

The current-voltage (I-V) and conductance-voltage (G-V) curves for a representative germanium unit are shown in Fig. 2.

The composite current-voltage (I-V) characteristics are illustrated in Fig. 3. Shown are the individual I-V curves of each diode, the composite current and the equivalent current (for noise purposes) as seen by the signal circuit. E_b is the value of bias set by the voltage sources as shown in Fig. 1. The most interesting feature is now shown by the composite conductance vs voltage characteristic presented to an input signal, and illustrated in Fig. 4. Three curves of conductance are shown, each for a different value of bias voltage E_b. For a value of $E_b = 0.165$ v, an extremely flat conductance characteristic is obtained for signal voltage deviations of over 100 mv. For a 115-mv interval on curve No. 2, a conductance change of less than 6 per cent has taken place. For the same bias point a single diode alone requires a voltage deviation of approximately 5 mv for a 6 per cent conductance change.

The constant conductance characteristic may be used with little or no degrading effect on noise figure. Curve No. 1 has been constructed for the characteristic obtained with $E_b = 0.150$ v, at which point the diode used has its minimum I/G ratio, and hence minimum noise figure. Curve No. 2 was displaced slightly to obtain better dynamic

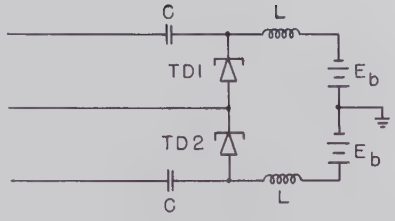

Fig. 1—Diode arrangement for push-pull operation.

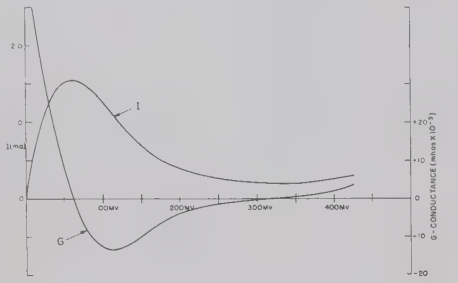

Fig. 2—Current-voltage characteristic of a typical germanium unit.

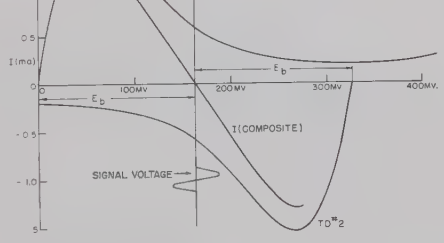

Fig. 3.—Composite current-voltage characteristic for push-pull arrangement.

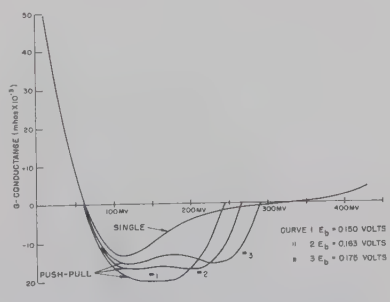

Fig. 4.—Conductance-voltage characteristic of a single unit and of the push-pull arrangement.

characteristics. The amount of displacement ($\Delta E_b = 12.5$ mv) resulted in negligible change in the I/G ratio, and hence in the expected noise figure.

The capacitance variations likewise are minimized with the diode combination. As the capacitance of a diode is a slowly increasing function of the junction voltage, for a given change in E_b the increase in capacitance of one diode is almost completely compensated by the decrease in the other. Thus, for signal voltages of the order of 100 mv, an almost constant capacitance characteristic is obtained. This will minimize the tendency toward loss in gain at high signal levels due to detuning of the resonant circuits.

Likewise, stability under large signal conditions will also be improved. For stability, the source conductance (G_s) (as seen by the diodes) must remain greater than the magnitude of the negative conductance ($|G_d|$). If the peaks of a large signal can drive the diode to the point where the negative conductance is greater than the source conductance, then instability may occur. The device may be "shocked" into oscillation if, due to rectification within the diode, the bias point can shift in the direction necessary to maintain the oscillations. If the "shocked" oscillations cannot persist, there is still the possibility of the building up of higher-frequency parasitic oscillations within that part of the signal cycle during which the condition $G_s - |G_d| < 0$ exists. With the double-diode scheme, when $G_s - |G_d|$ has been adjusted for proper gain, a much more stable arrangement is obtained, since now, under large signal peaks, the negative conductance will only decrease and not increase, as is obvious from the composite curves of Fig. 4.

A second and very important use would be for harmonic mixing. Because of the symmetry of the conductance curve about the bias point, the odd harmonic coefficients of the Fourier series expansion of the conductance evaluated about the bias point will all be zero. The even terms remain, allowing second- and higher-order (even) harmonic mixing. For the assumption that the image currents are short-circuited it has been estimated[1] that, if the diodes are biased as in curve No. 1, a local oscillator swing of 140 mv peak-to-peak would allow approximately 22 db of conversion gain with a noise figure of approximately 5 db. This noise figure represents a degradation of about one db from that expected if the same diodes were to be used as an amplifier. If tunnel diodes are to be used most efficiently in the high microwave or millimeter wave ranges, then the most efficient local oscillator scheme must be utilized. This double diode converter arrangement appears to be one such possibility.

L. E. Dickens
Rad. Lab.
The Johns Hopkins University
Baltimore, Md.

* Received by the PGMTT, April 2, 1961. This research was supported by the USAF Air Res. and Dev. Command.

[1] L. E. Dickens and C. R. Gneiting, "A tunnel diode amplifying converter," IRE Trans. on Microwave Theory and Techniques, vol. MTT-9, pp. 99–101; January, 1961.

Effects of Ferrite Strip Mounting Positions on Millimeter Wave Isolator Characteristics*

The position of the ferrite strip in a field displacement type isolator is an important problem. If x and L are defined as the mounting position of the ferrite strip and the width of the rectangular waveguide, respectively, as shown in Fig. 1, then, according to Soohoo,[1] Lax,[2] Fox, *et al.*,[3] and Button,[4] the optimum value of x ranges from $0.095L$ to $0.27L$. The sign of the directivity (backward to forward ratio of attenuation) for very thin ferrite strip is the same if $x<L/2$.

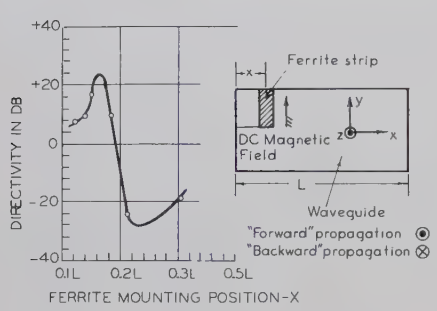

Fig. 1—Directivity and mounting position of ferrite strip.

The ferrite strip which the authors investigated was mounted on a polystyrene strip and was placed in RG-98/U waveguide as shown in Fig. 1. No attenuator film was coated on the ferrite strip in this case. The dimensions of the ferrite strip were 0.0117 inch×0.0325 inch×0.133 inch. The ferrite strip, made from a single crystal type sample LRR-1[5] ($BaFe_{12}O_{19}$, anisotropy field 18.4 koe, apparent density 5.13 g/cm³) was magnetized in the direction of easy magnetization. External dc magnetic field was applied in this direction as shown in Fig. 1, and the isolator was tested at frequency of 58.3 kMc.

The optimum position of the ferrite strip in this case was $x=0.16L$, which agreed with the results reported in the literature, but different results were obtained for directivity. The sign of directivity changed at $x=0.19L$. This is considerably smaller than $x=L/2$ reported in the literature. The experimental results obtained are shown in Fig. 1. The optimum values of backward to forward ratio of attenuation are plotted against the mounting position x. The results can be interpreted as a selective resonance of the ferrite structure against combined spatial harmonics as indicated by an arbitrary scale in Fig. 2.

When the applied dc magnetic flux density was changed, many peaks appeared in the attenuation curve as shown in Fig. 3. Several examples near the transition region of the directivities are shown in the figure. For each position of the ferrite strip, almost the same numbers of peaks were detected for backward attenuation. All the peaks were found at approximately the same magnetic flux density, even though the heights of the peaks were different. It can be considered that the peaks are due to complicated selective structural resonance of ferrite and spatial harmonics. In a certain mounting position, some peaks were accentuated and others were reduced. The sign of directivity corresponding to peak No. 2 did not change over the range of $x=0.109L$ to $0.303L$. It is thought that this is due to the local resonance with the TE_{10} mode. It is interesting to note that at the position where the directivity vanishes, most of the forward attenuation peaks are reduced as shown in Fig. 3(b).

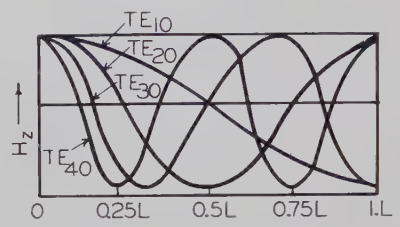

Fig. 2—Spatial harmonics in ferrite-loaded waveguide (arbitrary scale).

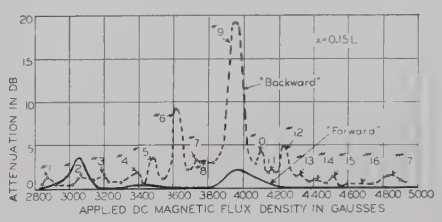

(a)

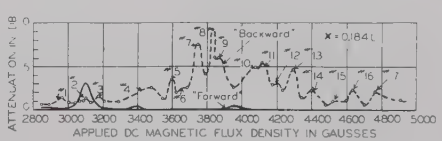

(b)

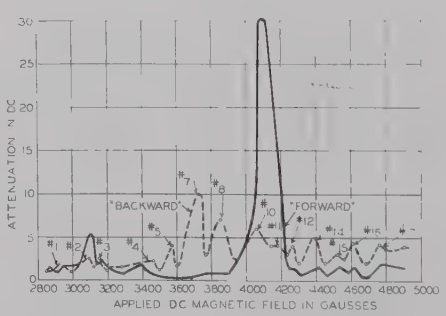

(c)

Fig. 3—Magnetic resonance characteristics.

* Received by the PGMTT, March 20, 1961; revised manuscript received, April 8, 1961. This research was supported by an A. O. Smith Corp. Res. grant.

[1] R. F. Soohoo, "Theory and Application of Ferrites," Prentice-Hall, Inc., Englewood Cliffs, N. J.; 1960.

[2] B. Lax, "Frequency and loss characteristics of microwave ferrite devices," PROC. IRE, vol. 44, pp. 1368–1386; October, 1956.

[3] A. G. Fox, S. E. Miller and M. T. Weiss, "Behavior and applications of ferrites in the microwave region," *Bell Sys. Tech. J.*, vol. 34, pp. 5–103; January, 1955.

[4] K. J. Button, "Theoretical analysis of the operation of the field displacement ferrite isolator," IRE TRANS. ON MICROWAVE THEORY AND TECHNIQUES, vol. MTT-6, pp. 303–308; July, 1958.

[5] Supplied by A. O. Smith Corp.

ACKNOWLEDGMENT

The authors thank A. Brault and S. Krupnik for their help in preparation of this manuscript, and the Raytheon Company for contributing the klystrons as a signal source.

K. ISHII
J. B. Y. TSUI
Dept. of Elec. Engrg.
Marquette University
Milwaukee, Wis.
F. F. Y. WANG
Long Range Res.
A. O. Smith Corp.
Milwaukee, Wis.

An *L*-Band Loop-Type Coupler*

The design of loop couplers for various loop length has been reported by Lombardini, Schwartz and Kelly.[1] This device is useful for many applications as the over-all length can be held to about 6 inches, whereas a comparable multihole coupler must be on the order of several feet long. The loop-type device couples a TE_{10} waveguide mode from a RG-69/U to a TEM mode in a $\frac{3}{8}$-inch coaxial line. A comb-type coupler, for coupling a coaxial line to TE_{10} waveguide, was reported by Lombardini and Schwartz.[2] This device made use of a multiple-capacitive probe situated in a longitudinal slot in the top wall of the waveguide.

The scattering matrix of the four-port device of Fig. 1 is

$$S=\begin{bmatrix} s_{11} & s_{12} & s_{13} & s_{14} \\ s_{21} & s_{22} & s_{23} & s_{24} \\ s_{31} & s_{32} & s_{33} & s_{34} \\ s_{41} & s_{42} & s_{43} & s_{44} \end{bmatrix}. \quad (1)$$

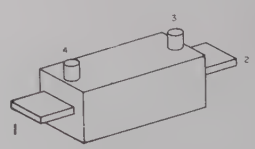

Fig. 1—A four-port device.

For matched ports, the principal diagonal elements of (1) will become zero:

$$s_{11}=s_{22}=s_{33}=s_{44}=0.$$

The energy coupled to the loop will travel in the direction opposite to that of the incident energy, therefore,

$$s_{13}=s_{24}=s_{31}=s_{42}=0.$$

For a lossless symmetrical network the uni-

* Received by the PGMTT, April 11, 1961.

[1] P. P. Lombardini, R. F. Schwartz and P. J. Kelly, "Criteria for the design of loop-type directional couplers for the *L*-band," IRE TRANS. ON MICROWAVE THEORY AND TECHNIQUES, vol. MTT-4, pp. 234–239; October, 1956.

[2] P. P. Lombardini and R. F. Schwartz, "A new type of directional coupler for coupling coaxial line to TE_{10} waveguide," 1957 IRE WESCON CONVENTION RECORD, pt. 1, pp. 22–29.

tary condition applies,[3]

$$S\tilde{S}^* = 1, \tag{2}$$

where $\tilde{S}^*$ is the conjugate transpose matrix. Considering the off-diagonal element of (2),

$$s_{12}s_{32}^* + s_{14}s_{34}^* = 0 \tag{3}$$

or

$$\theta_{12} - \theta_{32} = \pi + \theta_{14} - \theta_{34}, \tag{4}$$

where θ_{12}, θ_{32}, θ_{14} and θ_{34} are the argument of s_{12}, s_{32}, s_{14} and s_{34}, respectively. From the principal diagonal element of (2),

$$s_{12}s_{12}^* + s_{14}s_{14}^* = 1 \tag{5}$$

or

$$|s_{12}|^2 + |s_{14}|^2 = 1. \tag{6}$$

By choosing the location of the reference planes

$$\theta_{14} = \theta_{32} = 0, \tag{7}$$

(4) becomes

$$\theta_{12} + \theta_{34} = \pi. \tag{8}$$

A loop-type coupler, with the coupling loop placed near the side wall of the waveguide, is shown in Fig. 2. This device was tested for 15 kw average and 10 Mw peak. The coupling variation over the full waveguide frequency range is shown in Fig. 3. This figure shows the coupling with the loop at the center of the waveguide and near the side wall. The increase in coupling value as a function of coupling-loop position is

$$C = 20 \log \left(\frac{1}{\cos \pi d} \right), \tag{9}$$

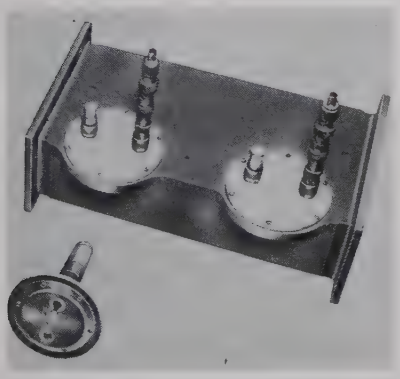

Fig. 2—Loop-type coupler.

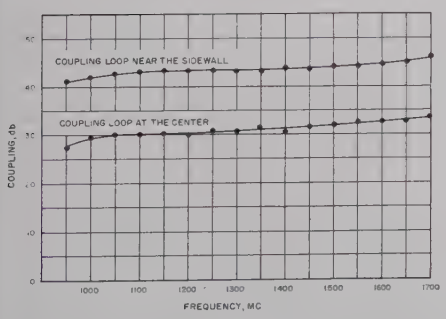

Fig. 3—Characteristics of loop-type coupler with coupling loop at the center and near the side wall.

[3] C. G. Montgomery, R. H. Dicke and E. M Purcell, "Principles of Microwave Circuits," McGraw-Hill Book Co., Inc., New York, N. Y., pp. 301–303; 1948.

where d is the displacement in fractions of the a dimension of the guide, and is measured from the center of the guide toward the side wall. The experimental and calculated values of this variation are shown in Fig. 4. Measurements were made at two frequencies differing by 10 Mc. The results show that the variation in coupling is frequency insensitive as indicated by (9). A minimum directivity of 30 db was achieved over 10 per cent of the band by adjusting the location, height and length of the rectangular-shaped plate situated around the coupling loop and grounded to the top wall of the waveguide. Fig. 5 indicates the change in directivity as a function of frequency. It is felt that a directivity greater than 40 db exists at the center frequency. This value could not be measured due to the lack of proper termination. A 50-Ω coaxial termination with VSWR of less than 1.03 was utilized with the auxiliary arm of the coupler.

ACKNOWLEDGMENT

The author would like to acknowledge many helpful discussions with S. Ammirati, who proposed the use of the hood over the coupling loop to increase the directivity, and with S. Lehr. He is also indebted to J. Ebert for his many helpful suggestions.

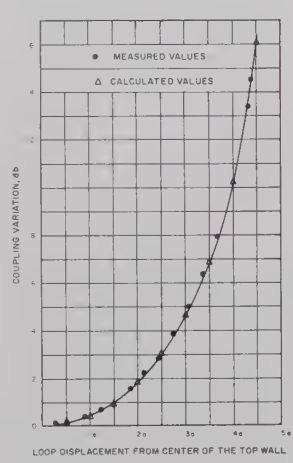

Fig. 4—Coupling variation as a function of loop position.

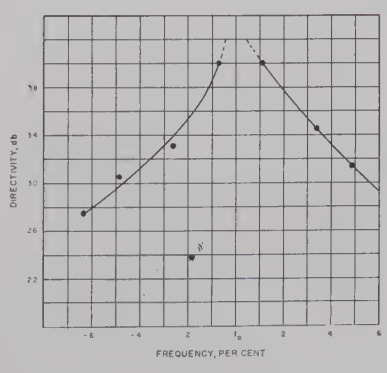

Fig. 5—Directivity vs frequency.

B. MAHER
Microwave Div.
FXR, Inc.
Woodside, N. Y.

The Cutoff Wavelengths of Composite Waveguides*

When electromagnetic waves propagate in waveguides of nonsimple cross section, no exact solution can be obtained by the conventional method of solving the wave equation by separation of variables. In such cases approximations are available such as perturbation methods, variational methods, etc.[1]

The Rayleigh-Ritz method has been used to obtain an approximate solution for the cutoff wavelength for waveguides with semicircular side walls and flat top and bottom walls, and for truncated-circular waveguides. See Figs. 1 and 2.

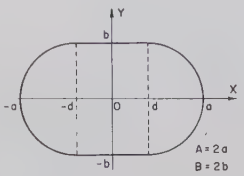

Fig. 1—Waveguide with flat tops and bottoms and semicircular side walls.

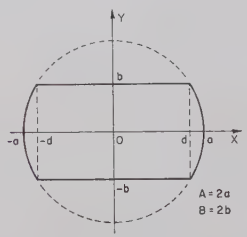

Fig. 2—Truncated-circular waveguide.

The results obtained for the cutoff wavelengths for waveguides of semicircular side walls and flat top and bottom walls disagree with the values shown by Montgomery, Dicke and Purcell[2] for aspect ratios of 0.406 and 0.450. From the nature of the problem and from experimental evidence it can be stated that the trial functions used to obtain the results[2] mentioned above was inferior to the one used here.

The boundary-value problem of electromagnetic waves propagating in a cylindrical waveguide can always be reduced to a simple two-dimensional problem.

If the longitudinal axis is in the z direction,

$$\nabla^2\psi_i(x, y) + k_i^2\psi_i(x, y) = 0, \tag{1}$$

where $\psi_i(x, y)$ is the eigenfunction and k_i is the propagation constant for the ith mode, respectively.

If ψ_i satisfies either Dirichlet or Neumann boundary conditions, a variational expression for the eigenvalue k_i^2 exists,

$$k_i^2 \leq \frac{\int |\nabla\psi_i|^2 d\sigma}{\int \psi_i^2 d\sigma} \tag{2}$$

* Received by the PGMTT, March 14, 1961; revised manuscript received, April 17, 1961.

[1] P. M. Morse and H. Feshbach, "Methods in Theoretical Physics II," McGraw-Hill Book Co., Inc., New York, N. Y.; 1953.

[2] C. G. Montgomery, R. H. Dicke and E. M. Purcell, "Principles of Microwave Circuits," M.I.T. Rad. Lab. Ser., McGraw-Hill Book Co., New York, N. Y., vol. 8, p. 45; 1948.

the integrals taken over the waveguide cross section.

Following the work of Kornhauser,[3] a trial function can be used to obtain an approximate value for the eigenvalue for the fundamental mode.[4]

Dropping subscripts, a legitimate trial function for the fundamental mode is

$$\psi(x) = \sum_{n=0}^{N} C_{2n+1}x^{2n+1}. \qquad 3)$$

Note that the trial function does not satisfy the boundary condition, also that the parameters C_{2n+1} will be adjusted to minimize the eigenvalue.

Let $N=1$; then

$$\psi = C_1x + C_3x^3. \qquad (4)$$

By inserting the trial function in (2), the eigenvalue takes the following form:

$$k^2 = \frac{\alpha C_1^2 + \beta C_1C_3 + \gamma C_3^2}{\delta C_1^2 + \epsilon C_1C_3 + \zeta C_3^2}, \qquad (5)$$

where $\alpha, \beta, \gamma, \delta, \epsilon$ and ζ are constants dependent on the dimensions of the waveguide.

The eigenvalue k^2 is next minimized with respect to C_1 and C_3. After eliminating C_1 and C_3, k^2 is obtained from

$$k^4 - 2\Theta k^2 + \Phi = 0, \qquad (6)$$

where

$$\Theta = \frac{2\alpha\zeta + 2\delta\gamma - \epsilon\beta}{4\delta\zeta - \epsilon^2}$$

$$\Phi = \frac{4\alpha\gamma - \beta^2}{4\delta\zeta - \epsilon^2}.$$

For the waveguide of semicircular side walls and flat top and bottom walls, the coefficients are

$$\alpha = a\left[p + \frac{\pi}{4}r\right]$$

$$\beta = a^3\left[2p^3 + \frac{3\pi}{2}p^2r + 4pr^2 + \frac{3\pi}{8}r^3\right]$$

$$\gamma = a^5\left[\frac{9}{5}p^5 + \frac{9\pi}{4}p^4r + 12p^3r^2 + \frac{27\pi}{8}p^2r^3 + \frac{24}{5}pr^4 + \frac{9\pi}{32}r^5\right]$$

$$\delta = a^3\left[\frac{1}{3}p^3 + \frac{\pi}{4}p^2r + \frac{2}{3}pr^2 + \frac{\pi}{16}r^3\right]$$

$$\epsilon = a^5\left[\frac{2}{5}p^5 + \frac{\pi}{2}p^4r + \frac{8}{3}p^3r^2 + \frac{3\pi}{4}p^2r^3 + \frac{16}{15}pr^4 + \frac{\pi}{16}r^5\right]$$

$$\zeta = a^7\left[\frac{1}{7}p^7 + \frac{\pi}{4}p^6r + 2p^5r^2 + \frac{15\pi}{16}p^4r^3 + \frac{8}{3}p^3r^4 + \frac{15\pi}{32}p^2r^5 + \frac{48}{105}pr^6 + \frac{5\pi}{256}r^7\right],$$

where $r=b/a$ and $p=1-r$.

[3] E. T. Kornhauser and I. Stakgold, "Application of Variational Methods to the Equation $\nabla^2u+\lambda u=0$," Cruft Lab., Harvard Univ., Cambridge, Mass., Tech Rept. No. 117; 1950.

[4] The fundamental mode is the equivalent to the H_{10} mode in rectangular waveguide and the H_{11} mode in circular waveguide.

The numerical results, the experimental points and the points obtained from Montgomery, Dicke and Purcell[2] are shown in Fig. 3.

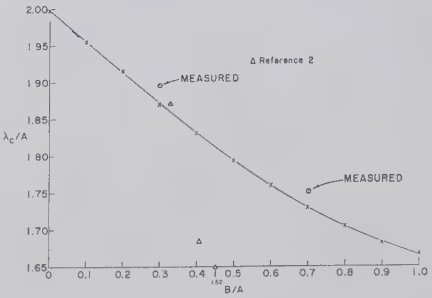

Fig. 3—The cutoff wavelengths for the waveguide with flat tops and bottoms and semicircular waveguides as a function of aspect ratio.

The method has also been applied to calculate the cutoff wavelengths for truncated-circular waveguides.[5]

G. R. Valenzuela
The Johns Hopkins University
Radiation Lab.
Baltimore, Md.

[5] G. R. Valenzuela, "The Cut-Off Wavelengths and Power-Voltage Impedance for Composite Waveguides for the Fundamental Mode," Rad. Lab., The Johns Hopkins Univ., Baltimore, Md., Tech. Rept., to be published.

A Mechanical Waveguide Hybrid Phase Shifter*

Some interesting results have been obtained on a waveguide-hybrid phase shifter under development for use in an *S*-band radio-astronomy interferometer antenna.

The phase shifter[1,2] illustrated in Fig. 1(a) comprises a waveguide hybrid junction, a rotating chopper, and a pair of variable lengths of a short-circuited waveguide: the variable lengths of the guide are provided by a movable short-circuit plunger. The operation of the phase shifter is as follows.

Let us assume that the chopper is initially closed. When power is injected at port 1, the power enters the hybrid junction where it is divided, one half being coupled to the adjacent waveguide where it continues to propagate in the same direction, while the other half of the power propagates in the main waveguide. The properties of the hybrid junction are such that the signal in the adjacent waveguide is in phase quadrature, lagging the signal in the main waveguide. At the chopper the two signals are reflected; power in the main waveguide enters the hybrid junction, recombining in phase with the power in the adjacent arm. The entire power leaves port 2, provided that the hybrid is matched. If, now, the chopper is opened, an additional path length is introduced into the hybrid system and the amount of phase shift is equivalent to an electrical length of twice the stub length. The phase shift can be made to be proportional to either the stub length s or to $(\lambda_g/2)-s$, where λ_g is the guide wavelength, depending upon how the chopper is introduced across the waveguide.

A sketch of the chopper used in the model under investigation is shown in Fig. 1(b). In the radio-astronomy application the chopper rotates at a speed of 900 rpm. The phase-shift characteristics as a function of chopper rotation are shown in Fig. 2 for two different plunger positions. Note particularly that the shorter stub length provides the greater amount of phase shift. For this case the phase shift is proportional to $(\lambda_g/2)-s$. This result can be explained quite readily if one analyzes the behavior of the chopper and stub in terms of an equivalent circuit.

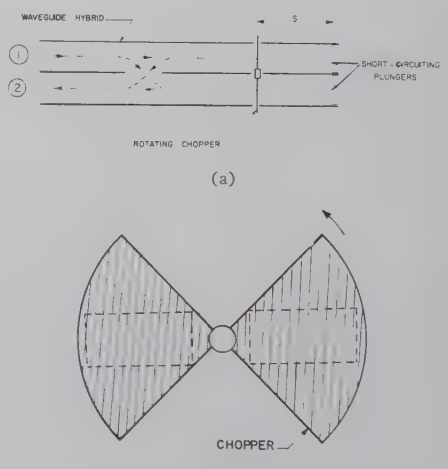

Fig. 1(a) Waveguide hybrid phase shifter. (b) Rotating chopper used in the phase shifter.

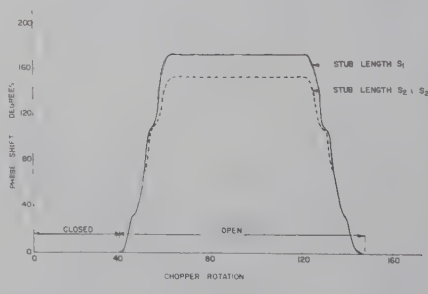

Fig. 2—Phase-shift characteristics as a function of chopper rotation.

The susceptance of the short-circuited stub is plotted as a point Y_{s1} on the Smith Chart diagram shown in Fig. 3. Placed in shunt with Y_{s1} is the susceptance of the chopper which behaves as a capacitive iris (positive susceptance). As the chopper is introduced, the net susceptance is reduced,

* Received by the PGMTT, April 17, 1961.

[1] H. Shnitkin, "Survey of electronically scanned antennas," *Microwave J.*, vol. 4, pp. 57-64; January, 1961.

[2] J. Blass, *et al.*, "A High Speed *X*-Band Conical Scanner," AF Cambridge Res. Ctr., Bedford, Mass., AFCRC Rept. TR-58-145-11; April, 1958.

causing the point to move counterclockwise around the Smith Chart. When the chopper is completely closed, the net susceptance becomes infinite, and this position is described by the point Y_{sc}. Hence the total phase shift is equivalent to twice the length of line $Y_{s1} - Y_{s}$, or proportional to $(\lambda_g/2) - s$.

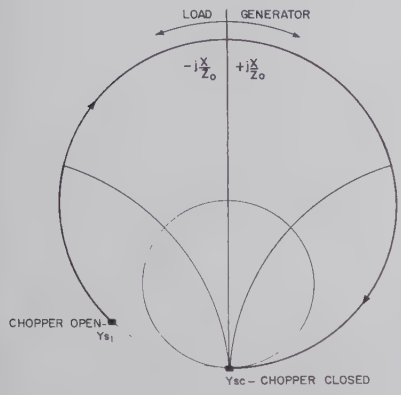

Fig. 3—Smith Chart representation illustrating the operation of the phase shifter.

It is not difficult to demonstrate that, if one provides a chopper which is equivalent to an inductive iris (negative susceptance), then the phase shift would be equivalent to twice the length of line $Y_{s1} - Y_{sc}$ measured in the opposite direction around the chart. In this case the amount of phase shift is proportional to the stub length s.

J. Y. Wong
Radio and Elec. Engrg. Div.
Natl. Research Council
Ottawa, Can.

Rectangular Waveguide Switches*

Introduction

Since the first disclosure by Reggia and Spencer[1] of the rectangular waveguide phase shifter, a number of investigators have presented qualitative analyses describing observed performances.[2–4] In general, these authors agree on two phenomena that occur. First, upon application of a longitudinal magnetic field to the ferrite (phase-shifter geometry shown in Fig. 1), there is a "trapping" process whereby the RF field is increasingly concentrated in the ferrite acting as if it were a "dielectric" waveguide. Second, there is a mode-conversion process that takes place simultaneously (probably a circularly polarized wave in the ferrite rod) that gives rise to an electric-field component in the ferrite region orthogonal to the electric field in the empty waveguide (TE_{10} mode).

It is possible to utilize these two effects to design a number of different reactive and absorption switches. It is the purpose of this paper to relate these devices to the phase-shifter phenomena and thus classify them. It is also desired to present preliminary experimental and behavioral data.

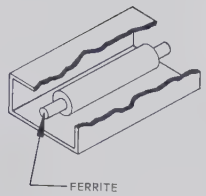

Fig. 1—Reggia-Spencer rectangular waveguide phase shifter geometry.

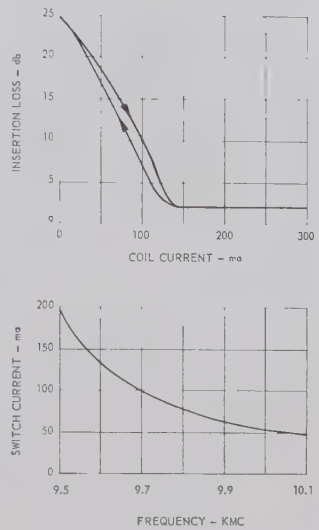

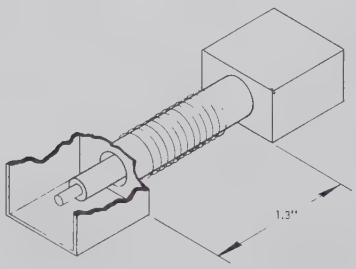

Fig. 2—Insertion loss vs coil current for reactive switch, normally off. Ferrite R-1, 0.260-inch diameter×2.0 inches long. Cutoff guide section, 1.3 inches long×0.4-inch diameter. Frequency is 9.6 kMc. Insert shows frequency sensitivity of switching current for minimum loss.

Types of Switches

1) *Reactive Switch, Normally Off:* Fig. 2 shows the geometry of the reactive switch.[5] Its operation depends upon the "trapping effect" mentioned earlier. Since the small tube containing the ferrite is normally at "cutoff," there is no energy propagation. When the magnetic field is applied, the energy is trapped in the ferrite and propagates through the cutoff section with low insertion loss. The input and output waveguides can be either in-line or crossed. This switch is similar to the tetrahedral junction described by Weiss[6] and Caswell.[7]

2) *Reactive Switch, Normally On:* Fig. 3(a) shows a reactive switch which is normally on. It is constructed with a thin metal septum, normal to the electric field of the dominant mode, soldered to the waveguide narrow-wall and extending to the ferrite in close proximity. With the absence of an applied field, energy is transmitted with low insertion loss. When a field is applied, the "mode-conversion" process takes effect, and an orthogonal electric-field component is generated so that the energy is reflected. The performance of the reactive switch is shown in Fig. 3(b).

3) *Absorption Switch, Normally On:* The switch shown in Fig. 3 is easily modified into an absorption switch by replacing the thin metal septum with a thin sheet of resistive material. The absorption switch is shown in Fig. 4(a) and its performance is plotted in Fig. 4(b). This switch would normally have a low VSWR for all coil currents. Reggia[8] has recently suggested a switch of this type. This switch design splits the ferrite and sandwiches the lossy material between the ferrite halves. In the design of Fig. 4, a resistive material was mounted close to the ferrite.

* Received by the PGMTT, May 8, 1961.

[1] F. Reggia and E. G. Spencer, "A new technique in ferrite phase shifting for beam scanning of microwave antennas," Proc. IRE, vol. 45, pp. 1510–1517; November, 1957.

[2] P. A. Rizzi and B. Gatlin, "Rectangular guide ferrite phase shifters employing longitudinal magnetic fields," Proc. IRE., vol. 47, pp. 446–447; March, 1959.

[3] A. Clavin, "Reciprocal ferrite phase shifters in rectangular waveguide," IRE Trans. on Microwave Theory and Techniques, vol. MTT-6, p. 334; July, 1958.

[4] Jerold A. Weiss, "A phenomenological theory of the Reggia-Spencer phase shifter," Proc. IRE, vol. 47, pp. 1130–1137; June, 1959.

[5] A. Clavin, "Problems Associated with Rectangular Waveguide Phase Shifters," presented at PGMTT Natl. Symp., San Diego, Calif.; May 9–11, 1960.

[6] J. A. Weiss, "The tetrahedral junction as a waveguide switch," IRE Trans. on Microwave Theory and Techniques, vol. MTT-8, pp. 120–121; January, 1960.

[7] P. A. Caswell, "Performance of Tetrahedral Junction Waveguide Switches," presented at the 6th Symp. on Magnetism and Magnetic Material, New York, N. Y.; November, 14–17, 1960.

[8] F. Reggia, "A new broadband absorption modulator for rapid switching of microwave power," Internatl. Solid State Circuits Conf., University of Pennsylvania, Philadelphia, Pa.; February, 1961.

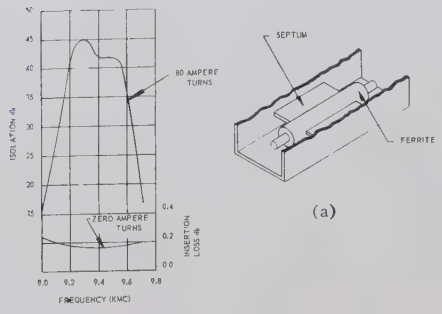

(a)

(b)

Fig. 3—Two-port reactive switch, normally on, utilizing mode-conversion properties of magnetized ferrite.

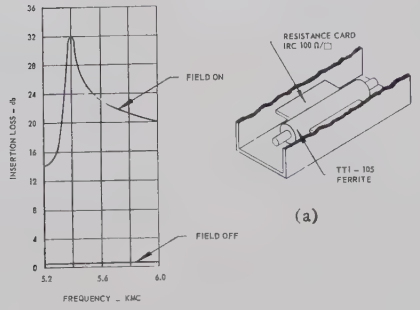

(a)

(b)

Fig. 4—*C*-band absorption switch, normally on.

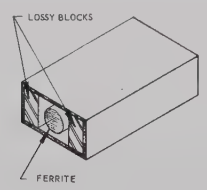

Fig. 5—Absorption switch, normally off. Field off, high insertion loss. Field on, low insertion loss.

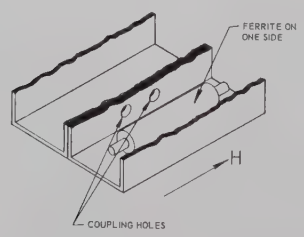

Fig. 6—Proposed variable coupler. With field applied, coupling to auxillary guide is reduced.

This indicates that there is a considerable field outside the ferrite even when saturated.

4) *Absorption Switch, Normally Off:* This configuration has not been fabricated as yet, but in principle should work well. The switch conception is illustrated in Fig. 5 and is similar to the reactive switch of Fig. 2. In this switch, the metal is replaced by lossy material so that, with zero field applied, most of the energy is absorbed. With an applied field, the RF energy is trapped to the ferrite and passes through the material with low insertion loss.

5) *Variable Coupling Devices:* A pair of coupled waveguides, one of which contains the phase-shifter geometry, is depicted in Fig. 6. When a field is applied, the energy is trapped in the ferrite and changes the coupling coefficient.

Conclusions

The suggested types of switches have a number of features which make them valuable. First, the magnetic field required is low, thus facilitating rapid switching. Second, they cannot be over-driven as in a Faraday rotation switch. Once saturated, additional field has little effect on the passage or reflection of RF energy. Excellent ratios of isolation to insertion loss can be obtained.

A. Clavin
Microwave Dept.
Rantec Corp.
Calabasas, Calif.

Comments on "Stepped Transformers for Partially-Filled Transmission Lines"*

The use of a lumped equivalent circuit for the transverse section of a waveguide has been used to determine the cutoff frequency of ridged guide.[1,2] In essence, the transverse section of the guide is equated to an LC tank and the resonant frequency of the tank is determined by the usual formula. Sullivan and Parkes[3] have extended this method to the analysis of a ridged guide partially loaded with dielectric. They account for the additional capacitance introduced by the dielectric and include this capacitance as part of the LC tank to be analyzed for the resonant frequency. While the simplified lumped-network equivalents are always desirable in analyzing microwave networks, we should be wary of overgeneralizing them. In the case of dielectric slab loading in a waveguide, the location of the added capacitance as well as its magnitude has an effect in determining the cutoff frequency. (This can also be said of the discontinuity capacitance at the edge of a ridge.) Note how a dielectric slab when centered in a rectangular waveguide will lower the cutoff frequency far more than when flush with the sidewall.[4] This is not accounted for in the LC tank equivalent. The effect of each increment of capacitance due to each lamina of dielectric will be largely determined by the distance from the lamina to the short-circuit walls. Therefore, the author believes that the case of a partially dielectric-loaded guide can only be genuinely analyzed by the transverse resonance method or by some other method which accounts for the distributed parameters involved.

Another point for consideration in analyzing dielectric slab-loaded guide is the relationship between the guide wavelength and the cutoff wavelength—or rather the lack of relationship. Formulas for guide wavelength are based upon the right triangle relationship that exists between the propagation constants $k_{0,\kappa t,\kappa g}$. These are, respectively, the propagation constants for free space, for the waveguide transverse direction, and for the waveguide longitudinal direction.

$$k_0^2 = \kappa_t^2 + \kappa_g^2, \tag{1}$$

where

$k_0 = 2\pi/\lambda_0$, λ_0 = wavelength of the traveling wave in free space,

$\kappa_t = 2\pi/\lambda_t$, λ_t = transverse resonant wavelength,

$\kappa_g = 2\pi/\lambda_g$, λ_g = guide wavelength.

* Received by the PGMTT, July 19, 1960.

[1] S. Ramo and J. R. Whinnery, "Fields and Waves in Modern Radio," John Wiley and Sons, Inc., New York, N. Y., 2nd ed., pp. 409–410; 1953.

[2] T. S. Chen, "Calculation of the parameters of ridge waveguides," IRE Trans. on Microwave Theory and Techniques, vol. MTT-5, pp. 12–17; January, 1957.

[3] D. J. Sullivan and D. A. Parkes, "Stepped transformers for partially filled transmission lines," IRE Trans. on Microwave Theory and Techniques, vol. MTT-8, pp. 212–217; March, 1960.

[4] N. Marcuvitz, "Waveguide Handbook," McGraw-Hill Book Co., Inc., New York, N. Y., p. 390; 1951.

$$\frac{1}{\lambda_0^2} = \frac{1}{\lambda_t^2} + \frac{1}{\lambda_g^2}; \tag{2}$$

$$\left(\frac{\lambda_0}{\lambda_g}\right)^2 = 1 - \left(\frac{\lambda_0}{\lambda_t}\right)^2; \tag{3}$$

$$\lambda_g = \frac{\lambda_0}{\sqrt{1 - \left(\frac{\lambda_0}{\lambda_t}\right)^2}}. \tag{4}$$

If the guide is completely filled with dielectric, (1) becomes

$$\epsilon_r k_0^2 = \kappa_t^2 + \kappa_g^2, \tag{5}$$

where ϵ_r is the dielectric constant of the medium relative to air.

Eq. (5) leads to

$$\lambda_g = \frac{\lambda_0}{\sqrt{\epsilon_r - \left(\frac{\lambda_0}{\lambda_t}\right)^2}}. \tag{6}$$

Usually when formulas (4) and (6) are presented λ_t is given as λ_c, the cutoff wavelength, because in the usual case where the guide has only one dielectric medium, λ_t is equal to λ_c. When the guide contains dissimilar dielectric media, however, λ_t is generally not equal to λ_c. Therefore, λ_c as well as f_c, the cutoff frequency, cannot be used to determine λ_g as in formulas like (4) and (6). This point is widely unappreciated. Sullivan and Parkes, for instance, have used the cutoff frequency in a formula akin to (6) attempting to determine λ_g for a dielectric slab-loaded guide.[5]

In a guide having one dielectric medium in the transverse plane, the transverse resonant wavelength for each mode is fixed and independent of the frequency of the traveling wave. In a guide having different dielectric media, however, the transverse resonant wavelength for each mode will vary as a function of the traveling-wave frequency as well as of the geometry of the system. Furthermore, each dielectric medium will contain a different transverse resonant wavelength.[6] In a dielectric slab-loaded guide, the air region and the dielectric region will each have a different transverse resonant wavelength, λ_{ta} in the air region and $\lambda_{t\epsilon}$ in the dielectric region. In all cases, λ_{ta} will be different from $\lambda_{t\epsilon}$, but both λ_{ta} and $\lambda_{t\epsilon}$ will yield the same λ_g when used in (4) and (6), respectively.

As the frequency increases, the *RF* tends to concentrate in the region of highest dielectric constant.[7] When the frequency is reached at which $\lambda_g = \lambda_0$, there is no longer any transverse propagation in the air region. λ_{ta} becomes imaginary, and in the transverse plane, the air region is a guide below cutoff. Nevertheless, (4) or (6) will still yield λ_g if we know λ_{ta} or $\lambda_{t\epsilon}$, respectively.

For the dielectric slab-loaded guide, (1) and (5) are modified respectively,

$$K_0^2 = \kappa_{ta} + \kappa_g^2 \tag{7}$$

$$\epsilon_r K_0^2 = \kappa_{t\epsilon} + \kappa_g^2 \tag{8}$$

where

$$\kappa_{ta} = 2\pi/\lambda_{ta}$$

$$\kappa_{t\epsilon} = 2\pi/\lambda_{t\epsilon}.$$

The determination of λ_g for this case is usually made by simultaneously solving (7), (8) and the transverse resonance equation of the given geometry.[6]

Michael R. Leibowitz
1620 Ocean Ave.
Brooklyn, N. Y.

Authors' Comment[8]

The authors would like to thank Mr. Leibowitz for his comments on the article, "Stepped Transformers for Partially-Filled Transmission Lines."[3]

The analysis of a ridged waveguide partially loaded with dielectric is intended primarily to outline a means of designing dielectric stepped transitions in ridged waveguide. Because of the approximations that have been made in the analysis, it is not intended to be a precise treatment of guide wavelength as a function of the dielectric geometry for the double-ridged guide. However, we feel the design procedure will yield good results for most engineering component applications. Similar stepped dielectric transformers have also been employed successfully in the 4000- to 7000-Mc range.

Although not reported in the paper, the VSWR of a linear dielectric taper (of the same length as the stepped transition) had also been measured. The maximum recorded VSWR in the 2000- to 4000-Mc band was 1.44 as compared to a maximum VSWR of 1.10 for the stepped transition.

D. J. Sullivan
D. A. Parkes
Advanced Microwave Dev.
Sperry Microwave Electronics Co.
Div. of Sperry Rand Corp.
Clearwater, Fla.

[5] Sullivan and Parkes, *op. cit.*, see (13).

[6] C. G. Montgomery, R. H. Dicke, and E. M Purcell, "Principles of Microwave Circuits," McGraw-Hill Book Co., Inc., New York, N. Y., pp. 385–390; 1948.

[7] T. Moreno, "Microwave Transmission Design Data," Dover Publications, Inc., New York, N. Y., Fig. 11–2; 1958.

[8] Received by the PGMTT, August 19, 1960.

Contributors

L. Paul Bolgiano, Jr., (M'56) was born in Baltimore, Md., on June 20, 1922. He received the B.S. degree in engineering from Haverford College, Haverford, Pa., in 1943. He received the M.A. degree in mathematics and the Ph.D. degree in physics both from the Johns Hopkins University, Baltimore, in 1947 and 1953.

L. P. Bolgiano, Jr.

During World War II, he served as a radar maintenance officer in the U. S. Navy. He taught at the U. S. Naval Academy, Annapolis, Md., for two years and at St. John's College, Annapolis, Md., for one year under a Ford Foundation Fellowship. In 1955, he joined the faculty of the University of Delaware, Newark, Del., where he is now an associate professor of electrical engineering. He has spent the past two summers at Stanford University, Stanford, Calif., as a research associate. His areas of interest include ionospheric propagation, radio astronomy, and noise theory.

Dr. Bolgiano is a member of Sigma Xi and the American Physical Society.

❖

Paul Diament was born in Paris, France, on November 14, 1938. He came to the United States in 1948, and attended Columbia University, New York, N. Y., where he received the B.S. and M.S. degrees in electrical engineering in 1960, and 1961, respectively. He is pursuing graduate studies at Columbia where he expects to earn the Ph.D. degree with the aid of a National Science Foundation fellowship.

P. Diament

In conjunction with his studies, he has been employed since 1958 by Columbia's Department of Electrical Engineering as a Research Assistant on a project dealing with surface wave structures incorporating dielectric and ferroelectric materials at microwave frequencies.

Mr. Diament is a member of Tau Beta Pi and Eta Kappa Nu.

❖

John J. Faris (M'59) was born in Grandview, Washington, on November 7, 1921. He graduated from Reed College, Portland, Oregon, in 1943, and received the Ph.D. degree in physics from the University of Washington, Seattle, in 1951.

J. J. Faris

From that time he has been teaching physics, first at Pacific University, Forest Grove, Ore., and since 1954, at Colorado A & M College, Fort Collins, Colo. During the summers of 1955 and 1958, he was employed at the Boulder Laboratories of the National Bureau of Standards, Boulder, Colo. His fields of major interest include secondary emission of electrons, solid-state physics, and microwaves.

Dr. Faris is a member of the American Physical Society, the American Association of Physics Teachers, Sigma Xi, and Phi Kappa Phi.

❖

Peter Foldes (M'58), for a photograph and biography, please see page 206 of the March, 1961, issue of these Transactions.

❖

Robert C. Hansen (S'47–A'49–M'55–SM'56) was born in St. Louis, Mo., on August, 3, 1926, His schooling at the Missouri School of Mines and Metallurgy, Rolla, was interrupted in 1944 for a period of U. S. Navy service as an RT and electronics instructor; he returned and received the B.S.E.E. degree in 1949. The M.S. and Ph.D. degrees were obtained from the University of Illinois, Urbana, in 1950 and 1955, respectively. While there he worked in the Antenna Laboratory on ferrite loops, streamlined airborne antennas, and DF and homing systems. Subsequently he was senior staff engineer in the Microwave Laboratory of Hughes Aircraft Company, Culver City, Calif., working on surface-wave antennas, slot arrays, near fields and radio-power transfer, electronics scanning and steerable arrays, and dynamic antennas. In 1960 he became a senior staff engineer in the Telecommunications Laboratory of Space Technology Laboratories, Inc., Los Angeles, Calif.; there he engaged in communications satellite, telemetry, tracking, and command studies. After the formation of Aerospace Corporation, Los Angeles, Calif., he became senior staff scientist in their Electronics Laboratory.

R. C. Hansen

Dr. Hansen is a member of the American Physical Society, Tau Beta Pi, Sigma Xi, Eta Kappa Nu, Phi Kappa Phi, and Commission 6 of URSI. He is a registered Professional Engineer in Missouri, and an Associate Editor of the *Microwave Journal.*

❖

Alexander Hessel (M'54) was born on October 19, 1916, in Vienna, Austria. He received his M.Sc. degree in physics from the Hebrew University in Jerusalem, Israel, in 1944, and the D.E.E. degree in 1960 from the Polytechnic Institute of Brooklyn, Brooklyn, N. Y.

From 1945 to 1948, he was engaged as a radio engineer with a broadcasting station in Jerusalem, Palestine. From 1948 to 1951 and from 1953 to 1956, he was employed with the Research Division of the Israeli Ministry of Defense, doing work in electron-

ics and microwaves. In 1955 and 1956, he was a lecturer in Microwave Transmission Systems at the Technion in Haifa, Israel. Since 1957, he has been with the Polytechnic Institute of Brooklyn at its Microwave Research Institute, where he is engaged in studies on leaky wave and modulated antennas and on the propagation of electromagnetic waves in plasmas.

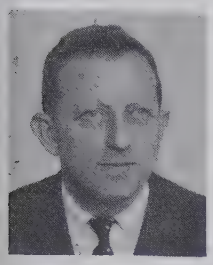

A. HESSEL

Dr. Hessel is a member of Sigma Xi.

❖

James D. Kellett (S'56–M'58) was born in Shinglehouse, Pa., on December 20, 1931. He received the B.E.E. degree from Rensselaer Polytechnic Institute, Troy, N. Y., in 1957. Since joining Sylvania Electric Products, Inc., in 1957, he has been engaged in the development of microwave components and system applications. In February, 1961, he transferred from Sylvania's Antenna and Microwave Laboratory at Waltham, Mass., to Sylvania's Communication Laboratory at Amherst, N. Y.

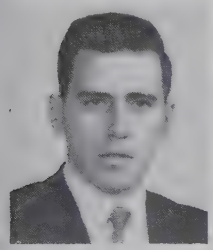

J. D. KELLETT

Mr. Kellett is an associate member of Sigma Xi.

❖

Howard E. King (A'46–M'55–SM'55) was born in Seattle, Wash., on October 16, 1924. He received the B.S.E.E. degree in 1945 from the University of Washington, Seattle, and the M.S.E.E. degree in 1955 from the University of Illinois, Urbana.

H. E. KING

From 1946 to 1952, he was a member of the broadcast section of the RCA Victor Division, designing FM and television transmittingantennas; he took part in the development of the Empire State Building multiple television antenna system. After a year with the Andrew Corporation, he was appointed a research assistant of the Antenna Laboratory of the University of Illinois, where he remained until 1955. Subsequently, he became a member of the technical staff of the Space Technology Laboratories, Inc., Los Angeles, Calif., where he engaged in the development of electronic countermeasures, antennas and components; and high-power transmitters, filters and diplexers. In January, 1961, he joined Aerospace Corporation, Los Angeles, where he is presently employed.

❖

L. Lewin was born in Essex, England, on July 22, 1919. He received his education at Southend High School.

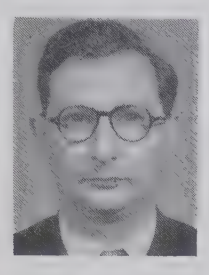

L. LEWIN

During World War II he was engaged at the Admiralty Signals Establishment on the design of radar antennas and waveguide components.

In 1946, he joined Standard Telecommunication Laboratories, Harrow, Essex, England, becoming head of the microwave department in 1951. He is engaged in research on waveguides and components, antennas, noise and electromagnetic theory, and has recently been appointed chief engineer in charge of the Research Group, responsible for advanced studies in several fields.

Mr. Lewin is a member of the IEE.

❖

Arthur A. Oliner (M'47–SM'52–F'61) was born in Shanghai, China, on March 5, 1921. He received the B.A. degree from Brooklyn College, N. Y., in 1941, and the Ph.D. degree in physics from Cornell University, Ithaca, N. Y., in 1946.

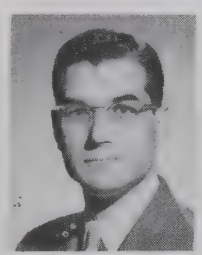

A. A. OLINER

While at Cornell, he held a graduate teaching assistantship in the physics department and also conducted research on an Office of Scientific Research and Development project. Since 1946 he has been with the Microwave Research Institute of the Polytechnic Institute of Brooklyn, N. Y., where he has conducted research on a wide variety of topics in the microwave field. He has also taught graduate courses in physics and electrical engineering, and is a research professor.

Dr. Oliner is chairman of USA Commission 1 and a member of Commission 6 of URSI. He also serves as chairman of a National Academy of Sciences Advisory Panel to the National Bureau of Standards.

❖

Frank Reggia (A'55–SM'59) was born in Northumberland, Pa., on October 30, 1921. He is a graduate of the Radar Materiel School, Naval Research Laboratory, Washington, D. C., and did his graduate and undergraduate work at George Washington and Maryland Universities.

F. REGGIA

While a member of the Armed Forces, he served as an electronic specialist in both the United States and South Pacific Theatre before and during World War II. He joined the technical staff of the National Bureau of Standards in 1945, where he was engaged in a research and development program on microwave standards.

Mr. Reggia joined the Microwave Branch of the Diamond Ordnance Fuze Laboratories, Army Ordnance Corps, Washington, D. C., in 1954, as an electronic engineer, where he has since been engaged in a study of the properties of ferrites and their applications to microwave systems.

❖

John M. Richardson (SM'56) was born in Rock Island, Ill., September 5, 1921. He received the B.A. degree in physics from the University of Colorado, Boulder, in 1942, and served as Electronics Officer in the USNR from 1943 to 1946 on the staff of various electronics officer-training schools. He received the M.A. and Ph.D. degrees in physics, the latter in 1951, from Harvard University, Cambridge, Mass.

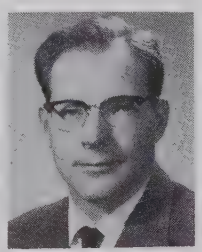

J. M. RICHARDSON

He was subsequently employed by the Denver Research Institute, Denver, Colo. Since 1952 Dr. Richardson has been with the Boulder Laboratories of the National Bureau of Standards, Boulder, Colo. There, his work has been in the area of microwave physics, including microwave spectroscopy, microwave interferometry and microwave diagnosis of ionized gases, especially, as these fields have bearing on standards and physical constants. His present position is Chief of the Radio Standards Laboratory.

Dr. Richardson is a Fellow of the American Physical Society, a member of Sigma Xi, the Research Society of America, and Commission 1 of the International Scientific Radio Union. He serves on the editorial board of the NBS *Journal of Research*.

❖

S. Perry Schlesinger (M'55) was born in New York, N. Y., on October 9, 1918. He received the B.A. degree from Michigan State College, East Lansing, in 1941, the M.S. degree from Union College, Schenectady, N. Y.,

in 1950, and the Dr. Eng. degree from The Johns Hopkins University, Baltimore, Md., in 1957.

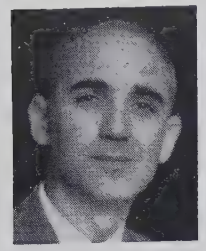

S. P. Schlesinger

In 1946, following war service as a destroyer engineer officer, he joined the General Electric Company, Schenectady. He subsequently served as an Assistant Professor of electrical engineering on the faculties of Union College and the U. S. Naval Academy, Annapolis, Md. From 1953 to 1956, he was a Research Associate at the Radiation Laboratory of Johns Hopkins, working on back-scattering problems, millimeter techniques, and problems in dielectric image line transmission. He is now an Associate Professor of electrical engineering at Columbia University, New York, N. Y., where, in addition to teaching and consulting, he is engaged in research on surface wave guiding and radiating structures.

Dr. Schlesinger is a member of Sigma Xi and Phi Kappa Phi.

❖

Roelif Stapelfeldt (M'58) was born in New York, N. Y., on August 31, 1929. He received the B.S. degree in 1954, the M.S. degree in 1955, and the Ph.D. degree in 1961 in electrical engineering from the Carnegie Institute of Technology, Pittsburgh, Pa.

R. Stapelfeldt

Since 1956, he has been associated with the Research Department of the Union Switch and Signal Division of the Westinghouse Air Brake Company, Pittsburgh, Pa., in the fields of transistor circuit design and infrared instrumentation. He has also been a part-time instructor at Carnegie.

Dr. Stapelfeldt is a member of Sigma Xi.

T. Bruce Thomson was born in Toronto, Canada, on March 27, 1934. He received the B.A.Sc. degree at the University of Toronto in 1957.

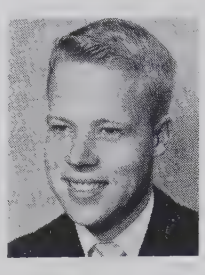

T. B. Thomson

Upon graduation, he joined the antenna design group of the RCA Victor Company, Ltd., Montreal, Canada, where he was engaged with various microwave problems, *i.e.*, branching filters, high-quality waveguide systems and antennas. Since September, 1960, he has been working for Computing Devices of Canada, Ltd., Montreal.

❖

Arvids Vigants was born in Bauska, Latvia, on February 19, 1932. He received the B.E.E. degree from the College of the City of New York, N. Y., in 1956. He then became an assistant in electrical engineering at Columbia University, New York, where he received the M.S. degree in June, 1957.

A. Vigants

At present, he is an instructor of electrical engineering at Columbia, and is working on a doctoral dissertation for the D.Eng.Sc. degree.

Mr. Vigants is a member of Eta Kappa Nu, Tau Beta Pi, and Sigma Xi.

❖

Max T. Weiss (S'43–A'45–M'55–SM'57) was born in Hungary, on December 29, 1922. He received the B.S. degree in electrical engineering from the College of the City of New York, N. Y., in 1943, and the M.S.E.E. and Ph.D. degrees in physics from the Massachusetts Institute of Technology, Cambridge, in 1947 and 1951, respectively.

He worked for RCA from 1943 to 1944, and then served in the U. S. Navy at the Naval Ordnance Laboratory. From 1946 to 1950, he was Research Associate at the M.I.T. Research Laboratory of Electronics, doing research on microwave spectroscopy. He joined Bell Telephone Laboratories, Holmdel, N. J. in 1950, where he was concerned with solid-state physics and, in particular, with the microwave properties and application of ferrites. More recently, he has done research in low-noise microwave amplification and in quantum electronics. He joined the Hughes Aircraft Company, Culver City, Calif., in 1959, where he was associate head of the Applied Physics Laboratory. Since March, 1961, he has been Director of the Electronics Laboratory of Aerospace Corporation, Los Angeles, Calif.

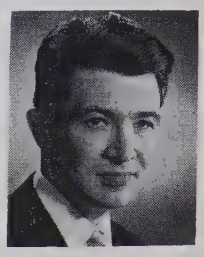

M. T. Weiss

❖

Frederick J. Young (S'54–M'57) was born in Buffalo, N. Y., on May 19, 1931. He received the B.S. degree in 1953, the M.S. degree in 1954, and the Ph.D. degree in 1956, all in electrical engineering from the Carnegie Institute of Technology, Pittsburgh, Pa.

F. J. Young

Since 1956, he has been an assistant professor of electrical engineering at Carnegie. He has been concurrently a research engineer in the Solid-State Physics Department of the Westinghouse Research Laboratories, Pittsburgh, where he is concerned with ferromagnetism. He has served as a consultant to Union Switch and Signal Division of the Westinghouse Air Brake Company, Pittsburgh, and to the Cornell Aeronautical Laboratories, Buffalo.

Dr. Young is a member of the Acoustical Society of America, the ACM, the ASEE, Phi Kappa Phi, and Sigma Xi. He is an associate member of the AIEE.

PGMTT News

1961 National Symposium Digests

There are a few extra copies of the "Digest of Technical Papers" of the 1961 National Symposium still available at $3.00 per copy. These Digests were a PGMTT Symposium "first" and were described as excellent by those who attended. While they last, Digests may be obtained from

Frank Reggia
Microwave Branch 250
DOFL
Washington 25, D. C.

Remittance should be made payable to 1961 IRE-PGMTT National Symposium.

The Digest covers twenty contributed papers which constituted four sessions describing Millimeter Waves, Parametric Devices, Ferrites, and Plasmas. Six invited papers for the two panel sessions on High Power Microwave Techniques and Low Noise Microwave Amplifiers are summarized. A complete paper "Elementary Considerations of Noise Performance," included in the Digest, formed the basis of discussion for the System and Receiver Noise Performance Clinic.

Available Back Issues

IRE Transactions on Microwave Theory and Techniques

Individual copies of the issues listed below may be purchased at the following prices: IRE members (one copy) $2.25, libraries and colleges $3.25, all others $4.50.

Vol. MTT-4, No. 3, July, 1956
Vol. MTT-5, No. 3, July, 1957
Vol. MTT-5, No. 4, October, 1957
Vol. MTT-6, No. 1, January, 1958
Vol. MTT-6, No. 2, April, 1958
Vol. MTT-6, No. 3, July, 1958
Vol. MTT-6, No. 4, October, 1958
Vol. MTT-7, No. 2, April, 1959
Vol. MTT-7, No. 3, July, 1959
Vol. MTT-7, No. 4, October, 1959
Vol. MTT-8, No. 1, January, 1960
Vol. MTT-8, No. 2, March, 1960
Vol. MTT-8, No. 3, May, 1960
Vol. MTT-8, No. 4, July, 1960
Vol. MTT-8, No. 5, September, 1960
Vol. MTT-8, No. 6, November, 1960
Vol. MTT-9, No. 1, January, 1961
Vol. MTT-9, No. 2, March, 1961
Vol. MTT-9, No. 3, May, 1961

INSTITUTIONAL LISTINGS

The IRE Professional Group on Microwave Theory and Techniques is grateful for the assistance given by the firms listed below, and invites application for Institutional Listing from other firms interested in the Microwave field.

AIRBORNE INSTRUMENTS LABORATORY
A Division of Cutler-Hammer, Inc.
Deer Park, Long Island, New York

Research and Development

AIRTRON, INC.
A Division of Litton Industries
200 East Hanover Ave., Morris Plains, N.J.

Designers and Producers of Complete Line of Microwave Electronic and Aircraft Components

ALFORD MANUFACTURING COMPANY
299 Atlantic Ave., Boston 10, Mass.

RF Instruments, Coaxial Components, Antennas and Air Navigation Aids

CASCADE RESEARCH
Div. of Lewis & Kaufman Electronics Corp.
5245 San Fernando Rd., Los Angeles, Calif.

Research, Development, Production: Microwave Ferrite Devices, Microwave Components & Subsystems

EIMAC TUBES, EITEL-McCULLOUGH, INC.
301 Industrial Way, San Carlos, Calif.

Microwave Tubes, TWT-VTM-Reflex Klystrons, Power Grid Tubes, Amplifier Klystrons

ELECTRONIC SPECIALTY CO.
5121 San Fernando Rd., Los Angeles 39, Calif.

Airborne and Ground Antennas, Towers, Waveguides, Microwave Components, Complete Radiating Systems

FXR, INC.
25-26 50th Street, Woodside 77, N.Y.

Precision Microwave Test Equipment, High Power Microwave Electronics, Microwave Components & Instrumentation

ITT FEDERAL LABORATORIES
500 Washington Ave., Nutley 10, N.J.

Line-of-Sight and Over-the-Horizon Microwave Systems; Test Equipment and Components

LITTON INDUSTRIES
Electron Tube Division
960 Industrial Rd., San Carlos, Calif.

Magnetrons, Klystron, TWT's, Noise Sources, BWO's, Display Devices, CFA's, Switch Tubes, MM Wave Tubes

MELABS
3300 Hillview Ave., Palo Alto, Calif.

Microwave Components and Systems for Communications, Countermeasures, Reconnaissance, Radar, Etc.

(See outside back cover for additional listings.)

The charge for an Institutional Listing is $50.00 per issue or $210.00 for six consecutive issues. Applications for Institutional Listings and checks (made out to The Institute of Radio Engineers, Inc.) should be sent to Robert A. Rivers, PGMTT Advertising Editor, Aircom Inc., 354 Main St., Winthrop 52, Mass.

INSTITUTIONAL LISTINGS

MICROLAB
570 West Mount Pleasant Ave., Livingston, N.J.

Designers and Manufacturers of a Complete Line of Coaxial Microwave Components and Cavity Filters

SCIENTIFIC-ATLANTA, INC.
2162 Piedmont Rd., N.E., Atlanta 19, Ga.

Complete Antenna Pattern Range Instrumentation, Special RF and Antenna Systems Development

MICROWAVE ASSOCIATES, INC.
South Avenue, Burlington, Mass.

Waveguide Devices, Microwave Diodes, Magnetrons, Duplexers, TWT's, Ferrite & Solid-State Devices

STEWART ENGINEERING COMPANY
Santa Cruz, Calif.

Backward Wave Oscillators & Other TW Type Tubes; Controlled Atmosphere Furnaces & Precision Spot Welder

THE MICROWAVE JOURNAL
1330 Beacon St., Brookline 46, Mass.

A Magazine Devoted to the Interests of Engineers Working at Microwave Frequencies

SYLVANIA MICROWAVE DEVICE OPERATIONS
Sylvania Electric Products Inc.
500 Evelyn Ave., Mountain View, Calif.

Magnetrons, Klystron, TWT's, BWO's, Ferrite Devices, Waveguide Windows, Microwave Diodes

PHELPS DODGE COPPER PRODUCTS CORP.
300 Park Ave., New York 22, N.Y.

Styroflex, Foamflex Air Dielectric Aluminum Sheathed Coaxial Cables, Connectors and Waveguides

TECHNICRAFT DIVISION, Electronic Specialty Co.
Thomaston, Conn.

Designers, Developers and Producers of Microwave Components, Transmission Lines, and Assemblies

PRD ELECTRONICS, INC.
202 Tillary St., Brooklyn 1, N.Y.

Complete Line of Microwave and Electronic Test Equipment Waveguide and Coaxial Components

WATKINS-JOHNSON COMPANY
3333 Hillview Ave., Palo Alto, Calif.

Res., Dev., Microwave Electron Devices, TWT's, BWO's, Parametric Amplifiers, Microwave Systems

SAGE LABORATORIES, INC.
3 Huron Dr., Natick, Mass.

Microwave Attenuators, Couplers, Crystal Holders, Filters, Hybrids, Mixers, Rotary Joints

WEINSCHEL ENGINEERING COMPANY, INC.
10503 Metropolitan Ave., Kensington, Md.

Attenuation Standards, Coax Attenuators, Insertion Loss Test Sets, Voltage & Power Calibrators

WHEELER LABORATORIES, INC.
Great Neck, N.Y.
Antenna Lab., Smithtown, N.Y.

Consulting Services, Research & Development, Microwave Antennas & Waveguide Components

(See inside back cover for additional listings.)